Acoustical Determination of Physical Properties of Porous Grounds

Thesis

Acoustical Determination of Physical Properties of Porous Grounds

Thesis submitted by

Heather Mary Hess M.Sc.

for the degree of

Doctor of Philosophy

May 1988

Department of Engineering Mechanics
Faculty of Technology
Open University
Milton Keynes
England

Date of Submission: 29.4.88

Date of Award: 4.10.88

Abstract

Conventional techniques for determining air porosity, moisture content, air permeability and crusting features are reviewed. Alternative approaches depending upon inversion of data for sound propagation near to and through the soil surface are presented and their results for both soils and snow are discussed. The inversion techniques depend upon models both for sound propagation near grazing incidence and for the acoustic properties of homogeneous and layered porous materials and these models are described.

Particular acoustic methods, based upon the difference in spectra received by two vertically separated microphones above the ground surface and the spectra received by probe microphones below the ground surface, are used on sand, silt, loam, clay and snow.

It is found possible using acoustical techniques to deduce air porosities at and near the surface to within 10% of their conventionally measured values. The acoustic measurements enabled deduction of an effective flow resistivity parameter in which the actual flow resistivity is multiplied by the square of a pore shape factor ratio. The use of this together with acoustically deduced porosity in monitoring soil condition is discussed. Changes in acoustically deduced parameters are shown to occur with moisture content both in soil bin and field experiments. The acoustic techniques prove successful in monitoring surface crusts and sub-surface layering with depth on a finer scale and at smaller depth intervals than those possible with conventional techniques.

Acknowledgements

I would like to record my sincere thanks to Dr.Keith Attenborough, whose guidance and encouragement have helped me through the smiles and tears of this research and the writing of this thesis. My grateful thanks also to Dr.Nick Heap and Dr.Peter Leeds-Harrison who have also provided helpful suggestions during the course of this work.

To those people who helped during field experiments, particularly Brendan Aengenheister, Dr.Margaret Price, Dr.Jim Rogers, David Berry, Dr.Jim Sabatier and Phil Payne, I would like to say a big thank you. Thanks are also due to those people who helped with the establishment of field trial sites. These include Tim Chamen at AFRC Engineering Silsoe, Stewart Miller and Gordon Soane at Silsoe College and Mr.Pillinger of Bulbourne Farm in Tring. Grateful thanks are also due to Dr.Sung Lee of KRC, Michigan for the opportunity to travel to Michigan, for his assistance in field experiments in the snow, and the chance to have a ride on a snowmobile!

A very grateful thank you also, to Dr.Kai Li for help in computer software development and to Julia Morris for number crunching and plotting. Also to everyone in the OU ACS Research Support Group particularly Andy Boddington whose ability to wander the mine-fields of LaTeX and whose wonderful sense of humour kept me going during the long dark hours of final thesis preparation.

Finally a heartfelt thank you to Tim whose shoulder was always there despite it being wrapped in a sling!

This work was sponsored by the Agriculture and Food Research Council and by the Open University Research Committee.

Contents

List of Figures

List of Tables

Chapter 1

Introduction

In agricultural research a knowledge of porosity of air connected pores, air permeability, moisture content, and near surface layering are desirable as indicators of soil structure, compaction and aeration. The precise dependence of crop yields on the soil parameters and structure is not understood. Nevertheless it is clear that poor structure and low air and water content and movement will inhibit plant growth, such as germination, root development, and ultimately crop yields. Thus the determination and monitoring of such soil characteristics in a tolerably non-invasive manner is a continual requirement. An examination of conventional methods of measuring the above soil parameters, used in soil science research, reveal the invasive and destructive nature of most techniques. This is not conducive to remonitoring of an area of soil throughout a growing season. In addition some techniques when made in close proximity to the soil surface are likely to be unreliable.

The application of this acoustic research is intended to develop an acoustically-based engineering solution to the continuing problem of determining and monitoring soil characteristics such as porosity of air-connected pores, moisture content, air permeability and near surface layering by non-invasive means or by methods that may be used *in situ* with the minimum of disturbance.

Reflection and refraction from a soil surface modifies near grazing propagation of sound and causes an interference pattern in the total sound field. This interference pattern can be modelled using knowledge of the acousti-

cal properties of porous materials (surface impedance) and the appropriate theory of sound propagation. Research has resulted in the development of various models for the prediction of sound levels due to outdoor sound sources on or near the ground. Most work has concentrated on characterising acoustical ground properties in terms of one parameter, the effective flow resistivity. This has met with limited success and other studies show that the influence of the ground surface on sound propagation is dependent upon the bulk parameters of the porosity of air-filled pores connected with the soil surface, the flow resistivity (equal to the dynamic viscosity divided by the air permeability), a pore shape factor and the tortuosity of the pores [1]. When layering occurs near the surface a layer depth parameter can also be included. In this research it is the intension to use these more sophisticated ground impedance models and their various approximations in an attempt to characterise the ground properties more realistically than the one parameter semi-empirical model. It is apparent that if the ground can be characterised in terms of its acoustical impedance, and this impedance can be expressed in terms of soil physical properties then from measurements of the acoustical characteristics of various soils these bulk parameters may be deduced by an inversion process.

Various acoustic techniques have been developed to measure acoustical impedance. The majority of these techniques were set up to examine the acoustical effect of sound reflection and refraction from differing ground surfaces, and not designed to study undisturbed soil samples *per se*. Some techniques cause disturbance of soil by the apparatus involved. Other techniques particularly long range sound propagation measurements are influenced by meterological conditions. In addition long range sound propagation measurements are influenced by a large area of the ground surface, thus the characterisation of small localised areas of soil, for example a tyre wheeling, is impossible. For the purposes of this work a short range level difference technique has been developed to try and overcome many of these problems. In some soils, for example those with a high flow resistivity crust close to the surface , reflected sound does not penetrate deep enough to characterise

subsurface layering features. This supports the need to measure sound transmission into the ground and for the purposes of this research a two probe microphone technique has been developed. The utilisation of a combination of sound reflection and sound transmission techniques in an effort to deduce soil parameters at the surface and at depth is a novel approach to acoustical ground characterisation. It is the purpose of this thesis to assess the feasibility and accuracy of using these acoustic techniques to determine ground parameters in close proximity to the surface, using more sophisticated impedance models than has previously been tried. If successful the acoustic technique could be used to measure soil parameters such as air permeability, air filled porosity and layer features simultaneously and with minimum disturbance of the soil condition.

1.1 Thesis Layout

The background to this study is described in Chapter 2 in the form of a literature review of published material relating to two topic areas. Firstly conventional techniques of soil parameter determination and the limitations of each method are considered. Secondly acoustic methods involving sound propagation above and below the ground surface are reviewed together with a summary of results for acoustically deduced ground parameters.

In Chapter 3 theoretical aspects of sound propagation above and below ground are discussed, together with a description of models used to predict impedance and propagation constant. The predictions are directly comparable to measurements carried out over several different soil types and snow. The dependence of level difference spectra on geometry and ground surface is also illustrated.

A description of each experimental location both in and outdoors is presented in Chapter 4. A description of the experimental procedure and the equipment used is also presented together with software developed to analyse the data obtained.

In Chapter 5 a summary of results are presented, each site being treated

individually. Results for different days at each site are compared and initial interpretation of results offered.

To assess the feasibility of using acoustic methods to determine ground parameters, five objectives are offered for discussion in Chapter 6, these are;

1. Acoustic determination of the air porosity of soils.
2. Acoustic determination of the flow resistivity of soils.
3. Acoustic determination and monitoring of soil moisture content.
4. Acoustic detection and characterisation of surface crusts, of a saturated surface layer and subsurface layering.
5. Acoustic determination of physical properties of snow.

Each objective is discussed in turn with a comparison of results from all sites.

A summary of the discussion and implications of this work for further areas of research and investigation are presented in Chapter 7.

Chapter 2

Background

2.1 Soil Porosity

Soil can be regarded as a three phase system as shown in Figure 2.1, consisting of solids, which are either mineral or organic matter, water and solutes, and air. The size and arrangement of solid particles determines the total amount of pore space that is occupied by water and air, which usually accounts for 30 to 60% of the volume of the soil, Hillel [2]. In terms of soil aeration for agricultural purposes such as crop growth, root development, and soil air movement, it is important to study the proportion of total porosity (V_f) occupied by air, the air filled porosity. The volume of air filled porosity (V_a) is related to water volume (V_w) because they compete for the same pore space.

$$V_f = V_w + V_a \tag{2.1}$$

2.1.1 Measurement Techniques

The standard technique for measuring total porosity, water content and air-filled porosity is called the gravimetric or difference method. The water content in a known volume of soil V_t is dried off by placing samples in an oven at 105°C for 24-48hours. The ratio of the mass of the dried soil M_s to its volume V_t is called the dry bulk density ρ_s and can be represented by

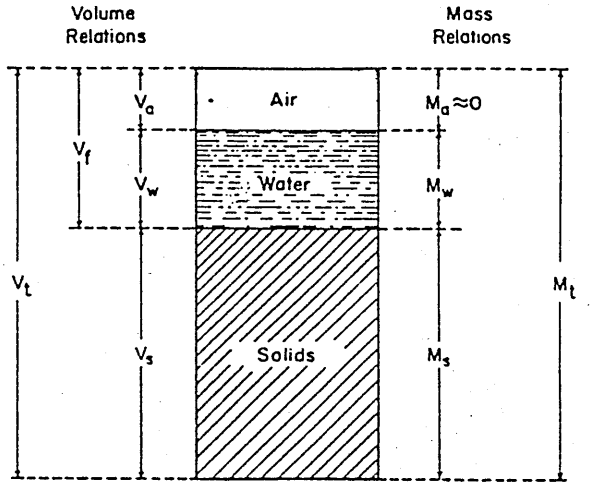

Figure 2.1 Schematic Diagram of the Soil as a Three Phase System.

$$\rho_s = \frac{M_s}{V_t} \tag{2.2}$$

The dry bulk density is always lower than the soil particle density ρ_g, which is accepted as $2650kg/m^3$ for most soils. This means only part of the bulk volume is occupied by solid particles, the rest is pore space. Total porosity can then be expressed as

$$V_f = 1 - \frac{\rho_s}{\rho_g} \tag{2.3}$$

By calculating the mass of water M_w as the difference between wet and dry sample weight and assuming the density of water ρ_w to be $1000kg/m^3$ the air-filled porosity V_a is found by subtraction from unity of the calculated percentage volumes of the water V_w and the solids V_s as shown in Equations 2.4, 2.5 and 2.6.

$$V_w = \frac{(M_w/\rho_w)}{V_t} \tag{2.4}$$

and

$$V_s = \frac{(M_s/\rho_g)}{V_t} \tag{2.5}$$

and

$$V_a = 1 - (V_w + V_s) \tag{2.6}$$

The technique described above is destructive, labour intensive and slow. It requires the replication of at least three soil cores from any one soil depth to give a representative value of V_a [3]. On a trial plot over the season this can result in a large area of the soil becoming disrupted and making the area unavailable for remonitoring. The extraction of undisturbed core samples is difficult to achieve particularly on very loose soils. There are also problems with stoney soils. Stones within the samples effect the volume and may give misleading results, Low [4]. After oven drying the soils the assumption is made that all the moisture has been removed, clay soils will however often retain appreciable quantities of water at that state of dryness, Hillel [2]. Clay soils also prove problematic due to volume shrinkage on

drying. Despite these disadvantages however this method is the reference technique to which all others are compared.

Alternative methods for determining air porosity include soil samples being saturated and then subjected to specific suctions or water tensions, measured in bars. The Blotter or Tension Table method of Learner and Shaw [5] and Jamison and Reed [6] were based on this principle. Present methods include sand tables designed after Van der Haarst and Stakman [7]. These are designed to look at moisture release characteristics under suctions from 0 (saturation) to 20KPa. Saturated samples are placed on an air free, porous sand table which is capable of retaining water against the suctions applied in the test. The suction can therefore be transmitted through the sand to the soil and the whole left until equilibrium is reached. The samples are then removed, weighed and replaced on the tension table under an increased suction. This procedure is continued until the maximum suction is reached for the apparatus at which point the sample is oven dried and the dry bulk density and the final soil moisture content by volume are calculated. The moisture contents are then calculated for all the other suctions. The volume of the air filled pore space for each moisture content can then be calculated from Equation 2.7.

$$V_a = \left(1 - \frac{\rho_s}{\rho_g}\right) - V_w \tag{2.7}$$

The pressure membrane cell technique as described in [3] is used from 200KPa to 1500KPa (permanent wilting point). The procedure involves placing a saturated soil sample on a cellulose membrane inside a pressurised cell. A pressure is applied which forces water out until the soil water suction is equal to the applied pressure. The water removed is collected and from its mass and the dry bulk density, the volume of water at each suction is determined as for the sand table.

These methods give a volume of drained pores at a series of water contents. There are various problems associated with using them. The saturation procedure can take several days to achieve, as long as 56 hours, Hunter [8]. Air entrapment is likely to make the assumption of complete

saturation invalid, Vomocil [9]. The time required to achieve equilibrium depends on the type of soil and the amount of suction applied. The higher the suction the smaller the amounts of water released and the longer it takes to reach equilibrium. This makes for a very time consuming process. The techniques rely on the use of undisturbed samples being transported to a soils laboratory and are unsuitable for soil samples that swell and shrink on wetting and drying, Page[10].

Techniques have also been developed that measure only the amount of air space present with no determination of the water content. Janse [11] suggests a porosimeter founded on Boyles' gas law, pV = constant, to measure the total porosity of dried soil samples whose acoustic properties were also measured using an impedance tube technique. Another method of measuring air filled porosity irrespective of moisture content, is the air space pycnometer. The pycnometer technique has been discussed by several authors Kummer and Cooper [12], Russell [13], and Pidgeon [14]. Its operation takes advantage of Boyles' gas law and is similar to the porosimeter used by Janse [11], although samples are not dried prior to the measuring of changes in gas volume. The volume of air space in a soil sample is measured by observing the resultant pressure when a known volume of gas at known pressure expands into a larger volume that includes the air space in the soil sample. A lengthy calibration involves gradually decreasing the % air space in the sample holder by infilling with metal discs. The resultant pressures for each known air space are then plotted. The calibration is particular to that sample holder size. The principle advantage of this method, once calibration has been undertaken, is speed. Determination of a single measurement can be obtained in two minutes. It is not necessary to pre-saturate the samples and measurements are not confined to any particular moisture content. However disadvantages involve daily adjustment due to changes in barometric pressure and temperature with different nomographs used. The pressure pycnometer has been suggested for use in the field, Page [10], however it is noted that the apparatus acts like a gas-filled thermometer and therefore precautions of rapid reading and shading should be observed, Vomocil [9].

The determination of air-filled porosity through measurement of bulk density and water content of core samples involves the assumption that the particular water content selected for sampling has some particular significance compared to other water contents. This is definitely the case for the moisture release techniques described above. If field samples are required with a characteristic wetness then this is usually accepted as field capacity, Vomocil [9]. Field capacity is the amount of water retained in the soil after the initial rapid stage of drainage eg. two days after a deep wetting, Hillel [2]. Jamison et al. [6] suggest techniques for taking core samples at field capacity but highlight the difficulties of actually finding field capacity sample areas in the field. If however the investigator is mainly interested in the physical quantities of air space and water volumes at the time of sampling the gravimetric technique is the best technique to use.

Measurement of air porosity *per se* does not give information on the continuity of pores which is important in soil aeration. A dynamic method for measuring soil air movement which relies on studying the air filled pores interconnected with each other and the soil surface is required. The measurement of air permeability is such a method.

2.2 Air Permeability

Soil air permeability is a measure of the ease with which air moves through a soil medium. Grable [15] says intuitively gases must flow through air filled pores and the quantity of flow is directly proportional to the air porosity. The area available for air flow and the ease of air movement is a function of pore volume, shape, tortuosity and continuity. Air permeability is important to know as an index of soil aeration for plant growth, but also as an indication of structure, Beuhrer [16].

Measurements of air permeability are based on Poiseuilles law of flow of a fluid through a cylindrical pore with a tube radius r, as shown in Equation 2.8.

$$\frac{Q}{t} = \frac{\pi r^4}{8\eta} \rho g \, \text{grad}\phi \tag{2.8}$$

where

Q/t = volume/time = volume flow rate

η = the viscosity of the fluid

gradϕ = the potential gradient

ρ is the density of the fluid

g = the acceleration due to gravity

From Childs [17] for a number (n) of pores Equation 2.8 can be written as

$$v = n\frac{Q}{t} = \frac{n\pi r^4}{8\eta} \rho g \, \text{grad}\phi \tag{2.9}$$

Taking into account porosity Ω, where Ω is equal to the area of the pore per unit area of cross section ($n\pi r^2$) Equation 2.10 can be written

$$v = n\frac{Q}{t} = \frac{\Omega r^2}{8\eta} \rho g \, \text{grad}\phi \tag{2.10}$$

When gravitational potential is negligible (assuming horizontal flow) or if small compared to the pressure potential then Equation 2.10 can be written

$$v = n\frac{Q}{t} = \frac{\Omega r^2}{8\eta} \frac{\Delta P}{L} \tag{2.11}$$

This is analogous to Darcys Law of flow through a single capillary tube shown in Equation 2.12

$$\frac{Q}{t} = K\frac{\Delta P}{L} A \tag{2.12}$$

where A is the area of the tube πr^2. Childs [17] expresses K the conductivity of the body as

$$K = \frac{\Omega r^2}{8\eta} = \frac{K_a}{\eta} \tag{2.13}$$

where $K_a = \Omega r^2/8$ is the intrinsic permeability and is an exclusive property of the porous medium dependent upon porosity and pore radius. K the conductivity and also called the permeability is dependent both on K_a and

on the viscosity of the fluid. In this case K_a is expressed in dimensions of area μ^2. In acoustics the specific air flow resistance (or resistivity) is

$$\sigma = \frac{\eta}{K_a} = \frac{8\eta}{\Omega r^2} \tag{2.14}$$

and is measured in $Pa\,s^{-1}\,m^{-2}$ where $1\,Pa\,s^{-1}\,m^{-2} = 1$ mks rayl/m

Darcys Law is valid for homogeneous and non-homogeneous porous media. However in this case it is assumed that the following conditions are met. Firstly: the medium is homogeneous and isotropic. That is the medium does not have preferred directions of flow by reason of its structure and hence flow is in the direction of the potential gradient. Secondly: flow is laminar. For flow to be laminar in the interior of the porous medium it is necessary for the Reynolds Number $\rho rv/\eta < 1$ where v is the velocity and other symbols are as described before. If the Reynolds Number exceeds 1 then turbulent flow will occur.

Kirkham [18] shows that Darcys' Law holds for gas flow as well as water provided that consideration is given to the compressibility of gases. In Equation 2.12 it was assumed that the volume Q crossing any section of the tube remained constant. This is valid if the fluid cannot be compressed. With air the volume changes because the air is compressed, and there is a change in density. At any one point along the tube $Q\text{mass} = \frac{Q}{t}\rho$ which is expressed in g/sec. Therefore for gases it is the mass flux crossing any section in a given time which is constant. For a fixed mass of gas the pressure and volume are inversely proportional to each other providing the temperature of the gas remains steady PV= constant . Therefore assuming flow through the soil sample is slow (ie isothermal conditions prevail) and laminar, and the mass flux along the tube remains constant and in a steady state, then Equation 2.12 can be applied for measuring air permeability. If these assumptions are made then an average flow rate Q(avg) and average pressure P(avg) can be substituted into Equation 2.12 to become

$$Q(\text{avg}) = \frac{K_a}{\eta}\,\frac{P(\text{avg})}{L} \tag{2.15}$$

Alternatively taking a convenient point where P and V are both known

for example at the soil surface, if a known volume of air Q is passed in time t through a soil sample then with the above assumptions, Equation 2.15 can be solved for K_a. This is the principle behind the constant pressure permeameter methods as used by Beuhrer [16], Grover [19], Brooks and Reeve [20] , Green and Fordham [21].

Kirkham [18] developed an equation and a variable pressure method.

$$Q = \frac{K_a}{\eta} . A \frac{P_{e1} - P_{e2}}{L} \tag{2.16}$$

where P_{e1} = pressure in excess of atmospheric at the beginning of the sample at t=0. P_{e2} = pressure in excess of atmospheric at the end of the sample length L, area A at t=1 sec.

2.2.1 Measurements of Air Permeability

The air permeability of a soil is relatively difficult to measure. In doing so porosity and structure of the soil grains and crumbs, which are probably the most important soil physical properties determining its permeability are usually changed unavoidably. Therefore it is necessary to find a permeability measuring technique which involves the minimum amount of disturbance to these parameters. Laboratory techniques involve the disturbance of cores during sampling, transportation to the laboratory and insertion into the permeability rig itself. An *in situ* technique appears preferable which includes a minimum amount of disturbance and which presents a measure of air permeability immediately.

Various techniques have been adapted for in-situ measurement and these fall mainly into two groups.

1. Variable pressure methods.

2. Constant pressure methods.

These will be discussed briefly together with their limitations. Two other techniques, the sphygmomanometer technique, Wilde and Steinbrenner [22], and the radiation emanation technique, Imre [23] are referenced here but are not the main methods used to calculate air permeability currently.

2.2.2 Variable pressure method

This method developed by Kirkham [18] used a constant volume air tank. Air at a given initial pressure P_e, and registered on a manometer as y was allowed to discharge through a soil sample of known dimensions located *in situ*. The dimensions of the permeameter and the volume and initial pressure of the air tank (regulated by a bicycle pump) could be varied to give a conveniently low rate of pressure drop during the test. The lower the rate of pressure change the more nearly the conditions approximate to the assumed isothermal expansion of air. As the tank pressure drops various values of y and time are recorded. A plot of log y against time on semilog paper reveals a straight line of slope -S. By measuring the slope S the intrinsic permeability can be calculated from

$$K_a = \frac{2.30\eta L V S}{A P_a} \tag{2.17}$$

where all variables are described as before except V which the volume of the tank, P_a = atmospheric pressure dynes/cm^3, y_1 is the displacement of the water in the manometer at P_{e1} and y_2 is the displacement of the water in the manometer at P_{e2} (from Equation 2.16) S is the gradient of log y versus time curve.$\frac{\log_{10} y_1 - \log_{10} y_2}{t}$. In the field situation $\frac{L}{A}$ was replaced by an appropriate function relating sample width to sample diameter.

Evans and Kirkham [24] also used a variable pressure method by introducing air from a tank through a tube radius R_1, the bottom of which just touched and was normal to the soil surface. Around this tube and pushed into the soil a small distance is an iron ring radius R_2. A thin layer of cooled hardened paraffin covers the surface of the soil in the space between the outside of the inlet tube and the inside of the ring. Air in the tank was pumped up to pressure and then allowed to fall. K_a was calculated from

$$K_a = \frac{2.30\eta V}{A^1 P_a t} \log_{10} \frac{y_1}{y_2} \tag{2.18}$$

where A^1 is a constant in centimetres which depends upon the ratio of $\frac{R_1}{R_2}$. This involves reading from a nomograph a value of A^1 for the particular pipe/ring arrangement.

The chief limitation to the variable pressure method, is the volume size of the air tank portable into the field. To cover a large representative sample to eliminate variation in readings a sampler or inner tube as large as possible is required. The bigger these are, the larger the volume of tank required. A 2.5cm tube requires a 245 litre tank. Therefore the volume of air limits the range of soils that can be studied. A highly permeable sand would require a large volume of air as it would pass through very fast. This technique then is more suitable to soils with an expected low permeability.

2.2.3 Constant Pressure Methods

Constant pressure methods were designed for high air permeable soils - where low pressures are required to prevent disturbances of the liquid phase and to avoid turbulent flow Alpan [25]. The original idea was developed for field use by Grover [19]. It consisted of an inverted cylinder of air, floating in an annular water chamber and an inlet tube positioned in the soil. Air in the chamber was at a known, constant pressure, recorded as a water head in cm on a manometer. As the float falls air from the chamber passed through the pipe into the soil. The weight of the float maintained a constant pressure independent of the rate of fall. The volume of air (V) entering the soil in time (t) when included into the equation as Q.

$$K_a = \frac{\eta Q}{A \Delta P} \tag{2.19}$$

where ΔP is the known constant pressure of air in the cylinder and A is a constant factor determined for different sampling cylinders and boundary conditions.

Grover [19] and Tanner [26] offer different values of A. Green and Fordham [21] using a constant pressure device offer an *in situ* permeability

$$\mathrm{K}(\textit{in situ}) = \mathrm{k(exhumed)} \times \frac{\text{flow of exhumed core}}{\text{flow of } \textit{in situ} \text{ core}}$$

this is to try and dispense with the $\frac{L}{A}$ factor for the *in situ* measurement.

2.2.4 Problems Associated with Measuring Air Permeability In Situ

As mentioned in Section 2.2.1 it is preferable to have an indication of air permeability *in situ*. However, whether the variable or constant pressure methods are used there are a number of problems common to both.

2.2.5 Boundary Conditions

In the Darcy equation it was stated that A was the cross sectional area and L was the length of the test piece in metres. However for *in situ* permeability measurements the sampler is inserted into the soil. According to the Laplace equation flow will occur through the soil along streamlines. Air flows down through the sample and then up through the soil around the outside of the sample. This changes the length of the sample to an unknown. Pressures will not be equal along these streamlines depending on their location and distance to the soil surface or cylindrical walls. If the pressures (or a combination of these) at the boundaries of the region of interest are known then the flow can be computed and if this flow is measured then the permeability can be determined. This is very difficult to solve. Various nomographs have been produced, Kirkham [27], Grover [19], for both the variable pressure and the constant pressure methods to give values for the $\frac{L}{A}$ or $\frac{R_1}{R_2}$ ratios.

2.2.6 Disturbance of Soil

In situ measurements, for the most part, do not rely on exhumed soil cores, however the insertion of a sampling container or the sealing of a soil surface with paraffin wax or wall-paper paste used in some techniques will disturb the natural soil conditions. This renders the measurements unrepeatable on soil plots particularly those where monitoring of changes in the permeability over a growing season is required. The occurrence of an inadequate seal between sample and sampler or inlet tube will overemphasize permeability readings.

2.2.7 Sample Size

This is problematic in terms of having a sampler or ring radius too small to represent the macro pore contribution to permeability. Janse and Bolt [28] recommend a sample comprising several units of the soils structural pattern; for sandy soils a sample 10cm wide and 6cm deep must be considered a practical minimum. Alternatively, the bigger the sample the more likelihood of including the effects of stones, cracks or worm holes. As stated by Evans and Kirkham [24], it is not the purpose of the equipment to study the air flow in worm holes and cracks.

2.2.8 Drying of Samples

By the very nature of the methods described to measure permeability forcing air through a soil sample is likely to have a drying effect, causing the permeability to rise as water is removed from some pores. Therefore the quicker the air flow passage the better. However, under rapid air flow steady state flow cannot be guaranteed, and turbulent flow may cause collapse of pore structure and disturbance of the water phase.

2.2.9 Variability of Data

The variability of the upper soil layers is usually large, accordingly determinations in the field tend to be inconclusive Janse and Bolt [28]. Taylor and Ashcroft [29] estimate that Kirkham and Evan's apparatus may require 160 determinations to distinguish between two soils with a 10% difference in mean K_a. Green and Fordham [21] have found that 8 to 10 permeability determinations per site are generally desirable, although a good correlation with soil moisture differences and air content has been detected with as few as four cores per site.

2.3 Measurement of Soil Water Content

Moisture content of a soil is related to air filled porosity as they compete for the same pore space. Moisture content can be determined effectively by the gravimetric technique already described in Section 2.1.1 and using Equations 2.4, 2.5 and 2.6. The advantages and disadvantages of this technique have been discussed. Two other methods for measuring moisture content available will be briefly discussed here along with their limitations.

2.3.1 Neutron Probe Method

The neutron probe is an instrument for measuring moisture content in the field. It consists of a probe, containing a radioactive source, a detector and a pulse counter. Measurements are made by lowering the probe into specially installed vertical aluminium tubes in the ground. The source emits fast (high energy) neutrons into the surrounding soil. The neutrons collide with soil and water particles and are slowed down. Collisions between fast neutrons and hydrogen atoms are the most effective in absorbing energy. These slowed neutrons are reflected and scattered in the vicinity of the probe detector which then measures the density of this slow neutron cloud. The density is closely related to the number of water molecules and hence the moisture content.

Each time the probe is used a standard water count, Rs, is measured in a tank of water. Field counts, Ra, are then referenced to Rs. Rs must be measured because of the instability of the instrumentation and must be done before each session of measurements in the field.

Calibration of the neutron probe can be done in two different ways. Bell [30] has produced standard curves of Ra/Rs versus moisture content (%vol) and from these calibration constants can be read off for a sand, loam or clay soil. In an alternative method Ra/Rs counts can be plotted against percentage volume moisture content determined by gravimetric methods from core samples made at the same time and place. Data collected over a period of time will establish equations relating the two variables.

Advantages of the neutron probe technique are that it is a non-destructive technique, once the initial access tubes have been installed, allowing frequent sampling at the same location. It is a good technique for providing a useful overview of moisture contents at different depths in a soil profile. Effectively large volumes of soil are taken into account, radii=10cm in a wet soil, 25cm in a dry soil Hillel [2]. This however makes the technique unsuitable for the detection of moisture profile discontinuities , eg. wetting fronts, or boundaries between distinct layers in the soil.

Disadvantages of the technique include its limitation on gravelly or stoney soils, or laminated soil. The stones and hard layers cause increased neutron scattering. In highly organic soils such as peat the hydrogen bonding of the organic particles also increases scattering. On shallow soils or with measurements close to the soil surface <15cms there is escape of neutrons into the air above the soil surface making readings in this vicinity unreliable. Correction factors, Grant [31], have been developed to account for this. Alternatively an extra layer of the same soil can be placed at the surface to block neutrons escaping or an hydrogenous material can be laid on the surface.

2.3.2 Gamma Ray Attenuation

This technique can be used to measure moisture content and wet bulk density in the field. The procedure is to place two adjacent probes, one a source of gamma rays eg. Caesium 137, the other a detector down parallel holes in the soil. Measurement is made of the attenuation of the gamma rays through the soil and the degree of attenuation increases with an increase in wet bulk density. The ratio of count rates measured in dry and moist soils can be expressed as

$$\frac{N_m}{N_o} = exp[-x(\mu_s \rho_s + \mu_w \theta)] \tag{2.20}$$

where

N_o is the count rate for gamma rays transmitted from the source through air to the detector and N_m is the count rate for wet soil, x is the path length through soil of dry bulk density ρ_s, water content θ is expressed as a volume,

μ_s and μ_w are mass attenuation coefficients for soil and water. In dry soil ($\theta = 0$) and therefore

$$\frac{N_d}{N_o} = exp[-x\mu_s\rho_s] \tag{2.21}$$

whereN_d is count rate for gamma rays transmitted from source to detector in dry soil. Hence it follows that

$$\theta = \frac{\ln(N_d)/(N_m)}{x\,\mu_w} \tag{2.22}$$

This requires a value of N_d in a dry sample of the soil for calibration. This is used for determining water content from gamma ray attenuation in a soil whose density does not change with water content Gurr [32]. On a swelling soil, a calibration curve is established for a particular soil type, Ferguson and Gardener [33]. Alternatively a two source technique has been described by Soane [34], and by Gurr and Jakobson [35] for use in the field, where two sources are used with different energies. Hence two sets of values of N_m, N_o, μ_s and μ_w are available for the calculation of θ and ρ_s.

An advantage of the gamma probe technique over the neutron probe is that it has a better resolution at depth and can be used closer to the soil surface. It is widely used in laboratories with considerable precision. However it is not widely used in the field due to problems of collimation and discrimination under field conditions [36]. The technique is very sensitive to small errors in the distance between source and detector . Rijtema [37] noted that a problem of interpretation of results is the separation of the systematical error due to the non parallelism of the two probes and the random variation due to sample errors and soil heterogeneity. For their equipment with the centre lines of the holes spaced 14cm apart, Gurr and Jakobsen [35], state that an error of 1mm in the spacing causes a 2% error in wet bulk density.

2.4 Monitoring of Surface Crusts

Surface crusts form due to the beating and dispersing effect of raindrops and the spontaneous slaking and breakdown of soil aggregates in water. Subsequent drying leads to the formation of a compacted layer of orientated particles close to the surface. Hillel [38] notes several physical differences between a crust and the under lying soil. These include a higher bulk density, a lower total porosity, and a higher proportion of micropores.

Measuring the structure, depth and effects on air permeability of surface crusts is problematic. Hillel [38] experimenting on artificially formed surface crusts suggested a modulus of rupture test to characterise a crust in terms of its hardness characteristics. Alternatively penetrometers can be used to measure the soils resistance to vertical push force as a cone ended rod is pushed a marked distance into the soil. These are generally used to study compaction with depth, searching for relatively more resistant layers. Crusts are usually difficult to monitor using penetrometers due to their fragility. Many varieties of penetrometers have been designed. There is no standard design and procedure for penetrometer operation and they are designed to give quantitative measurements of soil penetration resistance for correlation with density, shear strength and bearing values of soils for trafficability. They do not give an indication of the dynamic physical properties of soil such as air flow when a crust is *in situ*.

Grover [19] used an air permeameter to determine the air permeability of surfaced capped silty soils. From a very low level, permeability increased 20 times after 0.6cm of the capped soil was removed. Green and Fordham [21] encountered problems when trying to measure air permeability on surface crusted soils. The air permeability of an apparently well sealed moist surface crust at negligible flow rates which would suddenly increase through the moist cap. Examination of soil samples showed many cracks and pores were thinly bridged by washed soil. Rupture of this thin seal by the air flow allowed sufficient air flow to lift the cap contained in the sampler which in turn allowed even faster flow and thus inaccurate air permeability determinations.

2.5 Acoustic Measurement of Soil Parameters

2.5.1 Impedance

The acoustic impedance is a complex value which describes the acoustic properties of a material. It is composed of the real part, R, the resistance and the imaginary part, I, the reactance. De Bie and Groenewoud [39] define two types of impedance - the characteristic impedance and the specific impedance. The characteristic impedance is the impedance that can be measured at any place in the medium and is therefore a property of it. The specific impedance, otherwise called the specific surface impedance, is measured at the boundary of two media. It is equal to the characteristic impedance of the lower medium if the lower medium is semi-infinite. In acoustic modelling of ground surfaces and the prediction of sound propagation near these surfaces, a value of the normalised surface impedance Z is required, to characterise the surface acoustically. The normalised surface impedance is the specific acoustic impedance divided by ρc. When ρ is the density of air and c is the sound velocity in air, ρc is the characteristic impedance of the air for plane waves.

In sound propagation the surface impedance indicates how an incident wave is changed on reflection, it is related to the plane wave reflection coefficient which describes the absorption and phase shift on the wave due to the physical properties of the ground. It is therefore apparent that if the ground can be characterised in terms of its acoustical impedance, and this impedance can be expressed in terms of soil physical properties then determination of acoustical impedance provides an indirect way to look at soil physical properties, such as pore geometry, air porosity and air permeability or flow resistivity.

2.5.2 Impedance Prediction

Before proceeding with direct impedance measurements it is necessary to say a little about impedance prediction. Delany and Bazley [40] describe a method of relating acoustic impedance to the airflow resistivity of fibreglass

absorbents. They determined the following empirical relationships between impedance $R + I$ and flow resistivity.

$$R = 1 + 9.08\left[\frac{f}{\sigma}\right]^{-0.75} \quad I = -11.9\left[\frac{f}{\sigma}\right]^{-0.73} \tag{2.23}$$

where

f is the frequency and σ the flow resistivity in cgs rayls. These relationships have been used by many authors for predicted comparison with direct acoustic soil impedance measurements, with varying degrees of success. The difference in porosity between the fibreglass used by Delany and Bazley (porosity $\simeq 1$) and soils ($\simeq$ 0.1-0.6) shows a problem when using this model.

Work by Attenborough [41] has shown that impedance is also affected by the porosity, the tortuosity of the pores, and the pore shape and Embleton [42] suggests that σ in Equation 2.23 should be seen as an effective flow resistivity. More complicated models have been developed relating these physical parameters to impedance. In brief they model the ground as homogeneous, varying porosity with depth, or a combination of varying soil layers, with different depths and impedances. These models will be discussed more fully in Section 3.6.

2.5.3 Impedance Measurements

The main techniques used in direct acoustic measurements of soil impedance or related absorption coefficient and the results of these measurements will be discussed in the following sections.

Acoustic impedance measurements can be subdivided into two categories, normal incidence and oblique incidence. Normal incidence include the impedance tube or free field methods. Oblique incidence techniques are all free field.

Normal Incidence Techniques

Impedance Tube Measurements

The equipment traditionally used for measuring impedance is the impedance tube. Janse [11] has undertaken work on soils using such a technique. The

equipment consisted of a loudspeaker at one end of a long tube, at the other end of which is mounted a soil sample. Continuous pure tone sound waves were propagated down the tube so that they reflected from the soil surface. The sample absorbs some energy and reflects the remainder. The resultant standing wave pattern was then probed with a microphone to locate and measure pressure at the minima and maxima. These were then used to calculate the absorption coefficient.

Results in Figure 2.2 show that soils of the same porosity have different absorption characteristics when sample depth and aggregate shape was varied. Janse [11] suggested such measurements could help classify soils based on empirical subdivisions of porosity. Traditional measurements of porosity and air permeability as described in Sections 2.1 and 2.2.1 would determine the volume of air and ease of movement of a soil and the absorption technique would subdivide porosity groups in terms of aggregate size and shape.

The technique's main limitations were firstly that the soil samples were disturbed during insertion into the tube, and secondly difficulties arose because of an inadequate seal between tube and soil surface. Well known problems relating to the need for probe end corrections and the exact location of the soil surface are exacerbated by the relatively high impedances and rough surfaces encountered compared with architectural absorbents.

To overcome sample disturbance, impedance tubes were adapted for *in situ* measurements. Prout [43] designed a portable system, where the lower end of the tube was 'planted' into test beds of sand and outdoor surfaces of ploughed field and grass. Talaske [44] measured the impedance of various woodland soils, using a similarly modified tube. A disadvantage is the time consuming nature of the technique. Bearing in mind the inhomogeneity of soils from place to place, a large number of samples of each frequency are required to characterise the highly variable surface. Chung and Blaser [45] developed a 2-microphone impedance tube technique to overcome this problem. Measurements are obtained using two small microphones mounted in the side of the tube close to the ground. In this case white noise is

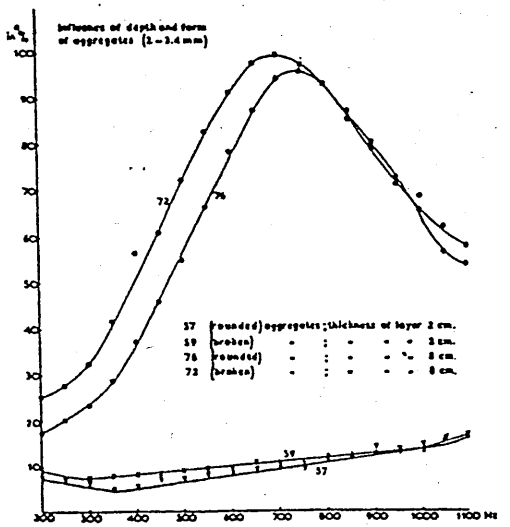

Figure 2.2 Influence of Depth and Shape of Soil Aggregates on the Absorption of Sound, after Janse.

used rather than pure tones. Theory involves the decomposition of a broad band stationary random signal into its incident and reflected components using the transfer function between the acoustic pressure received at the two microphone locations on the tube wall. This wave decomposition leads to the determination of the complex reflection coefficient from which the impedance is calculated. Heisler et al [46] made a series of measurements using both the above mentioned impedance tube techniques on forest floors. Apart from the saving of time by the second tube technique there were also a number of disadvantages.

The success of the measurements relies on the accurate measurement of the distance from the ground surface to the first minimum. The effect of an error in this by 0.5 or 1cm is small when the magnitude of the impedance is small, but when the magnitude of the impedance is large a difference of

0.5cm can lead to large differences in calculated impedances which includes erratic variations with frequency, Heisler et al [46]. It is therefore hard to determine whether scatter in the data is a feature of the ground's acoustic impedance or an artifact of the measuring technique without many measurements to calculate an average. Glaretas [47] reviews the impedance tube as a technique suitable for outdoor measurements on grass, sand and smooth surfaces, but unsuitable on gravel, rough soil and surfaces covered with dense vegetation, there being no proper seal made with the surface in these circumstances. Heisler et al [46] found that driving the impedance tube into the ground either loosens or compacts the soil and/or organic humus layer, particularly around the edges of the tube. Measured bulk densities inside the tube were higher than those measured outside. Soil sampling, for example, the measurement of layer depths and coring inside the impedance tube, was done by feel and therefore open to error.

As well as impedance measurements on soil the impedance tube technique has been used by Oura [48], Ishida [49], Tillotson [50] and Buser [51] to make impedance measurements of snow. In the most recent of these an automated impedance tube technique has been used in a cold room with samples extracted from larger samples brought in from snow layers outside. Lee and Rogers [52] in advocating a free field power cepstrum technique for determining snow properties maintain the impedance tube technique requires handling the snow which causes difficulties when working with, low density samples, and may alter irreversibly the snows properties.

2.5.4 Free Field Measurements

Free field techniques have been designed to avoid some of the difficulties involved in using an impedance tube on a real ground surface. Dickinson and Doak [53] used a sound source suspended from a tripod above the ground together with a microphone that moves along a vertical axis between the source and the ground. By probing the standing wave pattern created by pure tones in the open air the impedance can be deduced from the same principles as used in the impedance tube theory. The advantages are that no

seal is required with the soil surface and therefore there is minimum disturbance. There remains however the problem of accurate surface location and the problem of meteorological effects on the standing wave. Dickinson and Doak [53] ignore atmospheric turbulence as the path length they are using is only 4-5m and they are studying the low frequency range only. The error due to wind effects using this set up is, they calculate, about 0.02dB/25cm. Reflections from people and buildings close by were also a problem at low frequencies.

Legouis and Nicholas [54] designed a free field technique which involved measuring the phase gradient along a 'standing wave' above a porous material. Daigle and Stinson [55] have used this technique out of doors on various ground surfaces. Using Dickinson and Doak's technique at low frequencies the position of the first minimum becomes increasingly difficult to measure. However the phase goes through a rapid 180° phase change in the region of the interface minimum. Measuring phase directly using one microphone to 'find the flip' requires many tedious, precise measurements at various heights. A better way is to measure the phase difference or gradient between two vertically mounted microphones probing the standing wave. Phase gradients show a sharp peak during the rapid 180° change in the region of the amplitude minimum. At the amplitude maxima they show a valley feature. Knowing the peak-valley phase difference change and the distance to the first peak from the ground, a value of R_p, the plane wave reflection coefficient, is then calculated, for the sound field due to a point source above an impedance boundary, and hence the impedance can be calculated. Working at low frequencies has the problem of reflections from all other surfaces in the vicinity.

An alternative normal incidence technique which eliminates reflections is an impulse technique. This has been successfully used by Van der Heijden et al [56] on sand of varying thicknesses. The idea of using impulses is an attractive one. Any spurious reflections from immovable objects close to the experiment site can be separated from the main ground reflection in the time domain and gated out of the analysis. In addition a large number of

pulses can be averaged to obtain a better signal-to-noise ratio so decreasing the problems of background noise levels. Lee and Rogers [52] process pulses using the power cepstrum technique described by Bolton and Gold [57] to give the reflection coefficient and hence the impedance. Another pulse technique has been developed by Cramond and Don, but since this is used at oblique incidence it is described in the next section.

2.5.5 Oblique Incidence Techniques

Inclined Track

An array of microphones is used to measure the changes in interference patterns of pure tones along an inclined or oblique path. By changing the height and distance of the microphones the angle of incidence is kept constant therefore keeping the same point of reflection on the ground. This is necessary on outdoor ground surfaces because impedance varies from spot to spot.

To find the impedance, the real and imaginary parts are iterated in an optimisation routine until the minimum sum of squares of the differences between the measured and model predicted sound pressure level's at each microphone is calculated, for each frequency, Van der Heijden [58].

The techniques main disadvantage is the time involved. De Bie and Groenewoud [39] have 30 microphone positions but only five microphones, each having to be moved six times. At each position 22 pure tones were played, giving a total of 660 pieces of information. Each of those 660 had to be referenced to a free field measurement to take into account speaker directivity and frequency response. Hence it required 2-3 hours to make one set of impedance data on one particular soil site and also a great deal of computer time fitting the data afterwards.

Embleton et al. [59] made two sets of measurements, comparing impedances calculated over grass using an impedance tube and the inclined track method. In the first set the angle of incidence for the inclined track measurements ranged between 40° and 90°, and the assumption was made that the incident and reflected waves were plane. In the second set the angle of incidence

varied from 15° to 21°. In both cases the inclined track measurements gave similar results of impedances when compared to the impedance tube as shown in Figure 2.3. This indicates that the ground can be assumed to be locally reacting, that is impedance is independent of the angle of incidence. This is discussed in Section 3.1.

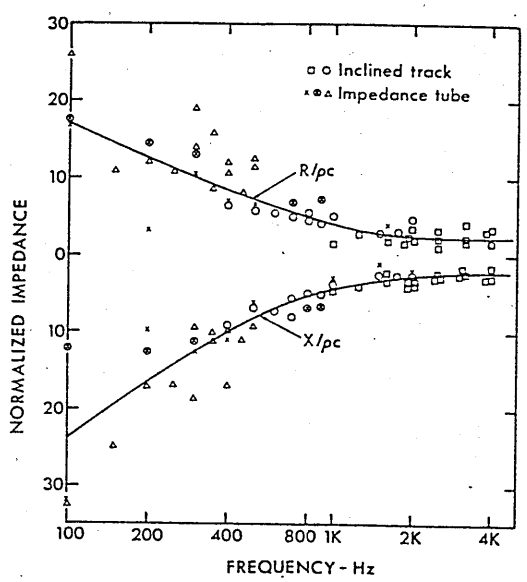

Figure 2.3 Comparison of values for the magnitude of the normalised surface impedance of a grass covered surface, using impedance tube and inclined track measurement techniques, after Embleton et al.

Another criticism of the inclined track technique is the susceptibility to meteorological effects, Mansbach and Holmer [60]. However Van der Heijden [58] by using small source receiver distances and low frequencies, sought to guarantee little effect from vertical wind or temperature gradients, turbulence and atmospheric absorption.

In the use of the calculation for plane waves with the local reaction assumption for outdoor propagation prediction it is obvious that as the angle of incidence, θ, increases r_2 the reflected path $\longrightarrow$ r_1 the direct path. The pressure at the microphone P_{tot} will decrease until at or near grazing incidence all frequencies will be cancelled. This is explained more fully in Section 3.2. At short range and grazing incidence ie. receiver and microphone

on the ground, all frequencies are received at the microphone. At larger ranges there comes a cut-off frequency where $Ptot \longrightarrow 0$ and the sound pressure level drops. This cut off frequency can be measured by studying the drop (3dB down) in sound pressure levels at a microphone with a source close to the ground. In a free field situation the drop in sound pressure level would depend on spherical spreading alone, 6dB/doubling of distance. With the ground present the cut off-frequency also depends on the ground's impedance, as well as distance.

Several authors have used the cut off frequency to provide an estimate of the magnitude of the normal specific impedance of the ground, Embleton et al [42]. Habault and Corsain [61] have used this technique over ranges varying from 0-50m over a grassy field and garrigue, a hard ground studied with small tufts of thyme and small pebbles. Comparisons were made at 0.0m and 0.22m source and receiver heights. There was very little difference and therefore the local reaction assumption made. From the values of excess attenuation, theoretical values of impedance were deduced using the identification method - or least squares minimization algorithm.

Excess Attenuation

Chessel [62] proposes that modification to propagating sound by reflection from a soil surface causes an interference pattern of the sound field. This interference pattern can be modelled using knowledge of the acoustical properties of porous materials and the appropriate theory of sound propagation. Research has resulted in the development of various models for the prediction of sound levels due to outdoor sound sources on or near the ground. These will be discussed more fully in Section 3.6.

From Embleton et al. [59], it is demonstrated that the sound propagation between a source and receiver both above the ground can also be used to predict impedance by measuring the excess attenuation spectra, over different surfaces. Excess attenuation is explained more fully in Section 3.3.

Excess attenuation measurements require the knowledge of the direct contribution to the total pressure at the receiver ie. that attenuation that

would occur naturally due to atmospheric absorption and spherical spreading without the impedance boundary present. Therefore the excess attenuation technique requires knowledge of the speaker frequency response and directivity. This can be measured either in an anechoic chamber, Rasmussen [63] or in the case of Habault and Corsain [61] and Soom and Gu [64] relative to the response over a perfectly reflecting plane ,a hard asphalt surface. Parkin and Scholes [65] referenced their measurements to excess attenuation measured at the shortest range at 19.2m. At this distance meteorological influences and turbulence are already contributing to disturbance of the interference pattern.

Advantages of measuring excess attenuation include no disturbance of the ground and that a large sample area can be studied. The knowledge of the ground surface location is not crucial. One particular problem is the meteorological influences on longer ranges and at high frequencies. The turbulence caused by wind and temperature profiles may 'fill in' the excess attenuation primary dip. As the location and magnitude of the dip is important to predict impedance, any predictions of soil parameters will be inaccurate. It is important therefore these kind of measurements are undertaken in calm conditions, preferably with a $< 2m/s$ wind speed, and by studying the lower frequencies only, for example up to approximately 4KHz, which are less effected by wind velocities Foss [66].

Although location of surface is not crucial, it is important that the surface be flat as demonstrated by Embleton et al. [59]. If the ground is on a slight slope or has irregularities in it then this can cause different interference patterns and hence location and magnitude of the important first minimum.

Background noise must also be accounted for. Soom and Gu [64] made corrections for all sound pressure levels measured within 4-12 dB of the background noise level. Nicolas et al. [67] ensured a received signal 10 - 20dB above background noise. Wempen [68] by measuring and recording a reference signal in an anechoic environment and then using this as the transmitted signal in the field, references all measurements to free field. At

the same time if the direct and ground reflected waves are synchronized (they are fed into an FFT with chosen time delay between them) then a high signal to noise ratio is obtained in a short averaging time.

Impulses

Cramond and Don [69], have developed a technique of measuring impedance using a novel impulse source, a blank cartridge fired from a gun barrel. By accurate positioning of two microphones the direct and reflected pulses can be isolated in time. From analysis of the direct and reflected pulse shapes the complex reflection coefficients can be determined. An advantage of this technique is that simultaneous recording of impulses at the two microphones means there is no need to correct for geometrical spreading and atmospheric absorption.

If a pulse is short then unwanted reflections are isolated and eliminated. The frequency content of the pulse limits the frequency range for which impedance can be measured. Don and Cramond [70] made a series of measurements made at various angles of incidence to the ground over grass, barren ground, a layered forest floor and a highly reflecting stone impregnated ground.

2.5.6 Level Difference Technique

In Section 3.4 it is discussed how the use of a second microphone eliminates the requirement of knowing the source frequency response and directivity. If broad band continuous noise is used as a source instead of pure tones or impulses then a wide range of frequencies can be studied simultaneously and speed up data collection c.2mins instead of two-three hours for the inclined track, pure tone method. Glaretas [47] suggests the use of a grazing incidence level difference technique. This enables the impedance deduction over the whole frequency range of interest at relatively short ranges and is based upon the transfer function or level difference between two vertically separated microphones, one of which is on the ground surface. Embleton et al. [42] demonstrated that if a receiver remains on or close to the ground

$r_1 = r_2$ there is no interference between waves caused by a path length difference. Therefore this microphone acts as a direct measurement. If the Sound Pressure Level (SPL) received at this microphone is subtracted from the SPL received at the top microphone any difference must be due to the reflection from the ground. As long as the lower microphone is sufficiently near the ground and the microphones are sufficiently separated the first dip in the level difference spectrum corresponds to that in the excess attenuation spectrum for the upper microphone.

The interference dips in Figure 2.4 show the level difference spectrum is equivalent to the that of excess attenuation but independent of the source spectrum. The dips coincide and implies that information is not lost using the level difference technique. The difference between the level difference and excess attenuation spectra is the contribution from the lower microphone which has been subtracted from the excess attenuation curves.

As with excess attenuation measurements meteorological effects on level difference measurements are assumed to be negligible, at short ranges. The lower microphone should be placed low enough to represent the direct path but high enough to be above any microclimatic conditions close to the soil surface, where steep sound speed gradients due to temperature and wind velocities are to be expected. Short range level difference measurements also sample a smaller area which is important when looking at trampled/wheeled areas of field when compared to other unwheeled areas nearby.

If the same level difference geometry is used over different ground surfaces then any shift with frequency of the first dip is probably due to differences in ground parameters. Figures 2.5 show dips for three level difference measurements over three very different surfaces, a dirt road, beneath pine trees with a deep humus layer and within a poplar tree wood, with loose leaves and twigs overlaying a mineral soil. The shift in frequency location of the dip is due to different impedances of the ground surface. Curves like this, exhibiting peaks and troughs can be fitted using a least squares fit to acoustical models of sound propagation to obtain predicted values of effective flow resistivity σ_e, porosity Ω and layer depths, depending on the model chosen.

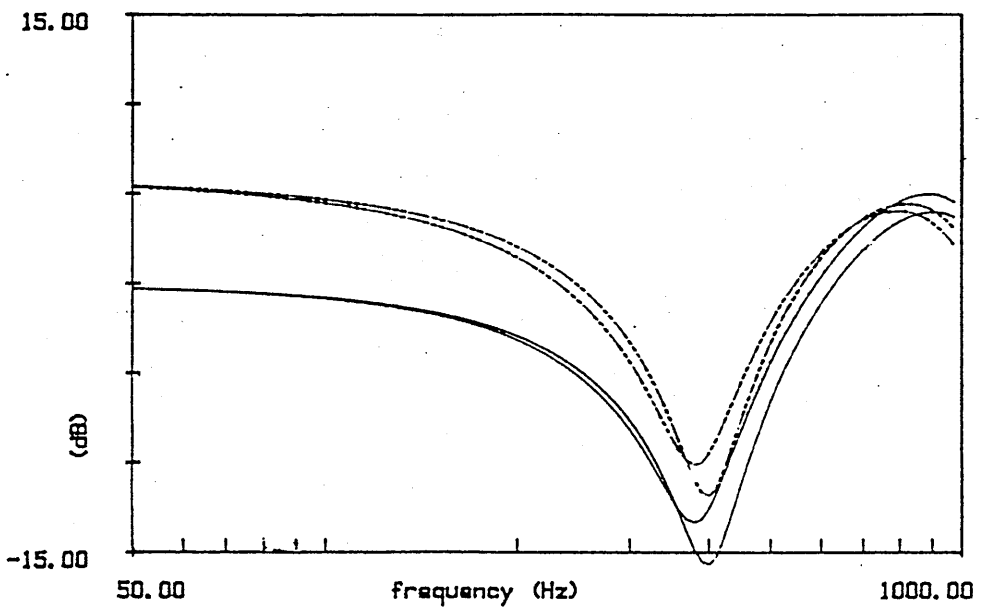

Figure 2.4 Comparison of Excess Attenuation (dash dot) and Level Difference (solid) Spectra for two different predicted flow resistivities, 400000 and 800000mks rayls/m , using a one parameter homogeneous model after [41], hs=1.26m, r=5m hrt=0.8m hrb=0.15m where distances are as shown in Figure 3.2

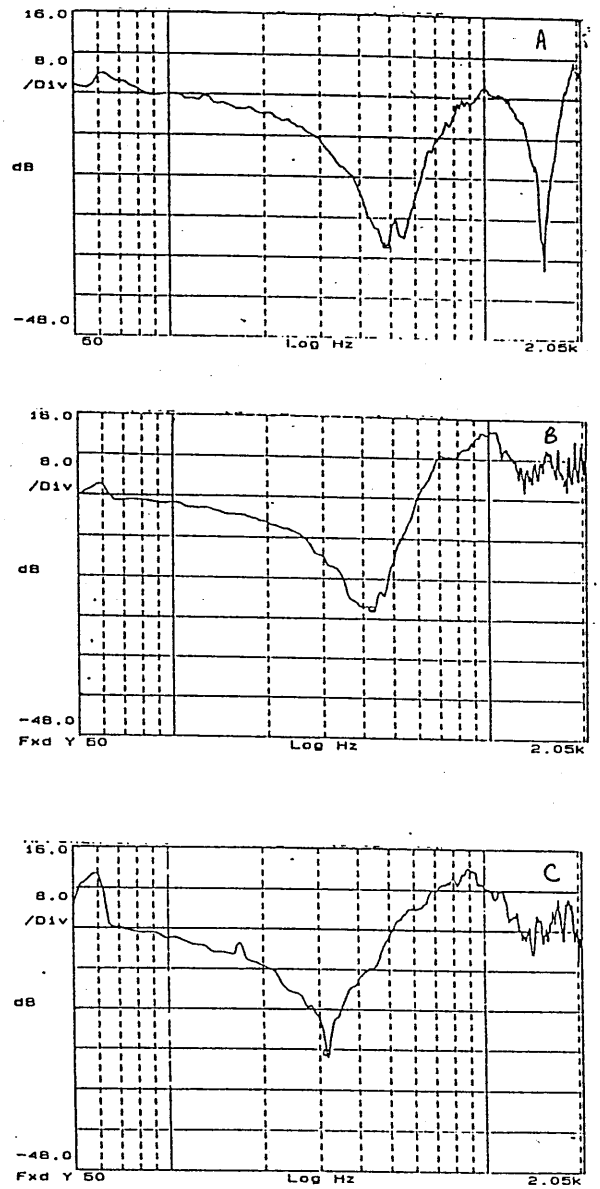

Figure 2.5 Comparison of Level Difference Spectra over Three Different Ground Surfaces, road a, woodland (poplar trees) b, and woodland (pine trees) c, hs= 0.5m, r=1.25m, hrt=0.5m, hrb=0.1.

Table 2.1 Best Fit Flow Resistivities of Various Ground Surfaces as Reported by Embleton et al. [42].

Description of Surface	Effective Flow Resistivity
	mks rayls/m
4 inches new fallen snow	10000 - 30000
Sugar Snow	25000 - 30000
Forest Pine Floor	20000 - 80000
Grassland	150000 - 300000
Roadside dirt (small rocks < 4 inches)	300000 - 800000
Sandy silt hard packed by vehicles	800000 - 2500000
Earth exposed and rain packed	4000000 - 8000000
Asphalt sealed by dust and use	> 25000000

2.6 Acoustic Prediction of Ground Parameters Deduced from Sound Reflection Techniques

2.6.1 Flow Resistivity

The parameter most commonly deduced from acoustic measurements of impedance is the effective flow resistivity. Table 2.1 expresses a range of values of effective flow resistivities for a variety of different surface types, Embleton et al [42]. Each surface type has a range of values. Range variation in soils may be due to moisture content, the presence of organic matter, root zones, the cracking of the soil surface and soil management practises. Martens et al. [71] study a forest soil, a grass covered soil and a bare sandy soil using the inclined track method. They are aware that other soil parameters, in addition to flow resistivity, also influence the acoustical impedance. However the over simplified semi-empirical relationships developed by Delany and Bazley are still used to classify the three different soil surfaces as acoustically soft, moderate and hard respectively according to the behaviour of impedance with frequency and to the corresponding best fit effective flow

Table 2.2 Comparison of Measured and Predicted Flow Resistivities

Surface	Measured	Predicted	Source
Grass	300000	200000	[72]
Bare Sandy Soil	63000	40000	[72]
Cultivated Farm Land	285000	150000	[72]
Hard clay Field	400000	250000	[72]
Uncultivated Grass	298000 - 341000	40000 - 75000	[73]
Forest Floor humus over A horizon	200000 - 540000	50000 - 60000	[71]
Grass field	220000	300000	[70]
	100000	250000	"
	30000	250000	"
	50000	200000	"

resistivities. To check these best fit deductions a classification of soils based on measured air flow resistivity was made but this was only roughly in agreement with the acoustical classification.

Table 2.2 shows a comparison between measured and predicted effective flow resistivities, made by several authors using a variety of measurement techniques. The predicted flow resistivities are made using the Delany and Bazley semi-empirical relationship. Martens et al. [71] and Bolen and Bass [72] found that the measured values of flow resistivity (σ) for these surfaces exceeded the best fit flow resistivity (σ_e) values needed to fit the impedance data, by a factor of roughly two. This discrepancy, also found by Talaske [44] on humus and soil layers of forest floors and Zuckerwar [73] on grassland is to be expected due to the differing values in porosity between fibreglass and soils as indicated in Section 2.5.2.

Don and Cramond [70] found in measurements over a grass field the reverse situation. The measured values of flow resistivity were considerably less than the values of σ_e predicted. The authors attribute the decrease of measured flow resistivity values from site to site to sub-surface cracks which the acoustic measurements do not show. This is not unexpected since the

Table 2.3 Predicted Flow Resistivities of Various Ground Surfaces as reported by various authors.

Surface	Flow Resistivity	Source
Grass	150000	[65]
"	300000	[64]
"	300000	[62]
Bare Soil	450000	[69]
Hard Clay	500000	[53]

acoustically deduced flow resistivity is determined from pulsed sound which penetrates to approximately 1cm depth in the soil and the measured flow resistivity values were obtained on samples 5cm deep. Table 2.3 shows other predicted values of σ_e for different surfaces.

The problems associated with a comparison between measured and predicted σ_e are threefold.

1. The Delany and Bazley semi-empirical relationship is used for prediction, which as shown above is inaccurate due to other soil parameters such as porosity not being included.

2. The techniques used to measure impedance and hence for deduction of σ_e have specific problems as mentioned above.

3. It is notoriously difficult to measure flow resistivity directly due to sample damage. The variability of flow resistivity between sites can also be very great and implies that an average flow resistivity value of one particular surface type is hard to achieve.

Some of the experimental data mentioned above have been reanalysed using models developed by Attenborough [74]. This work shows that some soils do not behave homogeneously but have a layered structure.

2.6.2 Layering

From studying Tables 2.1 and 2.3 above it is assumed that a grass covered soil tends to have a lower effective flow resistivity than a barren soil, even on sites adjacent to each other with comparable soil texture and structure, Van der Heijden [58]. Grass length as investigated by [72], [70] and [71] was not found to be an important factor affecting the impedance. It was assumed to be the presence of a root zone that loosened the top layer and influenced acoustic characteristics. However this is probably a gross over-simplification. When water is added to a grass covered soil the roots swell and fill the former air filled pores possibly long after a barren soil of similar structure has freely drained and the large pores are again air-filled. Under these circumstances a grass covered soil could have a higher flow resistivity than the barren soil. Hence the acoustically deduced flow resistivity will depend on when the acoustic measurements were made within a wetting and drying cycle. This situation is also complicated by the fact that roots also shrink at around midday due to maximum plant evapotranspriration and swell at night when evapotranspriration ceases. This diurnal effect is likely to create a slightly more porous soil during the day. Habault and Corsain [61] found differences between grassy field and garrigue (a kind of bare hard ground, studded with tufts of thyme and small pebbles). Talaske [44] also found that impedance is significantly influenced by the presence of an acoustically soft root and humus layer on top of a mineral soil, and this is also supported by Martens et al. [71].

There has been experimental work undertaken *in situ* to test the influence of a layer with depth. Dickinson and Doak [53] showed that a 10cm thick turf layer seemed to have the same absorption coefficient whether it overlaid either deep sandy loam or rock. Don and Cramond [70] artificially prepared layers outside by removing 2cm of turf and then overlaying the exposed earth with first 1cm and then 3cm of loose soil. The added soil was then removed, the base dug to a depth of 20cm and the finer top soil replaced. There was a marked decrease from the base impedance when the 1cm layer was present, while only marginal changes between 1cm, 3cm and

Table 2.4 Measured and Predicted Flow Resistivities of an Artificially Layered Ground Surface.

Surface	Measured σ	D&B predicted σ	Source
Base below turf	10 - 60000	2200000	[70]
loose soil layer	5000 - 12000	150000	"
1 cm thick			

the 20cm dug surface. It appears therefore that the acoustic pulse was only influenced by the top 1cm of soil. The results are set out in Table 2.4, in which D&B represents Delany and Bazley.

Forests usually have a naturally layered soil structure. Martens et al [71] define forest floor layers into litter, fermentation, humus and an A horizon mineral soil. This is similar to the definition reported by Talaske [44] and as reported by Wilde [75]. The litter/humus layers depend on the type of trees involved, either broadleaf or pine needles. Heisler et al. [46] measured a larger magnitude of impedance for a broadleaf forest with a shallow litter/ humus layer compared a relatively smaller magnitude of impedance in pine stand with a deeper litter layer. This would suggest, the thicker the litter layer the greater its effect on sound absorption. Don and Cramond [70] found when they artificially applied pine needles from 2cm up to 10cm deep over a sandy soil that increasing thickness of the layer generally decreases both the real and imaginary parts of the measured impedance, which is consistent with the layer reducing the reflected pulse amplitude. Resonances in the impedance plots due to a layered structure were visible when the litter layer was >6cm deep. There has been much conflicting experimental work on how deep the organic layer has to be before it influences the impedance. Heisler et al [46] showed that the properties of the mineral soil do seem to influence impedance even with an average of 3.5cm of organic matter on the soil. Talaske [44] found the litter layer to be acoustically transparent but that the deeper humus had an effect on the impedance.

2.6.3 Crusts

Other naturally occurring layer structures are surface crusts usually associated with the wetting and drying phase of soils. Soom and Gu [64] studied excess attenuation over a grassy meadow which was hard and dry from lack of rain. Prediction with a semi-infinite model using the Delany and Bazley empirical formulae was unsuccessful and a layered model was required, and more specifically one that modelled a thin, hard, less porous crust above a more porous ground. Unfortunately no soil measurements were made concurrently with the acoustic measurements and therefore the parameters could not be verified, although the general dry conditions were thought to have been consistent with the presence of a surface crust. Aylor [76] compares excess attenuation over a weather slaked, crusted sandy loam soil with the same site when disked. Between the two conditions the frequency of the first interference minimum shifts indicating a decrease in the effective flow resistivity, σ_e , at the surface although no soil parameters are acoustically deduced or measured using conventional techniques. This lack of verification raises a possible alternative interpretation which is that the differences between the two surfaces could also be due to the roughness of the disked surface, Attenborough [77].

2.6.4 Water Content and Porosity

In terms of acoustic interpretation the relationships between water content and porosity are difficult to understand. In essence it may appear simple as they compete for the same pore space. As moisture content increases it would be expected that the air porosity would decrease and therefore the flow resistivity would increase. This was the pattern found by Martens et al. [71] in experiments with peat dust samples where higher flow resistivities were found for higher water contents. Dickinson and Doak, using an impedance tube technique deduced flow resistivity values for sharp heath sand. Root free samples were dried and then 2% moisture content was added in stages with acoustic impedance measured at each stage. From initial flow resistivity measurements on this sand it was noticed that a slight addition

of water caused a decrease in flow resistivity which reached a minimum at 8-10% moisture content. After this minimum value there was a sharp increase in flow resistivity until the value equaled that of a layer of water. It appeared that a slight increase in moisture content, instead of filling up the previously air-filled pores, and increasing the flow resistivity rather brought about increased surface repulsion between the grains causing material to bulk and open up the pores. This behaviour was also determined from the acoustically deduced impedance measurements although the minimum flow resistivity and hence maximum sound absorption was predicted around 6% rather than the measured 8-10%. The presence of roots also affected the flow resistivity. For a sample of sandy soil with fine roots the minimum flow resistivity and hence maximum sound absorption occurred at 0% water content, but when the roots were carefully removed the flow resistivity behaved as before with a slight decrease in flow resistivity on the addition of a little moisture, followed by a sharp increase. This suggests that when a little moisture is added to a sandy soil containing roots any possible increase in porosity due to bulking is exceeded by root swell on intake of water. From this the authors conclude that a granulated inorganic soil is more sound absorbent when a little moisture is present, but when roots are present the greatest sound absorption occurs when there is no moisture. This is unexpected since under dry conditions roots shrink and contract resulting in vapour gaps which would facilitate the movement of gases within the soil, Huck et al [78], and increase space for sound waves to propagate, hence the reliability of these results is questionable. It would appear rather difficult to extract roots particularly very fine root hairs from a soil sample without disturbing the soil structure. Consequently the increase in flow resistivity when the roots were removed may be explained by grain movement and repacking to a more compact structure.

Cramond and Don [79] plot a series of impedance curves from measurements made over a grass site with increasing water content. The plots in Figure 2.6 show layer resonances and as the soil dries the number and frequency position of the resonances remains constant although their mag-

nitude decreases. The application of water to the soil caused the top 2cm of the soil to become saturated and formed a wetted crust. It seemed the technique was more sensitive to a crust structure and reduction in porosity brought about by structure deformation than by water actually filling the air connected pores. This was shown when the surface was broken to the original fairly loose state ie. removing the layer, then the original impedance pattern was regained.

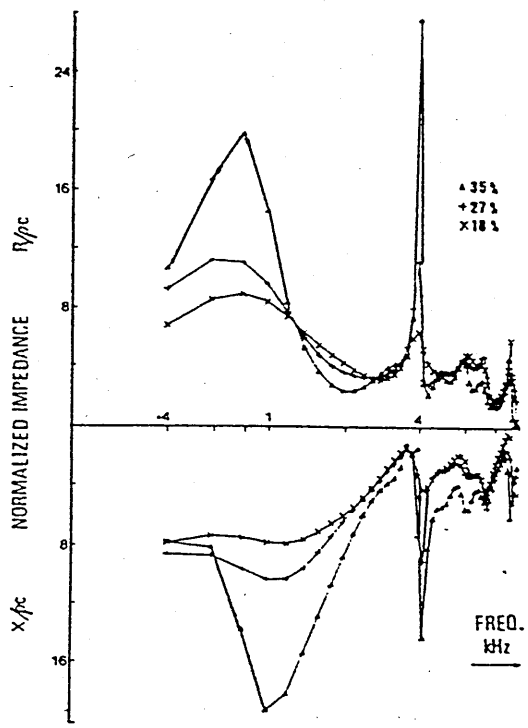

Figure 2.6 Impedance Measurements at One Site for Different Moisture Contents, after Cramond and Don.

Small "bumps" noticed in the tail of reflected pulse shapes in wetted soil have a major effect on the calculated impedance, causing resonances. These create difficulties in modelling and understanding of the subsurface layering. Hence Cramond and Don, in studying water relationships, concentrated on

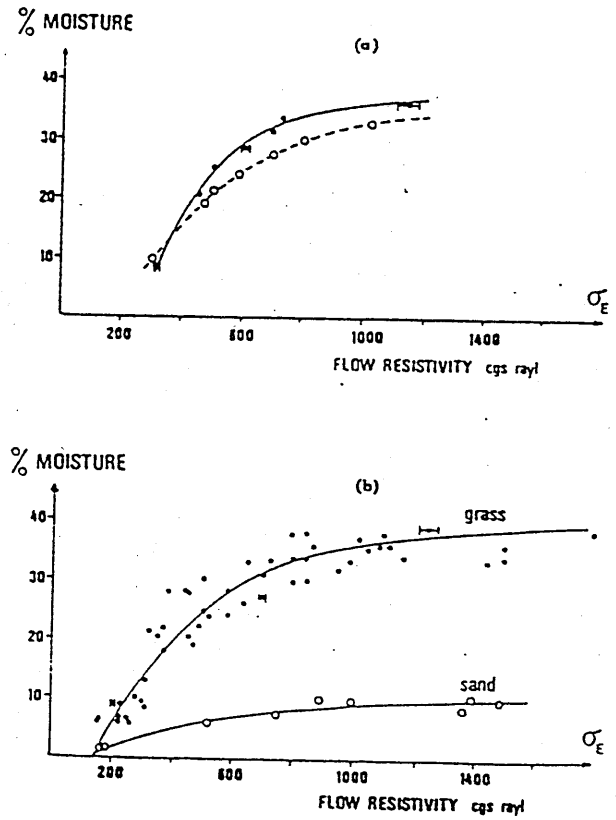

Figure 2.7 Variation of Effective Flow Resistivity with Moisture Content (a) grassland for two sites and (b) many grassland sites and sand, after Cramond and Don.

the amplitude of an ensemble average reflected pulse, where the "tail wiggles" are cancelled and reduced. Since the amplitude varies with impedance, choosing an effective flow resistivity which generates a signal with the same peak height as the measured pulse, can be used to investigate the variation of σ_e with moisture content.

Figure 2.7(a) shows a smooth increase in effective flow resistivity σ_e with moisture content, for the same soil type. Differences could be due to localised structure or root zones. Figure 2.7(b) shows the difference between a grass covered soil and a washed sand. The sand has a higher flow resistivity σ_e attained at a low moisture content $\approx$10% because the large pores are readily filled and the sand grains do not absorb water. The grassland soil does not

become a perfect reflector until a saturation of 40% is reached. Therefore deduction of moisture content from impedance measurements is difficult. Although the grassland and sand results do not overlap, it is possible to normalise the results to their maximum moisture contents. If this is done, then the sand results fall within the experimental scatter of the grassland. This implies that a unique curve of normalized moisture content versus impedance may be developed. Both sets of data have been fitted with a curve of the form.

$$\sigma_e = 360 \ln\left(\frac{1}{1-\frac{W}{Ws}}\right) + 150\text{cgs rayls}$$

where W is the moisture content and Ws is the saturation value of the soil.

2.7 Propagation Constant Techniques

The acoustic techniques described so far have focused on sound reflection and the measurement of the sound field above the ground to deduce the impedance and hence characterise the surface. When sound is incident on a porous surface most sound is reflected but some propagates through the air filled pores. The propagation through or within the porous medium can be studied by measuring the bulk propagation constant k_b which is expressed as a complex variable

$$k_b = a + ib \tag{2.24}$$

where a is termed the phase constant and b the attenuation constant. Delany and Bazley [40] have published a semi-empirical formula which characterises a and b in terms of the flow resistivity.

$$\frac{k_b}{k_o} = 1 + 0.0978\left(\frac{\sigma}{f\rho_0}\right)^{-0.7} + i0.1819\left(\frac{\sigma}{f\rho_0}\right)^{-0.595} \tag{2.25}$$

where

k_b is the propagation constant in the medium

k_o is the propagation constant in air

σ is the flow resistivity
ρ_0 the density of air
f is the frequency
and $i = \sqrt{-1}$.

Attenborough [41] has also characterised the bulk propagation constant in terms of four parameters mentioned in Section 3.6. Both these models assume that the only propagation is through the air-filled pores and that the frame is rigid. By using these relationships and measuring the way in which soil attenuates sound deductions may be made about its structure.

Attenuation in dB, sometimes called the transmission loss, can be written as

$$\text{attenuation} = 20 \log \left| \frac{P_0}{P_1} \right| \text{dB} \tag{2.26}$$

where
P_0 is the pressure at point 0 and
P_1 is the pressure at point 1. If studying attenuation over a certain sample length then the relationship can be written thus

$$\text{attenuation dB/unit length} = \frac{20\, Im(k_b) d}{\log_e 10} \tag{2.27}$$

where d is the distance between P_0 and P_1, and $Im(k_b)$ is the imaginary part of the propagation constant sometimes called the attenuation constant. The techniques reviewed in this section concentrate on trying to sense the variation in sound field with depth.

Nyborg et al. [80] studied the transmission loss through loam soil and sand samples under porous and water soaked conditions. For porous conditions a wooden chamber 1.5m long and 0.35m square in cross section was divided by a wire mesh screen at height 0.75m on which the soil samples were placed. The sound source, a whistle, emitted a series of single frequencies and the transmission loss was calculated by Equation 2.26 where P_0 was the level without a layer of soil present and P_1 when the soil was in place. Experiments were done on moist well aggregated samples which were gently stirred in a warm stream of air to create a drying effect. For the water-soaked

samples the whistle source was not sufficiently powerful to produce a signal the microphone could receive above background noise. This signal to noise problem resulted in the use of hydrophones buried directly in the samples. The source was a rochelle salt transducer whose radiating face was 7cm in diameter. The receiver hydrophones were small rochelle salt units 0.95cm in diameter. For both the porous and wet experiments the samples were artificially managed, there was no attempt to study undisturbed samples.

Ishida [49] conducted a series of experiments on the transmission loss through snow. In a rather awkward experiment a speaker was buried and sealed acoustically into the wall of a trench dug into the snow, as shown in Figure 2.8. A small opening was left into which freshly cut samples of

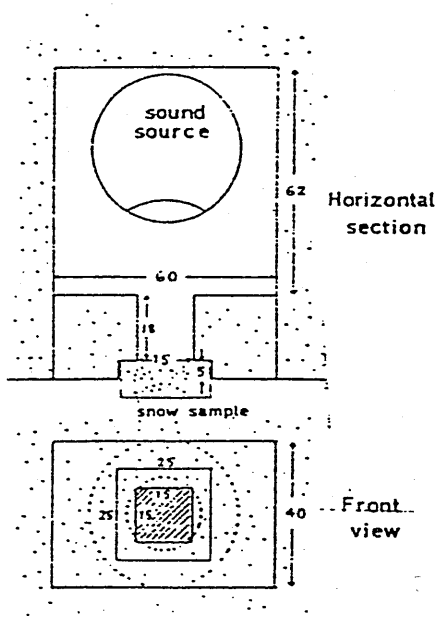

Figure 2.8 Sound room for measuring the transmission loss in snow, after Ishida, dimensions in cm.

snow, varying from 2cm to 10cm thick, were placed. The snow samples were always cut horizontally from deposited snow so that the texture of the sample was as uniform as possible. The frequency dependence of the attenuation (dB/cm) in snow are compared to results made by Scott [81]

on Stillite or rockwool. Scott measured the attenuation directly by inserting a small probe tube microphone into the Stillite. Ishida comments that it is difficult to apply this method to snow, since the texture of the snow may be destroyed by the insertion of the probe microphone.

The measurement of attenuation and phase speed using a probe microphone to monitor the sound field at depth has been successfully used by Attenborough et al [82] and [83], Richards et al [84] and Van Hoof [85]& [86]. Most have studied various soil types although Richards et al studied a 0.5m thick layer of fibreglass. Attenborough et al [82] and [83] study two kinds of sand, a wind blown loess and an institutional soil. Van Hoof [85] studied brickworks sand, rockwool, hardened clay grains and "Wezep soil".

Basically, in each set of experiments, the procedure is the same. A received signal is measured at the surface and another received at depth with the buried probe microphone. The magnitude and phase of the transfer function between the two signals enables calculation of the attenuation and phase change with depth. From this information the calculation of the real and imaginary parts of the propagation constant can be made and values compared to predicted ones. The surface signal can be received either by the probe microphone which is then subsequently buried, Attenborough et al [82] in sand, or by a microphone positioned at the surface adjacent to the probe location, in which case the signals are recorded simultaneously. If two different microphones are used a reference measurement of both side by side at the surface is made so any differences recorded can be equalised and attenuation and phase changes seen are due to the soil structure and not unmatched microphones.

The sound source in each of the above mentioned papers is different. Attenborough et al [82] and [83] broadcast swept tones between 30Hz and 1000Hz through a small speaker which were processed through a tracking filter. Richards et al [84] used three different sources namely a spark, an air jet of compressed air and a swept tone signal between 100Hz and 15 KHz. Van Hoof [86] used two different types of helicopter hovering above the ground surface. This makes the probe microphone a very versatile technique.

The most important criterion necessary in considering the source is that it has enough output power at the required frequency range of interest to enable a signal level to be detected by a buried microphone well above background noise.

When using the probe microphone technique in soils there are several problems which may occur. As Ishida [49] suggested burial of the microphone without destroying the soil structure is important. Scott [81] suggested a bullet-shaped probe head for ease of access and less disturbance. Attenborough et al. [83] recommend inserting the probe into a pre-augered hole particularly when the ground is very firm. For less cohesive soils like sand the probe could be pushed easily into the ground. Van Hoof [86] showed on his particular soil type that if, after the first measurement, the probe was simply pushed in to a deeper depth an unexpected decrease in attenuation was observed. This was assumed the result of improper sealing between the probe wall and the soil. Any leaks down the side of the probe which are open to the surface are alternative sound paths hence the increase in signal. To overcome this problem Attenborough et al [83] suggest placing a small amount of highly viscous, engine treatment oil around the probe at ground level to seal the probe entry. Another minor problem associated with probe burial was small soil particles getting into the microphone area which required regular cleaning.

2.7.1 Determination of Soil Properties from Sound Transmission Techniques

Measurements of attenuation or transmission loss of porous materials reveal that attenuation increases with increasing frequency. Ishida [49] found this to be the case in snow as shown in Figure 2.9. Attenuation also increases at any given frequency as the length of the sample increases, as shown by Nyborg et al [80] in Figure 2.10. Table 2.5 shows a comparison of attenuation/cm of different densities of soil and snow, at 10KHz. Nyborg et al [80] estimate an attenuation of 2dB/cm for nodulus loose soil aggregates and up to 20dB/cm at the same frequency for finely divided soils. For snow

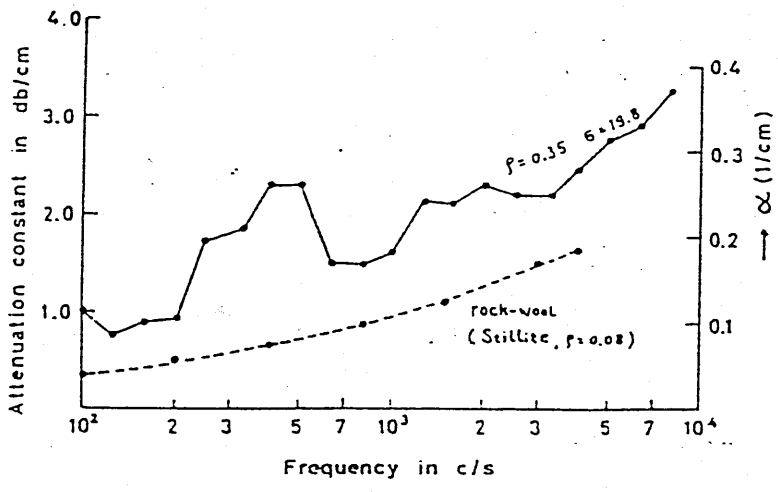

Figure 2.9 Measured Attenuation Constant of Compact Snow, density $350kg\,m^{-}3$, flow resistivity 19800mks rayls/m, after Ishida. The dotted curve shows the attenuation constant of Rockwool, after Scott.

Table 2.5 Comparison of Attenuation dB and Density for Soil and Snow

Sample	Frequency	Density $kg/m^3 \times 10^{-3}$	Atten dB/cm	Source
Soil				
Nodulus loose	10KHz	0.65	2.0	[80]
Finely divided	"	0.95	20.0	"
Snow	10KHz	0.10	0.9	[87]
	"	0.20	1.2	"
	"	0.30	1.6	"
	"	0.40	2.0	"
	"	0.50	3.0	"

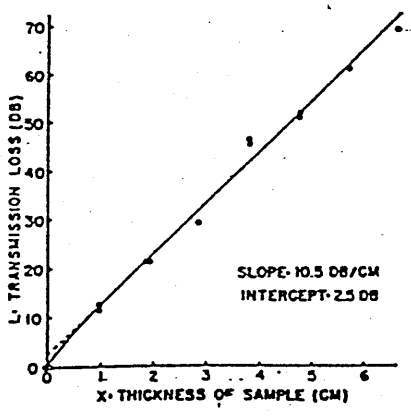

Figure 2.10 Transmission Loss vs. Sample Thickness for a Dry & Dusty Garden Soil at 10.5KHz, after Nyborg et al.

the density of the porous material also has an effect on the attenuation as shown by Ohgaki et al [87].

Figures 2.11 and 2.12, from Nyborg et al [80] show that at any one frequency as the soil and sand were progressively stirred and dried, the sample density was slowly increased as the particle size was reduced, and attenuation increased.

Due to the expected relationship between flow resistivity and acoustical measurements on porous material Nyborg et al [80] measured the flow resistivity of their samples. Figures 2.11 and 2.12 show for both sand and soil the rise in attenuation with increasing density could have been anticipated from observation of the increasing flow resistivity. However they also argue that monitoring flow resistivity itself is insufficient to predict attenuation. For example at 18KHz the loss in soil was 12.5 dB/cm at 80000mks rayls/m whereas, in sand at the same flow resistivity attenuation was 5.5 dB/cm. Although the authors realise other physical parameters are involved no effort was made to formulate these relationships.

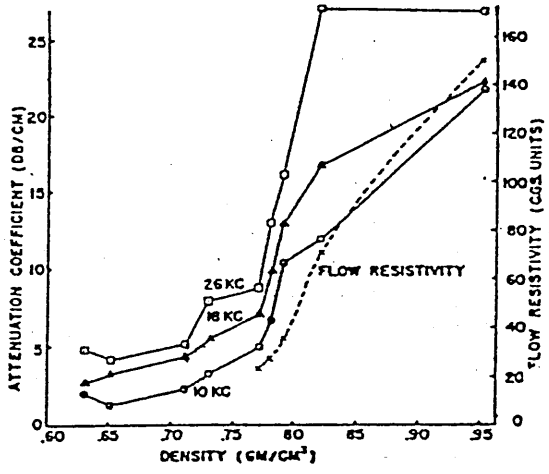

Figure 2.11 Attenuation for garden soil as a function of gross density for several frequencies, solid lines - attenuation constant, dotted line - flow resistivity vs density, after Nyborg et al.

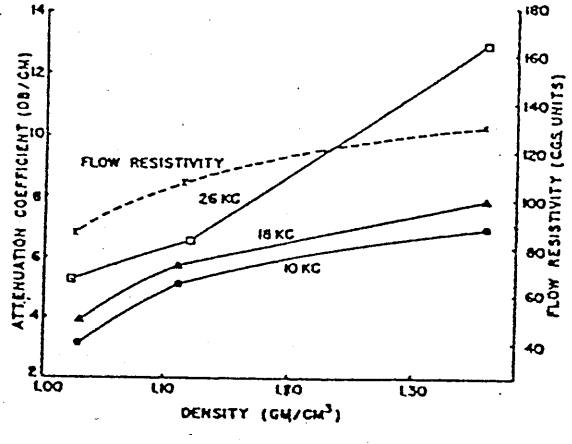

Figure 2.12 Attenuation Constants and Flow Resistivity for a Fine Sand after Nyborg et al.

Figure 2.13 shows attenuation measured by Richards et al [84] and a comparison made between these measurements and predicted attenuation using both the Delany and Bazley empirical formula [40] and the Attenborough [41] model. Using the measured flow resistivity of the fibreglass as recommended by the manufacturer of 11460mks rayls/m the Delany and Bazley prediction clearly over estimates the attenuation. This is surprising because the empirical formulae were developed on fibreglass. Using the Attenborough model which includes the measured flow resistivity, and porosity, tortuosity and grain shape factor all set to unity there is tolerably better agreement. The poor fit using Delany and Bazley shows that this empirically derived relationship is not a good representation of the physical relationships involved and does not have scope to include the other obviously important parameters including porosity, tortuosity and grain shape.

Ferraro and Sacerdote [88] using an impedance tube have measured the propagation constant of various types of sand and artificial porous material consisting of lead shot. Although measured with an impedance tube technique the results are worth including at this point for comparison. Delany and Bazley predictions using the measured flow resistivity compared to this measured data are too high. However if more parameters are included namely the measured porosity, an estimated tortuosity and a grain shape factor of 0.5 for spheres the prediction of the phase and attenuation constants are much improved, as shown by Attenborough [41].

Including more measured parameters into the prediction model does not always improve prediction. Attenborough [83] noted the measured attenuations per centimeter over the uppermost 2cm in dredged sand differed from those predicted using the measured mean flow resistivity and porosity shown in Figure 2.14. However by using an approximation technique and increasing the flow resistivity to fit the lowest frequency data point then better agreement is met over the whole frequency range. This illustrates the problems of making flow resistivity measurements on sandy soil with the possibilities of loosening the inherent structure and decreasing the flow resistivity.

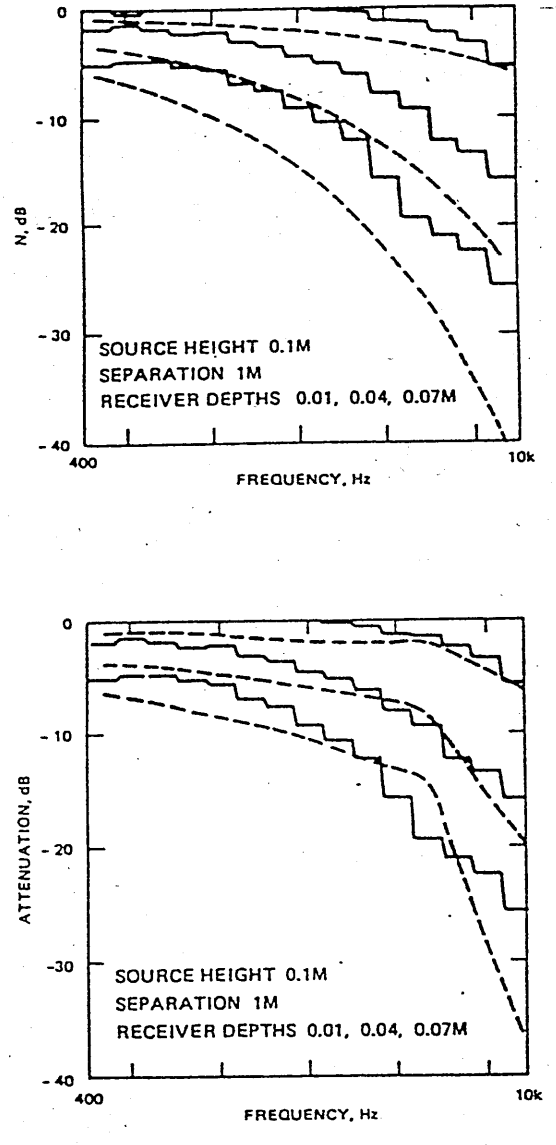

Figure 2.13 Comparison between measured attenuations between surface and subsurface receivers and those predicted (a) by the Delany & Bazley empirical formula [40] and (b) the Attenborough Model [41], after Richards et al.

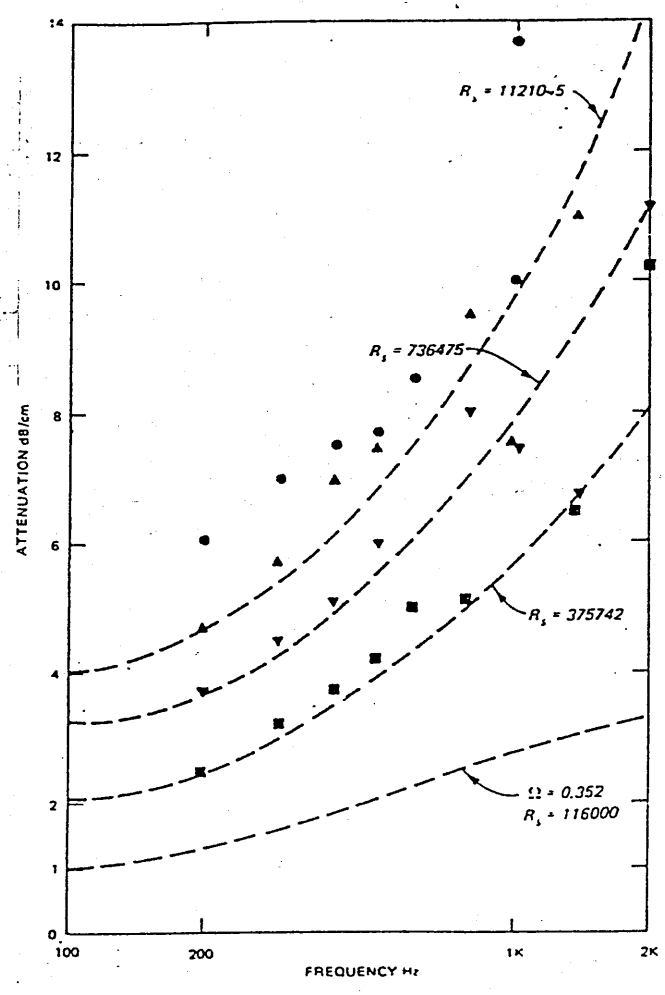

Figure 2.14 Measured and predicted attenuation in dredged sand, Measurements made with a probe microphone at 2cm for four different locations; After Attenborough et al. R_s = effective flow resistivity

2.7.2 Moisture Content

Little work has been done on the effects of moisture on the propagation constant. The effect of saturated moisture content was studied by Nyborg et al [80] as described in Section 2.7 . In water saturated media the attenuation was found to depend on the amount of gas present in the mixture. Air free mixtures prepared in an evacuated chamber had attenuations of 4dB/cm at 12KHz. Mixing in the presence of air the attenuation was extremely large: 26dB/cm at 10KHz to 64dB/cm at 30KHz.

Preliminary fitting of Van Hoofs data by Attenborough [86] showed that the Schweinfurt AMI ground was reasonably homogeneous with depth up to 0.045m with an estimated effective flow resistivity of 12800 - 103600mks rayls/m. After rain this value was increased to 1.6 million mks rayls/m.

2.7.3 Layering and crusts

In homogeneous sand Attenborough and Hess [89] found attenuation with depth was uniform. However probed measurements at one particular location on a weathered sand pile did not behave thus. Attenuation rates over the first two centimetres depth was greater than that of any other equal spacing below those two centimetres. It was noted that at this location a sand crust approximately 1cm thick had formed and below this the sand was much looser.

2.8 Prediction of Snow Parameters

2.8.1 Effective Flow Resistivity

Embleton et al [42] have measured excess attenuation over 10cm of new fallen snow covering 40cm of older snow. Using the Delany and Bazley [40] empirical homogeneous model an effective flow resistivity of 10000mks rayls/m is predicted, as shown in Figure 2.15. This is well below the average of 150000 - 300000mks rayls/m measured for grass covered soils by Bolen and Bass [72] and Van der Heijden [58]. It is also lower than 50000mks rayls/m

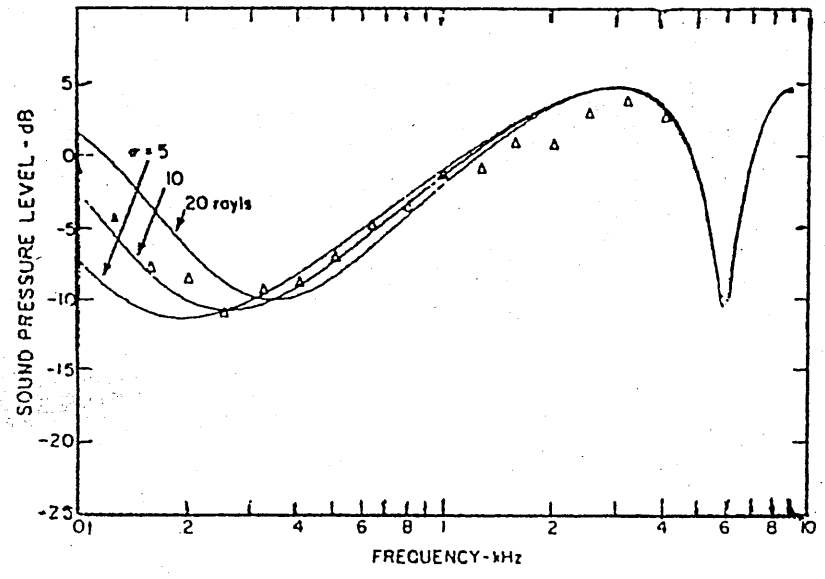

Figure 2.15 Comparison of measured and predicted sound pressure levels over snow after Embleton et al. Predicted flow resistivities at 5,10 and 20 cgs rayls/m.

measured by Van der Heijden [58] and 68000mks rayls/m measured by Price [90] over forest floors consisting of litter and humus layers above a mineral soil. Snow could therefore be categorised as an acoustically soft surface with an expected low flow resistivity.

Nicolas et al [91] show in Figure 2.16 four sets of excess attenuation data made over snow between 6 - 20cm deep, lying over a hard backing. The backing was either asphalt or old hardened snow or ice. Figure 2.16 shows the measured excess attenuation results compared to theoretical predictions assuming hard backed or semi-infinite layers. Good agreement is obtained between measured data and prediction curves for the hard backed cases at frequencies above 200Hz. However below 200Hz the results show better agreement with the semi-infinite case. The best fit effective flow resistivity values and layer depths are shown in Table 2.6.

Table 2.6 Predicted Effective Flow Resistivities over Snow

σ_e	depth cm	Snow type
15000	6	Snow over ice
15000	8	snow over asphalt
10000	10	10cm of new snow over 50cm of hard snow topped with ice crust
20000	20	

In Table 2.6 and Figure 2.16 (d) the 20cm depth of snow was sufficient to be considered as semi-infinite, there being no difference between the predicted excess attenuation using either the hard backed or semi-infinite case. On other measurements sites with 20cm of snow an infinitely thick layer could not be assumed. This, the authors suggest, is because the layer of snow behaves acoustically as one that is thinner than the actual measured thickness. When an effective depth was included after Donatos limiting case of variable porosity [92], then the dip location was better predicted. Some parameters deduced from this fitting are shown in Table 2.7.

Soom and Bollinger [93] use the Delany and Bazley [40] model to esti-

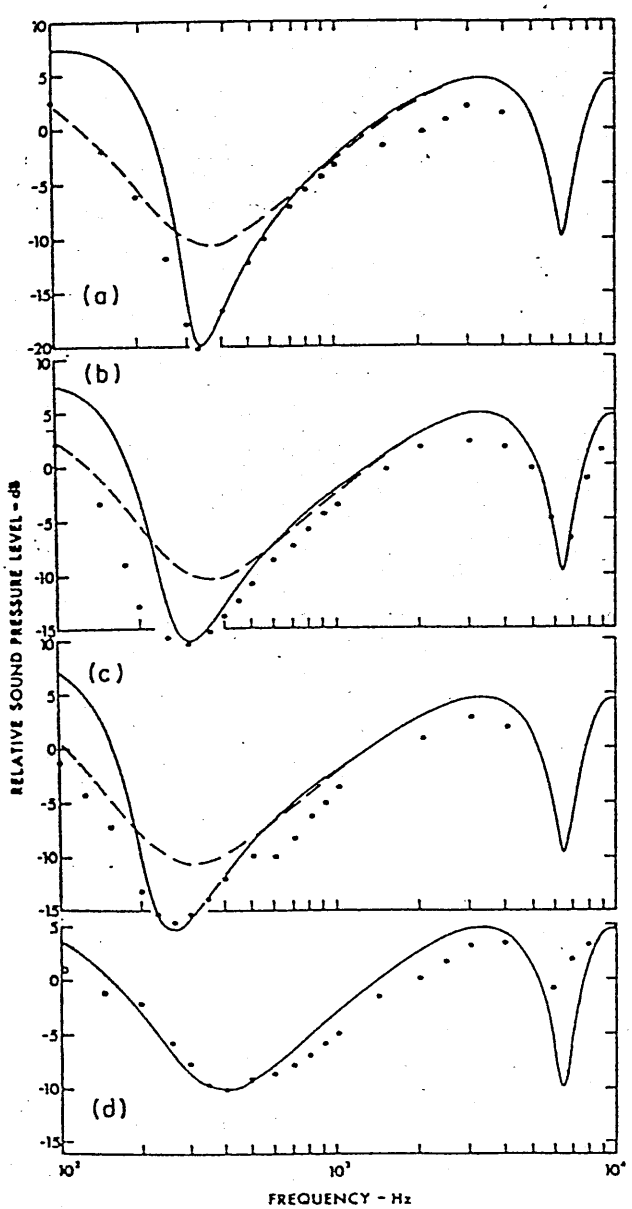

Figure 2.16 Measured and predicted sound pressure levels over snow layers after Nicolas et al, (a) σ = 15000 mks rayls and snow depth is 0.06m over ice, (b) 15000mks rayls and 0.08m deep new snow over asphalt, (c) 10000 mks rayls and 0.10m deep snow over old hard snow, (d) 20000mks rayls and 0.2m deep snow.

Table 2.7 Predicted Effective Flow Resistivities over Snow including Effective Layer Depth results after Nicolas et al.

σ_e	depth(cm)	effective depth	Snow Type
15000	20	10	
35000	10	4	snow exposed to sun and wind of 30-40km over frozen lawn
80000	6.5	2.5	snow over froze turf wind blown and compact

mate the flow resistivity of snow. Taking into account the thickness of the snow over a frozen lake and a frozen, ploughed forest road they find good agreement between predicted and measured attenuation using a value of 5000mks rayls/m. Bohlender et al [94] have measured a value of 30000mks rayls/m over 10cm of snow over a ploughed field.

The Delany and Bazley model is potentially more successful at fitting excess attenuation over snow than over soil. This is not surprising since the porosity of snow is generally much higher than for soils 0.6 -0.9. This is similar to the porosity of the fibreglass samples Delany and Bazley derived their empirical relationships on, hence better agreement is likely.

From the values of effective flow resistivity stated so far it appears that different types of snow have different flow resistivities. The meterological conditions the snow was laid down under, or experienced since, may have some influence over this. Ishida [49] in an extensive series of measurements on snow, including impedance measurements, attempted to clarify a relationship between acoustical properties and the internal structure of snow, by measurement of the flow resistivity. Table 2.8 summarises the ranges of parameters measured for various types of snow.

The measured values of flow resistivity σ in Table 2.8 are comparable to predictions mentioned in Tables 2.6 and 2.7. Ishida noted that two different snow samples with the same density may have different measured flow resistivities as shown in Figure 2.17. This implies that a value of flow resistivity

Table 2.8 Flow Resistivity, porosity and Density of Snow as measured by Ishida [49]

Snow Type	σ	density $kg/m^3 \times 10^{-3}$	porosity
new	3000-10000	0.08-0.20	0.9-0.8
compact	10000-22000	0.26-0.46	0.7-0.6
granular	5000-13000	0.35-0.48	
wet	3000- 4000		0.15-0.3

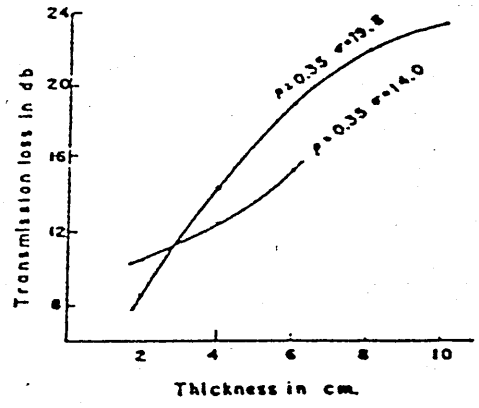

Figure 2.17 Transmission Loss vs. sample thickness for two snow samples with the same density after Ishida

is not only determined by its density but by its internal structure ie the shape and tortuosity of the pores.

2.8.2 Porosity of Snow

Buser [51] in an extensive series of impedance measurements on snow used Zwikker and Kosten's [95] impedance model to predict values of snow porosity, tortuosity and pore radii. These three parameters can be measured directly or indirectly to compare with acoustic predictions. Lee and Rogers [52] note that the direct measurement of porosity on snow is difficult. A value of porosity can be inferred from the gravimetric measurement of the density of snow compared to the density of ice.

$$\text{porosity} = 1 - \left(\frac{\rho_s}{\rho_i}\right) \tag{2.28}$$

where

ρ_s density of snow kg/m^3

and ρ_i density of ice taken as $917kg/m^3$

Buser [51] also notes that this could be the acoustic (effective) porosity as well since air bubbles in the ice grains are hardly ever observed in thin sections.

Attenborough and Buser [96] determine three parameters from fitting snow impedance measurements using an approximation technique. These three parameters are porosity, tortuosity and $sp^2\sigma$. Measured flow resistivities are compared to $sp^2\sigma$ where $sp^2\sigma$ includes flow resistivity σ being modified by sp^2 a pore shape factor ratio. The measured values of flow resistivity obtained with an air-flow rig enable further deduction of sp. The values of sp deduced lie between 0.4-0.6 which in some cases are $\geq$ 0.5 the maximum allowed in the theory.

Table 2.9 shows the difference between measured and predicted porosities determined by Buser [51] and by Attenborough and Buser [96] on the same impedance data. The results appear similar. The slight differences between the two predictions is due to the fitting technique used. Buser uses a least squares fit on 25 frequencies of data, whilst Attenborough and Buser

Table 2.9 Comparison of Measured and Predicted Porosity in Snow after Buser [51], and Attenborough and Buser [96].

		Buser	A & B
sample	measΩ	predΩ	predΩ
012	0.570	0.552	0.526
016	0.860	0.857	0.867
026	0.780	0.770	0.780
031	0.575	0.560	0.563

use an approximation technique that requires only five items of data information. These are the real and imaginary parts of hard backed and quarter wavelength air gap backed impedances at a single low frequency plus the frequency location of the first (half-wavelength) layer resonances.

Lee and Rogers [52] using a cepstrum impulse technique could distinguish between a thick layer of snow and 2cm layer of fluffy snow (density $0.05kg/m^3 \times 10^{-3}$) over a hard table backing. The reflected pulse from the layer situation was fitted to a prediction using Zarek's 6 parameter model [97]. The parameters deduced were typical of those in snow including a porosity of 0.99.

2.8.3 Layering

Snow accumulated to any significant depth is usually deposited by many independent snowfalls. These snowfalls may have been interspersed by days of sunshine or even melt. If a profile of snow is studied from the surface down then one is looking at a record of meterological conditions of the time when each deposit was laid and the subsequent effects the weather had on that snow between falls. It has also been seen that snow undergoes crystalline structure change with age Ishida [49], known as sintering. The deeper older snow at depth is likely to have experienced sintering. Consequently deep snow is unlikely to be homogeneous but have a layered structure, with different layers having different structures, porosities and densities.

Lee and Rogers [52] have noticed peaks in the tail end of some reflected

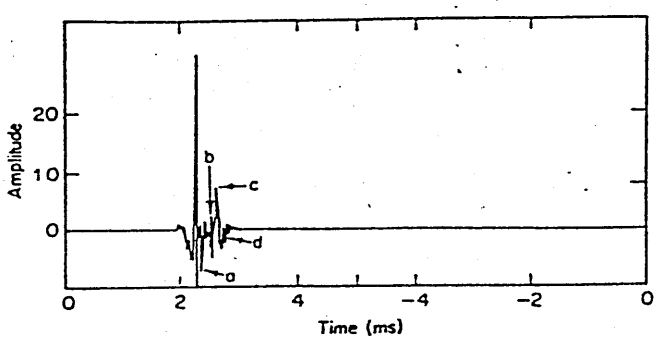

Figure 2.18 Power cepstrum for multi-layered snow. Events a,b,c and d are due to internal structure differences, after Lee and Rogers.

pulse spectra shown in Figure 2.18. They note that if the snow were homogeneous then only event "a" the main part of the pulse would be seen. Suggestion is made these peaks indicate an internal density and structure change and they represent secondary reflections from transitions from higher to lower acoustic impedance a few centimetres below the surface.

Acoustic monitoring of hoar-frost layers at depth has been suggested as desirable by Buser [98]. These very thin layers, with a loose density, sandwiched between layers of more compact snow are a point of weakness and the usual failure planes for avalanche genesis.

2.9 Choice of Acoustic Techniques

It was decided that the impedance tube technique was not suitable for the monitoring of outdoor soil conditions. This was due to the disturbance to soil properties caused by tube insertion into the ground. Free field normal incidence techniques looked more attractive due to non-disturbance of the soil. To explore this further an A-frame apparatus similar to that used by Dickinson and Doak [53] was constructed at the Open University and a series of experiments conducted on a Clay soil on the University Campus. This technique was found to have several limiting problems. Probing a pure

tone standing wave to locate pressure minima outdoors was a time consuming procedure and susceptible to meteorological effects. The experimental apparatus involved a 4m high A Frame, from which a loudspeaker was suspended. This frame was large and awkward to transport and erect in the field. The entire A-frame had to be moved several times to cover a large enough area to account for lateral soil inhomogeneity. Results of measured impedance were highly erratic and the technique was therefore abandoned.

Of the reviewed oblique incidence techniques, measuring the cut off frequency to determine ground impedance involved large distances between source and receiver. This characterised large areas of ground and was not suitable for monitoring changes in lateral soil inhomogeneity between areas close to each other, for example a wheel rut. Shorter distances between source and receiver could be achieved with the inclined track technique. This decreased the area of soil studied and reduced meterological effects to a minimum which was desirable. However the actual measurement procedure was deemed to be too time consuming and therefore the technique was not pursued.

Alternatively a quicker oblique incidence pulse based system was designed and investigated to study the potential of cepstrum analysis for the determination of the acoustical properties of soils. Pulse experiments were undertaken over sand within an anechoic chamber and over a sandy loam within a small soilbin. The soilbin results showed little or no improvement in the quality of measured data when compared to a continuous broad band source technique, despite the enclosed environment. The pulse technique also required an increase in the electronic hardware used in the experimental apparatus which complicated the procedure and its applicability in the field. A further complication was the inability of the speakers to produce repeatable pulses of sufficient volume at all the frequencies of interest.

The acoustic reflection technique chosen as the most reliable and producing the most repeatable results was the level difference technique. It involved the minimum amount of apparatus, important in a field application, which was easily transferred to another area of soil. The technique

could also be used in exactly the same set up for work over snow surfaces without significant disturbance. Unlike measuring excess attenuation it did not require a previous knowledge of speaker frequency response. Utilising continuous broad band noise allowed data collection at all relevant frequencies simultaneously and rapidly. The use of a small omnidirectional speaker proved successful and enabled the scaling down of the distances involved for the level difference measurements. This allowed meteorological factors to be ignored whilst still enabling examination of a large enough ground area approximately $1m^2$.

For measuring the propagation constant with depth a method using two probe microphones was developed. This allowed measurements to be made with the soil and crop, or snow in situ with the minimum disturbance. Depending on the ground properties the probe technique was able to monitor sound fields to a deeper depth than the reflection technique. Therefore it could detect sub-surface features such as crusting and layering that remained unseen by the level difference technique. In addition the area of ground affecting the sound field around the buried microphone was much smaller than that for the reflection technique. This meant the technique was suitable for detailed monitoring of parameter changes over very small areas or depths, for example within and eitherside of a wheelrut, or monitoring multiple layers with depth in snow. For this research the level difference and probe microphone techniques were used conjunctively in a novel approach to try and deduce ground parameters both at the surface and at depth.

Chapter 3

Theory

3.1 Local and Extended Reaction

When a sound ray r_2 is incident at angle θ on a porous ground surface its propagation into the ground can be described as locally or externally reacting. In Figure 3.1 for locally reacting medium $\theta_t = 0$, whilst for extended reaction $\theta_t > 0$. Extended reaction can be described in terms of the complex refraction index n, where by Snell's Law,

$$n = \frac{k_b}{k_o} = \frac{\sin\theta}{\sin\theta_t} \tag{3.1}$$

where k_b and k_o are the propagation constants in the ground and air respectively. A value of n considerably greater than unity indicates local reaction.

For soils local reaction is the general assumption. Similarity in measured impedance data made with normal and oblique incidence techniques as discussed in Section 2.5.5 upholds the assumption that wave refraction into soils is independent of the angle of incidence and normal to the surface. In snow the more porous nature of the medium raises the possibility of θ_t being significantly greater than zero since the propagation constant k_b in the snow is nearer k_o in air and hence the value of n becomes nearer unity. In the research reported here soils are assumed locally reacting and snow is allowed to be externally reacting.

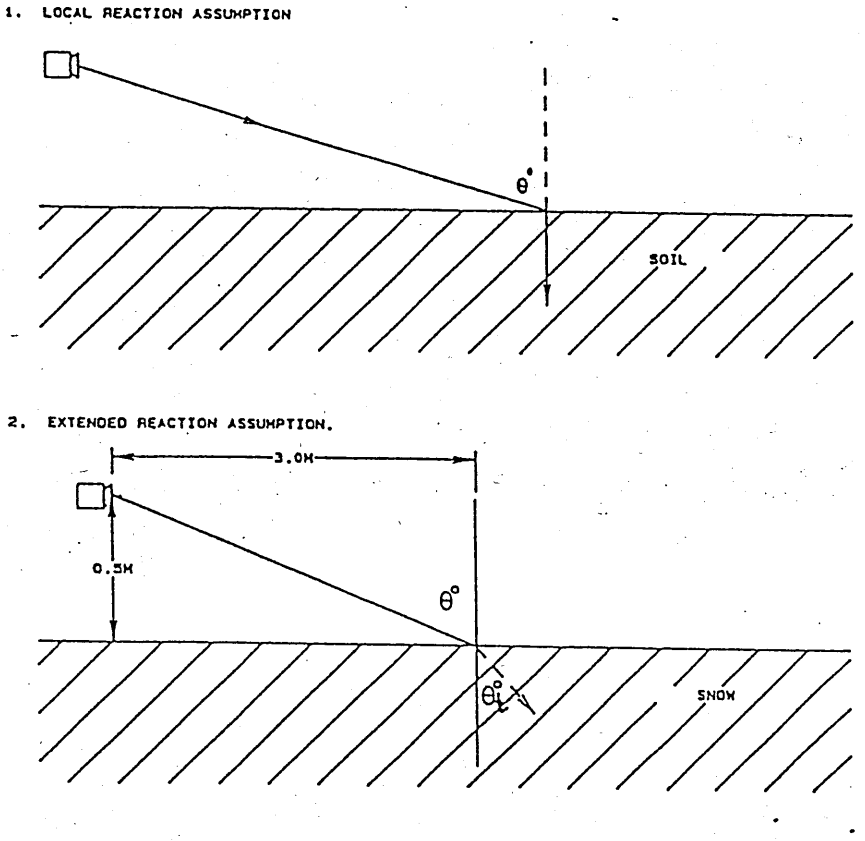

Figure 3.1 Local and Extended Reaction Assumption

3.2 Theory of Sound Propagation above the Ground Surface.

In Figure 3.2 a point source and receiver are located above a flat rigid surface. The total pressure received at the microphone is composed of the direct and the reflected sound rays. This can be expressed as

$$P_{tot} = \frac{e^{ik_o r_1}}{r_1} + Q\frac{e^{ik_o r_2}}{r_2} \tag{3.2}$$

after Attenborough and Heap [99], where k_o is the bulk propagation constant of sound in air, r_1 and r_2 the direct and reflected path lengths and Q is the reflection coefficient. Q depends on whether local or extended reaction is used and whether the wave front is spherical or plane. The spherical wave reflection coefficient Q can be approximated by R_p, the plane wave reflection coefficient, under certain circumstances. For the extended reaction case R_p is given by

$$R_p \simeq \frac{Z\cos\theta - \left(1 - \sin^2\theta/n^2\right)^{0.5}}{Z\cos\theta + \left(1 - \sin^2\theta/n^2\right)^{0.5}} \tag{3.3}$$

where Z is the normalized surface impedance. If n is very large then $\sin^2\theta/n^2$ is small and its contribution excluded hence the plane wave reflection coefficient for soils can be written

$$R_p \simeq \frac{Z\cos\theta - 1}{Z\cos\theta + 1} \tag{3.4}$$

At grazing incidence when $\theta \approx 90°$ and $r_1 = r_2$ then the substitution of R_p for Q in Equation 3.2 would result in zero pressure at the receiver which is false. To account for $R_p \neq Q$ at grazing incidence a term called the ground wave term is added to the plane wave reflection coefficient so that

$$Q \simeq R_p + (1 - R_p)\,F(w) \tag{3.5}$$

where $F(w)$ is the boundary loss factor and is given by

$$F(w) = 1 + i\sqrt{\pi}\,w\,e^{w^2}\,erfc(iw) \tag{3.6}$$

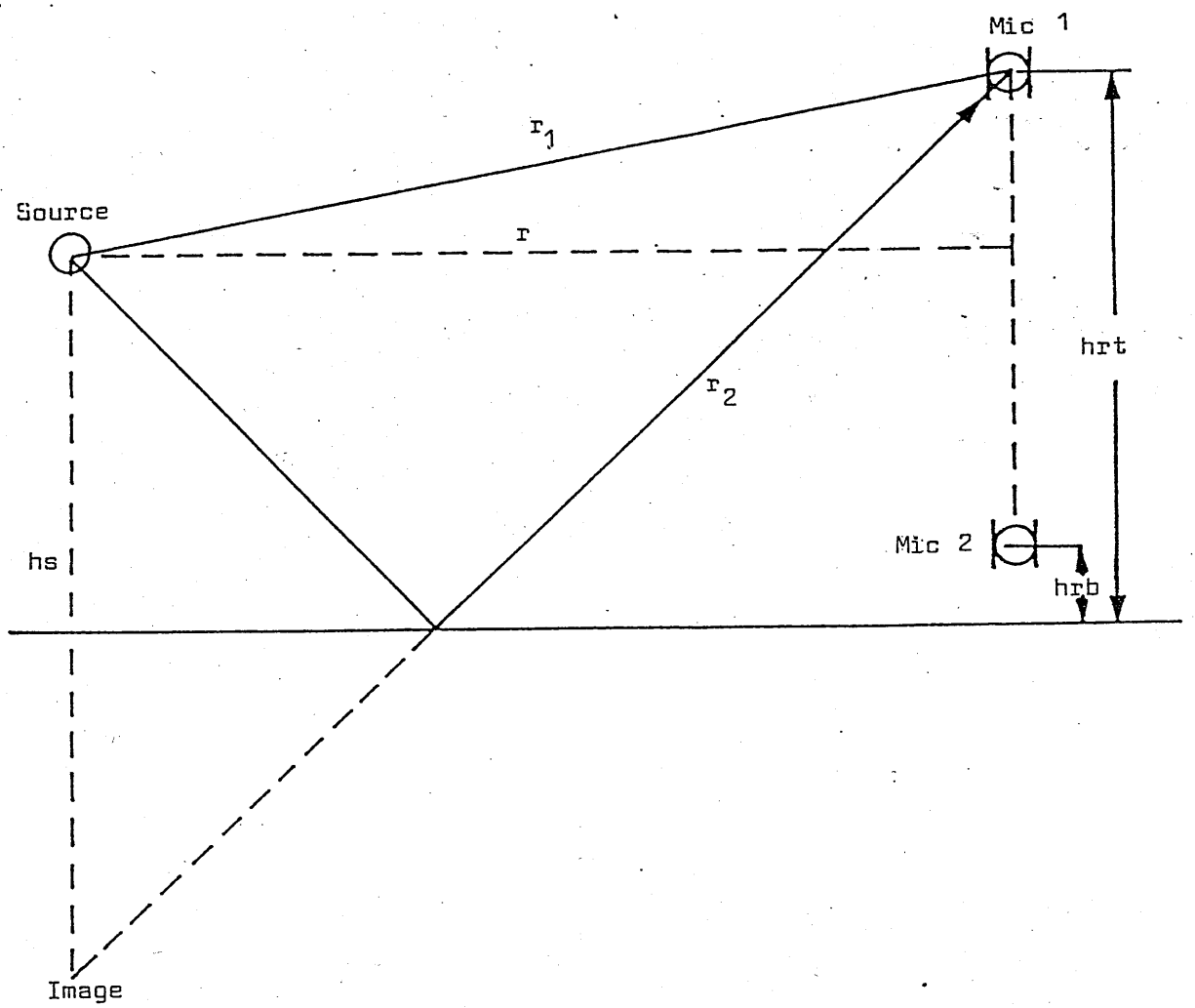

Figure 3.2 Geometry for Level Difference Measurement

where

$$erfc(iw) = \frac{2}{\sqrt{\pi}} \int_{iw}^{\infty} e^{-t^2}\, dt \tag{3.7}$$

is the complimentary error function and where w^2 for the local reaction case can be expressed as

$$w^2 = \frac{ik_o r_2 (\cos\theta + \beta)^2}{2} \tag{3.8}$$

where $\beta = \frac{1}{Z}$.

An approximation of $F(w)$ valid when $w \gg 1$ which implies for large source-receiver separations and/or small impedances is

$$F(w) = 2i\sqrt{\pi} W e^{-w^2} H\left[-Im(w)\right] - \frac{1}{2w^2} \tag{3.9}$$

where H is the Heavyside step function. For large values of w (very large ranges in wavelengths) $F(w)$ can be approximated by

$$F(w) = -\frac{1}{2w^2} \tag{3.10}$$

If the receiver and source are both located on the ground then the total field received will be

$$P_{tot} = 2\left(F(w)\right) \frac{e^{ik_o r}}{r} \tag{3.11}$$

In the propagation experiments described in this work the receivers are always located above the ground surface but such that θ is large ie at grazing incidence. Hence Equation 3.8 of w^2 is used for the local reaction case over soils. For an externally reacting media the calculation of the total field is expressed as

$$P_{tot} = \left[\frac{e^{ik_o r_1}}{r_1}\right] + \left[\frac{e^{ik_o r_2}}{r_2}\right] \left(R_p + B\left[1 - R_p\right] F(w)\right) \tag{3.12}$$

where

$$B = \frac{\left[\cos\theta + \beta(1 - \sin^2\theta/n^2)^{0.5}\right](1 - n^{-2})^{0.5}}{\left[\cos\theta + \beta(1 - n^{-2})^{0.5}/(1 - M^2)^{0.5}\right](1 - \sin^2\theta/n^2)^{0.5}} \times \frac{\left[(1 - M^2)^{0.5} + \beta(1 - n^{-2})^{0.5}\cos\theta + \sin\theta(1 - \beta^2)^{0.5}\right]^{0.5}}{(1 - M^2)^{1.5}(2\sin\theta)^{0.5}(1 - \beta^2)^{0.25}} \tag{3.13}$$

and where $F(w)$ is as in Equation 3.6 and w^2 given as

$$w^2 = ik_o r_2 \left[1 + (\beta \cos\theta(1 - n^{-2})^{0.5} - \sin\theta(1 - \beta^2)^{0.5})/(1 - M^2)^{0.5}\right] \tag{3.14}$$

where $\beta = Mn$. This is after Attenborough, Hayek and Lawther [100] as corrected by Quartararo [101]. The calculation of the function $e^{-w^2} erfc\,(iw)$ used in the analysis follows the method reported in Chien and Soroka [102]. The error introduced into a level difference prediction curve by $R_p = Q$ when using a geometry suitable for acoustical determination and using a four parameter homogeneous model is shown in Figure 3.3.

3.3 Excess Attenuation

The difference between the total and direct sound pressure levels at a receiver is called excess attenuation. That is the pressure received at the microphone over and above the effects of geometrical spreading and atmospheric absorption. When both source and receiver are above the ground surface excess attenuation in dB can be expressed as

$$\text{Excess Attenuation} = 20\log_{10}\left|\frac{\frac{e^{ik_o r_1}}{r_1} + \frac{Qe^{ik_o r_2}}{r_2}}{\frac{e^{ik_o r_1}}{r_1}}\right| \text{dB} \tag{3.15}$$

When both microphone and receiver are located on the ground, the path length difference and the grazing angle both tend to zero. Under these conditions $R_p \rightarrow -1$ and the pressure at the microphone reduces to Equation 3.11 and excess attenuation can be expressed as

$$EA = 20\log_{10}|2F(w)| \tag{3.16}$$

The result of an addition of the direct and reflected rays depends on their relative magnitude and phase. If the two rays are in phase then the sound from the two rays will add coherently, called constructive interference. If the two have a phase difference of 180° destructive interference occurs and the sound waves cancel each other out, causing a dip in the excess attenuation spectrum. Otherwise the rays partially interfere.

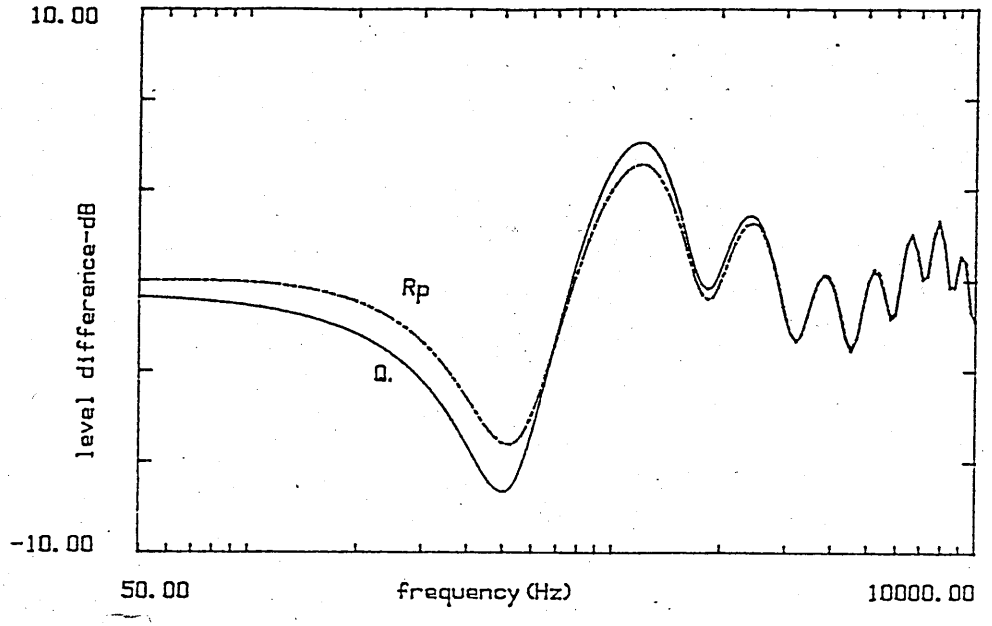

Figure 3.3 Error in Level Difference Prediction assuming Plane Wave Reflection Coefficient R_p compared to Spherical Wave Coefficient Q at Grazing Incidence, source height hs=0.44m, range r=1.75m, top microphone height hrt=0.55m, bottom microphone height hrb=0.1m,σ = 100000, Ω =0.44, T=1.0 sp=0.375.

Assuming plane waves and for a porous boundary the position of the first minimum will be located where

$$\Delta\phi^{\circ} = \frac{2\pi f \Delta r}{c_o} + \psi = \pi \tag{3.17}$$

where

ϕ= phase

c_0= speed of sound in air

Δr= path length difference between r_1 and r_2

f= frequency

and ψ= phase shift at the surface

where $\psi = \tan^{-1}\frac{a}{b}$ and reflection coefficient $= a + ib = R_p$

The first term $\frac{2\pi f \Delta r}{c_0}$ describes the phase change due to path length difference and ψ describes the phase change on reflection. From this the position of the frequency location and magnitude of the primary excess attenuation dip as shown in Equations 3.3 and 3.4, depends upon the angle of reflection and the acoustical impedance (Z).

3.4 Level Difference

The level difference technique has been discussed in Section 2.5.6. The pressure difference between two vertically separated microphones is equal to the total field at the top microphone minus the total field at the lower microphone. This can be expressed as

$$P\text{diff} = 20\log_{10}\left|\frac{r_1 t}{r_1 b}\left(\frac{\frac{e^{ik_o r_1 t}}{r_1 t} + \frac{Q_t e^{ik_o r_2 t}}{r_2 t}}{\frac{e^{ik_o r_1 b}}{r_1 b} + \frac{Q_b e^{ik_o r_2 b}}{r_2 b}}\right)\right| \tag{3.18}$$

where Q_t and Q_b are given by Equations 3.5,eqFw1 and eqw2loc with distances and angles appropriate to upper and lower receivers respectively. The lower microphones contribution is acting as the direct ray and eliminates the requirement to know the source characteristics relative to free field. Equation 3.18 is used to calculate all level difference measurements in this work. A typical experimental geometry is source height(hs) 0.44m, range(r) 1.75m, and microphone heights 0.44m top(hrt) and 0.1m at the bottom(hrb). The

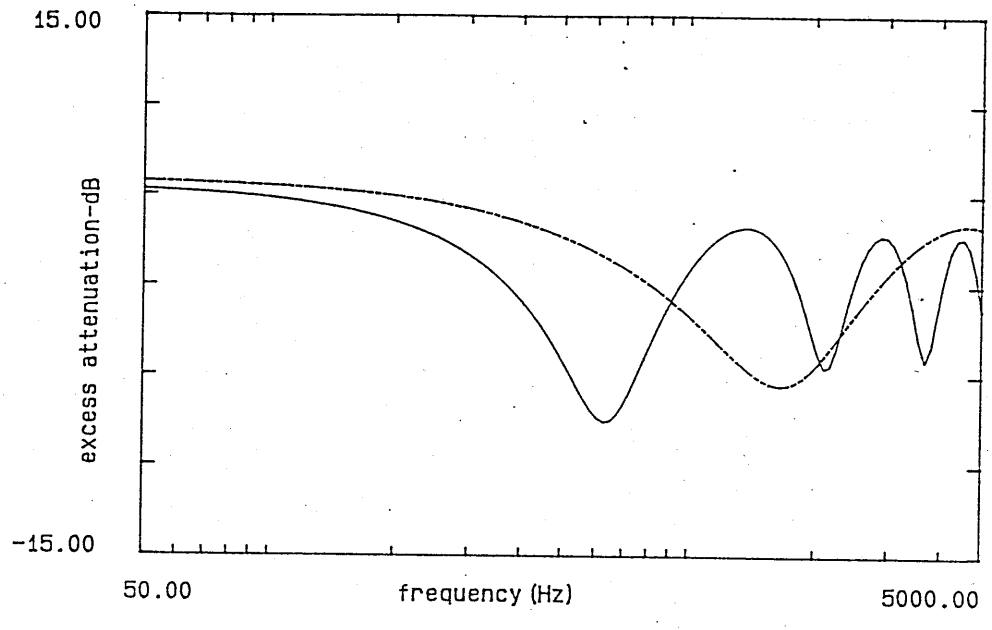

Figure 3.4 Excess attenuation spectra for two vertically separated microphones, hs=0.44m, r=1.75m, hrt=0.44m (continuous line) , hrb=0.1m (broken line), using a single parameter approximation (Equation 3.40), σ_e 50000mks rayls/m.

predicted excess attenuation spectrum at each microphone using a single parameter approximation (Equation 3.40) that requires a value of σ_e are presented in Figure 3.4. The geometries used are positioned such that the first minimum in the excess attenuation spectrum at the lower microphone is outside the frequency range of interest, so its contribution does not complicate the level difference spectrum unduly. Ideally the lower microphone should be position on the ground, where $r_2 = r_1$. In such a case there is no path length difference and its contribution can be considered as the direct ray. However microclimatic conditions are likely to involve steepest sound velocity gradients near the ground, Huisman et al [103], and the lower microphone was therefore usually located just above the ground surface.

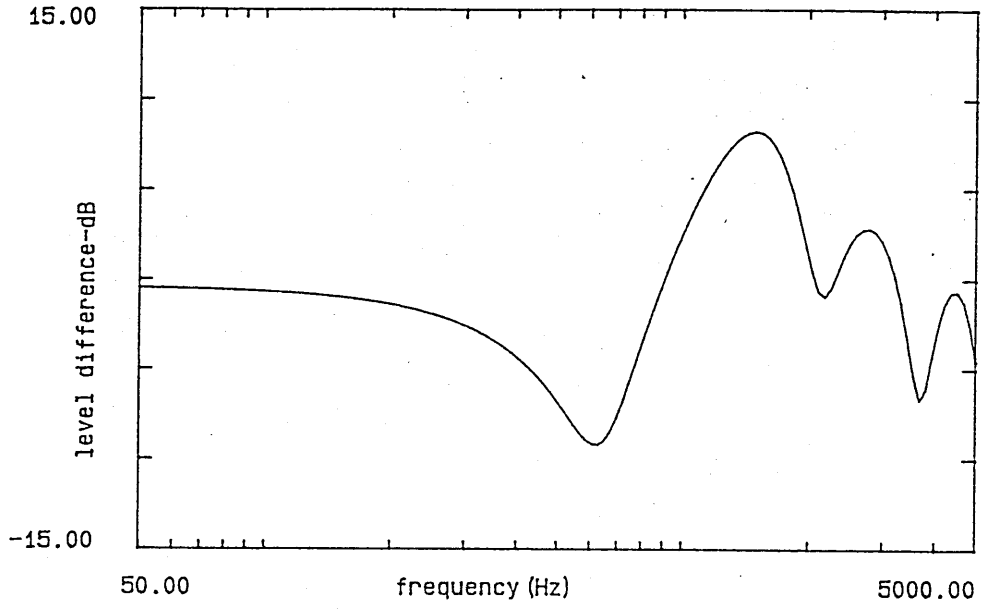

Figure 3.5 Reference Level Difference Spectrum for Two Vertically Separated Microphones, predicted using Equation 3.40, other heights, distances and flow resistivity parameters as for Figure 3.4.

The geometries chosen for level difference measurements except those in confined spaces (eg. the anechoic chamber) ensured that the frequency of the ground effect dip fell below 1KHz as shown in Figure 3.5. This enabled the use of low frequency/high flow resistivity approximation models for prediction of ground parameters. The position of the ground effect dip is not only influenced by geometry but also the ground impedance. Therefore preliminary experiments and predictions were made for most soil sites so that geometries were chosen that gave the best sensitivity in dip location for each soil type. Figure 3.5 is called the reference spectrum to which all the following predictions will be compared.

Figures 3.6 to 3.9 demonstrate the alteration to the reference spectrum when the geometry is changed. Source-receiver, separation and heights used

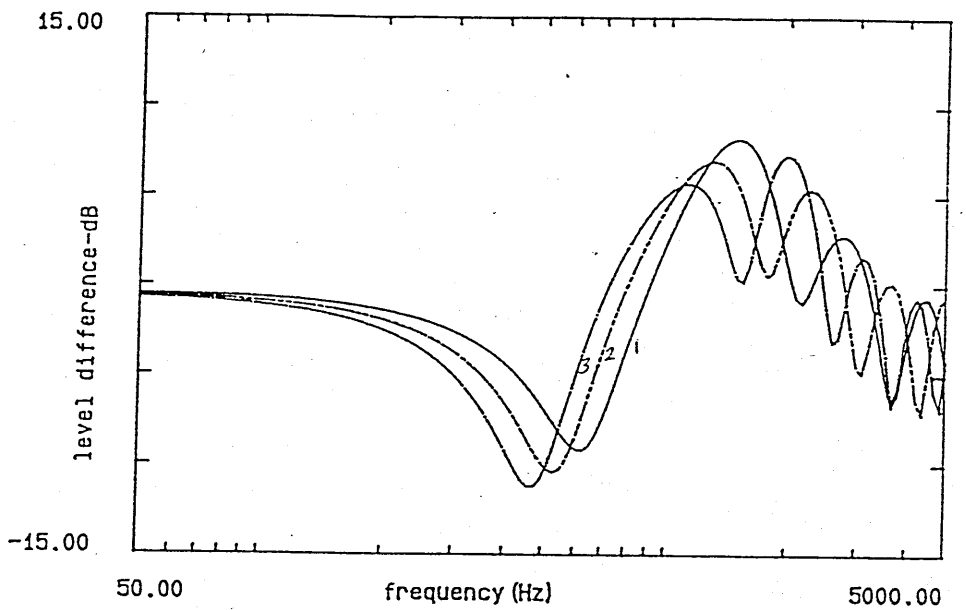

Figure 3.6 Effect of Raising Upper Microphone Height on Level Difference Spectrum, hrt=0.44m (1), 0.55m (2), 0.66m (3), predicted using Equation 3.40, other heights, distances and flow resistivity parameters as for Figure 3.4.

in the reference spectrum prediction have been changed by a 25% and 50% increase.

Figure 3.6 shows that when the top microphone height is increased the frequency location of the dip is lowered and the magnitude is increased. This is because r has been increased.

Figure 3.7 shows, by contrast, when the lower microphone is raised the primary dip location more or less remains static with only a slight decrease in the magnitude. This is because r is decreased.

Figure 3.8 shows primary dip movement to a higher frequency when the range is increased. As the range is extended the angle of incidence decreases and r_1 tends towards r_2.

Figure 3.9 shows the effect of raising the speaker height. The result is a

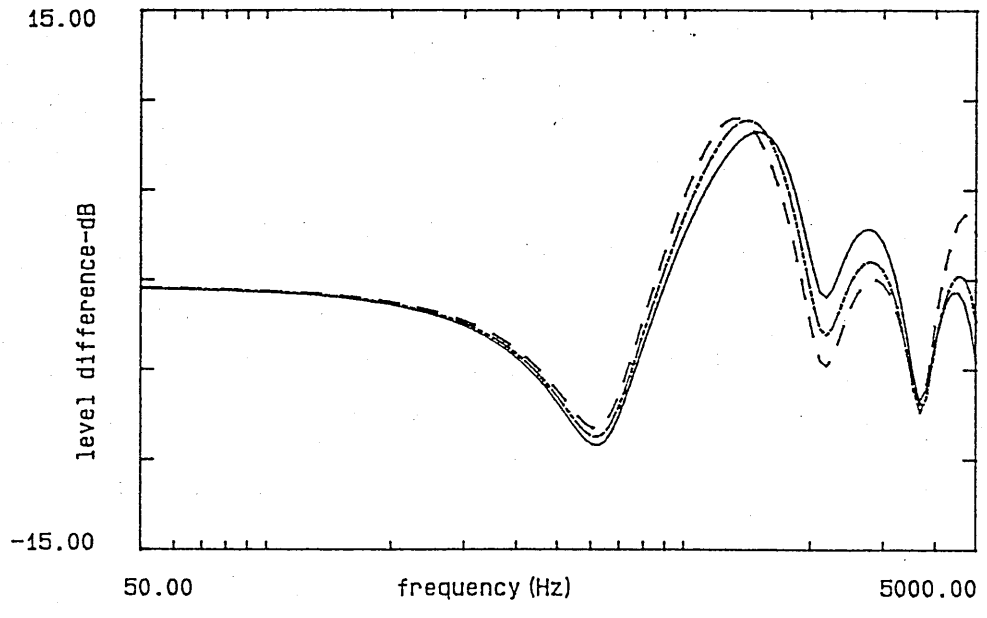

Figure 3.7 Effect of Raising Lower Microphone Height on Level Difference Spectrum, hrb=0.1m (solid), 0.12m (dashdot), 0.15m (dash), predicted using Equation 3.40, other heights, distances and flow resistivity parameters as for Figure 3.4.

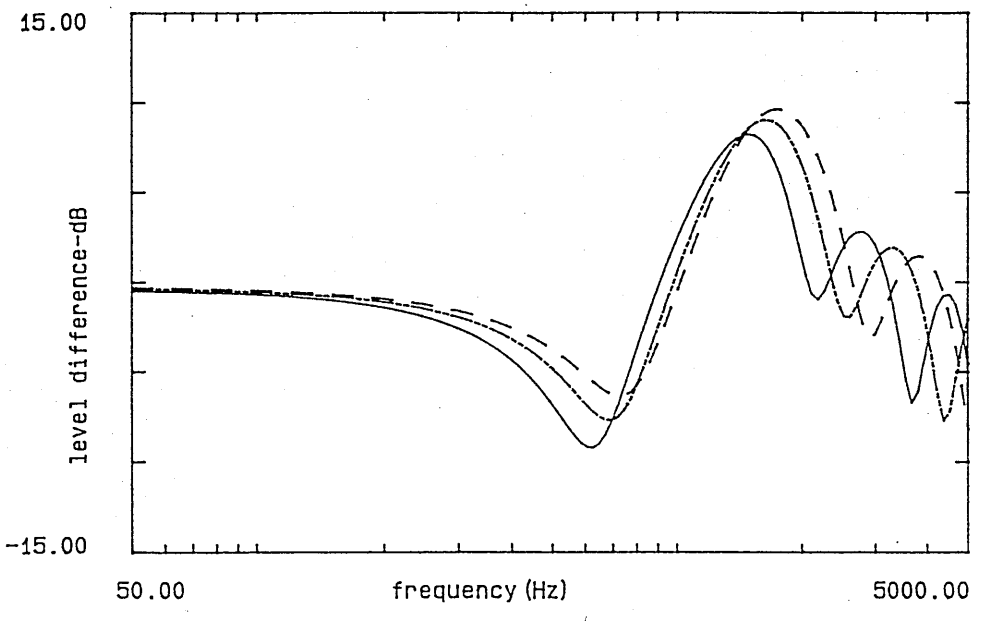

Figure 3.8 Effect of Increasing Range on Level Difference Spectrum, r=1.75m (solid), 2.18m (dashdot), 2.62m (dash), predicted using Equation 3.40, other heights, distances and flow resistivity parameters as for Figure 3.4.

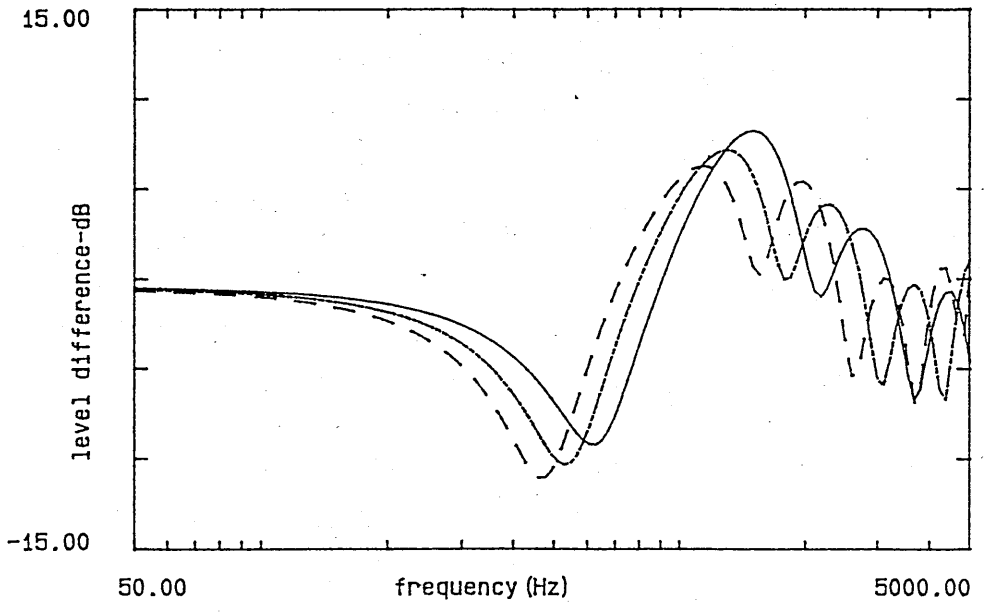

Figure 3.9 Effect of Raising Speaker Height on Level Difference Spectrum, hs=0.44m (solid), 0.55m (dashdot), 0.66m (dash), predicted using Equation 3.40, other heights, distances and flow resistivity parameters as for Figure 3.4.

similar pattern to that shown by raising the upper microphone and for the same reason r is increased.

The geometries used for this research are such that all angles of incidence are grazing angles. The range is short enough so that a relatively small area of soil can be studied, which has importance in agricultural applications. The short ranges reduce the influence of meterological conditions. On the other hand the range is sufficiently great that the source for the purpose of prediction is a point source.

A series of prediction curves shown in Figure 3.10 using the one parameter approximation, Equation 3.40in Section 3.6, demonstrates that for selected geometries the ground effect dip location is sensitive to impedance.

In Figure 3.10 the value of σ_e, the effective flow resistivity has been

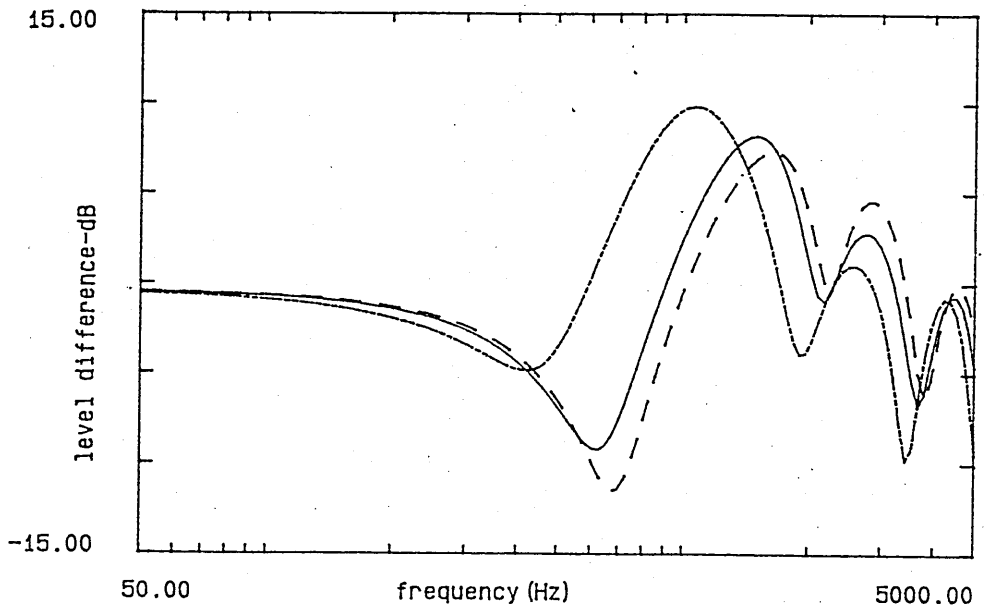

Figure 3.10 Effect of Increasing Effective Flow Resistivity on Level Difference Spectrum, geometry as for Figure 3.4, Flow resistivities(mks); 10000 dashdot, 50000 solid, 100000 dash.

incremented over a range expected for soils. The change in dip location and magnitude are large enough that distinction between different surfaces should be facilitated when comparing predicted and measured level difference spectra.

A series of prediction curves shown in Figures 3.11 and 3.12 , demonstrates how the ground effect dip location is sensitive to impedance using the three parameter approximation Equation 3.33.

Comparison of plots a and b in Figure 3.11 shows that the increase in tortuosity from 2 to 20 has very little effect on the location and magnitude of the ground effect dip for a high flow resistivity medium (100000mks rayls/m). However for a low flow resistivity medium (10000mks rayls/m), Figure 3.12a shows that when the tortuosity is fairly high (20) the frequency

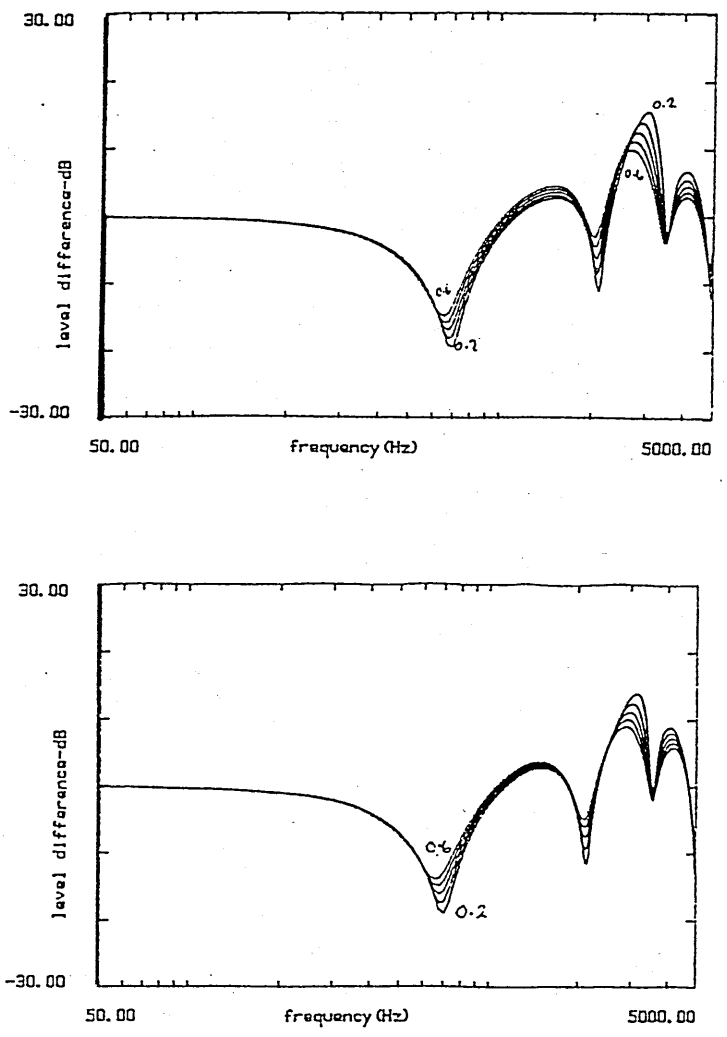

Figure 3.11 Sensitivity Analysis of Level Difference Spectrum using Three Parameter Approximation (Equation 3.33) showing effect of increasing Tortuosity and Porosity on a high flow resistivity medium, heights and distances as for Figure 3.4, a) Flow resistivity 100000, T=2.0, $\Omega = 0.2 - 0.6$ b) Flow resistivity 100000, T=20.0, $\Omega = 0.2 - 0.6$

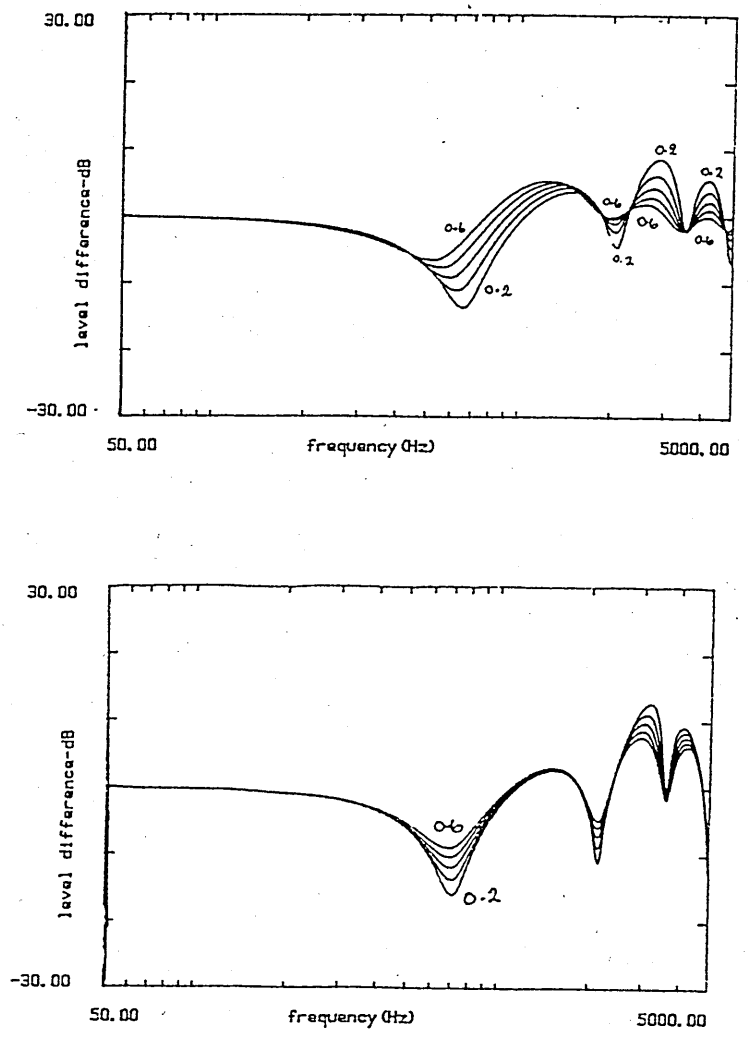

Figure 3.12 Sensitivity Analysis of Level Difference Spectrum using Three Parameter Approximation (Equation 3.33) showing effect of increasing Tortuosity and Porosity on a low flow resistivity medium, heights and distances as for Figure 3.4, a) Flow resistivity 10000, T=2.0, $\Omega = 0.2 - 0.6$ b) Flow resistivity 10000, T=20.0, $\Omega = 0.2 - 0.6$

location of the dip remains fairly constant but when the tortuosity is equal to 2.0 the frequency location of the dip is shifted depending on the porosity value. This would suggest that the tortuosity and porosity of the ground have a significant influence on the location of the level difference dip at low flow resistivities. At higher flow resistivities the influence of tortuosity is reduced, although porosity still influences the magnitude of the ground effect dip.

It has been stated earlier the extended reaction is assumed to be a more realistic description of sound propagation over and within snow 3.1. Figure 3.13 shows a level difference prediction using a four parameter model, discussed in Section 3.6 (Equations 3.30 and 3.31, and the same geometry as Figure 3.4 when the local and extended reactions are compared. With parameters similar to those expected for snow σ = 10000mks rayls/m, a porosity of 0.80, and with tortuosity and *sp*, a pore shape factor, set to 1.0 and 0.375, there is a large difference between the two prediction curves. When parameters similar to those expected for soil σ = 100000mks rayls/m, a porosity of 0.44, and the other two parameters remain constant, the two predictions curves coincide tolerably well Figure 3.14.

3.5 Theory of Sound Propagation through the Ground surface

Richards et al [84] give an approximation for the ratio of pressure at depth, received by a buried microphone, to the pressure received at the surface due to a point source above it as

$$\frac{P_b}{P_s} e^{i(\phi_b - \phi_s)} = \exp\left[ik_o d(n^2 - \sin^2\theta)^{0.5}\right] \tag{3.19}$$

where

P_b is amplitude pressure at depth d

P_s is amplitude pressure at surface

ϕ_b phase in soil at depth d in radians

ϕ_s phase in air at surface in radians

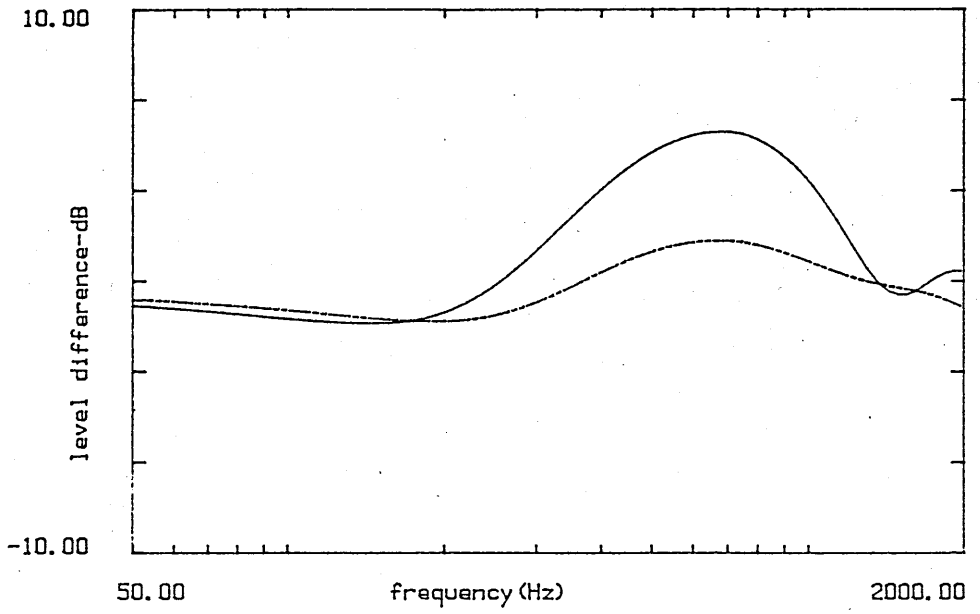

Figure 3.13 Effect of Local (solid) and Extended (dashdot) Reaction Assumption on Level Difference Spectrum over Snow, geometry as for Figure 3.4, Flow resistivity 10000mks, porosity 0.8, tortuosity 1.0, pore shape factor 0.375.

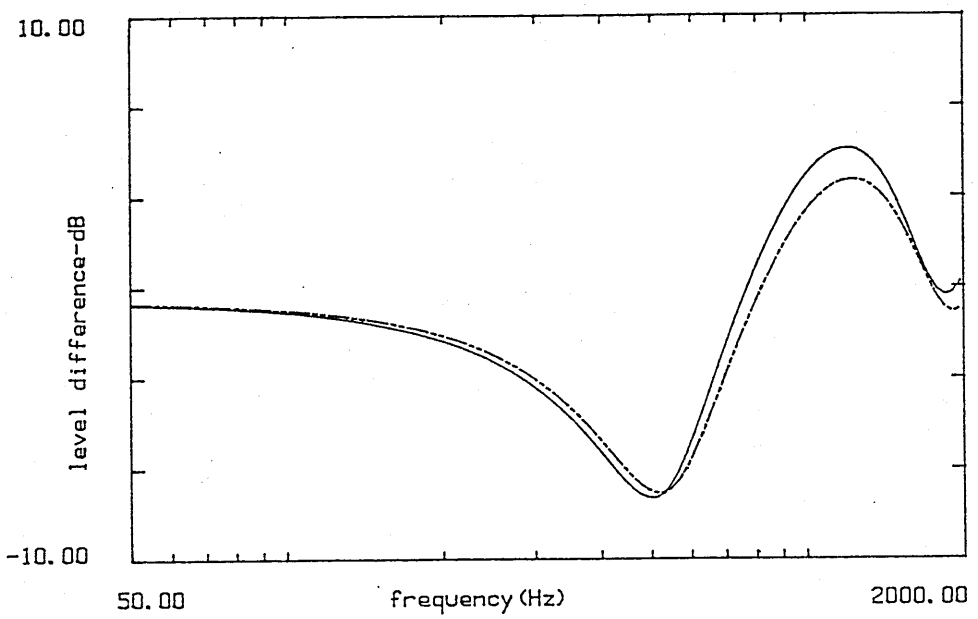

Figure 3.14 Effect of Local (solid) and Extended (dashdot) Reaction Assumption on Level Difference Spectrum over Soil, geometry as for Figure 3.4, Flow resistivity 100000mks, porosity 0.44, tortuosity 1.0, pore shape factor 0.375.

n refraction index $\frac{k_b}{k_o}$

θ angle of incidence in Figure 3.1.

d depth

k_o propagation constant in air

k_b propagation constant in ground

Equation 3.19 using $n^2 = {k_b}^2/{k_o}^2$ can be expressed as

$$\frac{P_b}{P_s}e^{i(\phi_b-\phi_s)} = \exp\left[id\left(k_b^2 - k_o^2\sin^2\theta\right)^{0.5}\right] \tag{3.20}$$

When $n^2 \gg 1$ as in a locally reacting situation then the $\sin^2\theta$ term can be neglected, hence, expressing the attenuation constant $k_b = a + ib$ equation 3.20 becomes

$$\frac{P_b}{P_s}e^{i(\phi_b-\phi_s)} = \exp[iad]\exp[-bd] = \exp[ik_bd] \tag{3.21}$$

From Equation 3.21 the attenuation with depth in dB can be expressed as

$$-\text{Atten} = 20\log_{10}|\exp(bd)|\,dB \tag{3.22}$$

and therefore

$$b = \frac{\text{Atten}\log_e 10}{20\,d} \tag{3.23}$$

From Equation 3.21 the phase constant may be related to the change in phase with depth by

$$a = \frac{\Delta\phi^{\text{rad}}}{d} = \frac{\pi\Delta\phi^{\circ}}{180\,d} \tag{3.24}$$

Where the medium is externally reacting it is necessary to write

$$h + ig = (k_b^2 - k_o^2\sin^2\theta)^{0.5} \tag{3.25}$$

if $k_b = a + ib$ then substituting into Equation 3.25 a can be expressed as

$$a^2 = \frac{p + \sqrt{p^2 + 4q}}{2} \tag{3.26}$$

where

$$q = h^2\,g^2 \tag{3.27}$$

and

$$p = h^2 - g^2 + (\frac{2\pi f}{c_0})^2 \sin^2\theta \tag{3.28}$$

and

$$b = \frac{gh}{a} \tag{3.29}$$

The determined values of a and b are then compared with prediction of k_b [2] as shown in Section 3.6.

3.6 Models for the Acoustical Characterisation of Porous Materials

The impedance models to predict ground parameters are presented here and their relative approximations and limitations discussed. In soils a good starting point for modelling is to assume homogeneity within the top few centimetres.

3.6.1 Models for Homogeneous Rigid Porous Materials

Attenborough [1] developed an impedance model based on theoretical analysis of the acoustic behaviour of rigid homogeneous, porous, granular materials. The model, called here the exact model, uses four physical parameters, flow resistivity σ, porosity Ω, a pore shape factor sp and a grain shape factor n'. Tortuosity q^2 can be calculated from the relationship $q^2 = \Omega^{-n'} = T$ The relative characteristic impedance is defined as

$$Z_c = \frac{\omega q^2}{k_b c_0 \Omega[1 - \frac{2}{Y}C(Y)]} \tag{3.30}$$

where

$$Y = \left(\frac{8\rho q^2 \omega}{\Omega \sigma sp^2}\right)^{0.5} \sqrt{i}$$

The normalised propagation constant is expressed as

$$\left(\frac{k_b}{k_o}\right)^2 = q^2\left[\frac{1+2(\frac{\gamma-1}{Y\sqrt{Npr}})C(Y\sqrt{Npr})}{1-\frac{2}{Y}C(Y)}\right] \tag{3.31}$$

where

$$C(x) = \frac{J_1(x)}{J_0(x)}$$

and

f=frequency

c_0 = speed of sound in air

Npr = Prandtl number in air

ρ = density of air

γ = ratio of specific heats

$J_1(x)$, $J_0(x)$ = First and Zeroth order Bessel Functions

k_b = bulk propagation constant

$k_o = 2\pi f/c_o$

The pore shape factor, sp gives a numerical value to the departure of the pore cross section from that of a circular cylinder. Extreme pore shapes were considered to be that of a circular capillary and of a parallel-sided slit of infinite extent. This gives a range of extremes of 0.5 - 0.25 The lower limiting value has been found appropriate for lead shot and sand where the grains are nearly spherical, whereas values for middle and upper range have been found to give best fits to acoustic data for various soils [82]. The value of the grain shape factor can range from 0.5 for the packing of spherical particles to 9.0 for the packing of flat mica chips. A value of n' for soil crumbs has found to be 1.0 [1].

A three parameter approximation of the four parameter model can be expressed

$$k_b = \sqrt{\gamma}\left[(\frac{4}{3} - \frac{\gamma-1}{\gamma}Npr)T + i\frac{2\sigma_{pe}}{\pi\rho_0 f}\right]^{0.5}(\frac{2\pi f}{c_0}) \tag{3.32}$$

and

$$Z_c = \frac{1}{k_b}\left[\frac{4}{3}\left[\frac{T}{\Omega}\right] + i\frac{2\sigma_{pe}}{\pi\rho_0 f}\right]\left(\frac{2\pi f}{c_0}\right) \tag{3.33}$$

where σ_{pe} is equal to a combination of $sp^2\sigma\Omega$, T is the tortuosity($= q^2$) and Ω the porosity. The three parameter approximation best approximates Equations 3.30 and 3.31 at low frequencies and using high flow resistivities. Equations 3.32 and 3.33 can be simplified following the further approximation that $4/3 \gg \frac{\gamma-1}{\gamma Npr}$ to

$$k_b = 0.0079\sqrt{f}\,[8.14\,T\,f + i4\sigma_{pe}]^{0.5} \tag{3.34}$$

and

$$Z_c = \frac{\rho_b\,(2\pi\,f)}{k_b\,\rho_0\,c_0} \tag{3.35}$$

where ρ_b is the complex density and is equal to

$$\rho_b = \frac{1}{\Omega}\left[\frac{4}{3}\,\rho_0\,T + i\frac{2\sigma_e}{\pi\,f}\right] \tag{3.36}$$

by assuming values of $c_0 = 343$m/sec, and the density of air as $\rho_0 = 1.2kg/m^3$ at $20°C$. For snow the speed of sound in air at$-5°C$ was taken as 328m/sec, with the density of air as $\rho_0 = 1.317kg/m^3$. Therefore the value of 8.14 in Equation 3.34 is recalculated to a value of 9.10.

This three parameter approximation was used for the main part of the reported analysis on soil and snow characterisation. The bulk propagation constant k_b was predicted for soils, and snow using extended reaction, using Equation 3.34, which enables the deduction of σ_{pe} and T from

$$Real(k_b^2) = \left(6.241^{-5}\right)\left(8.14Tf^2\right) \tag{3.37}$$

and

$$Imag(k_b^2) = \left(6.241^{-5}\right)(4\sigma_{pe}\,f) \tag{3.38}$$

A more severe approximation of Equation 3.30 is a one parameter approximation which expresses impedance in terms of only the effective flow resistivity. This is a very low frequency/very high flow resistivity approximation and can be expressed.

$$Z_c = (\pi\gamma\rho_0)^{-0.5}\left(\frac{\sigma_e}{f}\right)^{0.5}(1+i) \tag{3.39}$$

or

$$Z_c = 0.436 \left(\frac{\sigma_e}{f}\right)^{0.5} (1+i) \tag{3.40}$$

This approximation has equal real and imaginary parts and, the bulk propagation constant k_b can be written as

$$a \text{ or } b = 0.0112 \left(\Omega^2 \sigma_e\right)^{0.5} \sqrt{f}(1+i) \tag{3.41}$$

which includes an additional parameter porosity Ω. From Equation 3.41 the attenuation/cm in dB can be predicted from

$$\text{attenuation per cm} = 0.00097(\Omega^2\sigma_e)^{0.5}\sqrt{f} \tag{3.42}$$

The severe approximation in Equations 3.40 and 3.41 was used in analysis of preliminary experiments being the simplest available. They were also used in Equation 3.45 for simplicity in modelling a layered soil, as shown in Section 3.6.3. However as shown in the following paragraphs it is too severe to be useful on homogeneous cultivated soils. The propagation constant modelled as having equal real and imaginary parts $a = b$ meant that information on soil structure was potentially lost, since the difference between a and b includes information on tortuosity. However an approximation procedure for the deduction of σ_{pe} and T, from attenuation measurements only, has been used for one set of measurements on sand. This is explained in detail in Section 4.4.4.

3.6.2 Comparison of homogeneous impedance models

Figures 3.15,3.16 and 3.17 show impedance predictions using the four parameter model and the three and one parameter approximations. A list of input parameters are shown Table 3.1. With a low flow resistivity material accuracy of the three and one parameter approximations is better at low frequencies, particularly below 1kHz. The three parameter approximation is always a better approximation than the one parameter approximation. Figures 3.16 and 3.17 indicate as flow resistivity increases the difference between the exact model and the approximations becomes less, particularly in the mid and high frequency ranges. The approximations are closer to the

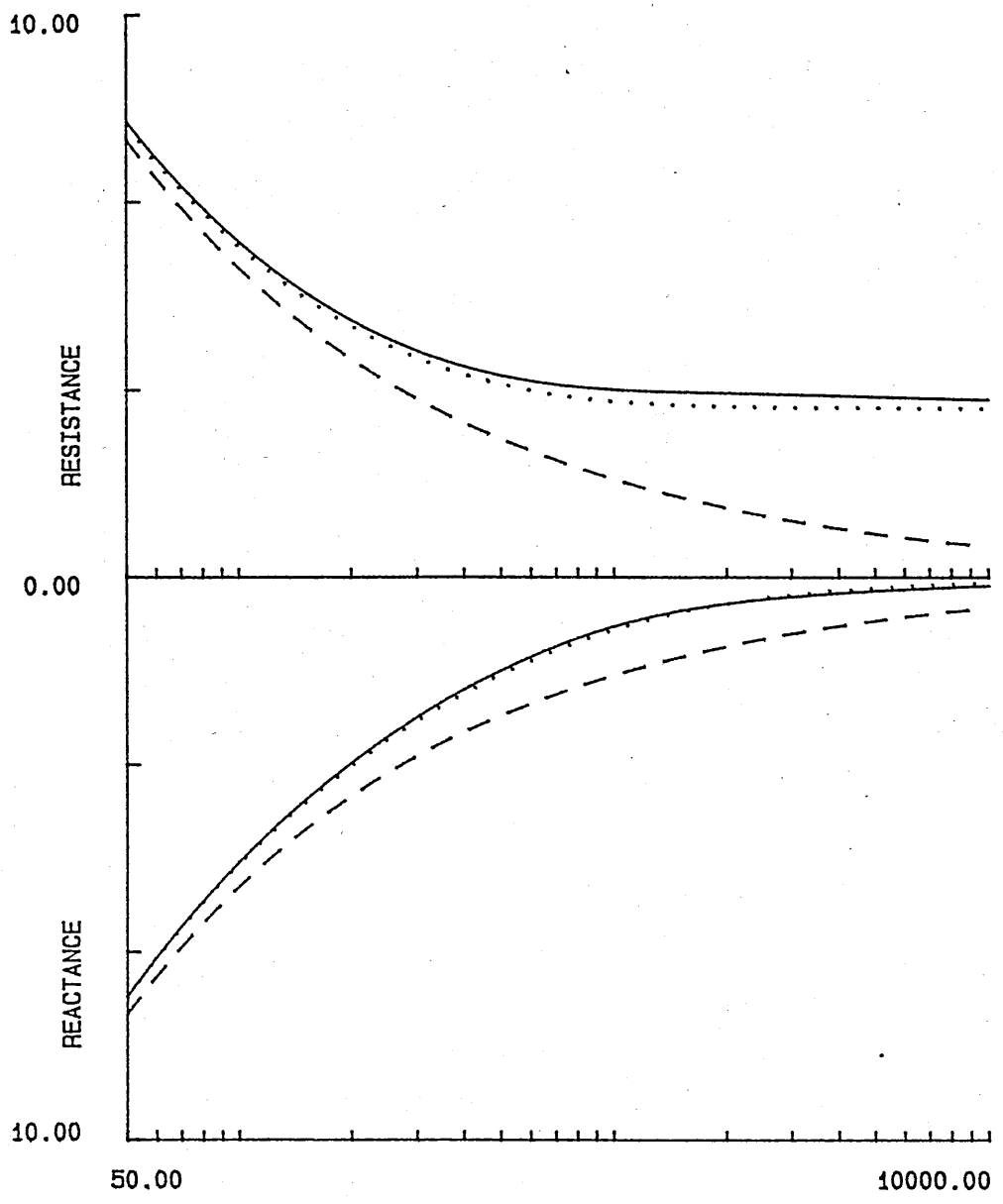

Figure 3.15 Comparison of Impedance Predictions from the Exact model Eqn 3.30(solid), and the 3 parameter Eqn 3.33 (dot), and 1 parameter Eqn 3.40 approximations (dash), assuming Homogeneity of the Ground Surface - Case 1 Low Flow Resistivity 50000mks.

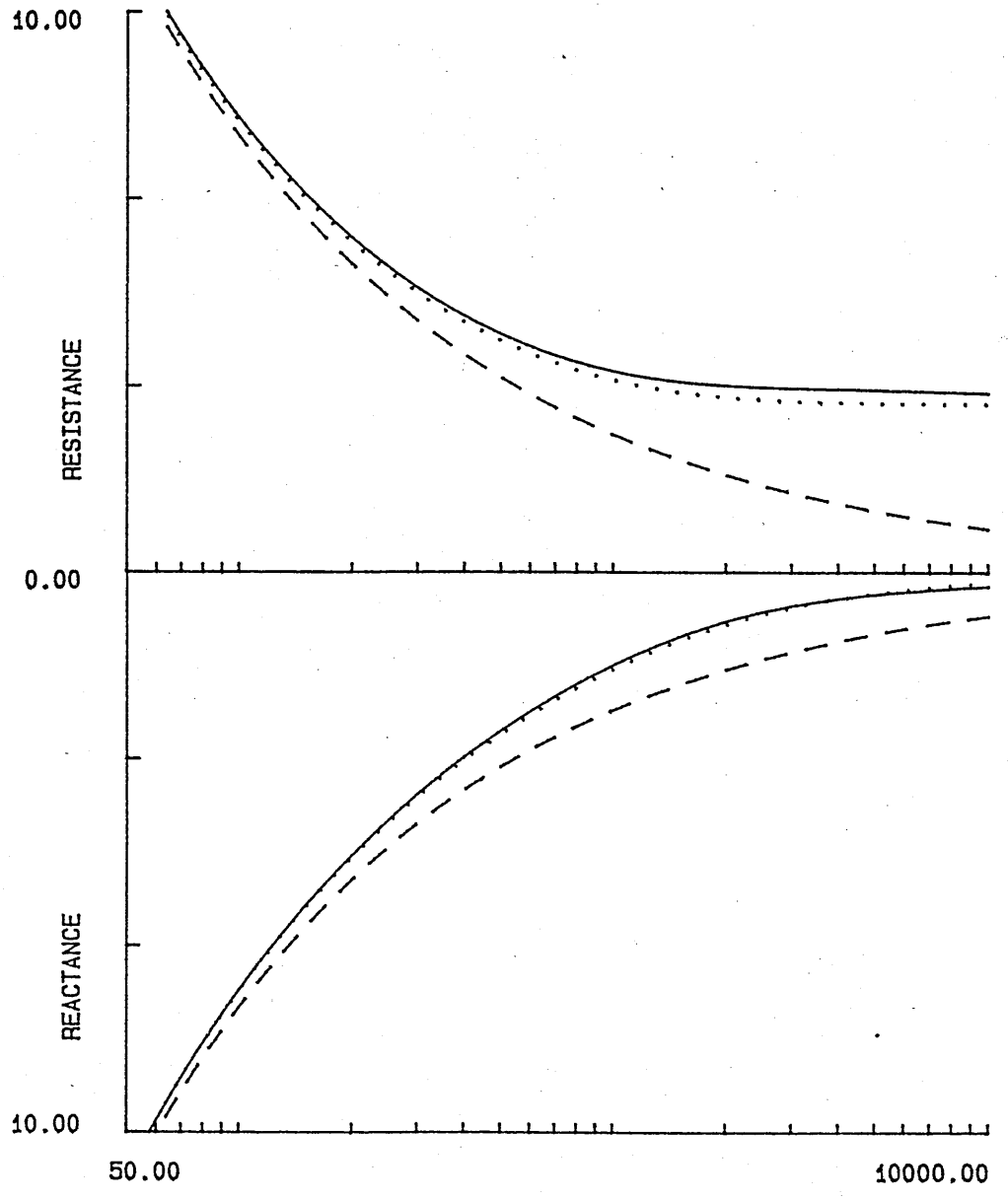

Figure 3.16 Comparison of Impedance Predictions from the Exact model Eqn 3.30(solid), and the 3 parameter Eqn 3.33 (dot), and 1 parameter Eqn 3.40 approximations (dash), assuming Homogeneity of the Ground Surface - Case 2 Medium Flow Resistivity, 100000mks.

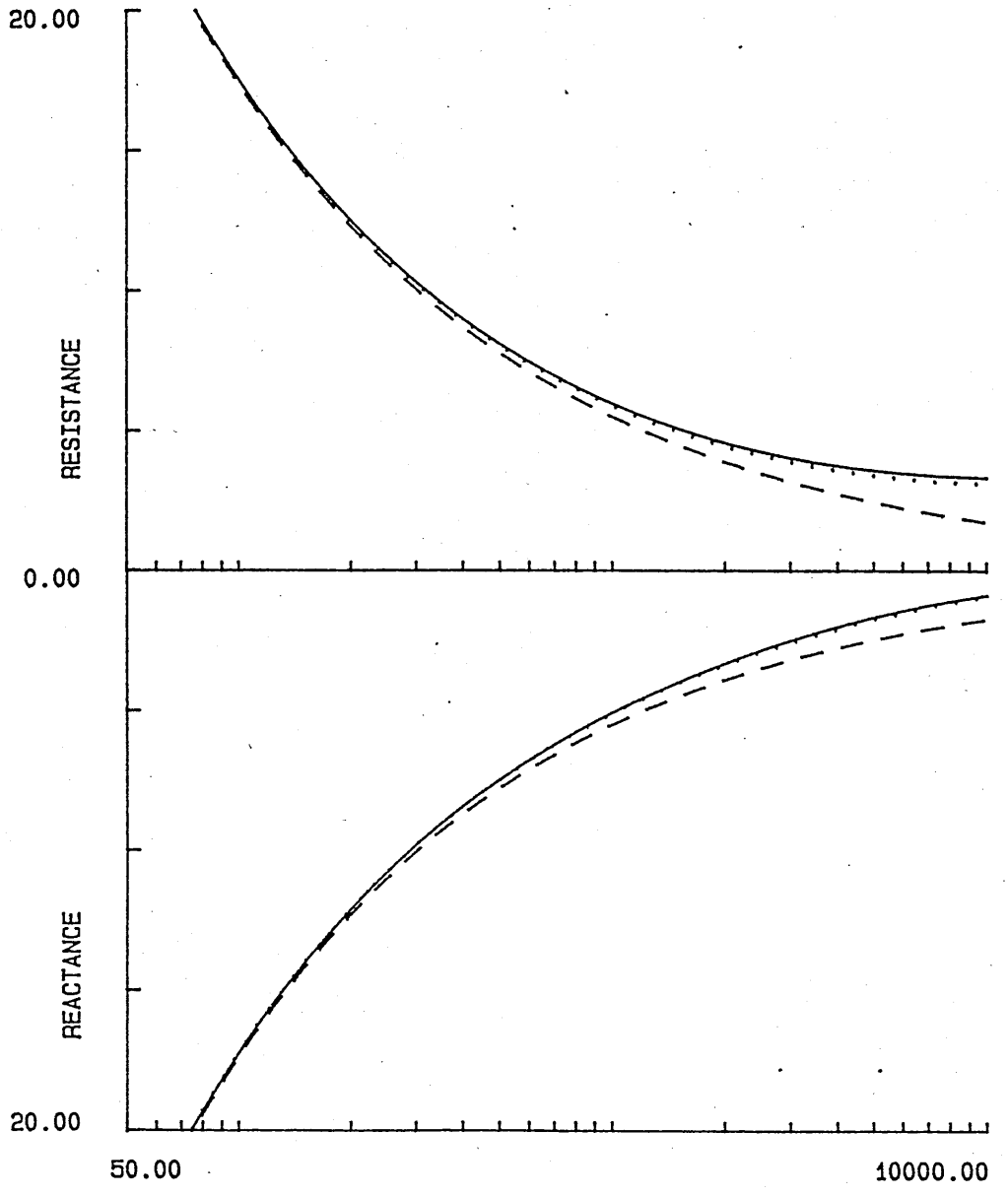

Figure 3.17 Comparison of Impedance Predictions from the Exact model Eqn 3.30(solid), and the 3 parameter Eqn 3.33 (dot), and 1 parameter Eqn 3.40 approximations (dash), assuming Homogeneity of the Ground Surface - Case 3 High Flow Resistivity 500000mks.

Table 3.1 Parameters used in Predictions to compare the Exact (4 parameter) Impedance Model with the Three Parameter and One Parameter Approximations over low, medium and high flow resistivity grounds.

Flow Resistivity	Model	σ	σ_e	Ω	sp	T	σ_{pe}
Low	Exact	50000		0.44	0.375	1.5	
	Three parameter			0.44		1.5	3080
	One parameter		15909	0.44			
Medium	Exact	100000		0.44	0.375	1.5	
	Three parameter			0.44		1.5	6160
	One parameter		31818	0.44			
High	Exact	500000		0.44	0.375	1.5	
	Three parameter			0.44		1.5	30800
	One parameter		159090	0.44			

exact model in the imaginary part than the real part at all frequencies and for all flow resistivities.

Figures 3.18, 3.19 and 3.20 show three corresponding families of prediction curves this time for level difference which shows indirectly the adequacy of the three and one parameter approximations for Z_C.

The geometry used is typical of the short range measurements in this work hs=0.44m, r=1.75m, hrt=0.55m, hrb=0.1m. At low flow resistivities, the one parameter approximation tends to under predict the frequency location and the magnitude of the ground effect dip and seriously over predict the magnitude of the first peak. As expected the difference between predictions becomes less as flow resistivity increases. It was rare that any soils analysed represented such high effective flow resistivities $\approx$160000mks rayls/m. The uncertainty at low flow resistivities of the one parameter approximation and a desire to deduce more physical parameters, which could be checked using conventional soil surveying techniques led to the choice of the three parameter approximation model to fit acoustically measured data. The three parameter approximation is more convenient than the four parameter model and the prediction curve lies very close to that of the four

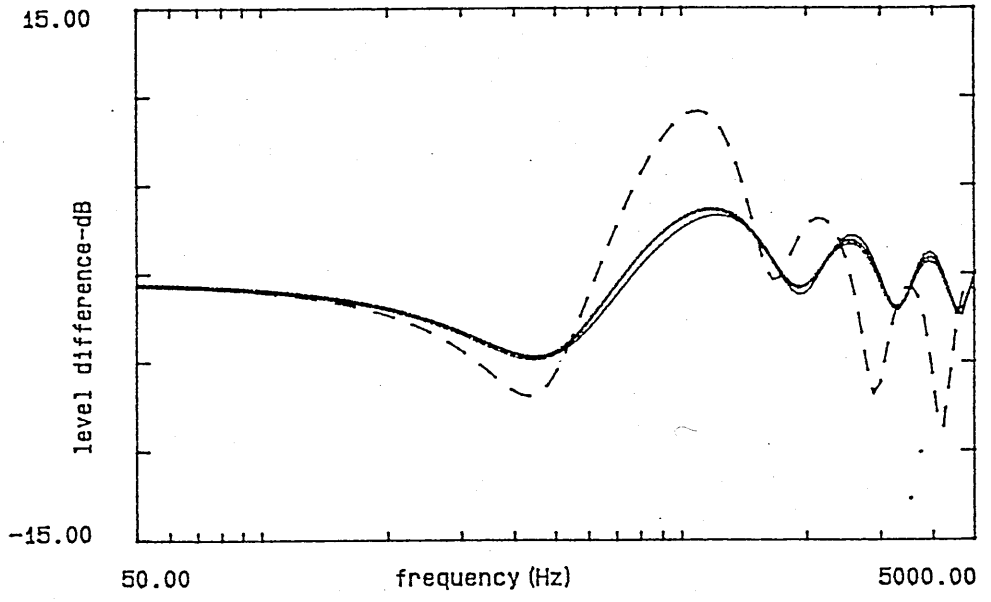

Figure 3.18 Comparison of Level Difference Predictions from the Exact model Eqn 3.30(solid), and the 3 parameter Eqn 3.33 (dashdot), and 1 parameter Eqn 3.40 approximations (dash), assuming Homogeneity of the Ground Surface - Case 1 Low Flow Resistivity 50000mks.

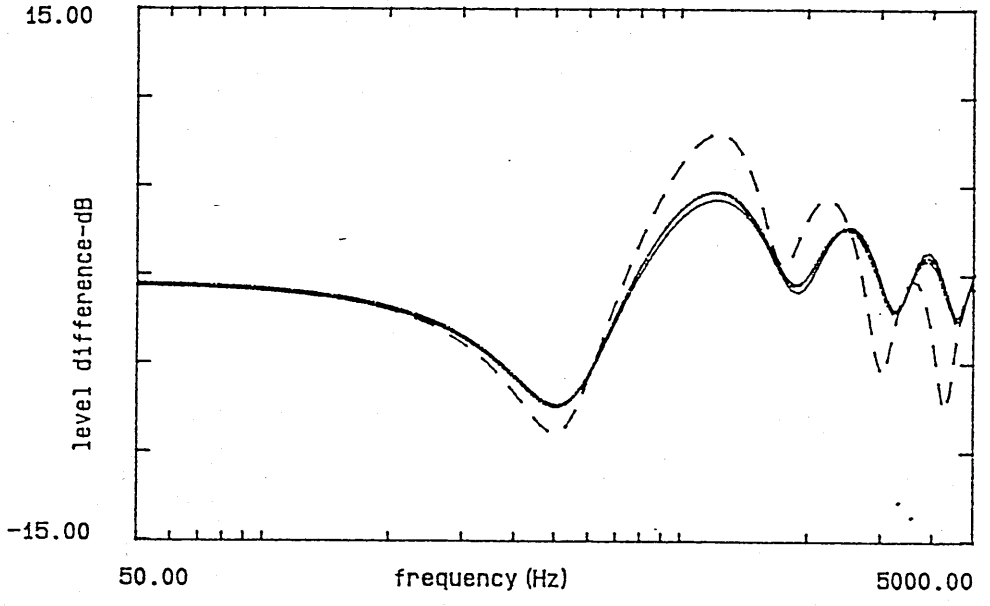

Figure 3.19 Comparison of Level Difference Predictions from the Exact model Eqn 3.30(solid), and the 3 parameter Eqn 3.33 (dashdot), and 1 parameter Eqn 3.40 approximations (dash), assuming Homogeneity of the Ground Surface - Case 2 Medium Flow Resistivity, 100000mks.

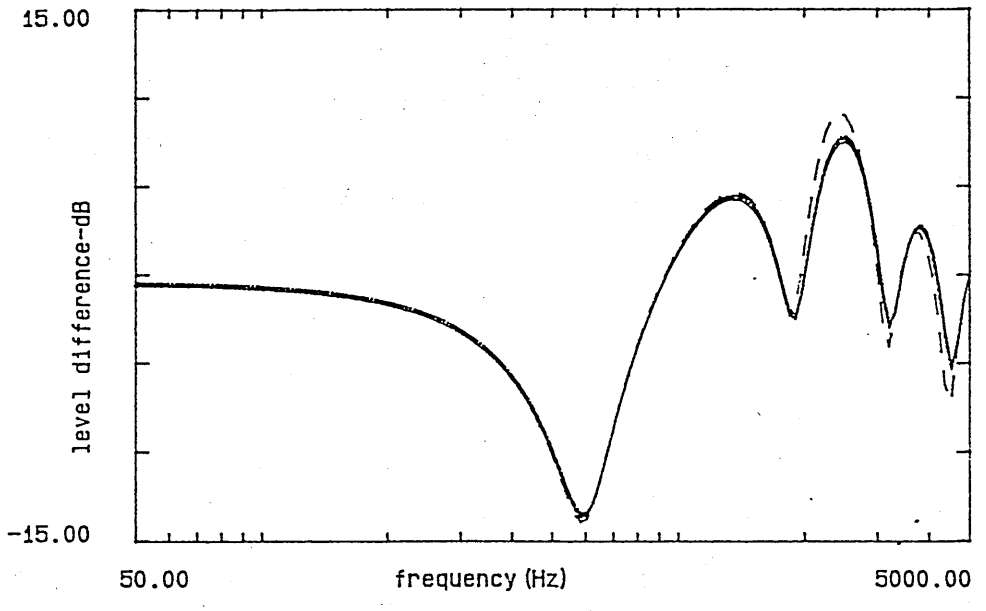

Figure 3.20 Comparison of Level Difference Predictions from the Exact model Eqn 3.30(solid), and the 3 parameter Eqn 3.33 (dashdot), and 1 parameter Eqn 3.40 approximations (dash), assuming Homogeneity of the Ground Surface - Case 3 High Flow Resistivity 500000mks.

parameter model for an appropriate range of flow resistivities.

Figures 3.21, 3.22 and 3.23 show comparisons of the complex propagation constant predicted by the four parameter model and the three and one parameter approximations for the low, medium and high flow resistivities mentioned in Table 3.1. In Figure 3.21, the three parameter approximation over predicts the real part (a) above 3kHz and under predicts the imaginary part (b) beyond 1.5kHz. The dashed line shows the one parameter approximation with equal real and imaginary parts. Figures 3.22 and 3.23 show the familiar pattern that as flow resistivity increases so the approximations are more exact up to a higher frequency and all the prediction curves move closer together.

For low flow resistivity media like snow the three parameter low frequency/high flow resistivity approximation proved adequate up to 1KHz. Above this frequency a high frequency/low flow resistivity approximation was used, after Attenborough and Buser [96], where the propagation constant is characterised in terms of σ_{pe} and T.

$$kb = \frac{T\left(\frac{2\pi f}{c_0}\right)\left[1+2\sqrt{i}\left(\frac{\sigma_{pe}}{4\pi\rho_0 T f}\right)^{0.5}\right]^{0.5}}{\left[1-2\sqrt{i}\frac{\gamma-1}{\sqrt{Npr}}\left(\frac{\sigma_{pe}}{4\pi\rho_0 T f}\right)^{0.5}\right]^{0.5}} \tag{3.43}$$

and where the characteristic impedance includes the additional term porosity Ω

$$Z_c = \left(\frac{\sqrt{T}}{\Omega}\right)\frac{[1+\sqrt{2}(1+i)(\frac{\sigma_{pe}}{4\pi\rho_0 T f})^{0.5}]^{0.5}}{[1+(\gamma-1)\frac{\sqrt{2}}{\sqrt{Npr}}(1+i)(\frac{\sigma_{pe}}{4\pi\rho_0 T f})^{0.5}]^{0.5}} \tag{3.44}$$

Figures 3.24 and 3.25 show Equation 3.43 has closer agreement to the exact model at higher frequencies and lower effective flow resistivities (16000 and 32000mks rayls/m), both in the real and imaginary parts.

Figure 3.26 shows the deviation away from the exact model at high flow resistivities 160000mks rayls/m. From studying Figures 3.24, 3.25 and 3.26 it is clear that Equation 3.34 is suitable for fitting the measured propagation constant over the entire frequency range of interest <4KHz on soils. On snow this model may only be used up to 1KHz and above this Equation 3.43 must

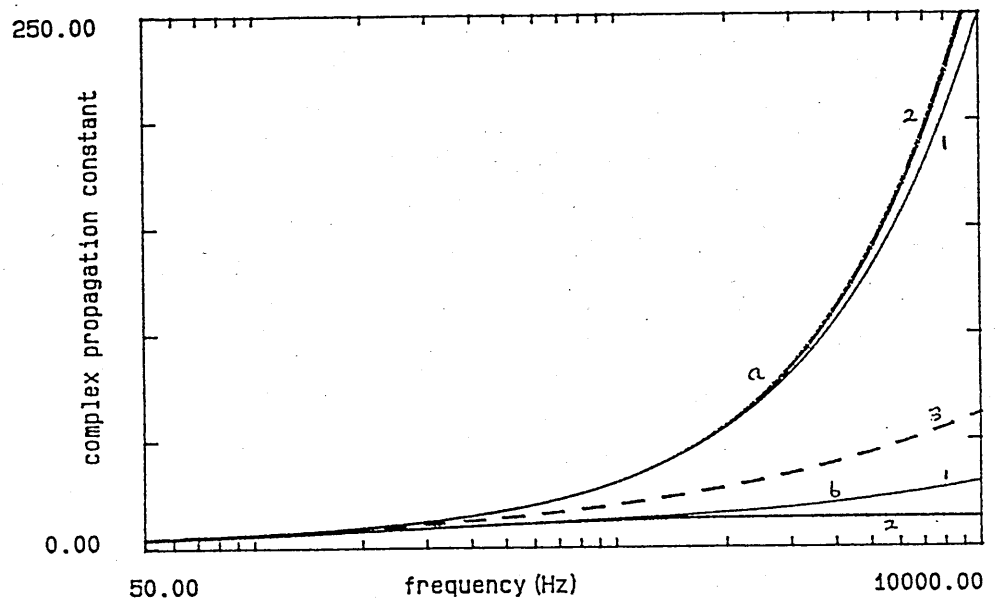

Figure 3.21 Comparison of Propagation Constant Predictions from the Exact model Eqn 3.31(solid), and the 3 parameter Eqn 3.34 (dashdot), and 1 parameter Eqn 3.41 (dash) approximations, assuming Homogeneity of the Ground Surface - Case 1 Low Flow Resistivity 50000mks (a)real part (b)imaginary part.

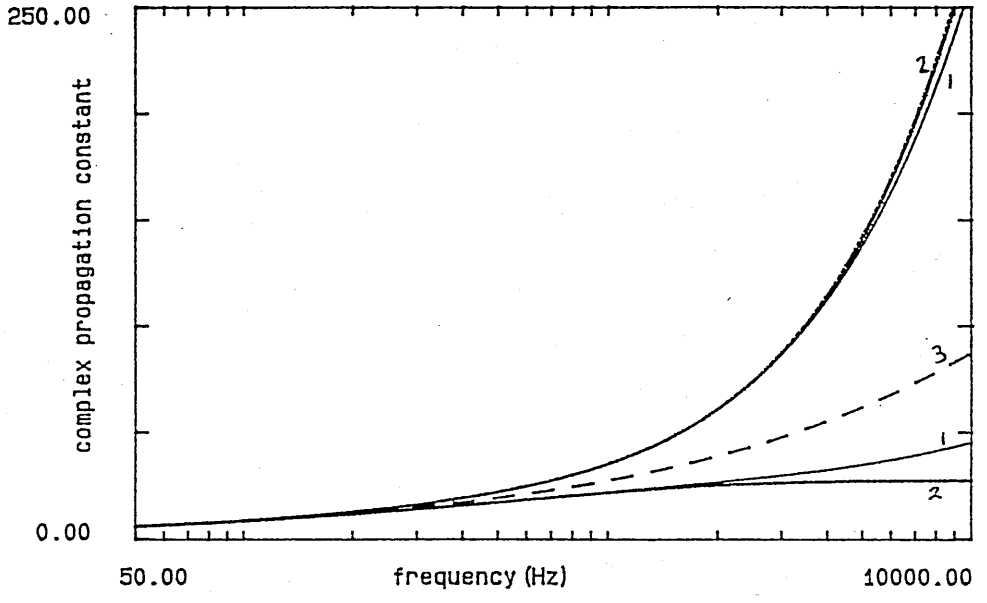

Figure 3.22 Comparison of Propagation Constant Predictions from the Exact model Eqn 3.31(solid), and the 3 parameter Eqn 3.34 (dashdot), and 1 parameter Eqn 3.41 (dash) approximations, assuming Homogeneity of the Ground Surface - Case 2 Medium Flow Resistivity, 100000mks.

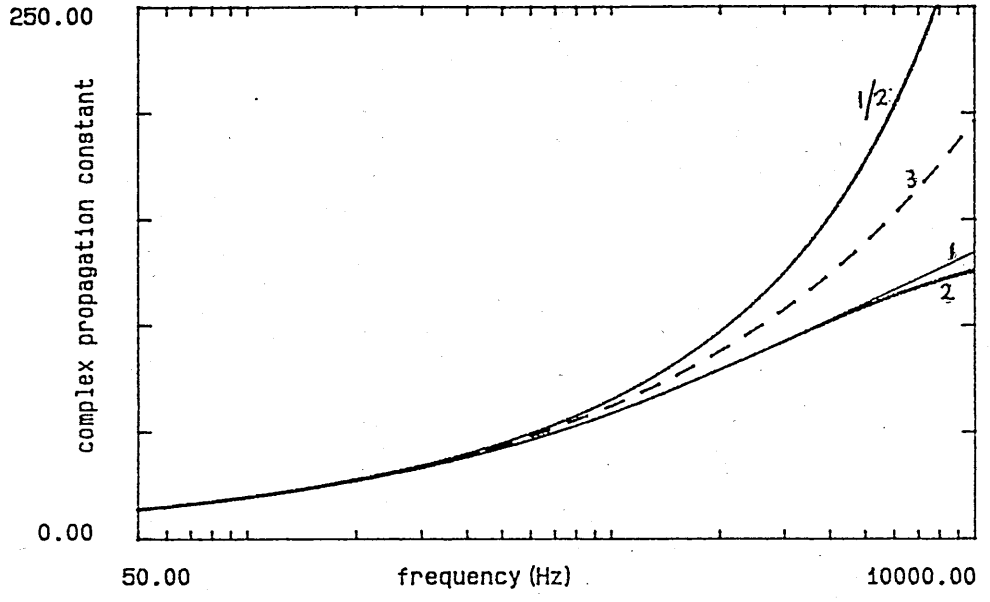

Figure 3.23 Comparison of Propagation Constant Predictions from the Exact model Eqn 3.31(solid), and the 3 parameter Eqn 3.34 (dashdot), and 1 parameter Eqn 3.41 (dash) approximations, assuming Homogeneity of the Ground Surface - Case 3 High Flow Resistivity 500000mks.

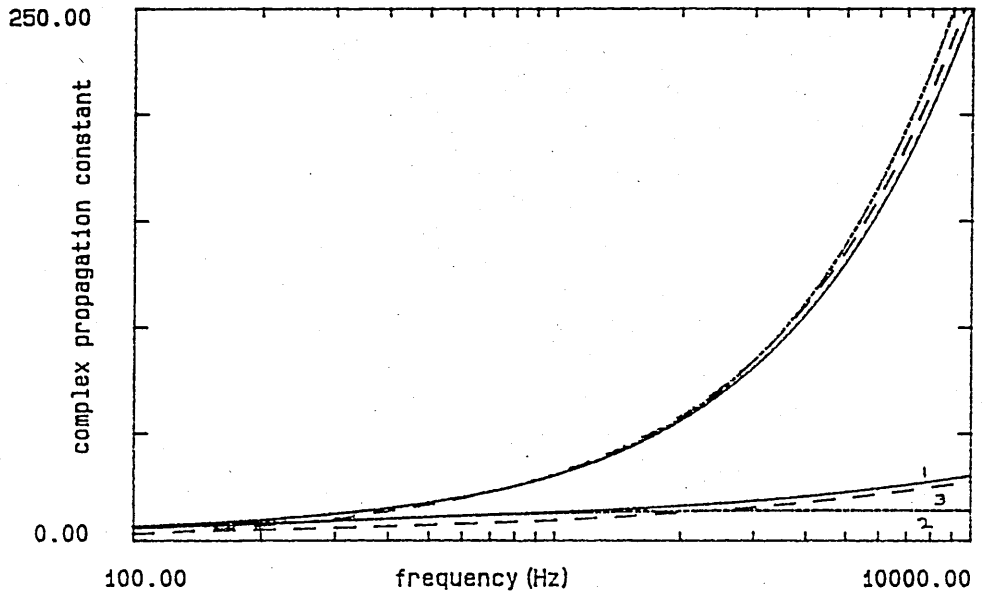

Figure 3.24 Predicted Propagation Constants compared for a Four Parameter Impedance Model (1)(Eqn 3.31), a low frequency/high flow resistivity approximation (2)(Eqn 3.34) and a high frequency/low flow resistivity approximation (3)(Eqn 3.43) - all assuming homogeneity of the medium Case 1 Low Flow Resistivity 50000mks.

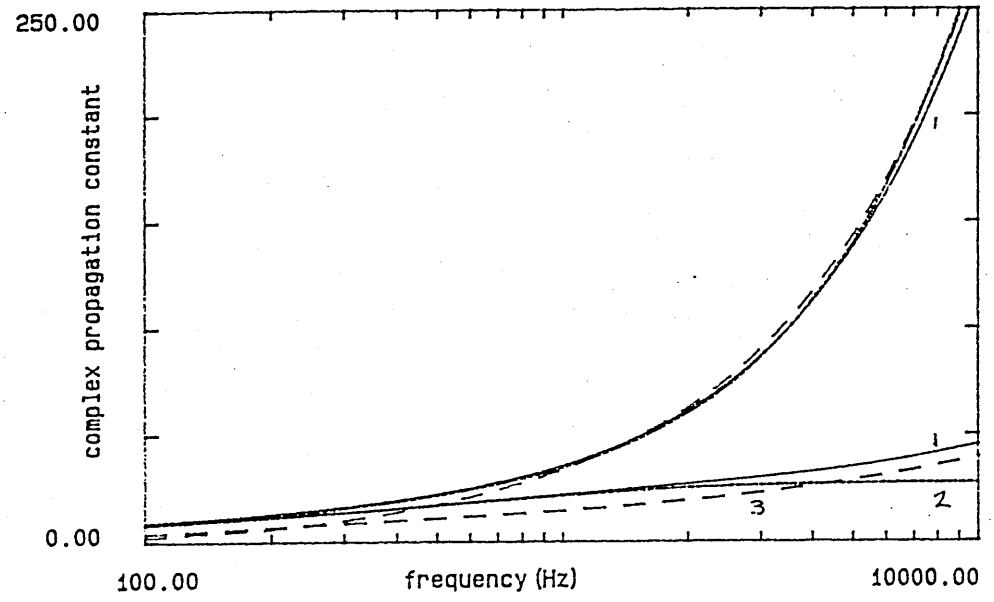

Figure 3.25 Predicted Propagation Constants compared for a Four Parameter Impedance Model (1), (Eqn 3.31), a low frequency/high flow resistivity approximation (2)(Eqn 3.34) and a high frequency/low flow resistivity approximation (3)(Eqn 3.43)- all assuming homogeneity of the medium, Case 2 Medium Flow Resistivity 100000mks.

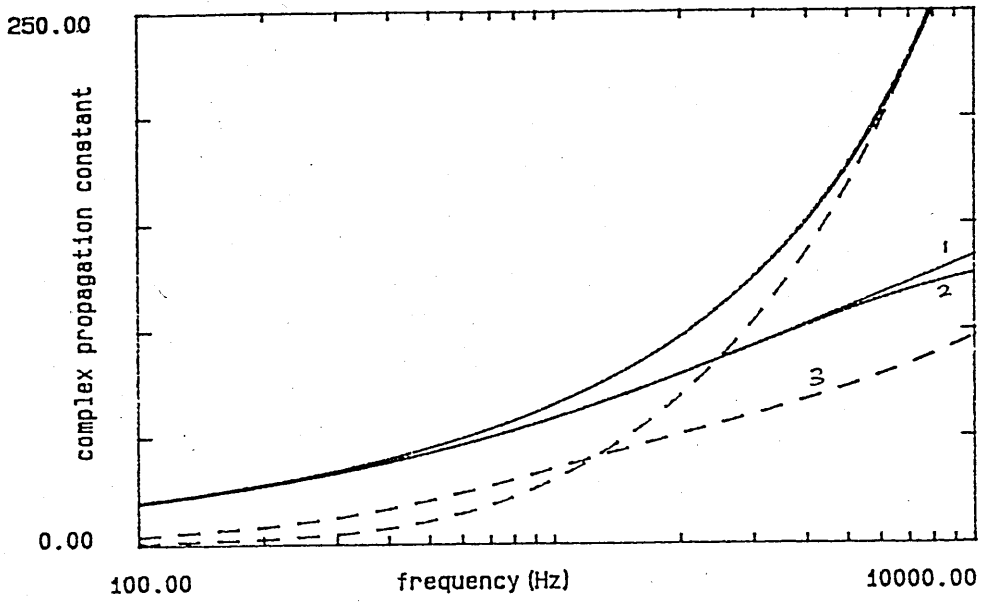

Figure 3.26 Predicted Propagation Constants compared for a Four Parameter Impedance Model (1), (Equation 3.31), a low frequency/high flow resistivity approximation (2)(Equation 3.34) and a high frequency/low flow resistivity approximation (3)(Equation 3.43)- all assuming homogeneity of the medium, Case 3 High Flow Resistivity 500000mks.

be used.

3.6.3 Multi-layered models

The assumption of soil homogeneity within the top few centimeters below the surface is not unreasonable where cultivation practises keep the soil turned over. Another model available for characterising impedance in terms of soil parameters was a variable porosity model [41]. It was thought unlikely that cultivated soil would exhibit an exponential decrease in porosity with depth which the model assumes. Therefore this model was not used. Some soils do, however, exhibit a layered structure. For example surface capping, saturated surface layers or forest floors with a litter and humus layer over a mineral soil. A multiple layer model was used in some instances to offer a more realistic prediction. According to the formulae presented by Brekhovshikh [104] the surface impedance Z_s of a two-layered fluid is given by

$$Z_s = Z_1 \left(\frac{Z_2 - iZ_1 \tan(k_b d)}{Z_1 - iZ_2 \tan(k_b d)} \right) \tag{3.45}$$

where
Z_1 is the normalised surface impedance of the upper porous layer
Z_2 is the normalised impedance of the lower porous halfspace
k_b is the bulk propagation constant in the upper layer
d is the depth of the upper layer

The model can be used for n layers but here for simplicity it was confined to two possible profiles. First, a high flow resistivity, low porosity layer over a more porous medium, a hard/soft case, and secondly, a low flow resistivity, highly porous medium over a more dense substrate, a soft/hard case. In either case the lower layer is considered semi-infinite and both upper and lower layers are modelled as homogeneous within themselves. Using the four parameter homogeneous model (Equation 3.30) for each layer, plus the depth of the top layer gives a total of nine parameters involved. The approximation Equations 3.40 and 3.41 using two parameters for each layer, flow resistivity σ_e and porosity Ω (required in the calculation of the propagation constant),

together with a depth, d, adds to a slightly more manageable total of five parameters.

Figure 3.27 shows impedance plots for a 0.02cm soft layer over a hard layer compared to a soft (ie low flow resistivity) homogeneous, semi infinite, case. For the layered case the flow resistivity contrast between surface layer and substrate results in impedance having a real part that is independent of frequency and an imaginary part that is comparatively large at low frequencies. The resonance peak from the harder lower layer is seen at 400Hz in the imaginary part and $\approx$550Hz in the real part.

Figure 3.28 shows impedance plots for a 0.02cm hard layer over a soft layer case compared to a hard (ie high flow resistivity) homogeneous, semi infinite, case. For the layered case the real part is always greater than the imaginary part at any frequency. No resonance peaks can be seen from the layer, although the influence of changing flow resistivity are clearly seen in comparing the imaginary parts at low frequencies.

Figure 3.29 compares level difference spectra for the soft/hard and hard/soft layer cases. Figure 3.29 also compares the five parameter approximation and the nine parameter model. With the soft/hard case the approximation slightly over estimates the magnitude of the primary dip and peak. For the hard/soft case Figure 3.29 shows the two prediction curves coincide extremely well around the first dip and peak.

Comparison of a soft/hard layered situation with the exact model prediction for an acoustically soft, homogeneous semi-infinite soil is shown in Figure 3.30. Again the possible contribution to reflection from the harder layer is seen in the sharp increase in magnitude and relocation of the primary dip.

Figure 3.31 shows little difference between prediction of a hard/soft case and a semi-infinite high flow resistivity surface. The high flow resistivity possibly effects the depth to which the sound waves penetrates before reflection. This demonstrates that level difference measurements alone are not enough to characterise sub-surface soils in terms of acoustic predictions and supports the need for probe microphone measurements at depth.

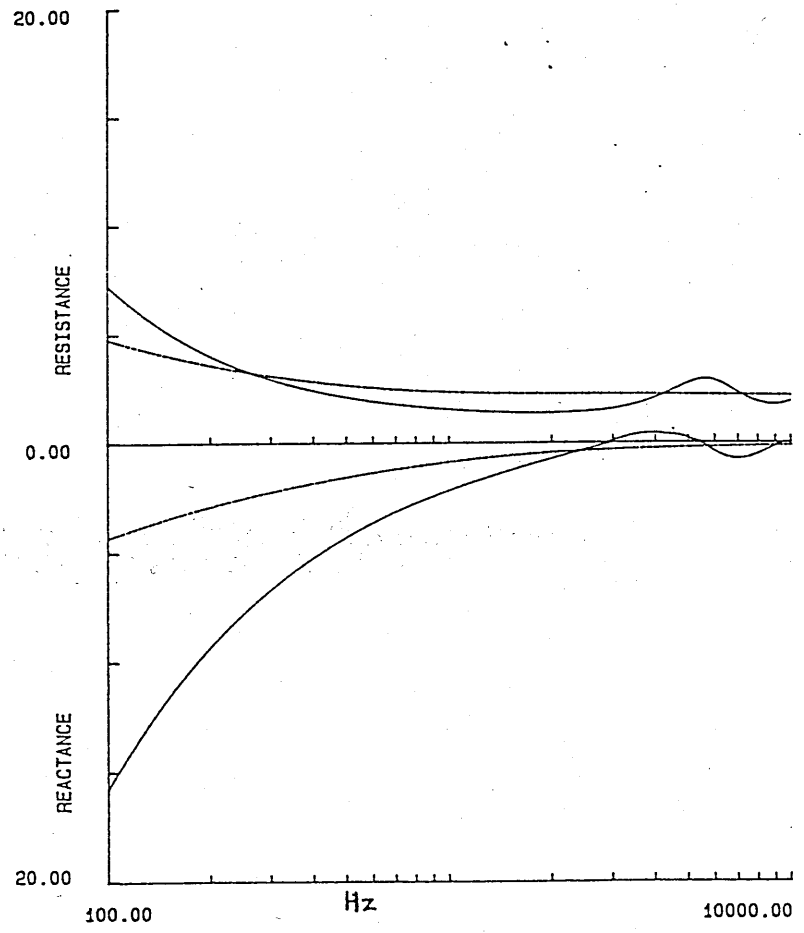

Figure 3.27 Impedance prediction for Soft/Hard layer case (continuous line) compared to a soft homogeneous semi infinite case (broken line). Parameters for the homogeneous semi-infinite case and for the top layer are σ=50000, Ω=0.65, T=1.5, sp=0.375, d=0.02 and for the lower layer σ=500000, Ω=0.25, T=1.5, sp=0.375.

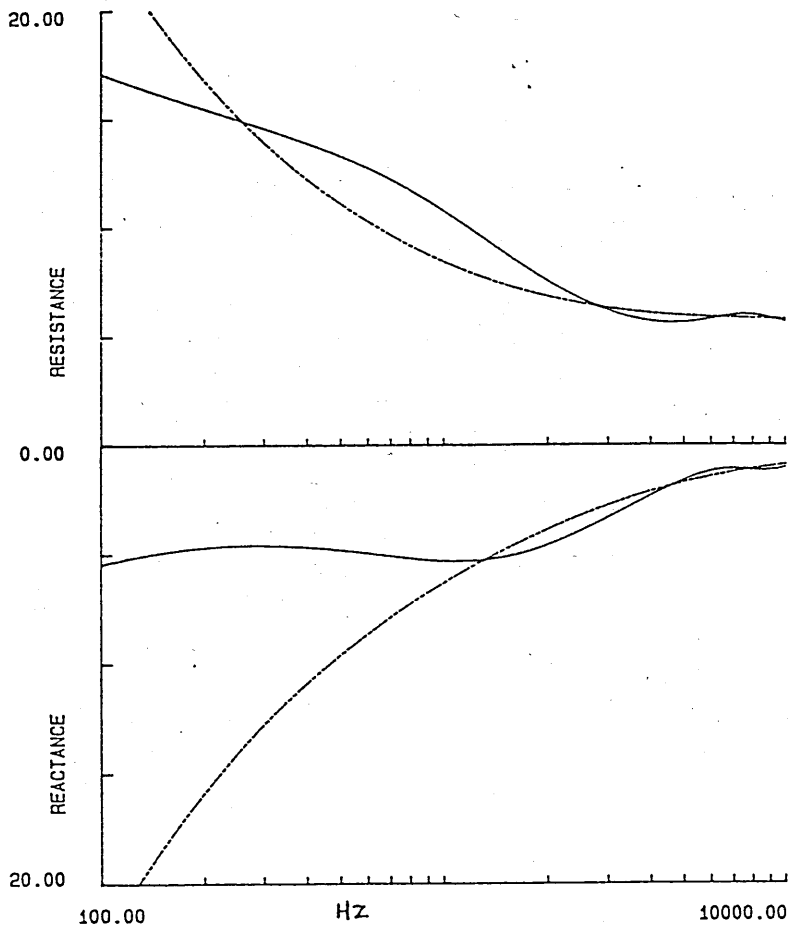

Figure 3.28 Impedance Prediction for Hard/Soft Layer Case (continuous line) compared to a hard, homogeneous, semi-infinite case (broken line). Parameters for the homogeneous semi-infinite case and for the top layer are σ=500000, Ω=0.25, T=1.5, sp=0.375, d=0.02 and for the lower layer σ=50000, Ω=0.65, T=1.5, sp=0.375.

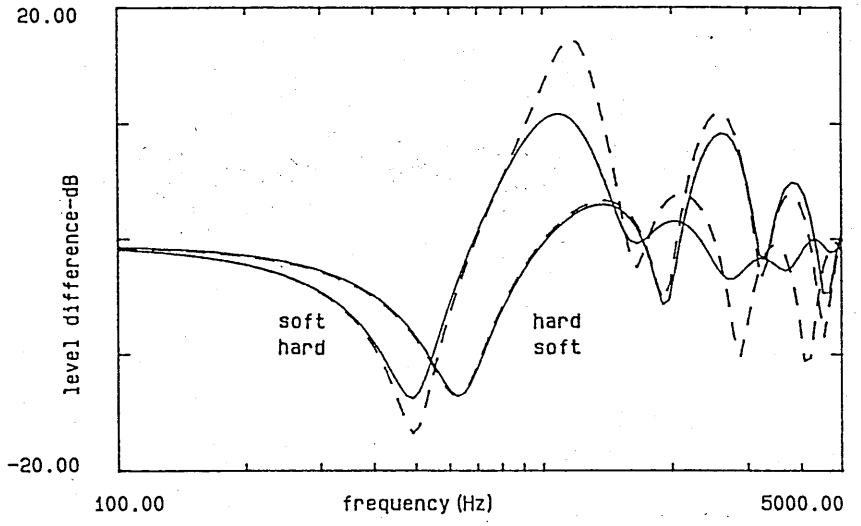

Level Difference Spectra Multi layer
Geometry hs=0.44 r=1.75 ht=0.55 hb=0.1

			σe	Ω	sp	T
soft	9 parameter	top	50000	0.65	0.375	1.5
hard		bottom	500000	0.25	0.375	1.5
	5 parameter	top	10770	0.65		
		bottom	280000	0.25		
hard	9 parameter	top	500000	0.25	0.375	1.5
soft		bottom	50000	0.65	0.375	1.5
	5 parameter	top	280000	0.25		
		bottom	10770	0.65		

depth of top layer = 0.02m

Figure 3.29 Comparison of Level Difference Predictions for Layered Soils, comparing the 9 parameter model (solid line) and 5 parameter approximation (broken line) for both a soft/hard (s/h) and a hard/soft (h/s) case, Ground Parameters as indicated above.

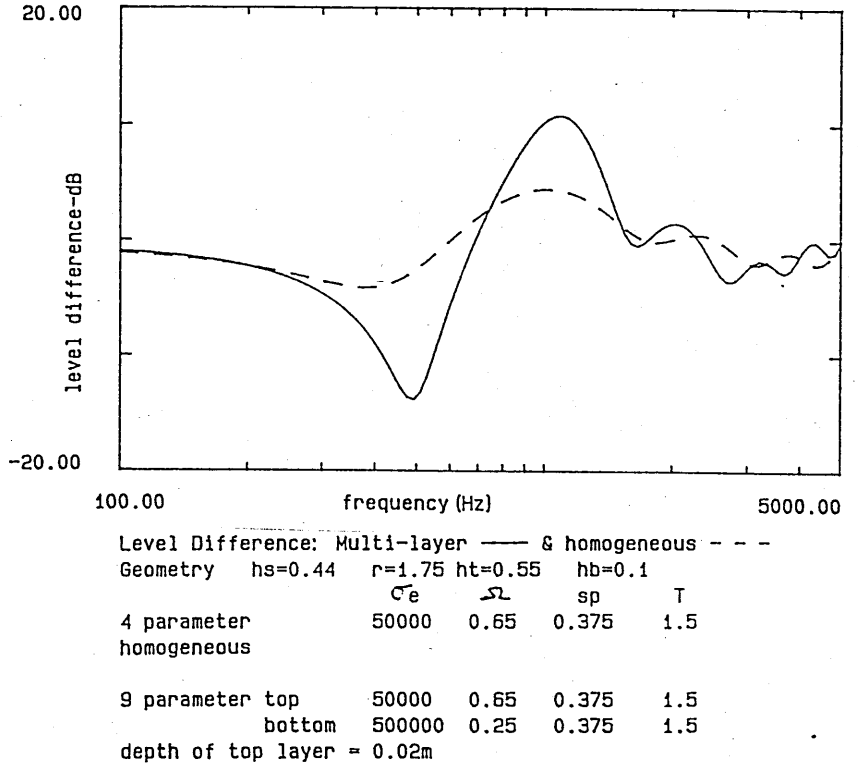

Figure 3.30 Comparison of Level Difference Prediction for a Layered Soil, comparing the 9 parameter (solid) for a soft/hard case and the Exact Homogeneous Semi-infinite Model (broken). Parameters as labelled.

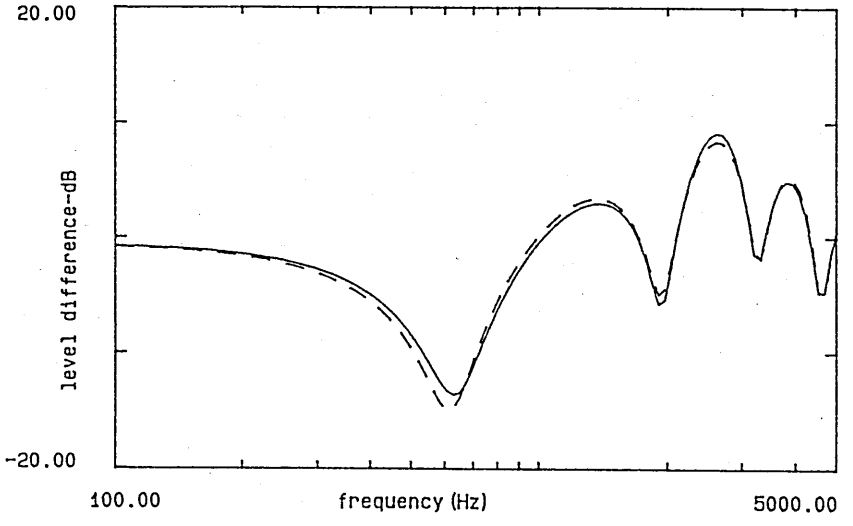

Fig. Level Difference: Multi-layer & homogeneous

Geometry hs=0.44 r=1.75 ht=0.55 hb=0.1

	σe	Ω	sp	T
4 parameter homogeneous	500000	0.25	0.375	1.5
9 parameter top	500000	0.25	0.375	1.5
bottom	50000	0.65	0.375	1.5

depth of top layer = 0.02m

Figure 3.31 Comparison of Level Difference Predictions for Layered Soils, comparing the 9 parameter (solid) for a hard/soft case and the Exact Homogeneous semi-infinite model(broken). Parameters as labelled.

3.7 Sound Penetration with Depth

Using the four parameter model (Equation 3.31) the propagation constant has been calculated for various combinations of σ, Ω, T and *sp* typical of results mentioned in Section 5. From predictions of the propagation constant and assuming a limiting value of 10dB attenuation then values of maximum penetration depth can be calculated for each frequency using Equation 3.23. Figure 3.32 demonstrates that by increasing σ and decreasing the porosity Ω the limiting depth of penetration is reduced with frequency. For snow with a flow resistivity of 10000mks rayls/m, porosity of 0.8, tortuosity of 1.0 and pore shape factor of 0.375 the depth of penetration ranges from 0.3m-0.15m, whilst if all parameters remain the same except σ which is increased to 20000mks rayls/m the depth of penetration is only between 0.23m-0.10m over the frequency range studied.

For a sand with a flow resistivity of 376000, porosity of 0.36, an *sp* of 0.55 and tortuosity of 1.0 the sound penetrates to between 0.05m at low frequencies and 0.02m at 1KHz. For a very high flow resistivity soil such as a crusted sand with parameters of an effective flow resistivity of 5000000, porosity 0.10 and the tortuosity and pore shape factor remaining at 1.0 and 0.375 respectively then penetration is from between 0.04m at low frequencies to 0.015m at 1KHz. Fitting of the homogeneous model to acoustic measurements is likely to be good if the soil remains homogeneous down to the maximum depth of penetration for example in the case of sand down to 0.06m. For a layered situation with a hard crust over a looser layer the effect of the lower layer will only be seen at low frequencies. At frequencies $>$ 1KHz a 1cm thick hard layer is regarded as semi-infinite, the sound never penetrating to the lower layer.

3.8 Rigid Frame Assumption

If the frame of the porous soil is assumed to be rigid, propagation of a sound wave below the ground surface only occurs within the air-filled pores. This is the only type of wave considered in the prediction models presented in

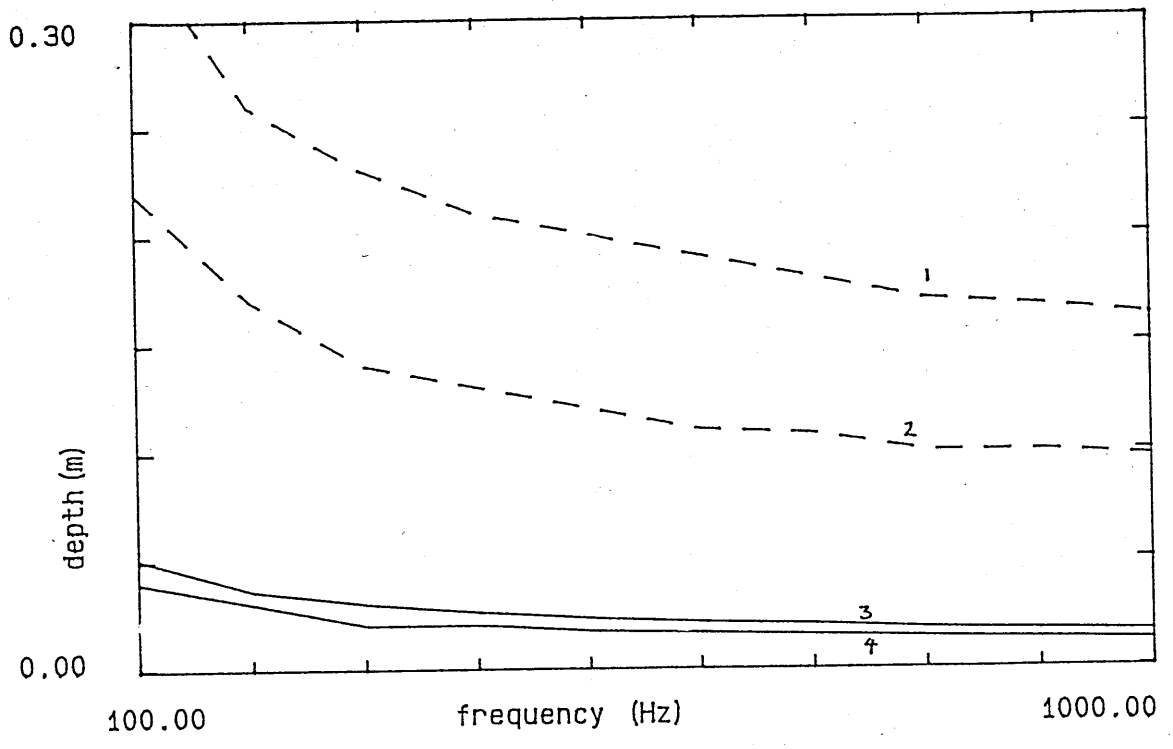

Figure 3.32 Prediction of Sound Penetration with Depth for Typical Soils and Snow using the exact, homogeneous model (Equation 3.31) assuming a value of 10dB attenuation as the critical value. Parameters are for snow (broken lines) (1) σ=10000, Ω=0.8, T=1.0, sp=0.375, (2) σ=20000, Ω=0.8, T=1.0, sp=0.375, for sand (3) σ=376000, Ω=0.36, T=1.0, sp=0.55, and for a typical wet soil or hard crust σ=5000000, Ω=0.10, T=1.0, sp=0.375.

Table 3.2 Comparison of Propagation Constants Prediction in Sandy Soil using both a Poroelastic Model and a Rigid Frame Model, after Sabatier et al.

Model	Rigid Frame Porous Model		Poroelastic Model	
Frequency Hz	Phase Constant	Attenuation Constant	Phase Constant	Attenuation Constant
100	13.01	12.61	12.89	12.49
200	18.70	17.56	18.53	17.38
300	23.26	21.18	23.06	20.96
400	27.29	24.09	27.06	23.83
500	31.00	26.53	30.74	26.24
600	34.50	28.64	34.22	28.32
700	37.85	30.49	37.56	30.15
800	41.09	32.14	40.79	31.77
900	44.26	33.62	43.95	33.23
1000	47.38	34.96	47.05	34.55
2000	77.21	43.91	76.84	43.88

this work. Biot [105] has developed a model which identifies three types of waves in a poroelastic soil; a pore-borne wave termed the slow wave, a fast wave travelling within the frame and a shear wave. Sabatier et al [106] present results from a series of propagation measurements using a probe microphone buried in sand. Measured and acoustically deduced parameters as shown in Table 3.2 are used to predict comparable values of slow wave phase and attenuation constants using both the above mentioned models.

Sabatier et al [106] comment that below 5KHz the two sets of predicted results are practically indistinguishable. Attenborough et al [83] calculate the results differ by 1%. Daigle and Stinson [55], using a phase gradient technique have however measured impedances below 200Hz which show a peaked structure. They attribute this to acoustic/seismic coupling and propagation of a fast wave within the frame.

Johnson [107] has applied Biots poroelastic model to wave propagation in snow. A series of theoretical impedance predictions, impedance measurements and comparison to results from Oura [48], Ishida [49], and

Bogordskii [108] on snow of different permeabilities and densities are presented. The high acoustic absorption coefficients measured over snow were considered to imply that a large proportion of sound within snow is transmitted through the air-filled pores as slow waves. Lee and Rogers [52] use Bogordskii's measured sound velocities in snow to show that for with low densities,$< 0.30kg/m^3 \times 10^{-3}$ and high porosities, sound is transmitted mainly by air motion in the pores. The majority of snow measurements made in this work are on snow possessing these properties.

It is therefore assumed that the more rigorous poroelastic theory is not necessary to predict acoustic attenuation on outdoor soil and snow surfaces, except perhaps at very low frequencies below 200Hz.

Chapter 4

Experimental Procedure

4.1 Detailed Description of Experimental Sites

The non-uniformity of soils between one area and another, maybe only a few metres away, makes the interpretation of measured acoustic spectra in terms of soil parameters difficult. Experimental sites therefore were selected where discrete soil types ie. a mainly clay, sandy or silt based soils occurred, so the acoustic characteristics of these three types could be determined. Two of the sites chosen were on agricultural traffic wheeling experimental plots which provided areas on the same soil type but with different compaction treatments thus deliberately creating adjacent physically contrasting areas for comparison.

4.1.1 Silt Soils

Tring

Access to farmland owned and managed by Farmers Weekly enabled two sites to be located on a Charity 2 series, silty soil, at OS reference SP 935137, near Tring in Hertfordshire. The two sites chosen in adjacent fields were close enough together to be on the same soil type but under different use. The two sites can be described as,

1. Cultivated, so called because the area was fallow and had recently been cultivated to keep the weeds from growing. The surface was quite

rough when first inspected due to passes with the weeder but had been flattened out by weathering by the time experiments started.

2. Compacted, so called because the area was located in a headland area of a field cropped with 'pick your own' strawberries!

Quadrates were marked out so that the same area of soil could be monitored each time. The permanent probe access tubes as described in Section 4.2.2 were also located within these quadrates. The soil here is called Silt A throughout the subsequent discussion.

Gosberton

This site was located on a Wisbech Series silty soil at OS reference TF 247307, near Gosberton in Lincolnshire. Two quadrates were set up on two different wheeling treatments which were part of a soil management experiment run by British Sugar, and monitored by Silsoe College, to study the effect of compaction on sugarbeet growth and yield. A plan of the experimental plots is shown in Figure 4.1. The treatments were described as

1. A poor practise plot which after initial ploughing had been completely flattened by machinery which repeatedly passed over the site.

2. A controlled wheeling plot on which, after initial ploughing, the first pass set out tramlines that were followed for every subsequent pass of machinery throughout the season, leaving the area between tramlines relatively untouched.

It was thought these two treatments would provide significant contrast and are described as poor practise and controlled wheeling sites. The soil here is called Silt B throughout the subsequent discussion.

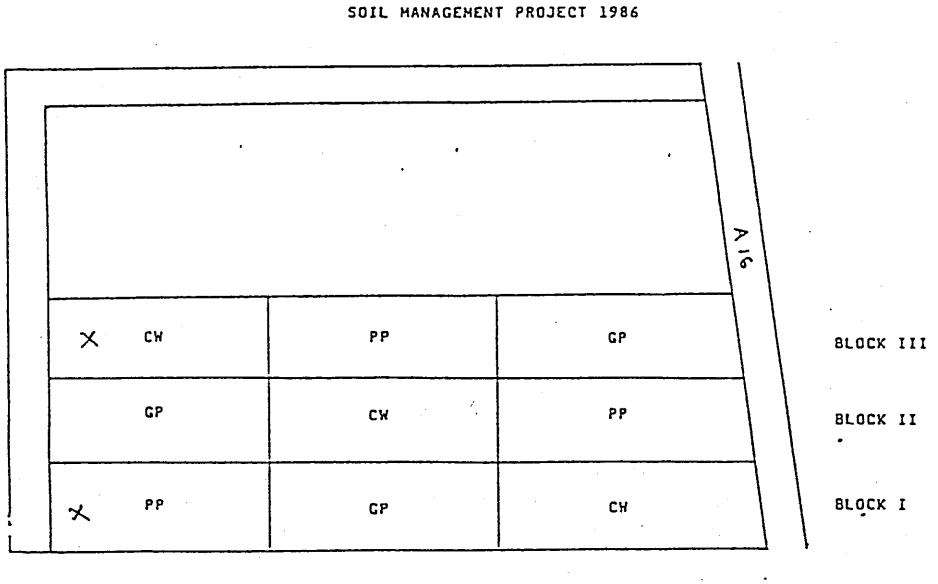

Figure 4.1 Soil Management Treatments at Gosberton, cw controlled wheelings, pp poor practise, gp good practise. Those used for acoustic experiments are marked x.

4.1.2 Clay Soils

Silsoe

This site was located on an Evesham Series clay at OS Reference Sheet 147 075345, near Silsoe, Bedfordshire. Two sites were subject to two different wheeling treatments which were part of a long term experiment to compare the effect of different tyre/soil contact pressures on soil and crop responses when growing winter wheat. Thus it was possible to attempt to distinguish acoustically between

1. A normal wheeled plot which had been direct drilled. Normal here means passed over with a standard tractor with standard tyre pressures.

2. A zero wheeled plot which had been shallow cultivated.

Subsequently these two sites are referred to as wheeled and zero sites. The growing crop was winter wheat.

4.1.3 Sandy Soils

Sand in Anechoic Chamber

A tray with dimensions 1.8m x 1.2m x 0.3m was located in a small anechoic chamber and filled with sand. In separate experiments two different sands were used, a sharp sand containing small pieces of gravel, labelled subsequently as Sand 1, and a more equigranular sand, Sand 2. For sand 2 experiments were also undertaken in a plastic dustbin, with a surface area of $1.25m^2$ and a depth of 0.5m. Sand in both cases was filled to the top of the containers flush with the sides to eliminate any reflections.

Harbour Project

This site was used by the Waterways Experimental Station Vicksburg, Mississippi for acoustic experiments. The area was a 12m high sand pile dredged

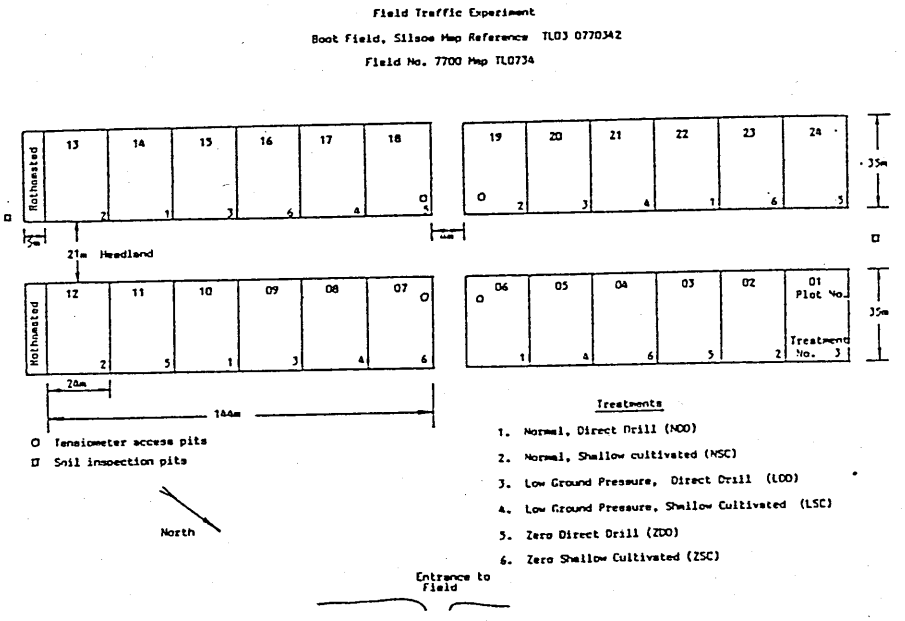

Figure 4.2 Soil Management Treatments at Silsoe. Those used for acoustic experiments are 06 and 07.

from the Mississippi River bed and graded to a level surface. This site, facilitated preliminary experiments both with level difference and probe measurements in conjunction with the University of Mississippi Physical Acoustics Research Group (Dr. J. Sabatier) and USAE Waterways Experimental Station (J. Lundien). The area was not homogeneous throughout. There also were areas of surface compaction and crusting on the surface, which were interesting to monitor acoustically. Subsequently this sand is referred to as Sand 3 throughout.

Soil bin

Measurements were made on a sandy loam soil contained in a large wooden box with the dimensions 2m x 1.5m x 0.8m, which was located on the floor of a large engineering workshop. The soil was levelled flush with the top of the box and preliminary tests showed the surface area large enough not to cause spurious reflections from the edges. Being in a workshop environment there were short periods of high background level noise, and although measurements were attempted during these periods, the background levels were checked frequently and every effort was made to undertake measurements during quiet periods, usually during tea and lunch breaks and after working hours.

The soil studied was a sandy loam from the Milford Series which was of the kind routinely used by Silsoe College in soil bin experiments. This soil had been bagged in storage consequently it was very dry, and because of reworking very pulverised and almost dust like with very small aggregates. Acoustic measurements were made on this soil when dry and again after the application of varying amounts of water such that three distinct soil conditions were achieved and subsequently described as dry, moist and wet.

For moist conditions the soil was wetted to approximately 20% (vol). This was attained by taking out a 50cm deep layer of soil from the box and wetting it with a hose pipe to try and obtain an even moisture distribution. The dry dust-like soil had a slow infiltration rate and an even water application from the surface with the soil *in situ* would have taken weeks to

achieve. The moistened soil was then replaced on top of the dry soil. The 50cm depth was considered sufficient to enable modelling as semi-infinite.

For the wet condition the soil moistened as mentioned above was sprayed further with water from a hose pipe directly onto the surface. This effectively saturated the surface, with small puddles forming in places, and the water was left to drain in overnight. In the morning a short sprinkling rewetted the very top of the soil. Subsequent examination showed the water had penetrated to a depth of approximately 1cm in the area of of interest. A series of probe and level difference measurements were then made.

4.1.4 Snow

Snow of any quantity and permanence was not found in the locality of Southern England. Acoustic measurements on snow were made at the Keweenaw Research Center, (KRC) part of Michigan Technological University, located on the Upper Peninsula of Northern Michigan USA. This area receives on average 2m of snow per annum falling mainly between November and March which collects to appreciable depths. Four areas chosen had between 0.4m and 1m deep snow depending on exposure of the site. The sites, called after their locations are

1. Site A - snow lying in close proximity to the KRC buildings.
2. Site B - snow over a forest road.
3. Site C - snow beneath pine trees.
4. Site D - snow in close proximity to poplar trees.

A criterion for choosing snow sites was that the snow layer was deep enough to allow it to be modelled as semi-infinite.

4.2 Measurement Procedure

Level difference and probe techniques and the equipment used for each are described in this section, together with measurement procedures for deter-

mining air porosity, water content and flow resistivity of soil samples. Data processing and analysis are described also.

4.2.1 Level Difference

Sound Generating System

The signal from a white noise source was passed through a Kemo low pass filter, amplified by an HHS150 slave amplifier and broadcast through a speaker. In intial experiments the speaker used was an Electrovoice S12-S two way speaker system. This had two drive units, a 30cm bass unit and a high frequency tweeter unit. The cross over network of the speaker system was specified as a nominal 3KHz. Pilot experiments Price [90] showed that the centre of the speaker drivers could be safely used as the location of an equivalent point source for long range propagation measurements, but for short ranges <2m this was not the case. Therefore a 40 watt Tanoy PD40 drive unit with a 30cm long brass tube attached to the front was used. Preliminary experiments proved this acted as a point source. Care was taken to filter out frequencies greater than 5KHz to reduce ringing of the brass tube. The PD40 was initially housed in a wooden box, however, it was soon realised there was significant reflections from the front of the box and this was removed. This set up was used for all indoor and outdoor experiments except those over snow and at the sand site in Mississippi. Over snow, the speaker used was an Electrovoice 1829 which acted as a point source. It was driven by an amplifier excited by the random white noise source of a Hewlett Packard 3561A dual channel spectrum analyser. For the sand 3 site the output from a General Radio white noise source was passed through a Hewlett Packard high and low pass filter, a power amplifier and finally broadcast through either, a smaller speaker for level difference measurements or a large speaker containing four drive units, but of which only one was used, for the probe experiments.

Microphone and Data Recording System

The recording system used varied with site and the successive upgrading of recording equipment during the 4 year period of the work. The microphones used for all level difference measurements over soil were two Bruel and Kjaer half inch condenser microphones, type 4165, with Bruel and Kjaer microphone preamplifiers, type 2619. In early outdoor experiments the microphones were connected via special input adaptors Type QSJP-BK to a two channel Nagra IV tape recorder, on which received signals for top and bottom microphones were recorded. Later the microphones were connected via 10m extension cables to a Bruel and Kjaer microphone power supply, type 2804, and from there to an Ono Sokki 910 dual channel FFT analyser where the magnitude and phase of the transfer function between the microphones was stored on an inbuilt floppy disk system. For the work on Sand 1 similar microphones were connected to two B& K measuring amplifiers from which signals for both top and bottom microphones were fed into a dual channel Nicolet 660B FFT analyser. The analyser was remotely controlled by a Nova 4 minicomputer and the digitized rms spectra were stored on the Nova 4 floppy disk system together with information on calibration tone voltage levels for each microphone. For the work on snow two Bruel and Kjaer sound level meters were connected to a HP 3561A analyser and level difference spectra stored as the real and imaginary parts of the transfer function on floppy disk. The recording system in Mississippi involved signals received by two Bruel and Kjaer microphones passing through two Tektronix AM502 differential amplifiers and into a dual channel HP 3580A spectrum analyser. The data was then recorded by plotting on to graph paper, no disk system being available.

All systems were calibrated using either a Bruel and Kjaer piston phone, type 4220, which produced a sine wave at 250Hz of 124dB, or a Bruel and Kjaer calibrator, type 4230, with a sine wave at 1000Hz of 94dB. For the Nagra tape recorder with the calibration tone switched on, the input attenuators for each channel were set to a level that gave a reading in the mid-range of the meter. Stepped input attenuators allowed the recording

level to be adjusted for each measurement without recalibration. The calibration tones were also recorded. For the systems involving the Ono Sokki and HP analysers, calibration tone levels were read as voltages from the peaks of the calibration tone spectra. These voltages were fed directly into the analysers internal memory and any subsequent sound pressure level measurements were automatically referenced to either 124dB or 94dB. The calibration tones were also recorded on floppy disk for use in data analysis.

Experimental Set Up

For initial experiments, as reported in [89], using the Electrovoice S12-S speaker, ranges of 5m, 8m and 12m were required to enable modelling the speaker as a point source. A speaker height, to the centre of the base unit, of 1.26m and microphone heights 0.8m and 0.15m were used. Such geometries were also used on the Mississippi Sand 3 site. The Tanoy PD40 and Electrovoice 1829 point sources enabled the geometry dimensions to be reduced. The geometries varied from site to site. As shown in Figures 3.6 to 3.12 the position of the ground effect dip is influenced by the by the geometrical set up and the flow resistivity of the soil. The choice of geometry was influenced by two things. Firstly geometries for a particular soil type were determined so that the distinction between different surfaces was shown by a large shift in the magnitude and location of the dip. Secondly, geometry was influenced by the physical space available. For example the indoor experiments had the geometrical set up delimited by the size of the trays used to hold soil. In general speaker heights were between 0.2 and 0.5m. Receiver heights were approximately 0.1m and 0.5m respectively above the soil and horizontal range from source to receiver between 1m to 2m. At some sites up to three different geometries were used.

Measurement

For each measurement white noise was broadcast for approximately one minute duration, approximately the time it took the FFT analyser to average 128 spectra. Figure 4.3 shows the improvement in signal to noise ratio

by increasing the number of samples in the average from 16, 32, 64 and 128 sample spectra. The 128 average spectra is definitely smoother having averaged any background noise and attaining a better signal to noise ratio. Extending the number of averages beyond 128 showed no significant improvement. Coherence between the received signals was frequently checked and if found to fall below 0.8 the data was discarded. An example of coherence for level difference data can be seen in Figure 4.4. Several level difference measurements were made over any one particular experimental plot to try and account for any unseen lateral soil inhomogeneity.

4.2.2 Probe

Sound Generating System

Continuous white noise, using the same equipment mentioned in Section 4.2.1, was broadcast through either an Electrovoice S12-S or S1202 model. The geometry of speaker height and source-receiver separation were not recorded over soil due to the local reaction assumption. For snow the geometry used was approximately 3.0m range and 0.5m source height. The cross-over frequency for the Electrovoice S1202 was 1.5KHz and the switch from lower to upper drive unit required a 0.2m adjustment to source height at this frequency for prediction purposes. Using either source it was important to ensure a probe microphone location in the far field of the speaker, in this case beyond approximately 2.5m.

Microphone System: Two Probe Technique

Initially only one probe microphone was used to measure attenuation. This consisted of a small miniature condenser and preamplifier housed in a sealed brass tube. Subsequently, it was realised more information on soil structure could be deduced from phase differences as well as magnitude differences with depth, hence two matching probe microphones were constructed. Each probe consisted of a Sony electret condenser microphone type ECM 150T inside a sealed brass tube, which was attached to a small amplifier. A

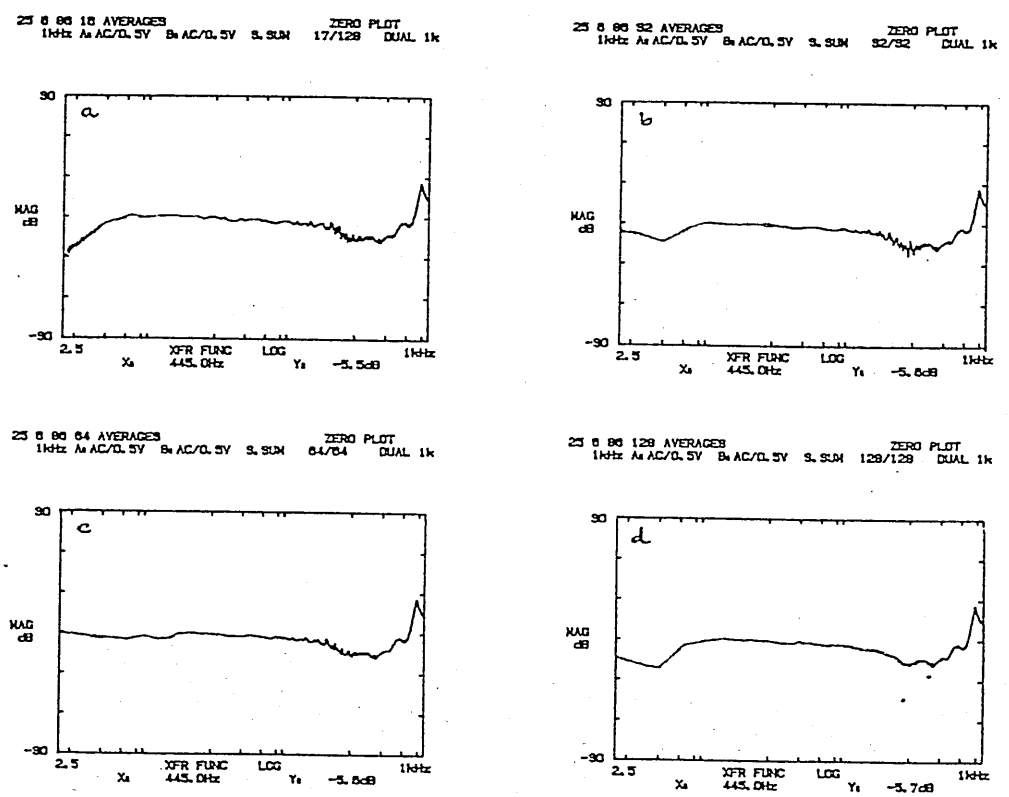

Figure 4.3 Comparison of Level Difference Spectra with Different Number of Averages - (a) 16, (b) 32, (c) 64, (d) 128.

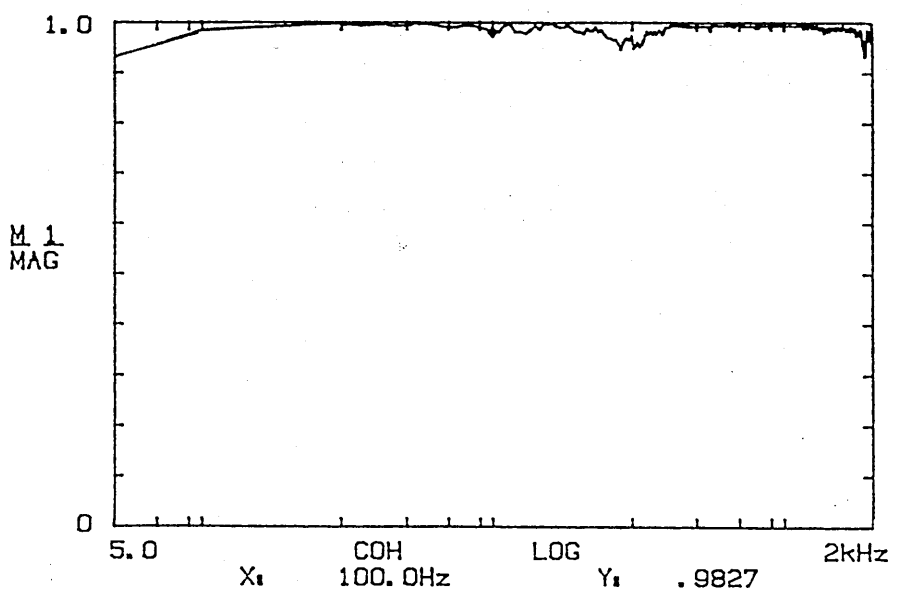

Figure 4.4 Typical Coherence for Level Difference Measurement hs 0.52, r 1.75, hrt 0.65, hrb 0.1

diagram of the probe is shown in Figure 4.5. Problems were found with hollow probe casings. Harmonic resonances appeared in the received spectra at wavelengths that were multiples of the length of the probe. To overcome this experiments using various casing fillers were made and the final solution was a combination of heat shrink plastic to fill the bulk of the tube and sand poured in to seal the little gaps. The electret microphones used were not phased matched, but the technique developed allows for unmatched phase response, as described in Section 4.2.2.

Figure 4.5 Construction of Probe Microphone

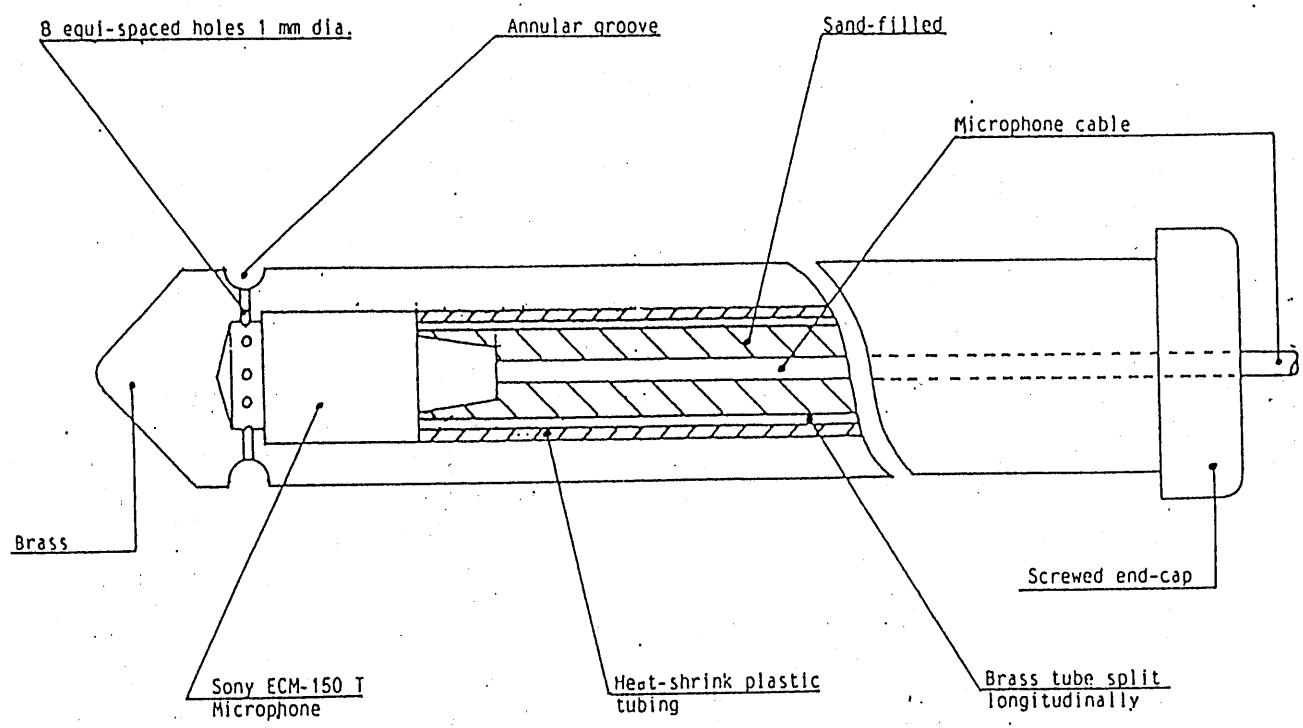

Experimental Set Up

For the buried probe microphone it was imperative to obtain a tight seal between it and the surrounding soil. Air spaces provided alternative paths for the sound waves other than the desired air-filled connected pores in the soil mass. In sand the probe was easily pushed in to the required depth but in most mineral soils a guaranteed close fit was not possible. Therefore a freshly augered hole just smaller than the diameter of the probe and to the required depth was made for each measurement. On very difficult soils a small amount of engine lubricant was put around the hole at the soil surface to ensure a perfect seal. In the snow other insertion and burial techniques were developed. Due to the porous nature of snow, sound penetration was significant to greater depths. Signals below 200Hz were received clearly at a depth of 70cm at one site, consequently the 30cm long probes were inadequate. An extension rod attached to the probe provided access to greater depths but also caused resonances in the received spectra. The development of a burial technique using an unhoused lapel microphone was more successful. Preliminary measurements showed the microphones were robust enough to withstand sub-zero temperatures and burial in snow overnight. The method that provided satisfactory results involved probing a hole of a diameter slightly greater than the diameter of the lapel microphone, to the maximum depth to be measured. The microphone was placed at the bottom of this hole and sand backfilled into the hole to block sound that might penetrate through the hole to the microphone. Subsequent to the acoustic measurement the microphone was withdrawn to a shallower depth through the sand and another measurement made. It was judged that the sand had a higher flow resistivity than the adjacent snow and that the received sound was indeed transmitted through the snow from the speaker.

Measurement

No calibration of the electret microphones was possible. The probe microphone at the surface served as a reference. By always taking a transfer function with respect to this reference it was possible to obtain data inde-

pendent of the spectral characteristics of the source. An initial measurement was made with both microphones side by side at the surface to provide information on their relative response characteristics. A plot of the magnitude of the transfer function between the two microphones at the surface is shown in Figure 4.6a beside which is a plot Figure 4.6b of the coherence.

After the reference measurement one probe or lapel microphone was placed successively at different depths in the snow or soil whilst the other remained at the surface. The phase and magnitude or real and imaginary parts of the complex transfer function between the two probe microphones at these locations were stored on floppy disk facilities of the Ono Sokki FFT and HP analyser respectively. Repeatability of the measurements was checked and background sound levels were recorded to determine depths where the buried microphone no longer received sufficient signal from the source to make a reliable measurement. An example of background noise and received signal for a typical probe microphone measurement made in snow are shown in Figure 4.7.

During probe measurements coherence between two probe signals was checked and Figures 4.8(a) and 4.8(b) show the decrease in coherence when the buried probe is at a deeper depth (14cm) at the clay zero site. The only improvement in the signal at depth due to increased averaging was a slight clarifying at the higher frequencies. For the clay wheeled site poor coherence was found at shallower depths as seen in Figures 4.9 and 4.10. Poor coherence at depth indicated that data should be excluded at frequencies >4KHz. This procedure gave an indication of the frequency range over which data was reliable.

Permanent Probe

To offer the facility of monitoring soil conditions at the same place and depth throughout a season, permanently situated access tubes into which a probe microphone could fit tightly, using an O-ring seal, were installed on the Silt A site. The technique experienced three major problems. Firstly the tubes were inserted into wet soil. Within a few weeks drying out caused huge

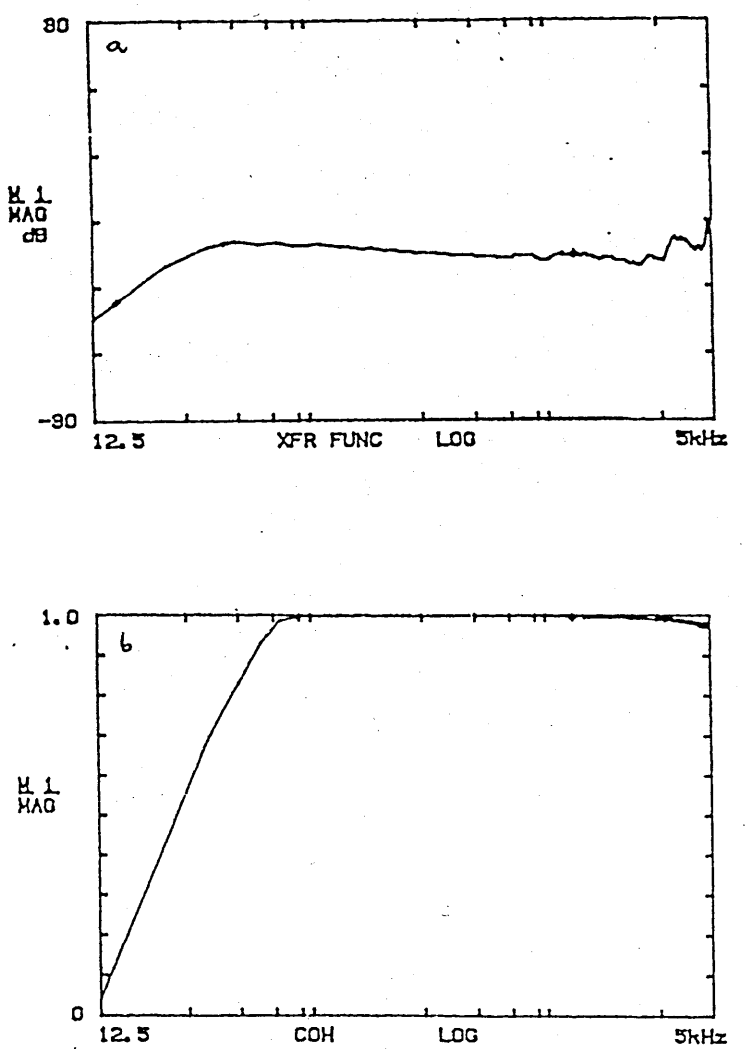

Figure 4.6 Magnitude dB (a) and Coherence (b) Between Two Probe Microphones at the Soil Surface.

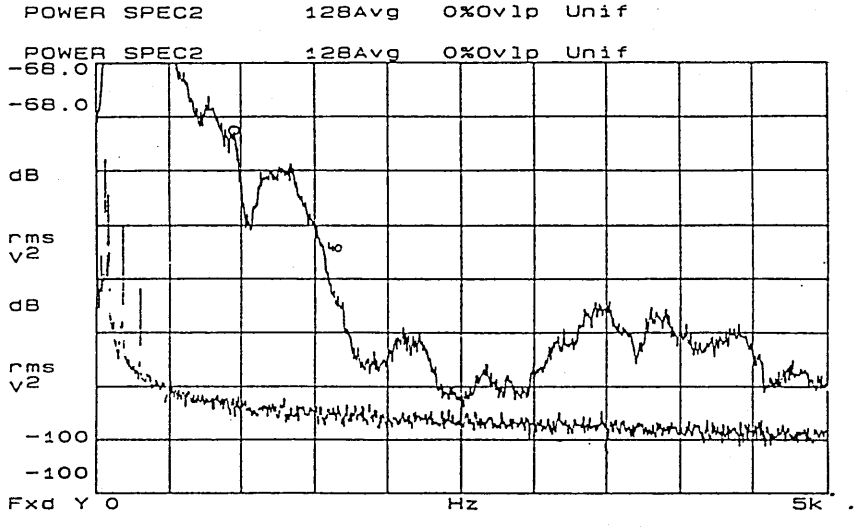

Figure 4.7 An example of background noise against received signal for a typical probe microphone measurement made in snow, at 0.4m depth.

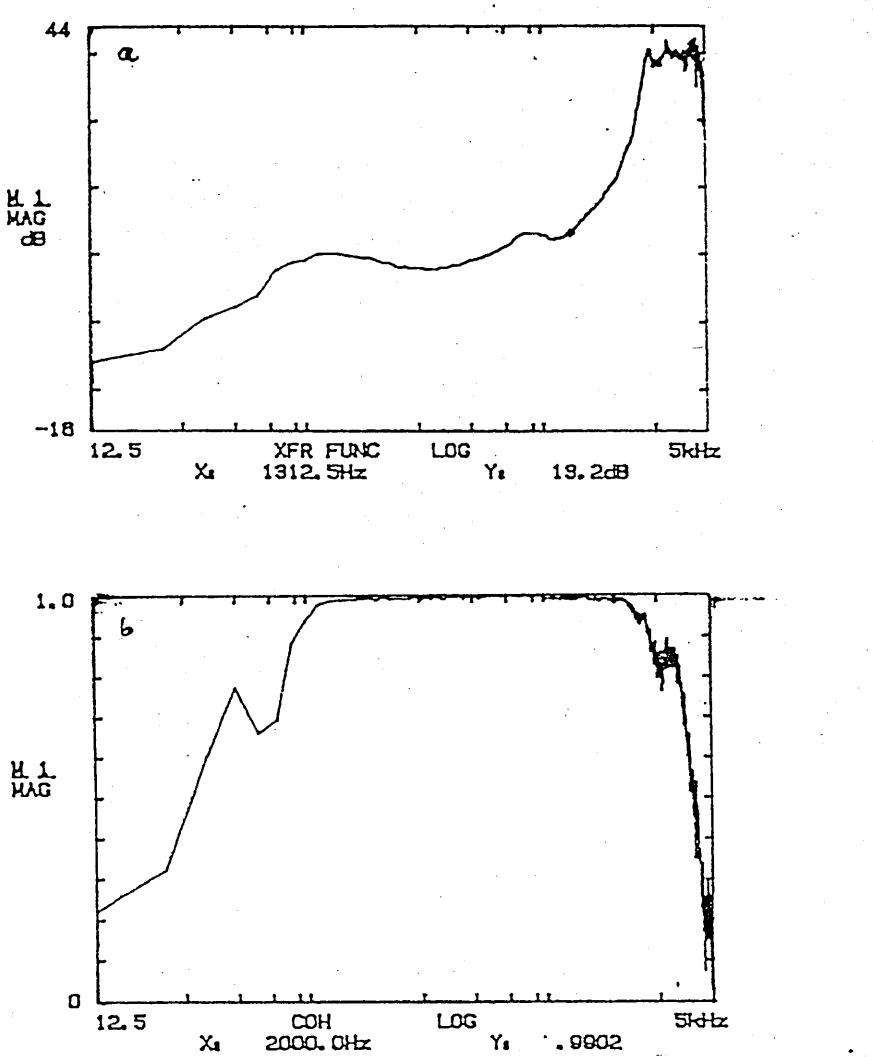

Figure 4.8 Magnitude dB (a) and Coherence (b) Between Two Probe Microphones one at the Surface the other buried in a clay soil at 14cm.

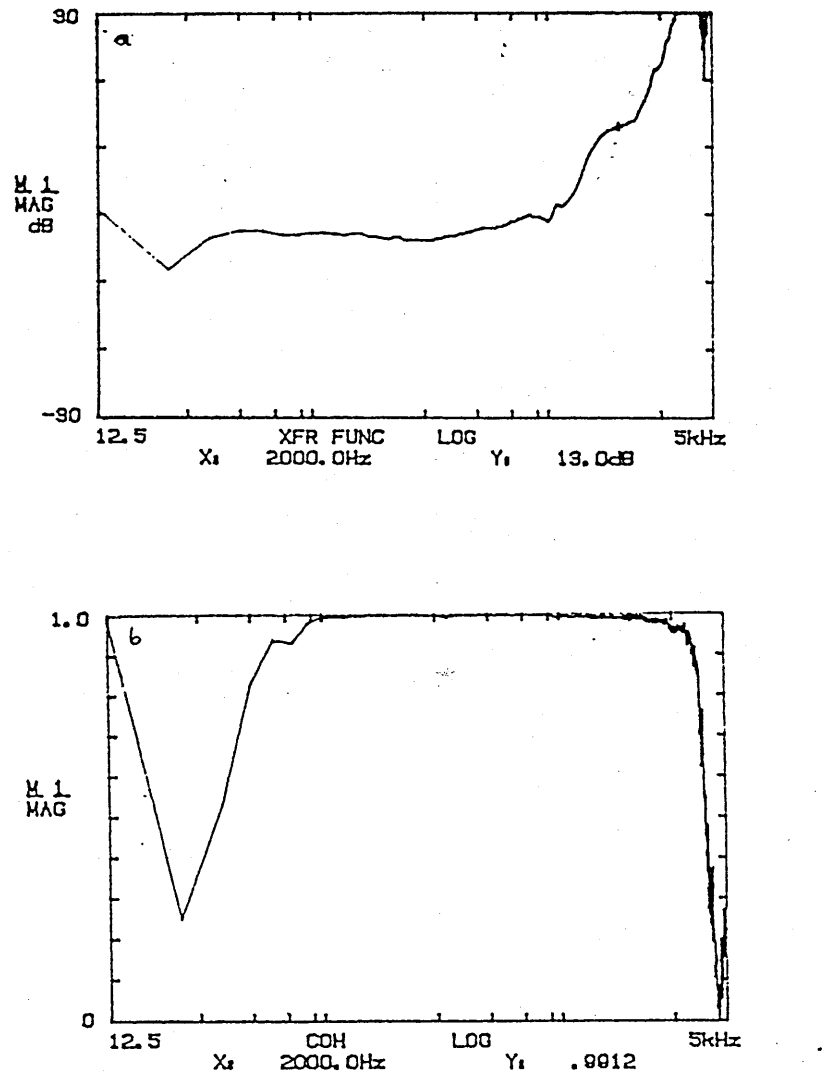

Figure 4.9 Magnitude dB (a) and Coherence (b) Between Two Probe Microphones one at the Surface the other buried at 6cm in a clay soil.

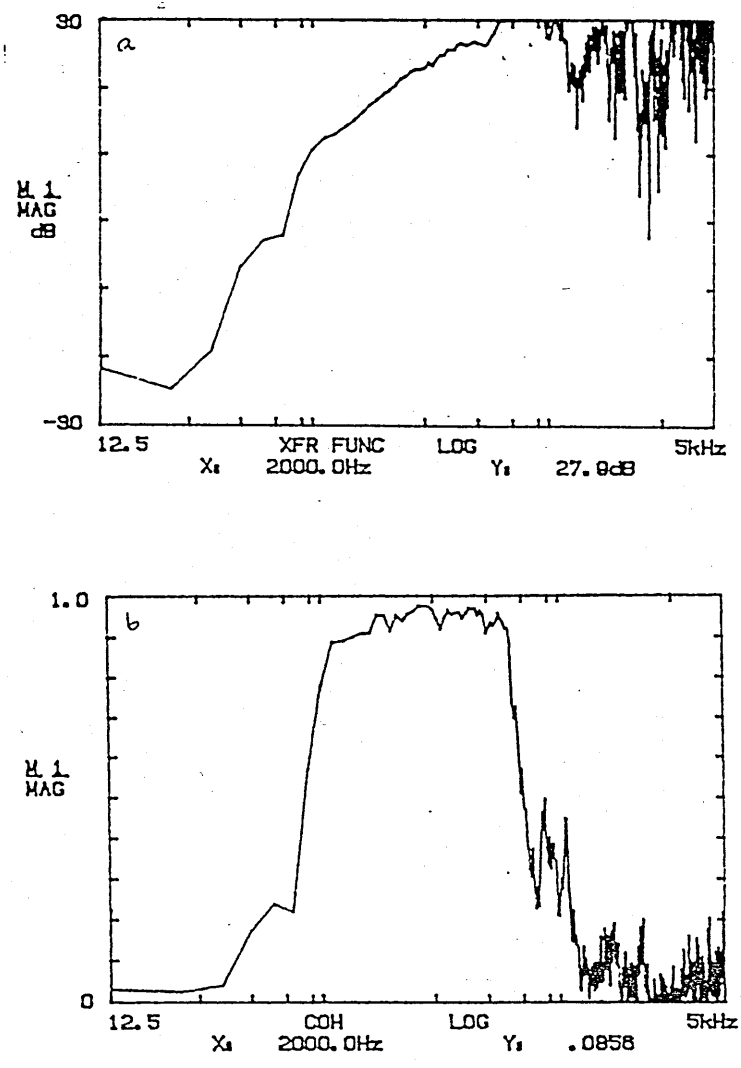

Figure 4.10 Magnitude dB (a) and Coherence (b) Between Two Probe Microphones one at the Surface the other buried at 8cm in a clay soil.

cracks around some tubes particularly on the compacted site which made measurement pointless. Secondly on the cultivated site a large wheeled farm vehicle accidently drove straight through the experimental quadrate and over the top of two access tubes pushing them into the ground and bending them. Consequently only very few measurements were made. Those measurements made experienced a third problem which was the actual insertion procedure of the probe into the tube. The fit between tube and probe was so tight that insertion was almost impossible without loosening the seal between access tube and soil.

4.3 Data Processing

Data processing is described for level difference and probe measurements in turn.

4.3.1 Level Difference

For measurements made in the anechoic chamber on Sand 1 the received signals at both microphones were passed into a Nicolet 660B FFT analyser which was remotely controlled by a Nova 4 minicomputer. The analyser calculated average RMS spectra of the voltage signals for each channel, over the frequency range selected, and these were transferred to Nova 4 floppy disks. Also recorded on disk was information about the analyser set up and voltage outputs for the calibration tones so that the RMS spectra could be converted to sound pressure levels. From the Nova minicomputer data was then transferred onto a Vax cluster. The calculation of level difference from these voltages was done by running the data through a specially written Fortran program DIF2VS, listed in Appendix A. At each frequency the SPL (in dB) for each microphone is calculated from

$$\mathrm{SPL} = 20 \log_{10} \left(\frac{V_m}{V_{m_{ref}}} \right) \tag{4.1}$$

where V_m is the measured voltage and $V_{m_{ref}}$ is the voltage output of the calibration tone for that microphone. The level difference in dB between

the lower A and upper B microphones can be calculated from

$$LD = 20\log_{10}\left(\frac{V_B/V_{B_{ref}}}{V_A/V_{A_{ref}}}\right) \tag{4.2}$$

After June 1986 all level difference measurements were recorded directly on the floppy disk of an Ono Sokki dual channel FFT analyser. The data was stored as the magnitude (in dB) of the complex transfer function. This was subsequently transferred via a Zenith PC remotely controlling the FFT analyser to a VAX cluster network. Subsequent to transfer , the data was converted from dB referenced to 1volt to dB referenced to 20μPa. A Fortran listing of the program to manipulate data called CAL is presented in Appendix A. This program calculates the level difference in dB from

$$LD = \frac{B}{A} - \frac{(cal_B)}{(cal_A)} \tag{4.3}$$

where B/A is the magnitude of the transfer function in dB and cal_B and cal_A are the overall levels in dB for the calibration tone received at each microphone.

4.3.2 Probe

Tape recordings of the simultaneous signals received at the surface and buried microphones were played into a two channel FFT analyser and the transfer function calculated. Alternatively disked recordings of transfer functions were recalled into the analysers internal buffer memory. The magnitude in dB, and phase in radians, of the transfer function between the two signals were transferred, using a specially developed data aquisition program, onto the hard disk system of a Zenith PC. From there the data was transferred to the Open University's Vax cluster network. The data was run through program CAL to eliminate data below 100Hz and to set up an array containing three columns, frequency, magnitude in dB (mag) and phase in degrees (phase). Each transfer function represented the difference between responses received by a probe microphone located at the surface and a microphone at depth. Subsequently this is called an equalised transfer

function. To calculate the measured attenuation and phase, and hence the propagation constant, between two equalised transfer functions at different depths (e.g. 2 and 4cm), the two equalised transfer functions are read into a program called OSABCALC (shown in Appendix A) as freq, mag1,phase1 and freq, mag2 and phase2 and the following calculations performed at each frequency point.

$$\text{attenuation} = 20\log_{10}\left|\frac{mag2}{mag1}\right| dB \tag{4.4}$$

and

$$\Delta\text{phase} = phase2 - phase1 \tag{4.5}$$

The real and imaginary parts of the propagation constant are calculated using equations

$$a = \frac{\pi\phi^{\circ}}{180\,d} \tag{4.6}$$

and

$$b = \frac{\text{atten dB } \log_e 10}{20\,d} \tag{4.7}$$

and where

$$k_b = (a + ib) \tag{4.8}$$

These values are then substituted into Equations 3.37 and 3.38 to calculate a value of T and σ_{pe} for each frequency.

For the measurements made over Sand 1 within the anechoic chamber the equalised transfer functions were calculated on a Nicolet 660B FFT analyser, temporarily stored on a Nova 4 floppy disk system and later transferred on to the Vax Cluster. The data were stored as the real and imaginary parts of the complex transfer function. To calculate the difference between two equalised transfer functions at different depths data was run through program PROPAB shown in Appendix A. Magnitude and phase for each transfer function were calculated from

$$\text{magnitude} = 20\log_{10}\left|\text{Re}^2 + \text{Imag}^2\right|^{0.5} dB \tag{4.9}$$

and

$$\Delta\phi^{\circ} = (\tan^{-1}\left[\frac{\text{Imag}}{\text{Re}}\right])57.296 \tag{4.10}$$

The real and imaginary parts of the propagation constant are calculated using equations 4.6, 4.7 and 4.8 and rearranged Equations 3.37 and 3.38 to calculate T and σ_{pe} at every frequency.

Data made on snow, as described in Section 4.2.2, involved recording the real and imaginary parts of the equalised transfer functions between surface and buried probe measurements. These data were passed from HP 3.5 inch discs via a controlling IBM PC onto 5.25 inch floppies which were then brought back to the UK. The procedure of transfer onto the Vax cluster is as described above. Data manipulation differs from the above described procedure due to a different data format and the need to take into account extended reaction and two models to calculate σ_{pe} and T.

Once on the Vax, differences between equalised transfer functions for different depths were calculated by processing data through NTFCALC (see Appendix A) which simply divides one transfer function by the other. The data is then passed through two further programs COPY5 for the high frequency model and COPY6 for the low frequency model, both of which are listed in Appendix A. In both programs the real (Re) and imaginary (Imag) parts of the equalised transfer functions are converted to magnitude dB and phase degrees by Equations 4.9 and 4.10. The magnitude of the equalised transfer function expressed in decibels, is equivalent to the attenuation between the two buried microphone locations.

From the measured attenuation and phase values and a knowledge of the geometry of source and receiver location values of a and b, are calculated from Equations 3.25, 3.26 and 3.29 and hence the real and imaginary parts of the propagation constant from Equation 4.8. For the low frequency/high flow resistivity model in COPY6 values of T and σ_{pe} are deduced using Equations 3.37 and 3.38. For the high frequency/low flow resistivity model in COPY5 Equation 3.43 has been rearranged to give values of σ_{pe} and T for each frequency. This is rather long and complicated and the reader is referred to the listing of the computer program COPY5 in Appendix A for

further details.

Data recording at Mississippi on the sand was a little more primitive and data points of attenuation with depth were read off from graph plots. Data processing was done by using an approximation technique and all analysis for these sites was done by hand on a calculator. This process will be described in full in Section 4.4.4.

4.4 Deduction of Ground parameters from Acoustic Data

The process of deducing ground parameters involved comparing measured level difference and probe measured propagation constants with theoretical predictions described in Section 3.6. The fitting procedures for both these techniques are described in turn.

4.4.1 Level Difference

For the three parameter homogeneous approximation, the procedure of deduction utilises curve fitting and the calculation of a least root mean sum of squares (rms) between the predicted curve and the measured level difference spectra, subsequently referred to the rms error. The fitting routine developed LDFIT utilises a Nag. library routine No. E04JAF and is listed in Appendix A. This is based on a quasi-Newton algorithm for finding a minimum of a function $F(\sigma_{pe}, T, \Omega)$ subject to upper and lower bounds on the independent variables using function values only. From a starting point supplied by the user there is generated, on the basis of estimates of the gradient and the curvature of the function a sequence of feasible points which is intended to converge to a local minimum of the function [109]. The least sum of squares value, rms, between the predicted curve and level difference spectra is calculated from the algorithm

$$rms = \sqrt{\sum_{n=1}^{N} \frac{[M_n - P_n]^2}{N}} \tag{4.11}$$

where N is the number of frequencies, M_n the measured data at the n_{th} frequency, and P_n the predicted value at the n_{th} frequency. The rms value indicates the goodness of fit, the lower the value the closer the predicted and measured curves lie.

A problem during fitting the three parameter approximation was non-uniqueness. For any one geometry there would be maybe two different combinations of σ_{pe}, T and Ω giving the same rms value. To overcome this, two or three different geometries for each site were fitted. A similar combination of parameters predicted for all geometries, was regarded as the most probable combination. This procedure can be seen in Table 4.1 where hs is the source height,r is the range, hrb is the height of the bottom microphone and hrt the height of the upper microphone. The similar combinations

Table 4.1 Non-Uniqueness of rms Values from Level Difference Fitting.

Ground	rms	hs	r	hrb	hrt	σ_{pe}	T	Ω	Meas. Ω
Sand 2	2.01*	0.21	0.76	0.05	0.21	12000	1.34	0.48	0.47
	2.01	"	"	"	"	16305	1.84	0.56	
	0.76*	0.10	0.37	0.02	0.17	20000	1.66	0.48	
	0.76	"	"	"	"	14310	2.66	0.51	
Sandy Loam	1.35*	0.10	0.37	0.06	0.15	25660	2.73	0.50	0.49
(dry)	1.35	"	"	"	"	32560	3.46	0.56	
	2.91*	0.40	1.05	0.05	0.40	20270	4.46	0.52	
	2.91	"	"	"	"	10000	10.0	0.55	
Clay Day 2	1.63*	0.50	1.77	0.10	0.53	6350	2.99	0.58	0.55
(dry)	1.63	"	"	"	"	3053	1.40	0.40	
	1.94*	0.50	1.77	0.10	0.65	6230	3.66	0.56	
	1.94	"	"	"	"	9338	5.49	0.69	
Snow Site B	0.31*	0.50	1.25	0.10	0.37	1751	1.85	0.90	-
(dry)	0.31	"	"	"	"	100	1.00	0.92	
	0.52*	0.55	1.65	0.13	0.51	2276	3.25	0.91	
	0.52	"	"	"	"	2860	4.28	1.00	

of predicted parameters, for each ground type, are the lines marked with an asterisk *. The proximity of the measured and acoustically deduced porosities was chosen as the main criterion in the combination selection.

For example on the Clay the predicted values of 0.58 and 0.56 are closer to the measured value of 0.55 than the other predicted values of 0.4 and 0.69. On some grounds, eg sandy loam, combinations of parameters showed all predicted porosities, for both geometries, were close to the measured porosity. When this occurred the similarity of the flow resistivity parameters (σ_{pe}) were examined to help make the combination selection. For the sandy loam the similarity between 25660mks and 20270mks is greater than between 32560mks and 10000mks for the other combinations. If both the porosities and flow resistivities were similar then the tortuosity values would be studied, however this was not necessary in the majority of cases.

In some instances, for example Snow Site B, there were no measured values of porosity available for comparison. When this occurred the most probable combination of parameters was made by examining the sensibility of the predictions. For example it is unlikely that snow will have a porosity of 1.0 whilst having a relatively high effective flow resistivity ($\sigma_{pe}2860$), similarly the extremely low effective flow resistivity of 100 is probably an unrealistic prediction over snow.

For the multi-layer model the fitting procedure was less precise as there was no routine available for iterating the five parameters (flow resistivity and porosity for each layer and the depth of the layer in centimetres) required by this model. In this case usually four parameters were set to either known or assumed values. These usually included a measured porosity for both layers, a measured flow resistivity of the lower layer and the depth of the layer. However in some cases, for example a 1cm saturated surface layer overlying a moist sandy loam, porosity and flow resistivity values for the lower layer were set equal to the best fit parameters from acoustic predictions made on the moist sandy loam before the surface layer was saturated. This procedure is best described by an example. From fitting the three parameter approximation to measured level differences made over a moist sandy loam the predicted values of σ_{pe}, 9000, and Ω, 0.39 were obtained. By using the relationship $\sigma_e = \sigma_{pe}/\Omega^2$ a value for σ_e of 59200mks can be calculated. The porosity of the top layer 0.11 was set at a measured value made on carefully

Table 4.2 Deduced Parameters for Layered Soil and RMS Value

Layer	σ_e	Ω	Depth	rms
Upper	2500000	(0.11)	(1.0)	2.93
Lower	(59200)	(0.39)		

extracted 1cm thick samples. Observation showed the layer depth (d) to be around 1cm thick. Hence these procedures estimated four out of the five parameters required for the multi-layer model and are indicated in Table 4.2 in brackets. All such assumed or conventionally determined parameters will be shown in brackets in future tables where the layered model is used. Those acoustically determined will have no brackets. With four out of five parameters estimated an iterative procedure was then developed to estimate σ_e for the upper layer. For each increment of σ_e the predicted curve was compared to the measured curve using Equation 4.11 until the smallest rms error was achieved. For some sites where layering occurred, only three parameters were known and both σ_e and Ω for the top layer had to be estimated using an iterative procedure until the smallest rms error was achieved. A high priority in future work will be the development of better fitting procedures, although iteration of five parameters will lead to non-uniqueness and even greater ambiguity from combinations of parameters.

4.4.2 Probe

The analysis of probe information required the fitting of the real and imaginary parts of the propagation constant at the same time. This was because σ_{pe} influenced the slope of the predicted curves and T their separation. No algorithm was available to undertake this complex fitting procedure. An added complication was a need to fit different models over different frequency ranges for probed snow data. Therefore an multi-frequency averaging method was used. For each frequency values of σ_{pe} and T were calculated using the relevant programs mentioned in Section 4.3.2. All values were then summed and this number was divided by the total number

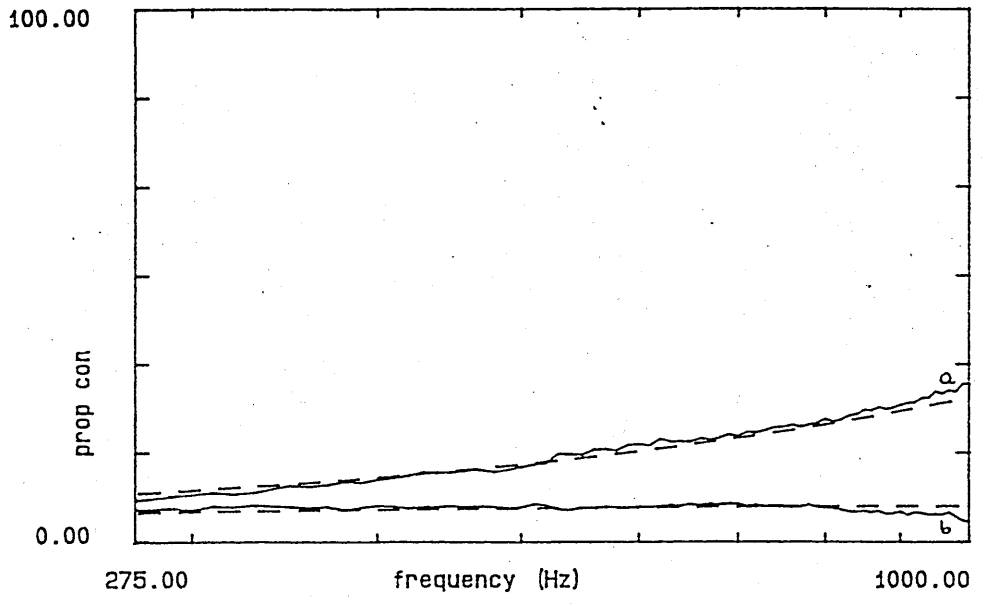

Figure 4.11 Example of Measured (solid) and Predicted Propagation Constant (broken) for a Clay Soil, Deduced parameters σ_{pe} =1450, T=1.46, depth 2-4cm.

of frequency points $\approx$ 200. This resulted an average σ_{pe} and an average T for that particular depth interval of soil or snow. Subsequent plotting of the propagation constant predicted from Equation 3.34 using these average values show tolerable agreement with measured data, an example of which is shown in Figure 4.11.

The consideration of a broad range of frequencies is a weakness of this procedure if the data is not well behaved. An example of badly behaved data is shown in Figure 4.12 which was made at between 13 and 15cms depth in snow. Erratic peaks in the low frequency range due to poor speaker output, and high frequency peaks due to poor signal to noise at the limits of the frequency range, clearly show over prediction of the flow resistivities and tortuosities deduced both from the low and high frequency approximations. To

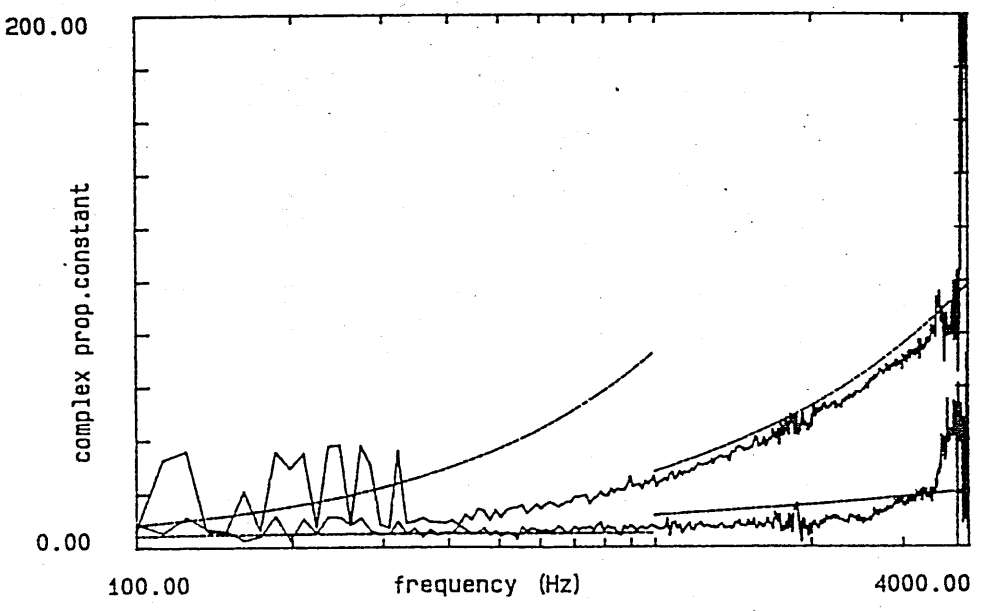

Figure 4.12 Example of Measured (solid) and Predicted Propagation Constant (broken), using multi-frequency averaging procedure, for Snow at 13-15cm deep, deduced parameters as shown in Table 4.3.

Table 4.3 Comparison of Average Multi and Single-Frequency Fitted Soil and Snow Parameters from the Measured Propagation Constant

	Depth cm	σ_{pe}	T	σ_{pe}	T
		low	low	high	high
Average	13-15	2945	2.95	4082	1.09
Approx	13-15	1347*	1.37*	1043*	1.09

overcome this problem a single-frequency average procedure is used similar to that used by Attenborough and Buser [96]. This involves data inspection and selection of measured values of a and b at single frequencies, where data is well behaved to calculate single values of σ_{pe} and T. The adequacy of the approximation model is frequency dependent as described in Section 3.6.2. Therefore for the low frequency/ high flow resistivity approximation single points are selected, from the lowest frequency behaved data for $\sigma_{pe}$and a well behaved higher frequency data point for T. For the high frequency/low flow resistivity approximation the highest well behaved data frequency are selected for both parameters. Deduced parameters from both the multi-frequency averaging and single-frequency average techniques for the data shown in Figures 4.11 and 4.12 are shown in Table 4.3. The * against the parameters denotes they were deduced using the single frequency average procedure. This will be the case for all probe deduced values of σ_{pe} and T mentioned subsequently.

For Figure 4.13 a value of 'a' at 500Hz and 'b' at 1KHz enabled the calculation of an σ_{pe} of 1347 and T of 1.37 for the low frequency approximation. For the high frequency approximation a value of 'a' at 3KHz resulted in an σ_{pe} of 1043 whilst the T value remained unchanged. The deduced parameters at either frequency extreme are now numerically close to each other and hence suggest homogeneity as expected from only 2cm thickness of snow. Another example of the use of the single frequency averaging technique to fit propagation constant data can be seen in Figures 4.14 and 4.15 for Sand 2. Figure 4.14 represents a fit using the multi-frequency average deduced σ_{pe} and T. In Figure 4.15, a fit is obtained by the selection of

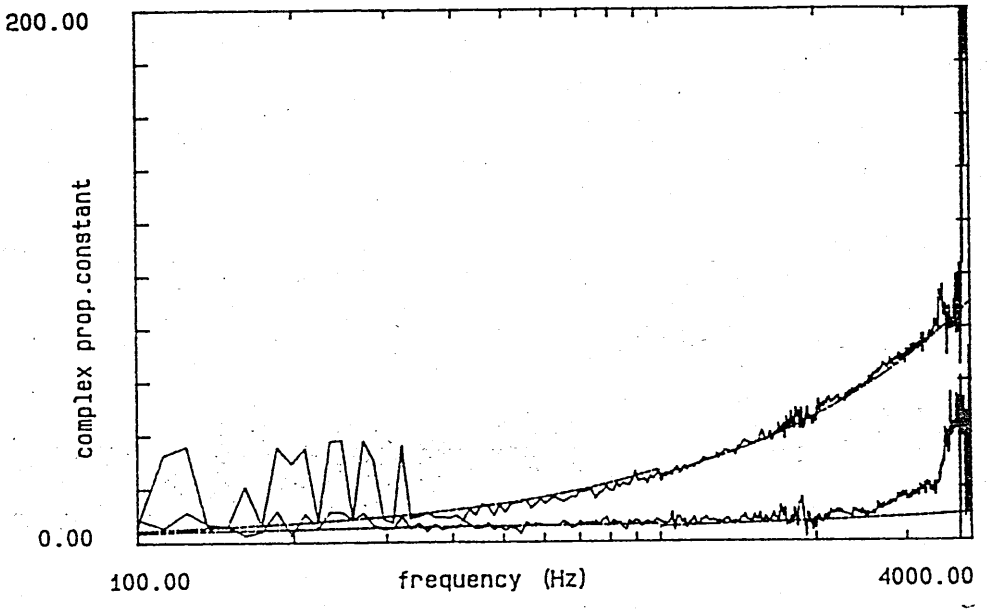

Figure 4.13 Example of Measured (solid) and Predicted Propagation Constant (broken), using single-frequency average technique, for Snow at 13-15cm deep, deduced parameters as shown in Table 4.3.

single-frequency values. The predictions are comparable and offer a way of speeding up the deduction process. The single-frequency averaging technique has advantages in terms of applicability to agricultural research on soils. Using these procedures the fitting and determination of parameters can be done rapidly on a calculator or micro computer without the need for the sophisticated and time consuming multi-frequency averaging technique.

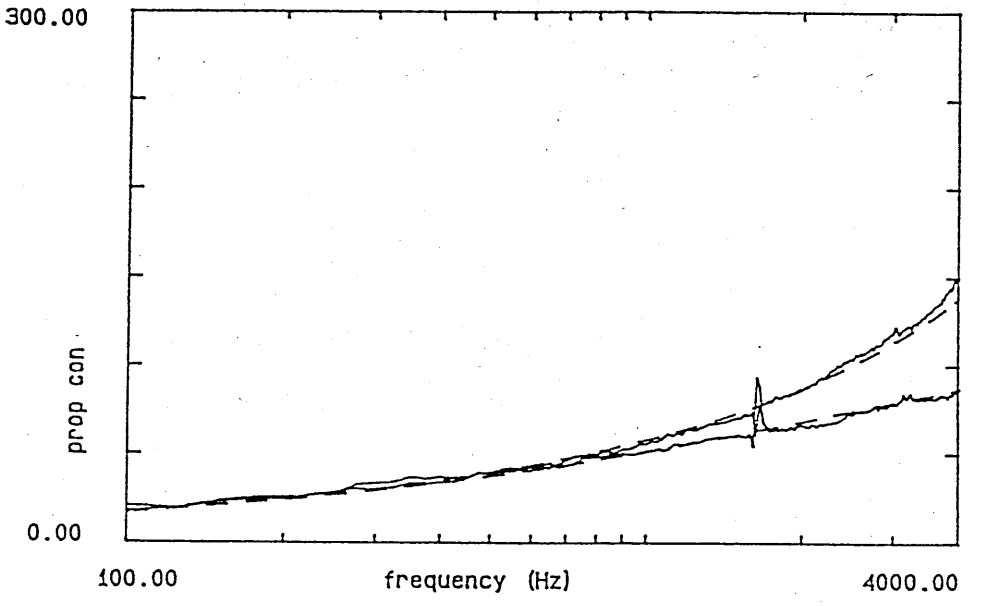

Figure 4.14 Example of Measured (solid) and Predicted Propagation Constant (broken), using multi-frequency averaging technique, for a Sand, Deduced parameters σ_{pe} =24240, T=1.55, depth 0-1.5cm.

4.4.3 Deduction of Porosity with Depth

From the two procedures in Sections 4.4.1 and 4.4.2 the deduction has been made of σ_{pe}, T and Ω from level difference measurements and σ_{pe} and T from probe measurements. Using the Bruggeman relationship where $T = \Omega^{-n'}$

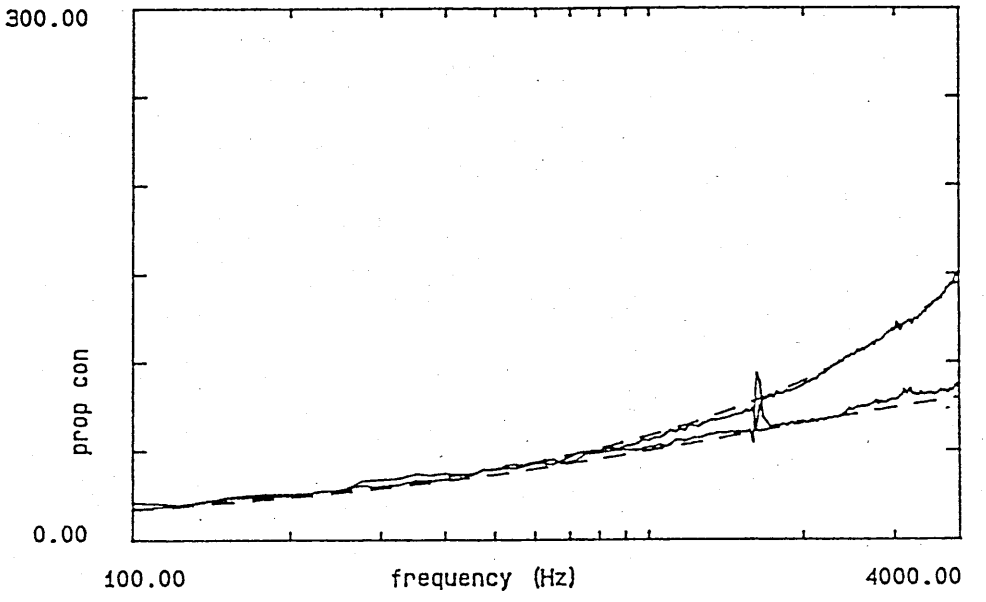

Figure 4.15 Example of Measured (solid) and Predicted Propagation Constant (broken),using single-frequency averaging technique, for a Sand, Deduced parameters σ_{pe} =23230 at 1KHz, T=1.99 at 4KHz ,depth 0-1.5cm

porosity can be expressed

$$\ln \Omega_o = -\frac{\ln T_o}{n'} \tag{4.12}$$

where T_o is the tortuosity and Ω_o the porosity both at the surface, in this case deduced from level difference measurements. At depth (d) T_d is the tortuosity and Ω_d the porosity, in this case T_d is deduced from probe measurements and hence

$$\ln \Omega_d = -\frac{\ln T_d}{n'} \tag{4.13}$$

Assuming that the grain shape factor n' remains constant with depth then

$$\ln \Omega_d = -\ln T_d \left(-\frac{\ln \Omega_o}{\ln T_o}\right) \tag{4.14}$$

$$= \frac{\ln T_d \ln \Omega_o}{\ln T_o} \tag{4.15}$$

hence porosity can be calculated at depth from

$$\Omega_d = \exp\left[\frac{\ln T_d \ln \Omega_o}{\ln T_o}\right] \tag{4.16}$$

using T_o and Ω_o from level difference fitting and T_d from probe measurements at various depths within soil. This procedure has been used to calculate profiles of porosity with depth.

4.4.4 Deduction of Effective Flow Resistivity and Tortuosity from Attenuation Measurements Only

Prior to measurements involving phase a theoretical deduction of T, the tortuosity, was derived based on a method described by Attenborough and Hess [89]. This involves looking at the difference between the first and second order approximations of k_b, the propagation constant,(Equations 3.34 and 3.40) at sufficiently high frequencies for their values to separate as seen in Figures 3.21, 3.22 and 3.23. Because attenuation/cm is the easiest to measure and most commonly used, the difference in the imaginary part between the two approximations is used. The technique is best explained by a worked example.

Using a measured value of attenuation eg 4.5dB at a relatively low frequency $f_1 = 200$Hz a predicted value of σ_{pe}, 107580, can be calculated using Equation 4.17 (see also Section 3.6).

$$k_b = \text{ a or b} = 0.0112\,(\sigma_{pe})^{0.5}\,\sqrt{f} \tag{4.17}$$

Using this value at a higher frequency where a and b are likely to have separated in value (say $f_2 = 2000$Hz), then the value of b, called b_1, can be predicted from

$$b_1 = (0.0112)\,(107580)^{0.5}(f_2)^{0.5} = 183.68 \tag{4.18}$$

Measured attenuation at f_2 is 15dB which from Equation 4.7 gives a value of $b_2 = 172.7$. Assuming that at high frequencies the measured b_2 is more closely predicted by the first approximation Equation 3.34 rather than the second approximation Equation 3.41 then the high frequency b_2 will be equal to

$$b_2 = b_1 - \frac{8.14\,T\,f[0.0112\sqrt{f}]}{8[\frac{b_1}{0.0112\sqrt{f}}]} \tag{4.19}$$

and hence T can be deduced from

$$T = \frac{8[\frac{b_1}{0.0112}]}{8.14\,(f_2)^2(0.0112)}(b_1 - b_2) \tag{4.20}$$

which can be rewritten

$$T = \frac{D\,F}{(f_2)^2}7824.4 \tag{4.21}$$

where $D = b_1 - b_2$, which for this worked example is 10.89, and $F = b_1$ = 183.68. Equation 4.21 therefore calculates a Tortuosity of 2.5. It should be noted that Equation 4.21 differs from that quoted in Attenborough and Hess [89]. Due to an algebraic error, multiplication by 0.7218 is necessary.

4.4.5 Summary of Deduction Processes

The flow diagram in Figure 4.16 outlines the procedures and steps taken for the acoustical deduction of effective flow resistivity, porosity, tortuosity at the surface and respective profiles with depth, from conjunctive use of

level difference and probe microphone deduced parameters. Alternatively an effective flow resistivity and porosity can be determined for a two layered soil together with an estimate of layer depth.

4.5 Measurement of Physical Soil Properties

Air Porosity and Moisture Content

Air porosity and moisture content were measured using the procedure described in Section 2.1.1. Samples of known volume were taken on sites within the area of level difference reflection and close to the probe positions. An core sampler taking 3cm deep samples and a another taking samples 5cm deep were used to extract undisturbed samples. The number of samples per plot at depths of 3,6 and 9cm or 5cm was usually 3, maybe more if time permitted, to try and give a representative sample of the localised area. Samples were weighed wet in the field using a small digital balance, sealed in polythene bags and labelled. They were carefully transported back to the laboratory in an adapted picnic cool box. Drying for 24-48hrs at 105° was done in an industrial oven. After drying and reweighing all required values (eg wet weight, dry weight, weight of sample tin) were run through a short computer program to calculate dry bulk density, % air porosity,% water content (vol), and % of solids. A Fortran listing of the program POROS3 is shown in Appendix A.

Dry bulk density and moisture content measurements were also available from AFRC Engineering for the Silsoe site. These measurements were part of a routine soil monitoring process made on the two different traffic wheeling sites. Dry bulk densities measured using the SIAE nuclear density probe, were made at 5cm intervals below the surface and at three sites per plot. Moisture contents were measured using a neutron probe also at 5cm intervals down through the profile. Although these measurements do not fall on exactly the same day as acoustic measurements it was recognised they provided a useful additional check on acoustic deductions particularly if it was known not to have rained in the intervening period.

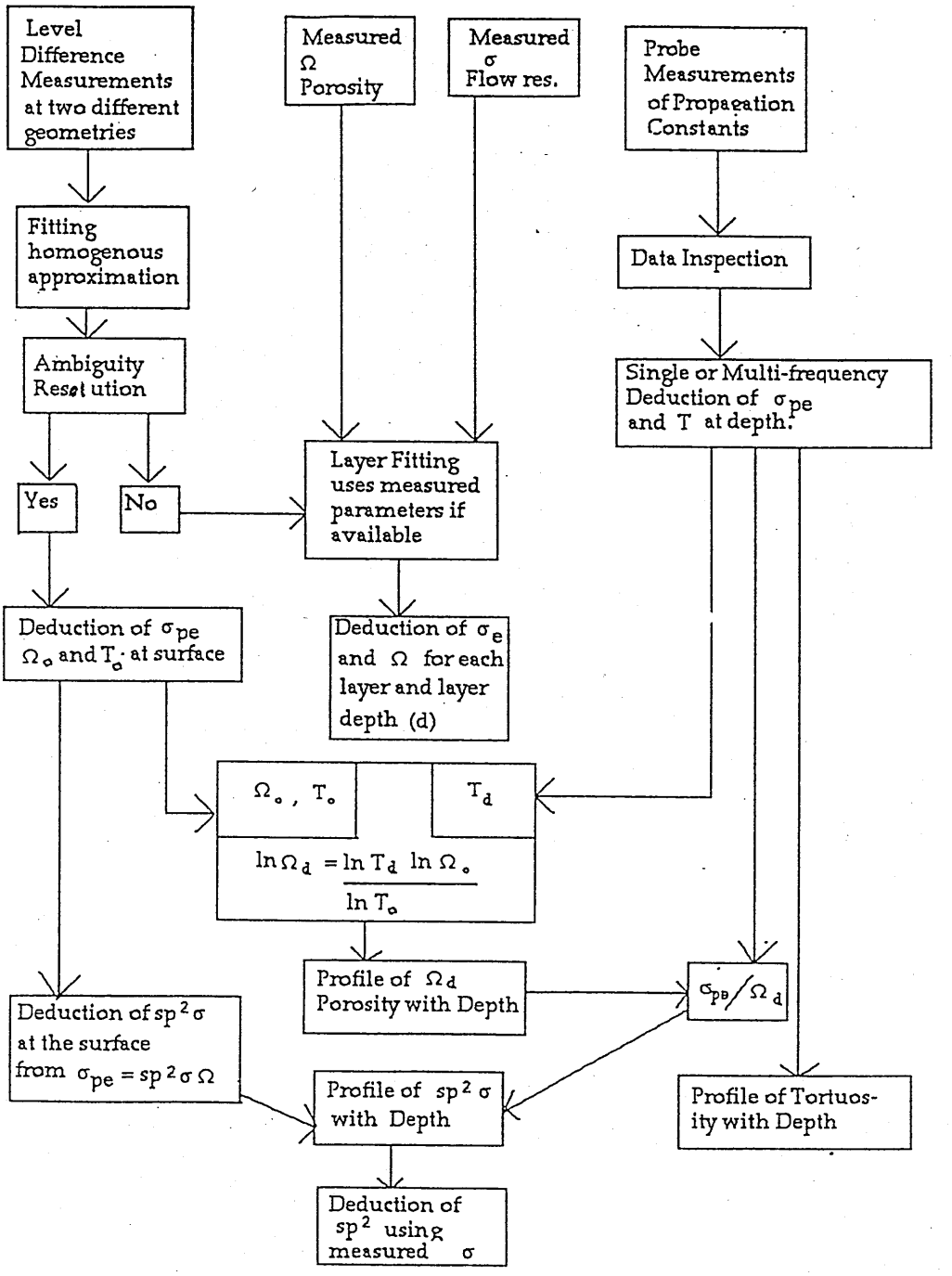

Figure 4.16 Flow Diagram of Deduction of Ground Parameters from Acoustical Measurements.

For snow, air porosity was deduced using Equation 2.28 mentioned in Section 2.8.2. Snow density calculations were made from weighing a known volume of snow using a Taylor - La Chappelle snow density kit.

Flow Resistivity

Three methods were used to measure the flow resistivity of soils.

Flow Rig

The arrangement of the flow rig is shown in Figure 4.17. Compressed air was passed through a series of regulating valves via a very narrow tube opening into chamber E. This created an area of low pressure immediately in front of the three tubes connected to the rest of the system. Consequently ,because of the pressure differential, air was drawn from the outside through the sample in the sample holder and into the system. The rate of air flow through the system was controlled by three flow meters, giving a total measurement range between 8.7 to 0.1 litres/minute. For these experiments the flow rate was kept below 3 litres/minute so that the sample structure would not be damaged. Starting at 3 litres/minute the flow rate was systematically decreased. At each flow rate the pressure drop across the sample was recorded from the Furness micromanometers as $mm\, H_20$. The flow resistivity in cgs rayls/m was calculated from

$$R = \frac{C_1\, A\, \Delta P}{Q\, L} \tag{4.22}$$

where
A is the area of the sample holder in cm^2
L is the length of the sample
Q is the flow rate in cm^3/sec
ΔP is the pressure drop in inches H_20
and C_1 is a conversion factor =2490 if the above units are used.

The measurement of flow resistivity in this manner involved the transportation of samples back to the laboratory. This sometimes damaged the samples or they dried out in transit. There was also the problem of insertion

into the sample holder causing further disturbance. To try and overcome these problems a second apparatus was developed at the OU based on the Leonards Apparatus [110] and a similar device was used in Mississippi.

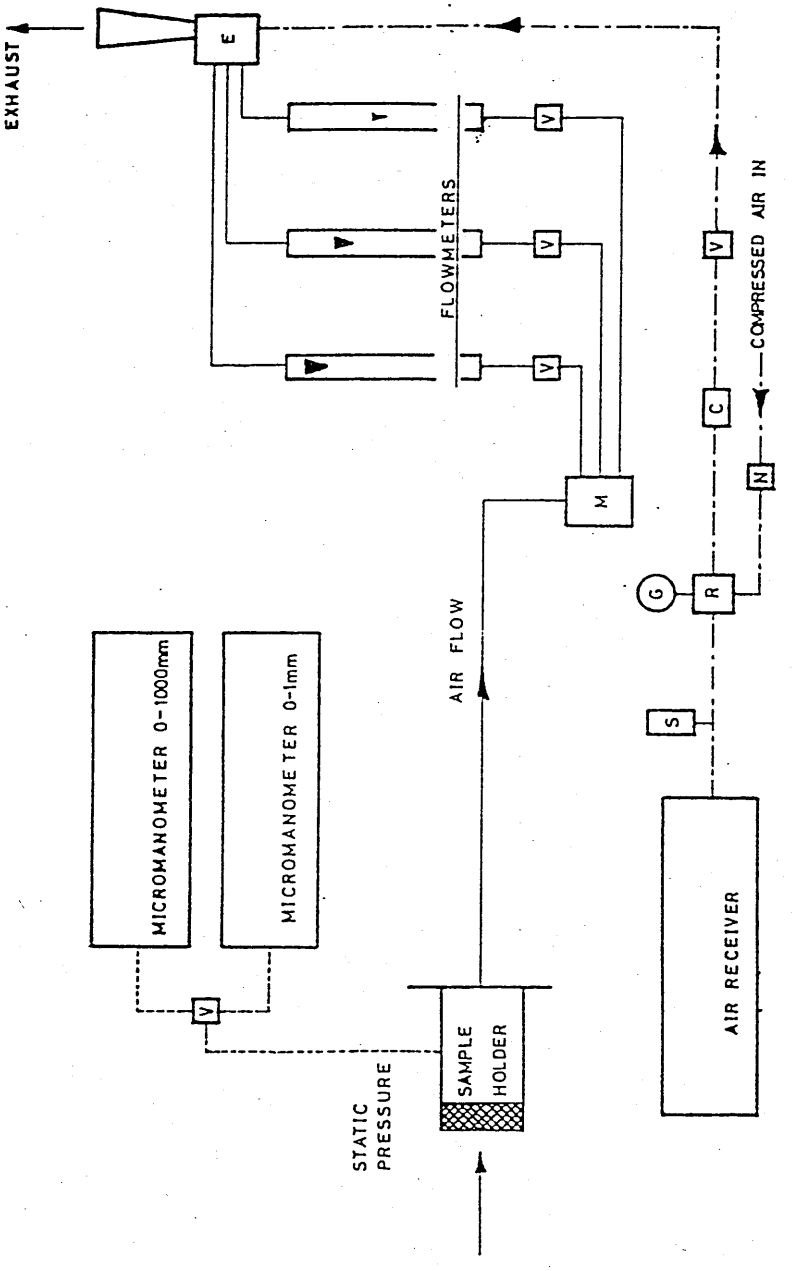

Figure 4.17 Diagram of Flow Rig

Leonards Apparatus

The apparatus is based on a balance mechanism as shown in Figure 4.18. The reader is referred to [110] for a detailed description of construction and operation. However, a brief description is offered here. Attached to one arm of a balance mechanism (see insert in Figure 4.18) is a displacement cylinder (A) floating in a double walled cylinder filled with parafin (D). The soil sample (C) is carefully placed into the sample holder (B). A known mass applied to the pan (E) causes the floating chamber to rise. The increased volume within the chamber creates a pressure differential and air is drawn in through the soil sample. The rate, in seconds, of air passing through the sample is monitored by noting the time taken for the central pointer (F) to pass from one gradation to another. Weights are applied so this swing is not too fast and flow is therefore kept slow.

The flow resistivity R in cgs rayls/m is calculated from

$$R = \frac{Fw\,\Delta t\,A_1}{A_2\,\Delta h\,A_2\,L} \tag{4.23}$$

where Fw is the force and is equal to (mass in grams) x (acceleration of gravity = 980cm/sec^2), Δt is the average time for that weight, A_1 is the area of the sample, A_2 is the area of the displacement cylinder and Δh the known length in cm for the 20 gradations the pointer passes across. When all known areas and constants are inserted into Equation 4.23 then flow resistivity can be calculated for the Mississippi measurements from

$$R = \frac{\text{mass}\,\Delta t\,2.27}{L} \tag{4.24}$$

and for the OU apparatus

$$R = \frac{\text{mass}\,\Delta t\,1.77}{L} \tag{4.25}$$

Indirect Method

The third and indirect method of calculating flow resistivity was using the relationship mentioned in Equation 2.14. Measurements of air permeability were made by Wall [111] on the Silsoe field site. Core samples were taken

from the same field treatments, normal and zero wheeled, on the same day as acoustic measurements. Air permeability of these samples was measured in a laboratory using a rig system described by Stanton [112], after Ball et al [113] and Hunter [8].

Figure 4.18 Diagram of Leonards Apparatus

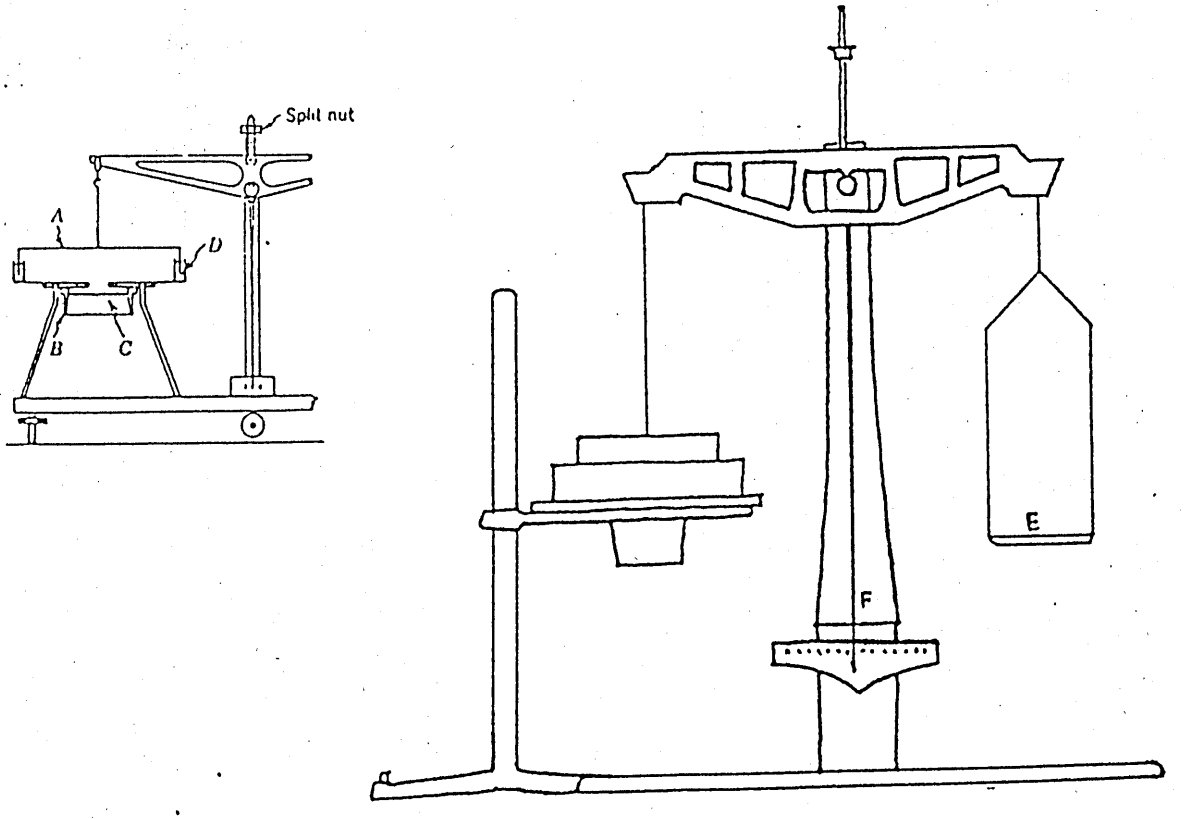

Chapter 5

Results

A summary of results, site by site, are presented here. An appendix reference is given for each site in which both level difference and probe measurement deduced ground parameters are presented in graphical and tabulated form. Measured air porosity, water content and flow resistivity calculations are also tabulated in specific appendices.

5.1 Results for Sand

5.1.1 Sand 1

Results of level difference measurements made for Sand 1 are presented in full in Appendix C. The best fit ground parameters using the three parameter approximation from level difference measurements are shown in Table 5.1. Also included are the best fit parameters using the Delany and Bazley semi-empirical formula. An example of a best fit prediction is shown in Figure 5.1.

Rms values (average 7.42) obtained using the Delany and Bazley semi-empirical relationship are significantly higher compared to the three parameter best fit rms values (average 1.88). This indicates that a prediction characterising the ground surface in terms of one parameter, the effective flow resistivity is an over-simplification of the ground properties.

From these results made at two different geometries it can be suggested the relatively high σ_{pe} values represent a fairly compacted sand. An av-

Table 5.1 Best fit ground parameters for Sand 1

	3 para approx				Delany and Bazley	
	σ_{pe}	T	Ω	rms	σ_e	rms
max	48311	2.20	0.38	2.06	1020000	7.72
mean	42000	2.15	0.36	1.88	906200	7.42
min	36800	2.08	0.35	1.56	790000	6.48

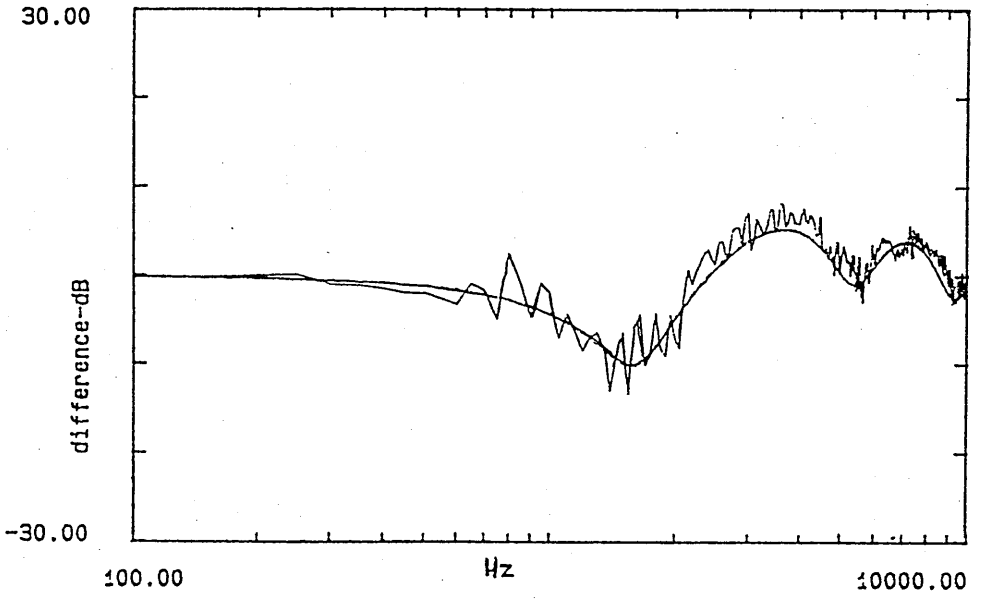

Figure 5.1 Example of Measured and Best Fit Level Difference over Sand 1, σ_{pe} =40910, T=2.21, Ω=0.36, rms=1.88, geometry hs=0.24,r=1.36,hrt=0.25,hrb=0.05.

erage porosity of 0.36 suggest an effective $\sigma_e$of 325000mks rayls/m using the relationship $\sigma_e\Omega^2$. Using the maximum theoretical value for the pore shape factor, so that $sp^2 = 0.25$, a predicted value of flow resistivity σ from $\sigma_{pe} = sp^2\sigma\Omega$ has a value of 468000mks rayls/m. Measured flow resistivities for this sand had an average value of 376000mks rayls/m and ranged from 326800 to 438000mks rayls/m. This suggests that sp^2 for this sand has a slightly larger value than 0.25. Measured values of porosity for the top 3cms of the sand averaged at 0.35 increasing slightly to 0.36 at 3 - 6cms deep. This compares favourably with an acoustically deduced value of 0.36. Values of measured porosity and flow resistivity can be seen in Appendix C.

Two separate sets of probe measurements were made on this sand. The first set were rather limited and experimental in that they involved the use of unhoused Sony Electret microphones, the buried microphone only protected by a coating of parafilm. The results of the first set are presented in Table 5.2.

Table 5.2 Ground parameters deduced from Measurements using Unhoused Microphones in Sand 1

Depth(cm)	σ_{pe}	T
0-1	27064	2.37
0-1	88897	9.45
0-2	27518	3.37
0-2	21906	1.76
1-3	23489	2.60

Examples of the propagation constant determined from these measurements are shown in Appendix C. They are very poorly behaved. This maybe due to the buried microphone being wrapped in parafilm which caused a signal to noise problem although coherence was checked and found to be above 0.8.

For the second set of probe measurements attenuation and phase were measured using a probe microphone signal referenced to a signal received by a Bruel and Kjaer microphone lying at the surface. An example of

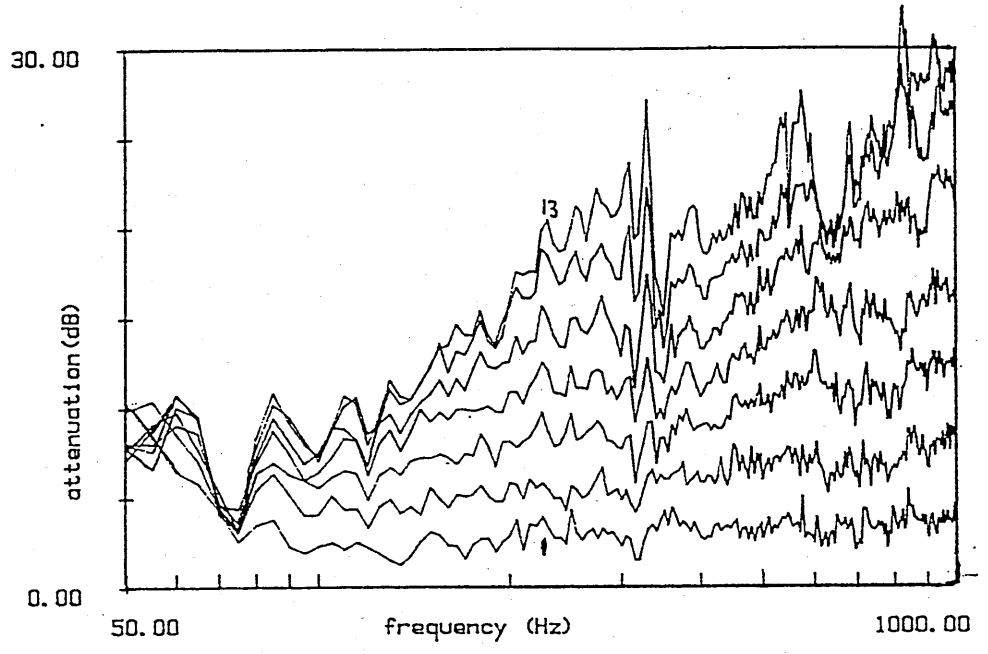

Figure 5.2 Measured attenuation dB at depths between 1-13cm in Sand 1

attenuation with depth for the second set of probe measurements can be seen in Figure 5.2. Measurements were at 1cm intervals down to a depth of 13cm although only 2cm intervals are plotted. Peaks in the received signal at approximately 350Hz and 630Hz limit the depth of analysis to 7cm. Table 5.3 shows an example of a profile of deduced σ_{pe} and T with depth, those with * beside them are deduced using the single-frequency averaging procedure. Examples of propagation constant fits for these measurements are shown in Figures 5.3 and 5.4, others are shown in Appendix C.

In Table 5.3 below 1cm the profile appears fairly homogeneous with σ_{pe} ranging from $\approx$ 7000-10000 and T around 2 - 2.5. The higher σ_{pe} and T

Table 5.3 Ground parameters deduced from Measurements using Probe Microphone in Sand 1

depth(cm)	σ_{pe}	T
0-1	30600	21.21*
1-2	6882	2.16
2-3	7112	2.12
3-4	9652	2.22*
4-5	8707	2.28*
5-6	7900	2.12*
6-7	7355	2.57*

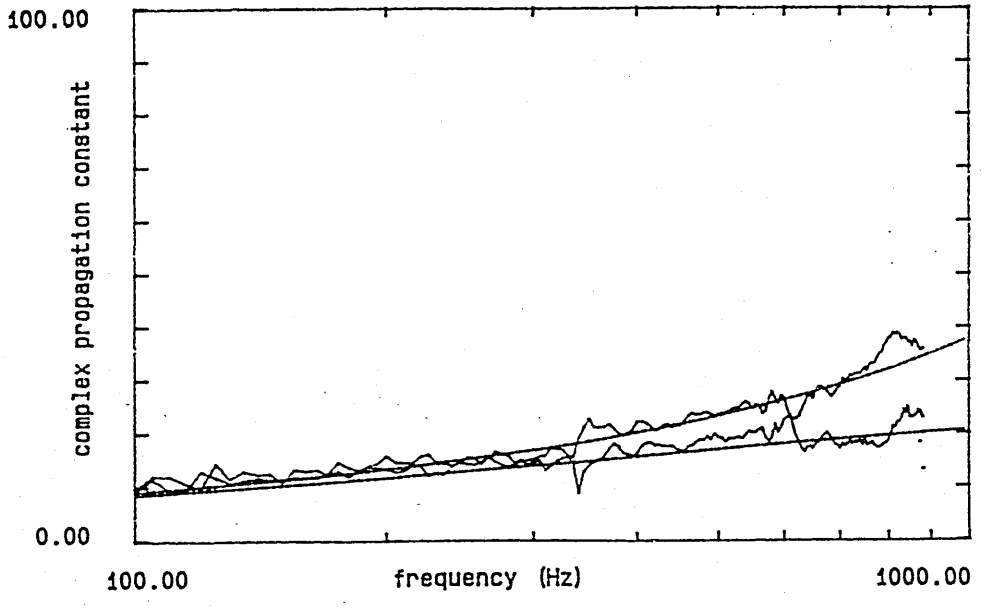

Figure 5.3 Measured and Predicted Propagation Constant for 1-2cm depth interval on Sand 1, σ_{pe} =6882, T=2.16.

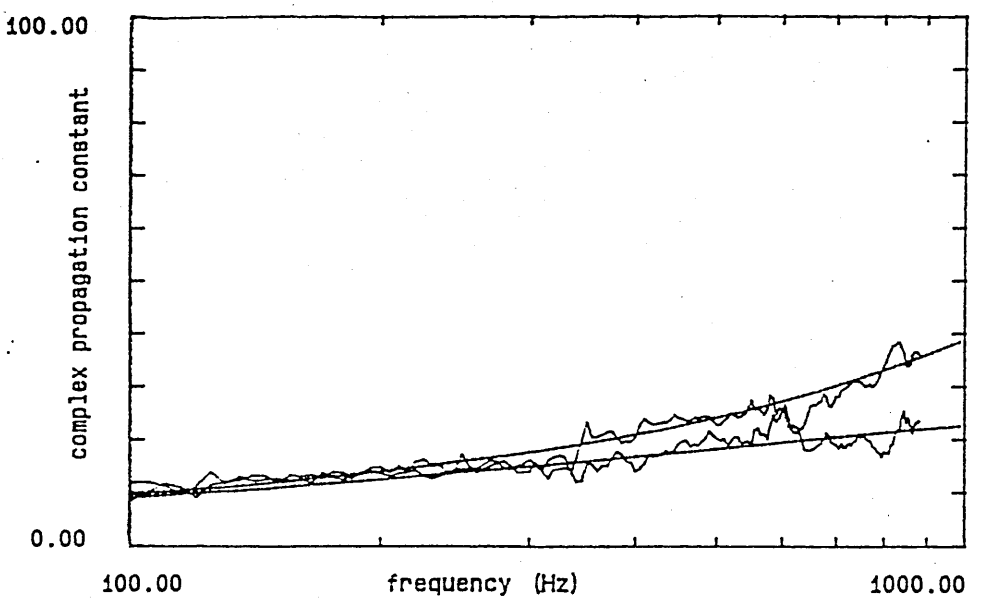

Figure 5.4 Measured and Predicted Propagation Constant for 2-3cm depth interval on Sand 1, σ_{pe} =7110, T=2.12.

values at the surface indicate the possibility of a harder surface. Comparison between surface interval probe results and the level difference predictions are shown in Table 5.4. The 0-1.5cm probe measurements show greater

Table 5.4 Comparison of level difference and probe Deduced parameters for Sand 1

measurement		σ_{pe}	T	Ω	rms
level difference	max	48000	2.21	0.38	2.06
	mean	42000	2.15	0.36	1.88
	min	36000	2.08	0.35	1.56
probe 0-1cm	max	88897	21.21		
	mean	40069	11.54		
	min	14470	2.37		

variability with σ_{pe} ranging from 14470-88897 and T from 2.37 - 21.21. This may result from the localisation of the probe measurements, giving a clearer picture of lateral inhomogeneity. Such high flow resistivity and tortuosity values close to the surface would seem to indicate the presence of a surface crust. However no such crust was visible in the sand tray. An alternative interpretation may be that for the probe measurements there are problems in the physical determination of the actual ground surface hence making these particular measurements unreliable.

An example of porosity deduction with depth is given here for one profile, shown in Table 5.5. Others are tabulated in Appendix B. With the exception of the surface measurement(0-1cm) the profile is homogeneous and the acoustic predictions match well the measured porosities at depth.

It has been suggested that the higher effective flow resistivity and tortuosity values at the surface indicate the possibility of a harder surface. However the sand could be successfully fitted with the homogeneous three parameter approximation and there was no visible surface crust. This inconsistency is due to an error in initial analysis of the data. During initial analysis the depth interval between the surface reference measurement and the first buried depth was assumed to be 1cm. During reanalysis of the

Table 5.5 Deduction of Porosity with Depth for Sand 1

Depth cm	T_o	Ω_o	T_d	Ω_d	Meas.Ω	Depth meas.
surface	2.15	0.36			0.36	0-3cm
0-1			21.21*	0.02		
1-2			2.16	0.36		
2-3			2.12	0.36		
3-4			2.22*	0.34	0.34	3-6cm
4-5			2.28*	0.33		
5-6			2.12*	0.36		

same interval data the depth was allowed to alter to 1.5cm and subsequently 2.0cm. The results of doing this can be seen in Table 5.6. It can been seen

Table 5.6 Reanalysis of Ground Parameters deduced from Measurements using Probe Microphone in Sand 1

depth(cm)	σ_{pe}	T
0-1	30600	21.21*
0-1.5	14487	11.22
0-2	8149	2.36*

that when the depth is allowed to be 0-2cm for this interval then the effective flow resistivity falls in line with those predicted for deeper depths, as shown in Table 5.3 and hence behaves more homogeneously. This depth error can be accounted for in the construction of the particular probe microphone used for this set of measurements. Examination of the probe revealed that there was in fact a 0.5cm difference between the position of the microphone diaphragm and the probe end holes. In addition there was approximately another 0.5cm error between the actual depth of the probe microphone and that indicated on the engraved 1cm intervals. This amounts to an error of c.1cm which explains the spurious values close to the surface. The intervals at deeper depths are however true 1cm intervals, relative to each other and the profile shown in Table 5.7 is a corrected profile for this sand.

Table 5.7 New Ground parameters deduced from Measurements using Probe Microphone in Sand 1

depth(cm)	σ_{pe}	T
0-2	8149	2.36*
2-3	6882	2.16
3-4	7112	2.12
4-5	9652	2.22*
5-6	8707	2.28*
6-7	7900	2.12*
7-8	7355	2.57*

5.1.2 Sand 2

Two sets of measurements were made over this sand. Set 1 was carried out on sand contained in a large dustbin. The second set was made over the same sand in a tray. Both the tray and dustbin were located within a small anechoic chamber. All results of level difference measurement best fit parameters, using both the three parameter approximation and the Delany and Bazley semi-empirical relationship, are presented in Table 5.8 to enable a comparison between the different locations. As with sand 1, the best fit rms values for the majority of cases of sand 2 are significantly higher when the single parameter model is used. Over the bucket of sand, however, the Delany and Bazley best fits are lower indicating a better fit than the three parameter approximation. Nevertheless when the average measured flow resistivity for this sand (134700)is used in conjunction with the semi-empirical prediction of effective flow resistivity in the relationship $\sigma_e = \sigma\Omega$ deduced porosities average at 1.87, which is unrealistic. The parameters predicted are similar for both locations. This indicates the area of sand actually sensed in a short range level difference measurement with a geometry of hs 0.1, r 0.37, hrt 0.15, and hrb 0.02, is likely to be smaller than $1.25m^2$, the surface area of the dustbin.

Using the relationship $\sigma_{pe} = sp^2\sigma\Omega$, an sp^2 of 0.25 and the average σ_{pe} and Ω values, a flow resistivity of 158800mks rayls/m can be predicted. The

Table 5.8 Best fit ground parameters for Sand 2

	3 para approx				Delany and Bazley	
location	σ_{pe}	T	Ω	rms	σ_e	rms
bucket	10750	1.21	0.50	1.17	260000	1.04
	20547	1.66	0.48	0.76	160000	0.58
tray	11910	1.34	0.48	2.01	170000	4.49
	25629	1.00	0.54	2.08	260000	4.54
	21698	1.00	0.49	1.90	270000	7.28
	21428	1.34	0.44	2.46	330000	6.41
	21450	1.34	0.44	2.45	320000	7.35
average	19058	1.27	0.48	1.84	253000	4.54

average measured flow resistivity for this sand was 134700mks rayls/m and values ranged from 109200 to 153700mks rayls/m. Like Sand 1 this would suggest a value of sp^2 greater than 0.25. A predicted average porosity of 0.48 compares with a measured porosity of 0.47. Measured values of air porosity for replicates and flow resistivity measurements are listed in Appendix D.

Magnitude dB and phase at increments of 1cm depth within Sand 2 are shown in Figures 5.5 and 5.6. Deduced values of σ_{pe} and T for Sand 2 in the tray location are shown Table 5.9. An example of σ_{pe} and T deduction from propagation constant data is shown in Figure 4.14. Plots and tables of propagation constant fits for other depths from both tray and dustbin location are shown in Appendix D.

Studying the profiles in Table 5.9 the fairly constant values of σ_{pe} and T for the bucket location would indicate a fairly homogeneous sand with depth. For the tray sand there would appear to be a harder slightly more compact layer at between 3-5cm depth where σ_{pe} and T both increase. Porosity measurements were only made for this sand down to a depth of 3cms due to its very loose nature and difficulty in sample extraction and so unfortunately confirmation of this acoustically sensed harder layer cannot be made. Comparison of the deductions from level difference and probe measurements is shown in Table 5.10. There is good agreement between level difference and probe predicted values of σ_{pe} and T, unlike those for Sand 1.

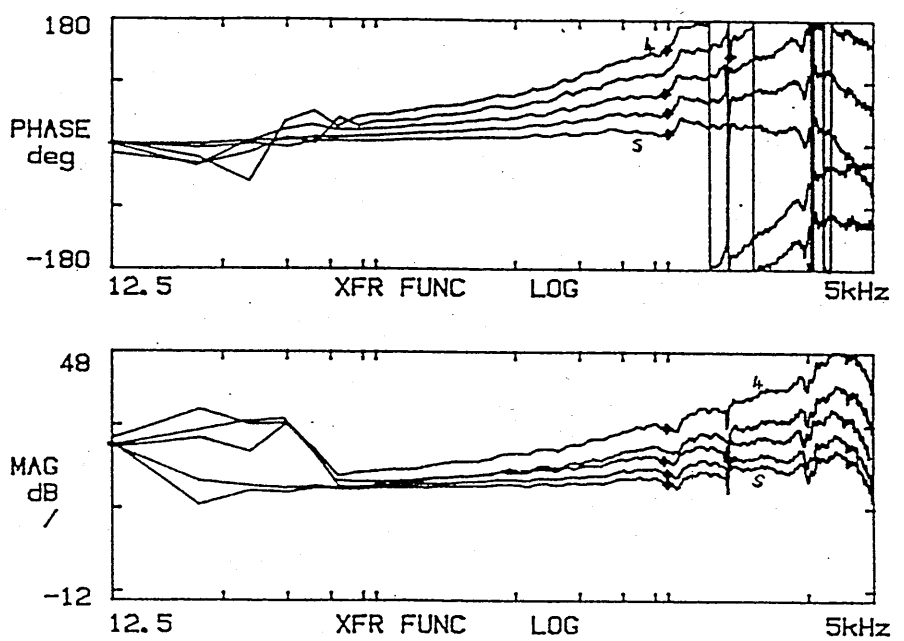

Figure 5.5 Measured magnitude dB and Phase at depths between 1-4cm in Sand 2

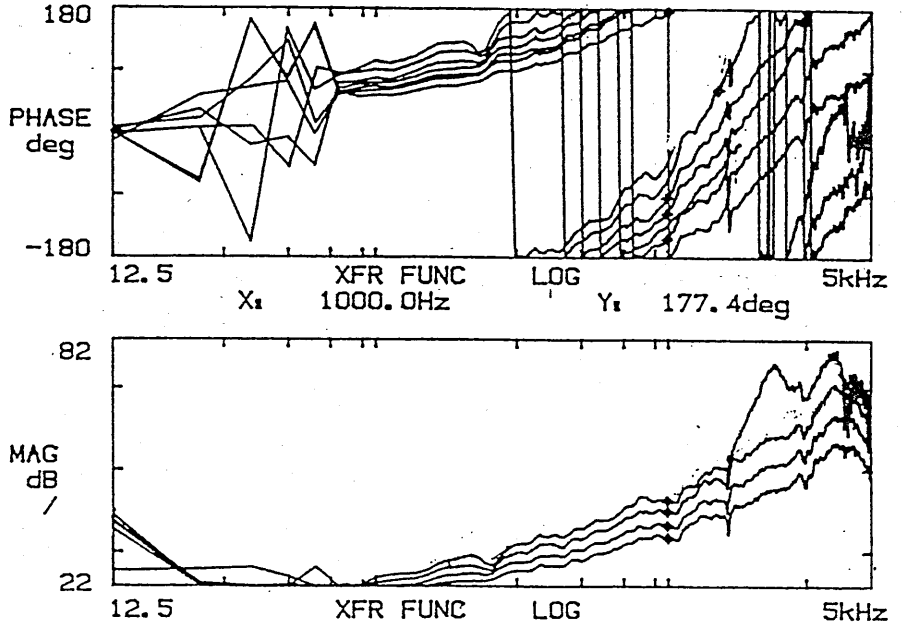

Figure 5.6 Measured magnitude dB and Phase at depths between 5-8cm in Sand 2

Table 5.9 Ground parameters deduced from Measurements using Probe Microphone in Sand 2

location	depth(cm)	σ_{pe}	T
dustbin	0-1	21444	3.38*
	1-2	14161	2.15*
	2-3	13382	1.85*
	3-4	10766	1.35*
	4-5	19819	1.85*
	5-6	11618	1.65
	6-7	12533	1.59
tray	0-1.5	24242	1.55
	2-3.5	13159	1.11
	3.5-4	33250	3.27*
	4-5	25844	2.25*
	5-6	18477	1.85*
	6-7	26457	2.10*

Table 5.10 Comparison of Level Difference and Probe Deduced Parameters for Sand 2

measurement		σ_{pe}	T	Ω	rms
level difference	max	25629	1.66	0.54	2.08
	mean	19058	1.27	0.48	1.84
	min	10750	1.21	0.44	0.76
probe 0-1cm	max	24242	3.38		
	mean	18947	2.68		
	min	11156	1.55		

Examples of porosity deductions with depth for Sand 2 are tabulated in Appendix B.

5.1.3 Summary for Sands 1 and 2

A summary of results comparing deduced with measured parameters for both sand types is presented in Table 5.11.

Table 5.11 Comparison of Measured and Predicted Ground Parameters for Sands 1 and 2

Sand Type	Predicted σ $\star$	Measured σ	Range Measured σ	Depth of Meas Sample
sand 1	467000	376000	326000- 438000	0-3cm
sand 2	158000	134000	109000- 153000	0-3cm
	Predicted Ω	Measured Ω		Depth of Meas Sample
sand1	0.36	0.35		0-3cm
sand2	0.48	0.47		0-3cm

$\star$ assumes a pore shape factor of 0.5

From these results the acoustic measurements have distinguished the main physical differences in terms of flow resistivity and porosity. Sand 1 is predicted and measured as having a higher flow resistivity than Sand 2, whilst also having a lower porosity. Close agreement is likely because the acoustic level difference technique is sampling a layer similar in depth to the 3cm thick samples made for the conventionally measured samples.

5.1.4 Sand 3

Level difference measurements were fitted using the layered model to deduce ground parameters. The results are presented in Table 5.12.

Prediction fitting shows a hard crust overlying a more porous sand beneath. The porosity values are set close to measured porosity values, see Appendix E, for the two distinct layers . The depth (d) was set to 1cm the observed layer depth. Fitting was then under taken by iterating the two effective flow resistivities until a least rms value was obtained. Measured

Table 5.12 Parameters Deduced from Level Difference Measurements for Sand 3.

Layer	σ_e	Ω	Depth(cm)	rms
Top	5000000	(0.13)	(1.0)	1.75
Bottom	100000	(0.27)		

flow resistivity of the sand measured with the Leonards Apparatus averages at 71000mks rayls/m taken for a sample 5cm deep. Consequently monitoring of the crust flow resistivity was not possible using this conventional technique. Details of flow resistivity measurements are in Appendix E.

Probe results for this sand were made using the procedure mentioned in Section 4.4.4 from attenuation measurements only. A typical profile is shown in Table 5.13 whilst others are presented in Appendix E.

Table 5.13 Ground parameters deduced from Propagation Constant Measurements using Probe Microphone in Sand 3.

depth(cm)	σ_{pe}	T
0-1	106950	5.97
1-2	47520	3.22
2-3	21020	1.92
3-4	21120	19.30

The deductions from studying the imaginary part of the propagation constant confirm the presence of a harder surface layer with a looser layer beneath. The T value of 19.30 at 3 - 4cm is probably untrue. This is because attenuation was only reliably measured up to 800Hz due to background noise and calculation was therefore at a frequency where the real and imaginary parts of the propagation had not separated sufficiently in value.

5.2 Results for Sandy Loam

Level difference and probe measurements were made on a sandy loam soil contained in a soil bin. Measurements were made after the application of varying amounts of water with the soil described as dry, moist and wet. The results are presented here in the three moisture content categories.

5.2.1 Dry

Level difference predictions of the 3 parameters σ_{pe}, T and Ω are presented in Table 5.14, together with the best fit predictions using the single parameter relationship of Delany and Bazley. An example of a best fit predicted curve

Table 5.14 Best Fit Ground Parameters from Level Difference Measurements over a Sandy Loam Soil (dry)

	3 para approx				Delany and Bazley	
	σ_{pe}	T	Ω	rms	σ_e	rms
max	28800	4.59	0.59	2.92	530000	19.94
mean	24050	3.32	0.52	2.00	370000	10.95
min	20270	1.06	0.47	1.35	210000	3.84

against measured data is shown in Figure 5.7. All best deduced parameters are shown in Appendix F. It can be seen that the average Delany and Bazley rms value is much higher than that for the three parameter approximation fitting. The average acoustically deduced porosity for this soil is 0.52. Measured porosities for the top 5cms ranged from 0.47-0.51 and are tabulated in Appendix F. The predicted surface porosity is likely to be higher than that measured over 5cm as the acoustic reflection technique takes into account less depth of soil than the core samples. The relatively high values of σ_{pe} may indicate a fairly compact soil. Measured flow resistivities for this dry soil, shown in Appendix F, ranged from 212000 - 306000mks rayls/m with an average of 259000mks rayls/m. From the relationship $\sigma_{pe} = sp^2\sigma\Omega$ and using the average predicted porosity an inferred value for sp^2 is 0.17, which is similar to that deduced previously for soil [83].

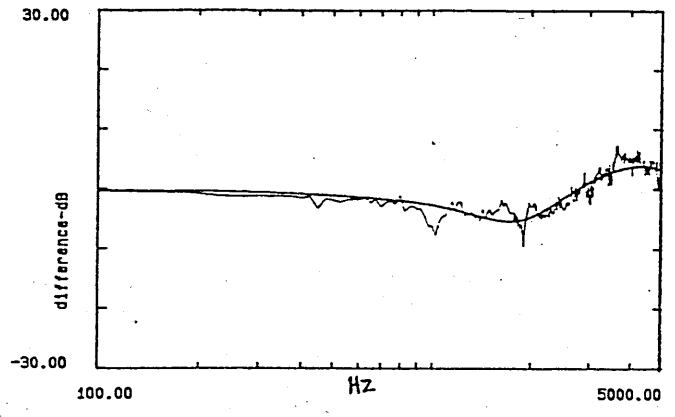

Figure 5.7 Example of Measured and Best Fit Level Difference over a Dry Sandy Loam σ_{pe} =28800, T=4.29, Ω=0.47 rms=1.57, geometry hs=0.2, r=1.05, hrt=0.2, hrb=0.05.

Figure 5.8 shows an example of attenuation and phase with depth down to 6cms. Although measurements were made up to 4KHz, analysis concentrates on frequencies between 100Hz and 1KHz. This is due to poor coherence and hence the unreliability of the high frequency data. This is true for all measurements made under all three moisture contents. The compact nature of this soil both when dry and dust like, and when saturated, is possibly the reason for poor coherence. Sufficient signal above background noise level was not received by the probe microphone at the high frequency range.

Deduced parameters of σ_{pe} and T from probe measurements are shown in Table 5.15 for intervals of 0-1, 1-3, and 3-5cm. Examples of fitting the propagation constant deduced from probe data are shown in Appendix F.

In Table 5.15 with the exception of 0-1cm for Run #2 the profiles do appear homogeneous with depth and the high values of σ_{pe} and T suggest a compacted soil. They are comparable with data obtained from the level difference measurements. A comparison between the two techniques predictions is shown in Table 5.16.

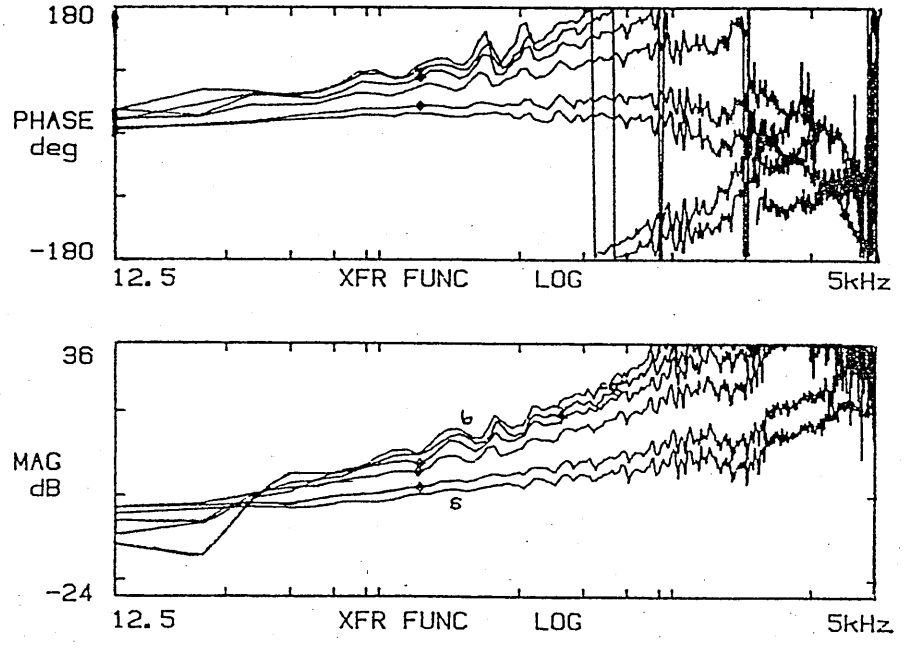

Figure 5.8 Example of measured magnitude dB and phase for a dry sandy loam at 0,1,3,4,5 and 6cm depths.

Table 5.15 Parameters deduced from Probe Measurements using Probe Microphone in a Sandy Loam Soil (dry).

Depth(cm)	σ_{pe}	T
0-1	31255	5.44
1-3	20957	3.45
3-5	20143	5.29*
0-1	8675	5.79
1-3	23101	2.02
3-5	26227	6.31
0-1	23839	3.48
1-3	34158	3.89
3-5	29250	9.81

Table 5.16 Comparison of level difference and probe Deduced parameters for Sandy Loam (dry)

measurement		σ_{pe}	T	Ω	rms
level difference	max	28800	4.59	0.59	2.92
	mean	24050	3.32	0.52	2.00
	min	20270	1.06	0.47	1.35
probe 0-1cm	max	31255	5.79		
	mean	21590	4.90		
	min	8675	3.48		

Porosity with Depth

Using the relationship described in Section 4.4.3, porosities with depth have been calculated for the profiles mentioned above. These are shown in Table 5.17.

Table 5.17 Deduction of Porosity with Depth for Sandy Loam (dry)

Depth cm	T_o	Ω_o	T_d	Ω_d	Meas.Ω	Depth meas.
surface	3.32	0.52			0.49	0-5cm
0-1			5.54	0.40		
1-3			3.45	0.51		
3-5			5.29*	0.38		
average				0.44		
0-1			5.79	0.38		
1-3			2.02	0.68		
3-5			6.31	0.37		
average				0.49		
0-1			3.48	0.51		
1-3			3.89	0.48		
3-5			9.81	0.29		
average				0.43		

In Table 5.17, Run 1 has a lower porosity 0.40 just below the surface followed by a much looser layer with a porosity of 0.51. This is reflected in the σ_{pe} values in Table 5.15. Run 2 also exhibits this porosity pattern. Looking at Table 5.15 the value of 8675 for σ_{pe} is obviously uncharacteristic although 5.79 for T is average. Therefore it enables a consistent deduction of porosity with depth. Run 3 has a gradual decrease in porosity with depth. This is indicated by the gradual decrease in T but not in the values of σ_{pe} in Table 5.15 . From this it is indicated that the value of σ_{pe} alone does not automatically indicate a relative compaction or looseness of the soil, values of T must be considered an important indicator.

Average porosities for each 0-5cm profile deduced from by probe measurements are comparable to porosities measured using the conventional technique. The predicted values of porosity 0.44, 0.49 and 0.43 are close to

the measured range of 0.47-0.51. However from studying smaller intervals the probe technique may show greater detail of porosity changes with depth.

5.2.2 Moist

Level difference predictions of the three parameters σ_{pe}, T and Ω, together with the effective flow resistivities obtained using the Delany and Bazley semi-empirical relationship, are presented in Table 5.18. The average rms value obtained using the former approximation (1.16) is much less than that obtained using the latter relationship (5.25).

Table 5.18 Best fit Level Difference Parameters for Sandy Loam (moist)

	3 para approx				Delany and Bazley	
	σ_{pe}	T	Ω	rms	σ_e	rms
max	10240	1.33	0.41	1.84	230000	9.02
mean	9380	1.23	0.39	1.56	218000	7.25
min	8710	1.02	0.38	1.16	170000	5.61

Figure 5.9 is an example of best fit parameters, other best fit deduced parameters are listed in Appendix G. In Table 5.18 there is an obvious reduction in σ_{pe}, T and Ω compared with Table 5.14. The average deduced porosity for the moist soil is 0.39, whilst the average measured porosity over 5cm depth is 0.33 with a scattered range of 0.26-0.40. Details of the porosity measurements are shown in Appendix G.

The mean level difference deduced parameters of σ_{pe} and T are 9380 and 1.23 respectively. This indicates a much less compact soil structure than for the dry situation. The lower rms value of 1.56 compared to the rms for dry conditions 2.00 indicates a greater homogeneity when the soil is moist. The average measured flow resistivity value was 54000mks rayls/m (see Appendix G) and the average measured porosity for these samples 0.39. Using this information, and the relationship $\sigma_{pe} = sp^2\sigma\Omega$ a value of 0.44 can be suggested for the squared pore shape factor. This is much larger than the $sp^2 = 0.25$ for the dry conditions. The reduction in the flow resistivity σ_{pe}

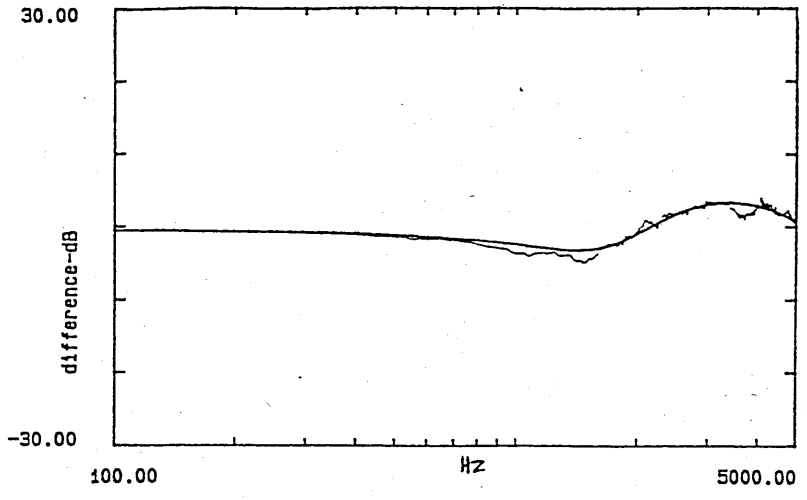

Figure 5.9 Example of Measured and Best Fit Level Difference over a Moist Sandy Loam, Geometry hs 0.1, r 0.37, hrt 0.15, hrb 0.06, σ_{pe} =8708, T=1.02 Ω=0.41 rms=1.84

and the tortuosity T when compared to the dry soil is consistent with the reduction in measured flow resistivity from 259000mks rayls/m to 54000mks rayls/m.

Successful probe measurements were difficult to make on this moist and relatively loose soil. Many measurements were abandoned due to leaking holes. An example of fitting the measured propagation constant is shown in Figure 5.10 others are in Appendix G. Deduced σ_{pe} and T parameters for the successful measurements are presented in Table 5.19.

The deduced values of σ_{pe} are grouped mainly below 11000 and T between 2 and 10. One point in the second profile at the 4-6cm interval appears uncharacteristic, this may be because the signal was less than the background noise. The predicted values of σ_{pe} at 0 - 2cm are compared to those deduced from level difference in Table 5.20. The predictions of σ_{pe} are in rough agreement, whilst predicted values of T are between four and five times higher.

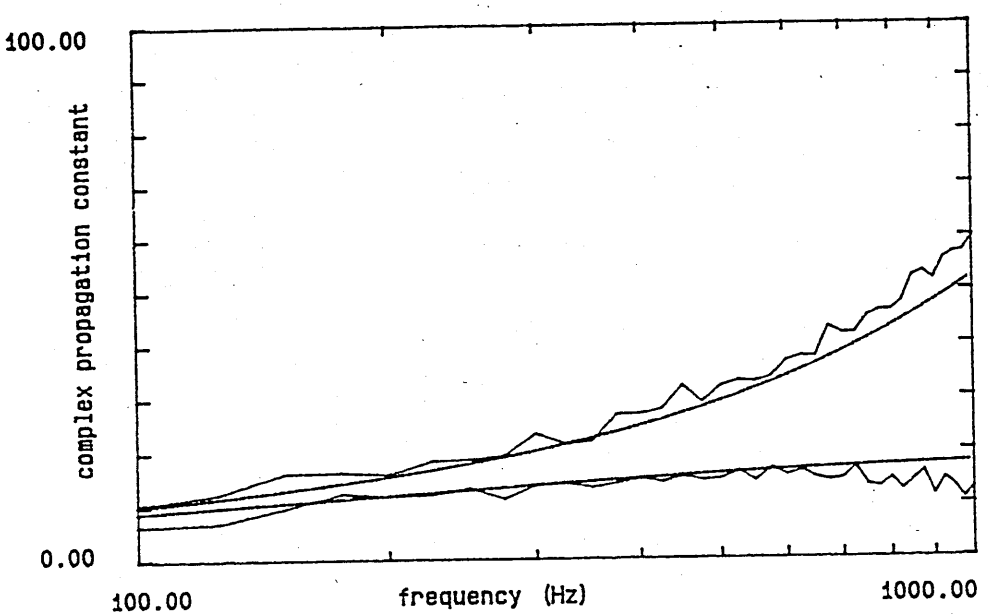

Figure 5.10 Measured and Predicted Propagation Constant for 2 cm depth interval on Moist Sandy Loam σ_{pe} =7470*, T=5.20*

Table 5.19 Ground parameters deduced from Propagation Constant Measurements using a Probe Microphone in a Sandy Loam Soil (moist).

Depth(cm)	σ_{pe}	T
0-2	7470*	5.20*
2-4	9510	1.30*
4-6	10643	4.77*
0-2	1340	1.50*
2-4	7992	4.65*
4-6	35805	7.50*

Table 5.20 Comparison of Level Difference and Probe Deduced parameters for Sandy Loam (moist).

measurement	depth (cm)		σ_{pe}	T	Ω	rms
level difference		max	10237	1.33	0.41	1.84
		mean	9381	1.23	0.39	1.56
		min	8708	1.02	0.38	1.16
probe	0-1	max	7222	7.47		
	0-1	mean	4280	5.34		
	0-1	min	1337	3.22		

Porosity with Depth

Calculation of porosity with depth using the profiles mentioned above were made using the procedure in Section 4.4.3. The deduced profiles are shown in Table 5.21. The deduced profiles are very poor. The large contrast between the T_d values and the T_o value results in the deduction of extremely low and unlikely porosities. Only where the T values are similar are porosities roughly in agreement with the measured predicted. An explanation of this behaviour may be the grain shape factor n' is not constant with depth after the considerable disturbance caused by the wetting process.

Table 5.21 Deduction of Porosity with Depth for Sandy Loam (moist)

Depth cm	T_o	Ω_o	T_d	Ω_d	Meas.Ω	Depth meas.
surface	1.23	0.39			0.33	0-5cm
0-2			5.20*	0.0005		
2-4			1.30*	0.35		
4-6			4.77*	0.0008		
0-2			1.50*	0.17		
2-4			4.65*	0.001		
4-6			7.50*	-		

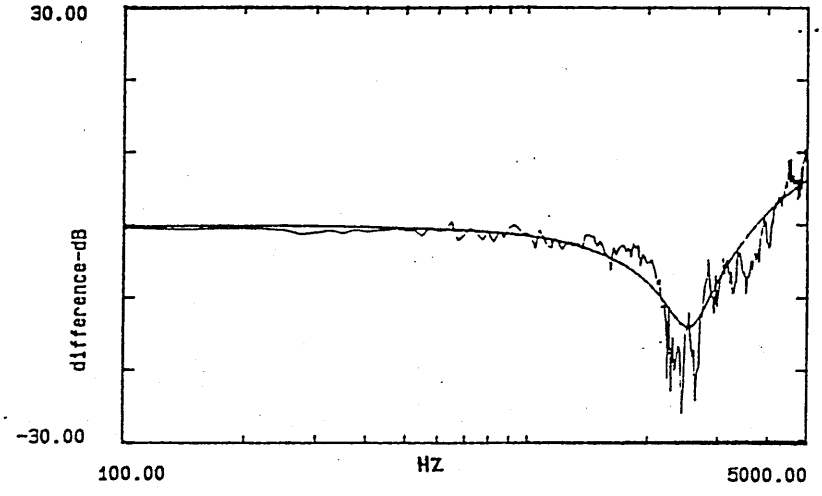

Figure 5.11 Example of Measured and Best Fit Level Difference over a Wet Sandy Loam, hs=0.2, r=1.05, hrt=0.17, hrb=0.05, Deduced parameters, top layer σ_e =2500000, Ω= 0.11, bottom layer σ_e =59200, Ω=0.39 rms=2.93

5.2.3 Wet

Analysis of the acoustic results for the wet condition is based upon the assumption that wet soil has a layered structure. Prior examination showed a 1cm very wet surface layer was overlying an assumed semi-infinite moist soil. The parameters predicted by the layered model, are shown in Table 5.22. An example of a level difference fit can be seen in Figure 5.11.

Table 5.22 Average Parameters Deduced from Level Difference Measurements for Sandy Loam (wet)

Layer	σ_e	Ω	Depth(cm)	rms
Top	2875000	(0.11)	(1.0)	3.12
Bottom	(59200)	(0.39)		

Parameters for the lower layer were assumed to be the average values of effective flow resistivity and porosity determined from the level difference fitting over the moist soil condition (σ_{pe} of 9000 and Ω of 0.39 respectively) from which σ_e = 59000mks was deduced using the relationship $\sigma_{pe} = \sigma_e \Omega^2$. The porosity of the upper layer 0.11 was a measured porosity of the top 1cm

layer, and the layer depth was set equal to 1cm which was actually observed and measured with a rule. Iteration of the flow resistivity of the upper surface layer allowed a fitting to deduced values of σ_e, listed in Appendix H, which have an average of 2875000mks rayls/m. Using the relationship $\sigma_e = (\sigma sp^2)/\Omega$, and a mean measured flow resistivity of 1500000mks rayls/m a squared pore shape factor (sp^2) of 0.21 can be predicted. The range of measured flow resistivities for this wet sandy loam ranged from 830000 - 2170000mks rayls/m,(see Appendix H) .

Examples of probe measured attenuation dB and phase are shown in Figure 5.12. The increased attenuation between the surface and 1cm compared to other 1cm intervals confirms the presence of a 1cm deep wetter layer. Typical σ_{pe} and T parameters with depth for this wet sandy loam soil are shown in Table 5.23, other measurements are shown in Appendix H.

Table 5.23 Ground parameters deduced from Propagation Constant Measurements using a Probe Microphone in a Sandy Loam Soil (wet).

Depth(cm)	σ_{pe}	T
0-1	53930	9.24
1-3	13230	5.39
3-5	9500	4.74
5-6	9490	6.15

The higher deduced values of σ_{pe} and T confirm the presence of a wetter layer close to the surface. The σ_{pe} and T values remain relatively high to a depth of 3cm and therefore suggestion can be made that while the layer is more wet and compacted within 1cm of the surface it extends to 3cm deep in some places. Below 3cm the σ_{pe} and T values revert back to numbers similar to those obtained under moist conditions. This suggests the technique has monitored a wetting front within the soil profile.

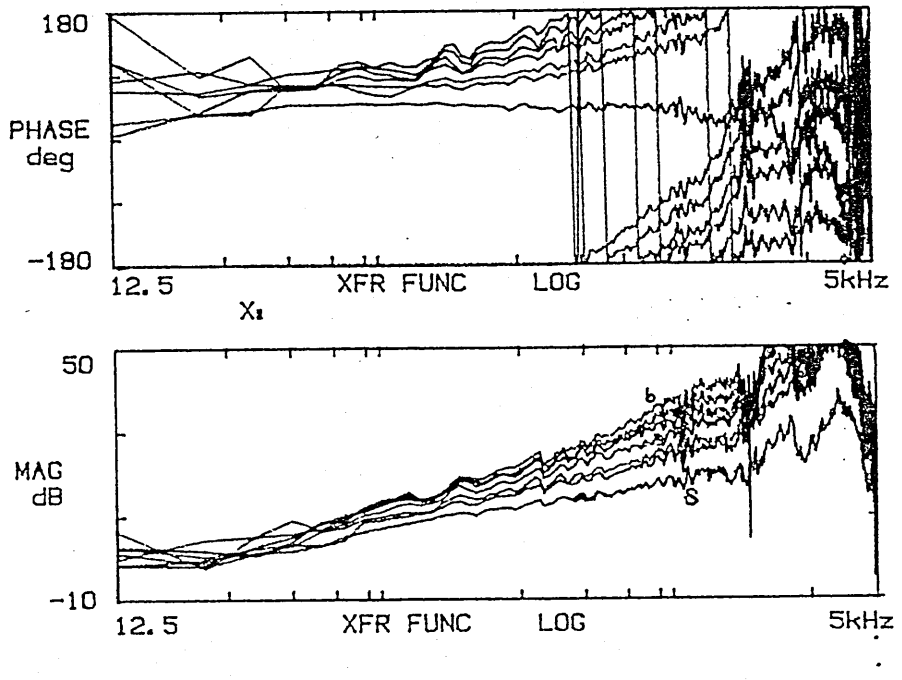

Figure 5.12 Example of measured magnitude dB and Phase for a Wet Sandy Loam at 1cm depths between 0-6cm

5.3 Results for Clay Soil

Acoustic measurements were made on the two treatments on five different days throughout one summer. The results are presented here day by day.

5.3.1 Day1

Level difference measurements were made on the wheeled and zero treatment sites. The best fit ground parameters using the three parameter approximation from level difference measurements are shown in Table 5.24. Also included are the best fit parameters using the Delany and Bazley semi-empirical formula. A more detailed listing of best fit deduced parameters and examples of best fits are shown in Appendix I.1. Values of rms in Table 5.24 show the improved fitting obtained using the three parameter approximation.

Table 5.24 Parameters Deduced from Level Difference Measurements for Clay Day1

	3 para approx				Delany and Bazley	
Wheeled site	σ_{pe}	T	Ω	rms	σ_e	rms
max	17300	4.8	0.59	1.09	190000	2.53
mean	14085	3.87	0.53	1.08	168000	2.29
min	12570	3.51	0.5	1.06	160000	1.90
Zero site						
max	15015	2.67	0.64	2.74	118000	5.65
mean	12070	1.94	0.57	1.58	106000	2.75
min	10140	1.13	0.51	1.30	90000	1.30

The mean σ_{pe} value is higher for the wheeled plot 14085mks rayls/m compared to 12070mks rayls/m on the zero treatment plot. The higher T value also indicates the wheeled plot has a less porous soil surface with a more tortuous path for the sound waves to follow. Measured porosity values have an average of 0.55 for the zero treatment plot which compares favourably with the acoustically predicted value of 0.57. For the wheeled

plot there is some disagreement between the acoustically predicted value of 0.53 and the measured value of 0.62. The reason for this is thought to be poor extraction of the core samples. Measured porosities are listed in Appendix I.1.

No measured flow resistivities were made on this day. However the higher σ_{pe} and T and slightly lower predicted porosity suggest that the wheeled site has a more compacted profile at least close to the surface. Probe measurements were also made on both sites. They are summarized here in Table 5.25 with details of results in Appendix I.1.

Table 5.25 Ground parameters deduced from Measurements using Probe Microphone in Clay wheeled site day 1

Wheeled			
Depth cm	σ_{pe}	T	n
0 - 2	4090	10.20	3
2 - 4	81770	55.80	1

The probe results for the wheeled site suggest that there is a looser surface layer overlying a much more compacted layer. Measured values of σ_{pe} for the 0 - 2cm depth ranged from 734 to 7178 and T from 1.67 to 16.86 so there appears a large variation with probe location, however compared to the very high values predicted for 2 - 4cms they can all be classified as representative of a looser layer. Taking the most reasonable pair of values for the 0 - 2cm interval as σ_{pe} 4352 and T 12.04 and used in conjunction with the level difference predictions of T and Ω for the same site, a limited picture of the porosity change with depth can be predicted. This is shown in Table 5.26.

For the zero site probe measurements in full are listed in Appendix I.1. A summary is presented in Table 5.27. These results can be interpreted as suggesting a fairly loose surface with a harder layer prominent between 4 - 6cm.

A profile of porosity with depth can be deduced and is shown in Ta-

Table 5.26 Deduction of Porosity with Depth for Clay wheeled site day1

Depth	T_o	T_d	Ω_o	Ω_d	Meas. Ω	Depth
Surface	3.87		0.52			
0 - 2		12.04		0.29	0.62†	0 - 3
2 - 4		55.8		0.14	0.20	3 - 6

† possible core sampling error

Table 5.27 Ground Parameters Deduced from Probe Measurements in Clay, Zero Site, Day 1

Zero	Depth cm	σ_{pe}	T	n
	0 - 2	2550	4.08	6
	2 - 4	6270	7.95	6
	4 - 6	9443	25.00	3
	6 - 8	4100	16.98	2

ble 5.28. The predicted values of porosity indicate a much more compacted

Table 5.28 Deduction of Porosity with Depth for Clay zero site day1

Depth	T_o	T_d	Ω_o	Ω_d	Meas. Ω	Depth
Surface	1.94		0.57			
0 - 2		4.08		0.30	0.55†	0 - 3
2 - 4		7.95		0.17		
4 - 6		25.00		0.08	0.40†	3 - 6
6 - 8		16.98		0.10	0.10	6 - 9

† possible core sampling error

profile than the core sampling technique. There is however some question over the reliability of the measured values, due to core sampling error. Again the high tortuosity (T) values and consequently low porosities deduced by assuming constancy of the grain shape factor calls this assumption into question for the clay sites. Furthermore there is poor agreement between the values deduced acoustically from level difference measurements and near surface probe measurements.

Table 5.29 Parameters Deduced from Level Difference Measurements for Clay Day2

	3 para approx				Delany and Bazley	
Wheeled Site	σ_{pe}	T	Ω	rms	σ_e	rms
max	4620	3.41	0.44	1.74	127000	9.04
mean	3680	2.68	0.42	1.43	112700	6.34
min	2985	2.00	0.40	1.25	104000	4.59
Zero site						
max	6620	3.81	0.58	1.94	98000	7.40
mean	6280	3.35	0.57	1.76	91500	6.28
min	5730	2.97	0.56	1.61	87000	5.56

5.3.2 Day 2

Level difference measurements were made on the same wheeled and zero treatment sites as Day 1. A summary of predicted parameters using the three parameter approximation and the Delany and Bazley semi-empirical model are shown in Table 5.29. A more detailed listing of the parameters and plots are in Appendix I.2. It is noticeable how much improved the rms values are when the three parameter approximation is utilised for ground characterisation.

For this day the wheeled site has a lower average σ_{pe} deduced than the zero treatment plot. The reverse of the predictions for Day 1. On the otherhand conditions in the field between the two days differed considerably. In the two weeks preceeding Day 1 rainfall had totalled 33mm compared to 7mm for the two weeks prior to Day 2. Consequently field conditions on Day 2 were much drier than for Day 1, although soil moisture measurements for these days, as shown in Appendix I.2, do not corroborate this because of the poor core samples for Day 1. An explanation of the lower values of σ_{pe} could be moisture content but it is more likely the acoustic technique was sensing cracks within the clay, which were commented upon in the field notes, and made the plots more air-permeable. This would also explain why the wheeled site has a lower σ_{pe} value than the zero wheeled plot having experienced

Table 5.30 Deduction of Ground Parameters from Probe measurements for wheeled and zero sites on clay day 2

Wheeled	Depth cm	σ_{pe}	T	n
	0 - 2	3740	4.16	3
	2 - 4	2090	1.84	1
	4 - 7	7120	3.45	1
Zero	Depth cm	σ_{pe}	T	n
	0 - 2	1467	3.36	1
	0 - 2	393	3.36	1
	2 - 5	414	0.92	1

more severe cracking. It is worth commenting that the single parameter predictions do not show this feature. Using this prediction formula the wheeled site has a higher effective flow resistivity than the zero wheeled site. It is thought the poor sensitivity of the single parameter model does not permit detection of the cracks.

Air permeability measurements were made on this day by Wall [111]. These values, an average of three replicates, have been converted to flow resistivities by the relationship described in Equation 2.14 and show a higher flow resistivity for the wheeled site (81200mks rayls/m) than for the zero site (41230mks rayls/m). The samples were $\approx$ 5cm in diameter and deliberately sampled away from any cracks. This confirms the interpretation therefore that for this day the acoustic reflection technique is sensing a crack feature particularly on the wheeled site. Small sample flow resistivity measurements can not sense this feature. Examples of σ_{pe} and T deduced from probe measurements can be seen in Table 5.30.

For the wheeled site σ_{pe} and T values deduced from probe measurements, Table 5.30 indicate the possible presence of a crust close to the surface beneath which there is a looser layer, followed by more compacted soil below 4cm. It is interesting that level difference measurements detect a cracked surface whilst the more localised probe measurements,made away from the cracks, detect a crust feature. For the zero treatment plot the measurements

Table 5.31 Deduction of Porosity with Depth for Clay Wheeled & Zero Sites Day 2

Treatment	Depth	T_o	T_d	Ω_o	Ω_d	Meas. Ω	Depth
wheeled	Surface	2.68		0.41		0.47	0 - 3
	0 - 2		4.16		0.27		
	2 - 4		1.84		0.57		
	4 - 7		3.45*		0.33	0.28	3 - 6
zero	Surface	3.35		0.57		0.55	0 - 3
	0 - 2		3.36		0.55		

are limited by the surface being dry and loose and consequent leaking around probed holes. This is shown by the very low values of σ_{pe} and T. Profiles of porosity with depth can be deduced and are shown in Table 5.31.These again confirm the presence of a crust on the wheeled site, and represent rather better validation of the constant grain shape assumption than those for Day 1.

5.3.3 Day 3

Only probe measurements were made on this day on both the wheeled and zero sites. A summary of the determined parameters can be seen in Table 5.32, more detailed tabulation of results and propagation plots can be seen in Appendix I.3. Studying these two profiles it can be suggested that there is a harder surface layer between 0-2cm on both the sites which becomes looser with depth.

5.3.4 Day 4

Only level difference measurements were made on this day. On the wheeled site they were made before and after rain. Whereas on the zero site they were made before rain only. A summary of the determined parameters can be seen in Table 5.33 whilst a listing of deduced parameters and examples of best fit plots are shown in Appendix I.4.

Table 5.32 Deduction of Ground Parameters from Probe Measurements for Wheeled and Zero Wheeling Sites on Clay Day 3

Wheeled	Depth cm	σ_{pe}	T	n
	0 - 1	6860*	7.36*	1
	1 - 2	5670	3.45	1
	1 - 3	3130	3.16	3
	2 - 5	1250	2.31	1
	3 - 5	1550	3.22	1
Zero	Depth cm	σ_{pe}	T	n
	0 - 2	4780	5.03	5
	2 - 4	1334	2.18	2
	4 - 6	1456	1.21	1

Table 5.33 Parameters Deduced from Level Difference Measurements for Clay Day 4

Wheeled Site before rain	σ_{pe}	T	Ω	rms	n
max	9640	7.25	0.45	1.47	
mean	9390	6.82	0.45	1.42	3
min	9200	6.21	0.44	1.33	
Wheeled site after rain					
max	7710	11.3	0.50	1.39	
mean	6650	10.41	0.48	1.25	6
min	5390	8.11	0.42	1.07	
Zero Site before rain	σ_{pe}	T	Ω	rms	n
max	9430	5.53	0.52	1.64	
mean	7320	4.51	0.47	1.45	8
min	6315	3.34	0.41	1.33	

Before the rainstorm the deduced parameters suggest that the wheeled site is a more compact and has a less porous surface than the zero site. However after the rain the deduced σ_{pe} decreases and deduced porosity increases suggesting that the soil structure on the wheeled site has changed and become looser than the dry, zero site.

5.3.5 Day 5

Only probe measurements were made on this day on both the wheeled and zero sites. A summary of the acoustically determined parameters can be seen in Table 5.34. The wheeled site has very low values of σ_{pe} between 0-4cm

Table 5.34 Deduction of Ground Parameters from Probe measurements for Wheeled and Zero Sites on Clay Day 5

Wheeled	Depth cm	σ_{pe}	T	n
	0 - 2	755	3.19	2
	2 - 4	915	4.39	2
	4 - 6	19454	33.14	2
Zero	Depth cm	σ_{pe}	T	n
	0 - 2	1193	4.19	3
	2 - 4	1506	2.77	3
	4 - 6	6378	7.30	2
	6 - 8	1526	2.80	2
	8 -10	1282	3.04	1

depth, these could possibly be explained by sub-surface cracking. For the zero plot there is the suggestion of a harder layer between 4 and 6cm. Plotting of the measured and fitted propagation constants are in Appendix I.5.

5.4 Results for Silt

5.4.1 Silt A Day1

For Day 1 level difference and probe measurements were made only on the cultivated site. Level difference best fit ground parameters using the three

parameter approximation are summarised in Table 5.35 and shown in full in Appendix J.1. Also included are the best fit parameters using the Delany and Bazley semi-empirical formula. The improved fits obtained by using the three parameter approximation indicated by the lower rms values are noticeable.

Table 5.35 Parameters Deduced from Level Difference Measurements for Silt A, Cultivated Site, Day1

	3 para approx				Delany and Bazley	
Cultivated	σ_{pe}	T	Ω	rms	σ_e	rms
max	8750	2.97	0.58	1.38	130000	6.50
mean	8670	2.89	0.56	1.29	110000	4.40
min	8590	2.81	0.54	1.21	90000	2.29

Level difference predictions in Table 5.35 show a very porous surface. Using the average value of σ_{pe} (8670) and the average porosity of 0.56 a σ_e of 30000mks rayls/m is predicted. No measurements of flow resistivity were made at this site but the predicted porosity of 0.56 compares favourably with a measured porosity of 0.54 for the 0 - 6cm interval. Field notes describe the surface as having a crumb structure which was quite wet and sticky particularly below 6cms. Probe measurements were difficult to make due to the looseness of the surface however a few successful measurements were made (see Table 5.36) which show a looser profile down to 4cm overlying a less porous, acoustically harder layer. Looking at the measured porosities

Table 5.36 Deduction of Ground Parameters from Propagation Constant Measurements for Silt A, Cultivated Site, Day 1

Cultivated	Depth cm	σ_{pe}	T	n
	2 - 4	1530	2.49	2
	4 - 6	14190	6.11	1
	6 -10	10550	8.58*	1

for this site in Appendix J.1 there is a marked decrease in porosity with

depth from an average of 0.54 for the 0-6cm interval to an average of 0.35 for the 6-9cm interval. This pattern is also suggested by the increasing σ_{pe} and T values. Examples of fitting the propagation constant are shown in Appendix J.1.

An acoustically deduced profile of porosity with depth predicts porosities similar to those measured as shown in Table 5.37.

Table 5.37 Deduction of Porosity with Depth for Silt A, Cultivated Site, Day 1

Depth	T_o	T_d	Ω_o	Ω_d	Meas. Ω	Depth
Surface	2.89		0.56		0.54	0 - 6
2 - 4		3.91		0.47		
4 - 6		6.11		0.37		
6 - 10		8.58*		0.31	0.35	6 - 9

5.4.2 Silt A Day 2

For Day 2 level difference and probe measurements were made on both the cultivated and compacted sites. Level difference predicted parameters using both the three parameter approximation and the Delany and Bazley semi-empirical one parameter relationship are summarised in Table 5.38 and shown in full in Appendix J.2.

As with the silt soil on Day 1, the three parameter approximation gives a better average rms fit than the single parameter model. The predicted porosity indicates a slightly less porous surface than for Day 1. It does not compare favourably to the measured value of 0.65 (see Appendix J.2). This is probably due to the measured value being in error, the soil being very loose and difficulty was experienced extracting the core samples. The surface, in field notes, was described as very dry, loose and friable, however there was also a short shower of rain just before measurements started. Although porosity has decreased, the reduction of the effective flow resistivity (σ_{pe}) indicates a more permeable soil. Predicted parameters for the com-

Table 5.38 Parameters Deduced from Level Difference Measurements for Silt A, Cultivated and Compacted Sites, Day 2

	3 para approx				Delany and Bazley	
Cultivated	σ_{pe}	T	Ω	rms	σ_e	rms
max	6400	2.49	0.52	1.27	120000	7.32
mean	6040	2.24	0.49	1.23	106000	4.27
min	5830	1.78	0.46	1.20	90000	2.64
Compacted						
max	17070	2.94	0.19	1.38	1600000	3.43
mean	14260	2.41	0.18	1.23	1045000	2.29
min	11440	1.88	0.18	1.11	490000	1.15

pacted site show a marked contrast with the cultivated site. The porosity is noticeably reduced to around 0.20 and the effective flow resistivity (σ_{pe}) has approximately doubled. The acoustic technique can distinguish well between the two soil conditions. The measured porosity for the compacted site compares favourably with the measured value of 0.23 for the 0-6cm interval.

Probe measurements on these two sites were made using the probe microphone inserted into permanently placed access tubes. The few successful results can be seen in Table 5.39 for both sites. Examples of propagation constant measurements and best fits are shown in Appendix J.2.

Table 5.39 Deduction of Ground Parameters from Probe Measurements for Silt A, Cultivated and Compacted Sites, Day 2

Cultivated	Depth cm	σ_{pe}	T	n
	2 - 4	2527	3.72	1
	4 -6	3250	8.95	1
	4 -6	3870	11.90	1
	6 -8	3280	1.35	1
Compacted	0 -2	13630	31.00	1

The results show between 2 - 8cm depth a fairly uniform profile on the cultivated site. For the compacted site the results show a high σ_{pe}

similar to that indicated by the level difference technique in Table 5.38. The T values are dissimilar however. These measurements show that the permanent positioning of access tubes could measure changes in the soil. The access tube technique proved less successful on the compacted site, cracks formed around the tubes providing alternative paths for sound waves to reach the microphone, hence the lack of results.

5.4.3 Silt A Day 3

For Day 3 level difference and probe measurements were made on both the cultivated and compacted sites. Level difference predicted parameters for the cultivated site are summarised in Table 5.40 and shown in full together with an example of best fit level difference in Appendix J.3.

Table 5.40 Parameters Deduced from Level Difference Measurements for Silt A, Cultivated Site, Day3

Cultivated	σ_{pe}	T	Ω	rms	n
max	4483	2.60	0.48	1.41	
mean	4370	2.44	0.48	1.32	3
min	4300	2.20	0.47	1.14	

The cultivated site is very loose with lower σ_{pe} than on Day 2, although the porosities remain about the same. The acoustically predicted porosity 0.48 compares tolerably well with a measured porosity of 0.53. For the compacted site it was not possible to fit successfully with the homogeneous model and therefore the multi-layered model was used. The results are presented in Table 5.41 and shown in Appendix J.3. The parameters in Table 5.41 indicate a crust on the compacted site 1cm thick and which has a porosity of 0.23 overlying a looser soil of porosity 0.32. The porosity of the lower layer is set equal to the measured value obtained over a 0-3cm interval. Examples of best fit level difference measurements are shown in Appendix J.3. Measured values of porosity are also shown in Appendix J.3.

Probe data taken on Day 3 on the cultivated and compacted silt sites

Table 5.41 Parameters Deduced from Level Difference Measurements for Silt A, Compacted Site, Day3

Layer	σ_e	Ω	Depth(cm)	rms
Top	300000	0.23	(1.0)	2.59
Bottom	75000	(0.32)		

are shown in Table 5.42 and examples plotted in Appendix J.3. The mea-

Table 5.42 Deduction of Ground Parameters from Probe Measurements for Silt A Cultivated and Compacted Sites Day 3

Cultivated	Depth cm	σ_{pe}	T	n
	0 - 2	1330	8.73	2
	2 -4	870	2.28	2
	4 -7	715	4.45	1
	7 -8	555	4.65	1
Compacted	0 -0.05	61720	4.37	1
	0.05- 1	25550	1.44	1
	0 -1	6865	10.47	1
	0 -2	1295	1.81	1

surements in Table 5.42 are very erratic particularly on the compacted site. This probably reflects the non-homogeneous nature of the compacted site and the difficulty experienced trying to probe through a surface crust and ensure a good seal. For the compacted site The effective flow resistivity values from probe measurements do not compare with a level difference prediction of σ_{pe} 16000mks rayls/mhaving used the relationship $\sigma_{pe} = \sigma_e\Omega^2$. On the other hand the cultivated site has an extremely loose profile with the localised probe measurements indicating a much lower surface σ_{pe} than that deduced from the level difference measurements. A profile of porosity with depth deduced for the cultivated site is shown in Table 5.43.

The parameters here indicate that the more localised probe measurements are sensing a surface crust over a very loose soil which the reflection technique using a homogeneous model does not.

Table 5.43 Deduction of Porosity with Depth for Silt A Cultivated Site Day 3

Depth	T_o	T_d	Ω_o	Ω_d	Meas. Ω	Depth
Surface	2.44		0.47		0.53	0 - 6
0 - 2		13.9		0.11		
1 - 2		10.43		0.15		
2 - 4		2.28		0.50		
4 - 7		4.45		0.28	0.32	6 - 9
7 - 8		4.65		0.28		

5.4.4 Silt B

Using a summary of probe deduced parameters presented in Table 5.44 as a guide for parameter choice, the multi-layered prediction model has been fitted tolerably well to the level difference curves as shown in Appendix K. On the controlled wheeling site the probed σ_{pe} value of 6520mks rayls/m and the measured porosity of 0.48 were used to calculate a value of σ_e of 36600mks rayls/m for the bottom layer. The depth (d) was fixed at the observed crust depth of 1cm. For the upper layer the σ_e and Ω were iterated until a combination that predicted a value of 13500mks rayls/m for σ_{pe} and gave a least sum of squares were found. The result predicts a top layer of 1cm thick with the parameters shown in Table 5.45. The level difference fits are tolerable but not good with rms values >3.0. The growing crop was sugarbeet and it was quite difficult to obtain a large enough area of ground without spurious reflections from sugarbeet plants , hence the large rms values. The acoustically predicted and measured porosities are not in agreement for the surface layer (0.15 compared to 0.48) because the coring technique with samples 3cm deep is not sensing the crust present.

For the compacted site the same fitting procedure was adopted for choosing the parameters of the bottom layer. Here the rms values are similar to those for the controlled wheeling site but the best fits are obviously in error, as plotted in Appendix K. The location and magnitude of the ground effect dip is well predicted but the first peak is predicted at too low a frequency.

This may be explained by spurious reflections due to the proximity of the sugarbeet and therefore the measurements must be viewed with some caution. However, the probe results in Table 5.44 and in Appendix K show without doubt that a crust is present on both sites and that the crust on the poor practise site is acoustically harder with higher σ_{pe} and T values, than the crust on the controlled wheeling site. Measured flow resistivities and porosities for these sites are shown in Appendix K

Table 5.44 Deduction of Ground Parameters from Probe Measurements for Silt B Controlled Wheeling and Poor Practise Sites

Treatment	Depth cm	σ_{pe}	T	n
Controlled Wheeling	0 - 2	16470	9.35	2
	2 -4	7480	7.00	2
Poor Practise	0 -2	57940	24.00	3
	2 -4	4050	12.64	2
	4 -6	6530	5.98	1

Table 5.45 Parameters Deduced from Level Difference Measurements for Silt B Controlled Wheeling and Poor Practise

Treatment	Layer	σ_e	Ω	Depth(cm)	n	rms
controlled	Top	600000	0.15	(1.0)	4	3.01
wheeling	Bottom	(36600)	(0.48)			
poor	Top	2500000	0.12	(1.0)	2	3.89
practise	Bottom	(40800)	(0.42)			

5.5 Snow Results

Four different areas of snow were studied as mentioned in Section 4.1.4 and the results are presented according to their location.

5.5.1 Site A

At Site A four different areas were studied, A1, A2a, A2b and A3.

Site A1

Probe measurements were made at depths of 0, 4, 6, 9.5, 11, 13 and 15cms. Measured attenuation (dB) with depth is shown in Figure 5.13 which shows increasing attenuation with depth and with frequency. The poor quality of the data above 4KHz is probably due to lack of received signal at these higher frequencies. While the poor data below 100Hz is due to the weak output of the electrovoice speaker in the low frequency range. Therefore analysis is undertaken on data between these two frequencies. This is the case for all probe results presented here. An example of measured and predicted propagation constants is presented in Figure 5.14, and the predicted values of σ_{pe} and T for this profile are presented in Table 5.46.

Table 5.46 Deduction of Snow Parameters from Probe Measurements for Site A1

Depth cm	σ_{pe} Low	T Low	σ_{pe} High	T High
0-4	2990	2.40	6530	1.15
4-6	2150	1.98	2890	1.25
6-9.5	1690	1.43	1600	0.95
4-9.5	1850	1.95	1800	1.07
9.5-11	12820	5.83*	13680*	4.23*
11-13	5030*	4.50*	5280	2.93
13 -15	1350*	1.37*	1040*	1.09

Interpretation of results in Table 5.46 indicates a fairly homogeneous profile down to a depth of 9.5cm. Between 9.5-11cm σ_{pe} and T values increase noticeably. The measured density and porosity profile in Table 5.47 show a decrease in porosity, from 0.65 at 5cm to 0.56 at 10-12cm. The acoustic technique has successfully located the hard layer mentioned in the stratification description. Below the harder layer at 12cm the σ_{pe} and T

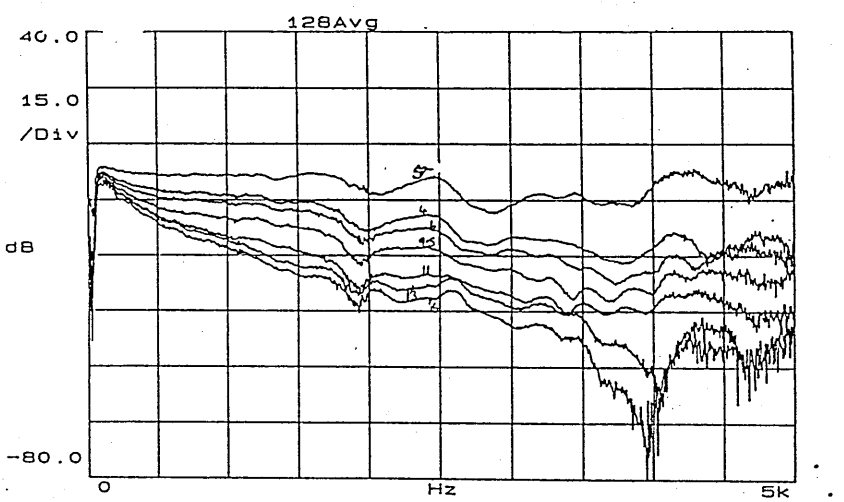

Figure 5.13 Measured Attenuation dB with Depth at Snow Site A1

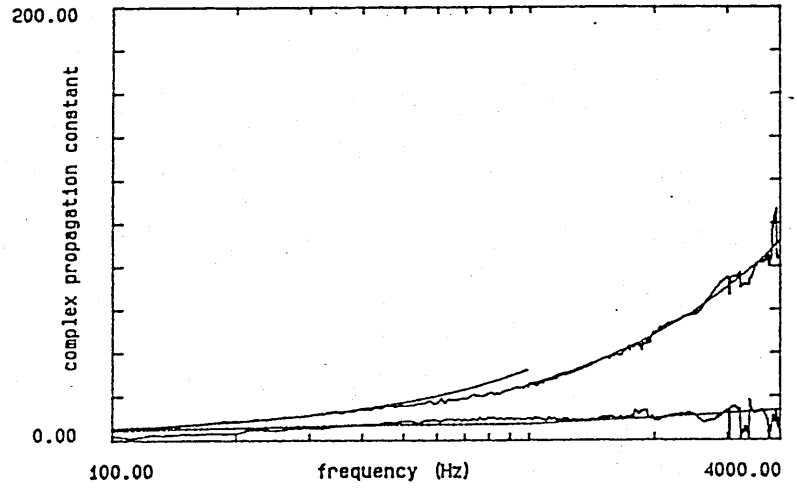

Figure 5.14 Measured and Predicted Propagation Constant in Snow Site A1, depth interval 4-9.5cm, low frequency parameters σ_{pe} =1847 T=1.95, high frequency parameters σ_{pe} =1796 T=1.07.

Table 5.47 Measured Density Profile of Snow at Site A1

Depth cm	Density $kg/m^3 \times 10^{-3}$	Porosity	Stratification
0	0.38	0.58	(hard layer at depth)
5	0.32	0.65	
10	0.40	0.56	10-12cm
15	0.23	0.75	
20	0.22	0.76	
25	0.34	0.62	
30	0.39	0.57	30cm

values suggest a less dense snow which a measured porosity of 0.75 confirms.

Site A2a

Fewer measurements were made at this location, which was approximately 10m away from Site A1. Successful results were obtained at 0,7,10 and 20cm depths. Figure 5.15 shows attenuation (dB) with depth. Measured and predicted propagation constants are shown in Appendix L.1. Table 5.48 shows deduced values of σ_{pe} and T with depth.

Table 5.48 Deduction of Snow Parameters using Propagation Constant Measurements for Site A2a

Depth cm	σ_{pe} Low	T Low	σ_{pe} High	T High
0-7	1060	2.26	2520	1.23
7-10	2990	2.45	4810	1.01
10-20	2600	1.33	1130	1.39

The presence of a harder layer at 12cm depth is noted in the stratification description shown in Table 5.49 although its presence is not detected by the density sampling technique. The value of σ_{pe} of 4810mks rayls/m at 7 - 10cm for the high frequency model may suggest a relatively harder layer but the low frequency model indicates a uniform profile with depth. The hard layer probably lies deeper and falls within the 10 - 20cm interval. The hard layer maybe thin enough, possibly less than 1cm, so the probe and density sampling intervals, 10 and 5cm respectively, cannot detect it. At Site A1 the harder layer was at least 2cm thick occurring at 10 and 12cm depth and easily detectable by both techniques.

Measured attenuation with depth suggests the presence of a looser top 7 cm at Site A2a compared to the top 4cm layer at Site A1. Table 5.50 compares features between these two sites at 1.5KHz and 3KHz. The more dense 4cm layer at Site A1 attenuates the sound as much as 7cm of less dense snow at Site A2a.

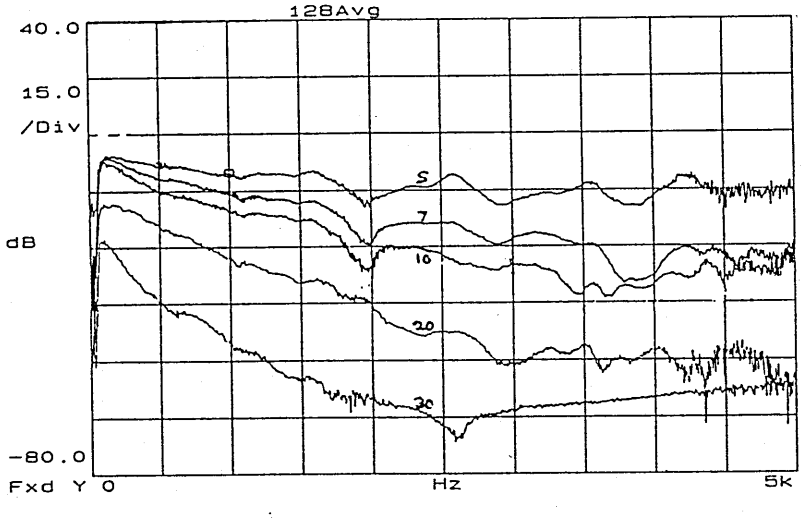

Figure 5.15 Measured Attenuation dB with Depth in Snow Site A2a

Table 5.49 Measured Density Profile of snow at site A2a

Depth cm	Density $kg/m^3 \times 10^{-3}$	Porosity	Stratification
0	0.30	0.67	hard layers
5	0.24	0.73	
10	0.22	0.76	12cm
15	0.26	0.71	
20	0.32	0.65	
25	0.29	0.68	23cm
30	0.30	0.67	
35	0.27	0.70	

Table 5.50 Comparison of Attenuation with Depth in Snow at Two Different Sites

Site No.	Depth cm	Frequency	Attenuation	Snow Density	Porosity
		KHz		$kg/m^3 \times 10^{-3}$	
A1	0 - 4	1.5	7.5 dB	0.38	0.58
A2a	0 - 7	1.5	7.5 dB	0.30	0.64
A1	0 - 4	3.0	9.2dB	0.38	0.58
A2a	0 - 7	3.0	10.0dB	0.30	0.64

Table 5.51 Deduction of Snow Parameters using Probe Measurements for Site A2b

Depth cm	σ_{pe} Low	T Low	σ_{pe} High	T High
0-2	3520	3.00*	5100*	2.14
2-8	2960	3.07	3490	2.55
8-16	2050	3.96	2170	1.89
16-18	23920	13.94	30330	15.75
18-24	4030	1.62	2590	1.44
24-30	2570	2.36	2130	1.95

Site A2b

Measurements were made successfully at 2, 8, 16, 18, 24 and 30cms depth. Figure 5.16 shows these and other less well behaved attenuation measurements made at 6 and 12cm for this site. Figure 5.16 also shows the high frequency data is erratic, particularly >3.5KHz for depths 0 - 8cm and >1.5KHz for depths 16 - 30cm. Figures of the measured and predicted propagation constants in Appendix L.2 show this poor behaviour at higher frequencies and therefore the parameters deduced using the high frequency model must be interpreted with caution. Parameters deduced from probe measurements are shown in Table 5.51.

In Table 5.51 the low frequency values of σ_{pe} (3523mks rayls/m) and T (3.0) could suggest a very slight crust feature at the surface. A much harder layer can also be deduced from the high values of σ_{pe} (23920) and T (13.94) at between 16 - 18cm. Comparing this to the stratigraphy and measured density profile in Table 5.52, a hard packed snow layer with a density of $0.38kg/m^3 \times 10^{-3}$ was seen at 13 - 16cm depth. The detection of this layer by the probe microphone at 16-18cm probably means that the boundary between the two layers was undulating and varied by at least 2cm between the probe location and the snow sampling pit. The density measurements do not however measure a surface crust.

Level difference measurements were also made at this particular site and

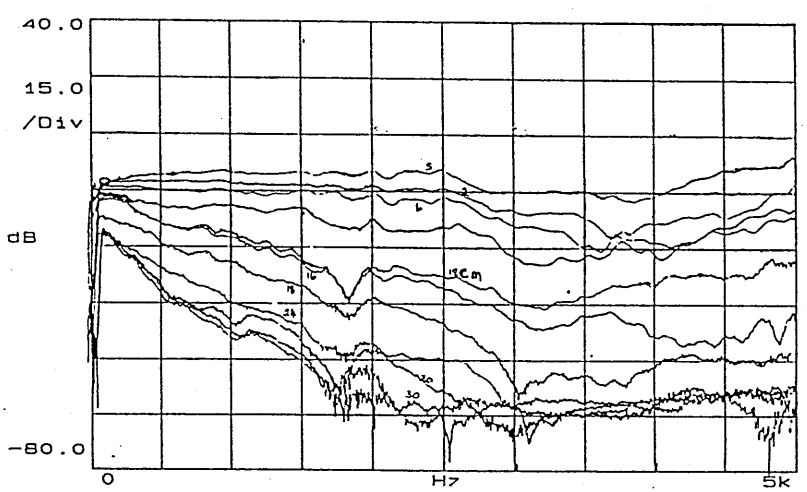

Figure 5.16 Measured Attenuation dB with Depth in Snow Site A2b

Table 5.52 Measured Density Profile of snow at site A2b

Depth cm	Density $kg/m^3 \times 10^{-3}$	Porosity	Stratification
0cm	0.22	0.76	hard layers
5	0.22	0.76	
10	0.29	0.68	13cm Hard packed
15	0.38	0.58	snow layer
20	0.29	0.68	16cm (not ice)
25	0.30	0.67	
30	0.30	0.67	
35	0.30	0.67	

the acoustically predicted parameters σ_{pe}, T and Ω can be seen in Table 5.53. A total of four level difference measurements were made but two suffered

Table 5.53 Parameters Deduced from Level Difference Measurements for Snow Site A2b

σ_{pe}	T	Ω	rms
3810	2.83	0.92	0.72
3120	2.57	0.85	0.64

high back ground noise levels from a snow-blowing machine clearing the airport runway adjacent to the test site. An example of a typical best fit curve assuming extended reaction is shown in Figure 5.17. The ground effect dip is located at 200Hz. The geometry used for this measurement was a source height of 0.5m, microphone heights of 0.1 and 0.5m and a range of 1.63m. The level difference deduced parameters show a highly porous snow surface, 0.85 - 0.92 which is not indicative of a crust as suggested by the more localised probe measurements. The acoustically deduced porosity is higher than the measured porosity 0.76 for the top 10cms of snow.

Site A3

These measurements were made in a deeper snow drift area where the snow was described as 'soft and fluffy'. Attenuation and phase were measured at

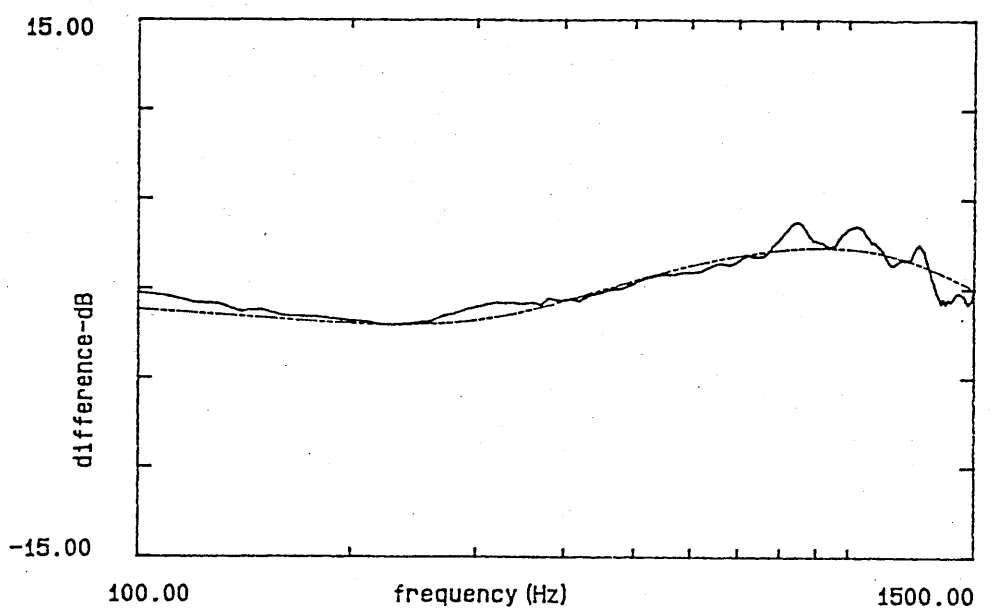

Figure 5.17 Example of Measured and Best Fit Level Difference over Snow Site A2b hs=0.5m, r=1.63m, hrt=0.5m, hrb=0.1m, Best Fit Parameters σ_{pe} = 3120, T=2.57, Ω=0.85, rms=0.64.

depths of 0,2,5,10,15,20,30 and 40cms and the attenuation with depth can be seen in Figure 5.18. Figure 5.18 shows little attenuation difference between the 2 and 5cm measurements at frequencies below 1KHz, and would explain the very small σ_{pe} 321 for this interval. Figure 5.18 also shows measurements at 2 and 5 cms receiving more signal than the reference surface measurement at frequencies <400Hz . This could mean the holes were leaking and the measured values of the propagation constant and hence deduced values of σ_{pe} and T were unrepresentative. The averaged values of σ_{pe} and T are presented in Table 5.54 with propagation constant plots in Appendix L.3 and stratigraphy data in Table 5.55.

Table 5.54 Deduction of Snow Parameters using Probe Measurements for Site A3

Depth cm	σ_{pe} Low	T Low	σ_{pe} High	T High
0-2	8600	28.58	12700	34.69*
2-5	320	1.29	1320*	1.51*
5-10	7490	10.88	7230	6.82
10-15	7000	2.46	5770	4.08
15-30	2050	2.01	1890	1.86

Features detected acoustically in this profile are dissimilar to those measured using the snow density kit. The high values of σ_{pe} and T close to the surface infer the presence of a crust feature which is overlying a much softer, less dense snow. The measured porosity is 0.76 - 0.77 for the first 5 - 10cm. The possibility of poor quality measurements at the shallow depths could account for this discrepancy.

At a depth of 10cm, the stratigraphy profile in Table 5.55, shows a harder more compacted snow between 10 - 23cms with densities increasing to $0.33-0.38kg/m^3 \times 10^{-3}$. The probe technique senses this layer as beginning at 5 - 10cm deep but is unable to detect the base because the next successful interval measured is 15 - 30cms. For 15 - 30cm the predicted values of σ_{pe} and T using both low frequency and high frequency approximations, (2050mks

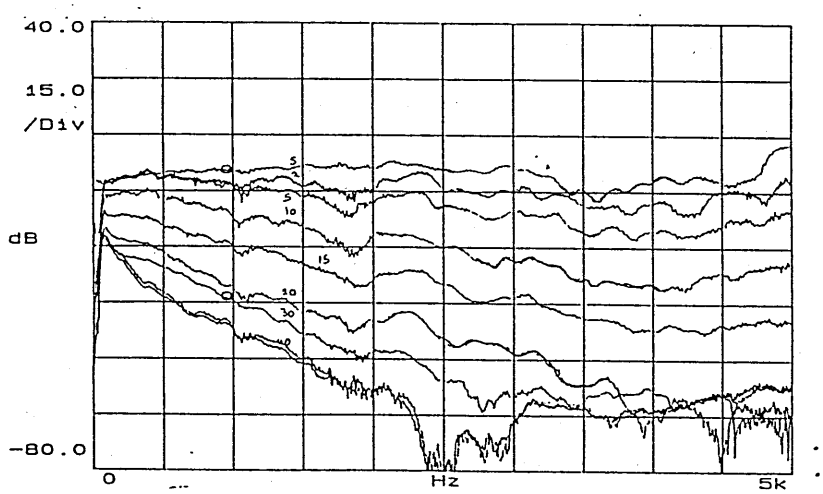

Figure 5.18 Measured Attenuation dB with Depth in Snow Site A3

Table 5.55 Measured Density Profile of snow at site A3

Depth cm	Density $kg/m^3 \times 10^{-3}$	Porosity	Stratification
0cm	0.22	0.76	0cm undisturbed snow
5	0.21	0.77	(1 week old)
10	0.33	0.64	10cm Hard compacted
15	0.38	0.58	snow
20	0.38	0.58	
25	0.35	0.61	23cm soft compacted
30	0.31	0.66	snow
35	0.32	0.65	35cm granular snow no
40	0.30	0.67	cohesion
45	0.28	0.30	
53			soil surface

rayls/m and 2.01, 1890mks rayls/m and 1.85) respectively can be interpreted as indicating a more porous layer of snow.

5.5.2 Site B

Measurements were made at 5, 10, 15, 20 and 30cms depth at this site. Analysis of the data has proved difficult. In most intervals except those listed in Table 5.56 averaged values of σ_{pe} have been extremely low and tortuosity values have been calculated as negative. This probably means the holes at 10,15 and 30cm were leaking. In Table 5.56 the relatively high values of σ_{pe} and T for the 0 - 5cm interval implies the presence of a harder surface crust, which is described in the stratigraphy column between 3-5cm as shown in Table 5.57.

Level difference predictions, tabulated in Table 5.58, and plotted in Appendix L.3, for this site are varied. They appear to fall into two categories; those that predict a high surface porosity 0.9 - 0.91 and those that predict a lower surface porosity 0.56 - 0.67. This would imply a non-uniform surface crust over the area.

Table 5.56 Deduction of Snow Parameters using Probe Measurements for Site B

Depth cm	σ_{pe} Low	T Low	σ_{pe} High	T High
0-5	10531	35.10	5319	33.30
5-20	1580	1.61	560	1.23

Table 5.57 Measured Density Profile of Snow at Site B

Depth cm	Density $kg/m^3 \times 10^{-3}$	Porosity	Stratification
0cm			powdery snow
3-5			crust layer
10	0.22	0.76	powdery snow
16	0.36	0.61	"
17.5			ice layer
22	0.21	0.77	powdery snow
24	0.32	0.65	hard layer

Table 5.58 Parameters Deduced from Level Difference Measurements for Snow Site B

Category 1	σ_{pe}	T	Ω	rms	n
max	2276	3.25	0.91	0.52	
mean	2010	2.55	0.90	0.41	2
min	1751	1.85	0.90	0.31	
Category 2					
max	1560	1.35	0.67	0.64	
mean	1270	1.10	0.63	0.53	4
min	1118	1.00	0.56	0.31	

5.5.3 Sites C and D

These two sites were located beneath or in close proximity to trees. The average accumulation of snow here was approximately 13 -16 cms deeper than the snow depth over the road. Level difference measurements shown in Table 5.59, beneath the pine trees predict a surface porosity of 0.57 - 0.65 and beneath the poplar trees a surface porosity of 0.45. Prediction fits to level difference data beneath the pine trees and the poplar trees are shown in Appendix L.4.

Table 5.59 Parameters Deduced from Level Difference Measurements for Snow Sites C & D

pine trees C	σ_{pe}	T	Ω	rms	n
max	1690	1.32	0.65	1.0	
mean	1420	1.11	0.60	0.90	3
min	1130	1.0	0.57	0.81	
poplar trees D					
max	1580	1.58	0.45	0.72	
mean	1570	1.58	0.45	0.69	2
min	1550	1.58	0.45	0.66	

Probe measurements beneath the pine trees measurements were made at 0, 2, 5, 10, 15, 22 and 25cm depths and adjacent to the poplars a rather limited set of measurements at 0, 3, 5 and 18cms. These are shown in Table 5.60. For both areas the surface interval 0 - 2 and 0 - 3cm respectively were leaking and the results unreliable. At depths of 2-5cm for Site C and 0-5cm for Site D however, both locations indicate the presence of a hard surface crust. The relatively higher σ_{pe} values for the poplar tree area, σ_{pe} of 17750 and 19400 for each model is greater than those under the pine trees, 9005 and 5520. This suggest a harder surface in the poplar tree area. This interpretation is also supported by the predicted level difference parameters, which predicts higher σ_{pe} and T values and a lower porosity for the poplar tree area, D, compared to the pine tree site, C.

Density profile measurements, Table 5.61, at the pine tree site show a

Table 5.60 Deduction of Snow Parameters using Probe Measurements for Sites C and D

Site	Depth cm	σ_{pe} Low	T Low	σ_{pe} High	T High
C	0-2	1660	0.03	2860	1.857
	2-5	9000	37.30	5520	29.20
	5-10	4370	12.60	3740	7.57
	10-15	460	0.87	260	0.93
	15-22	5450	13.10	6050	12.02
	22-25	3610	1.08	3520	2.00
D	0-3	1000	-1.27		
	0-5	17750	7.79	19400	9.02
	5-18	890	0.63		
	5-18	850	0.61		

Table 5.61 Density Profile of snow at sites C and D

Site	Snow Pit	Depth cm	Density $kg/m^3 \times 10^{-3}$	Porosity	Stratification
C	1	0.0			surface layer hard
					resistant crust
		3.5			powdery snow
		6.5			pine needle layer
		9.0	0.32	0.65	
		15.5			resistant hard layer
					including pine needles
					powdery snow beneath.
		26.0		0.30	
		30.0			resistant layer
					including pine needles
C	2	5.0	0.44	0.52	very difficult to penetrate
		16.0	0.28	0.69	
		22.5	0.35	0.61	
		31.0	0.28	0.69	
		35.0			soil surface

resistant surface layer existed between 0 - 3.5cm at Pit 1 and 0 - 5cm at Pit 2. A porosity of 0.52 was measured at 4.9cm deep. No density profile was made for the poplar tree area but the very much higher values of σ_{pe} and T 19404 and 7.79 respectively would suggest a density in excess of $0.44kg/m^3 \times 10^{-3}$ at between 0 and 5cm depth.

For the pine tree area between 5 - 10 cm the probe measurements can be interpreted as a fairly compacted layer σ_{pe} of 4370 and T of 12.6 but less dense than the surface measurement. The measured density corroborates this with a measured density of $0.32kg/m^3 \times 10^{-3}$. The interval between 10-15 cm is hard to explain. The low values of σ_{pe} and T indicate that there was hardly any attenuation between these two depths, which may indicate the 15cm hole was leaking. The measurement between 15 - 22 cm however predicts similar values of σ_{pe} and T to that between 5 - 10 cms and a similar measured density at 22.5cms of $0.35kg/m^3 \times 10^{-3}$ seems to support the validity of the 15cm measurement.

Chapter 6

Discussion

The first thing discussed in this chapter is the justification for the choice of prediction models used to determine ground properties. Secondly each of the five objectives are discussed one by one. The five objectives are;

1. Acoustic determination of the air porosity of soils.
2. Acoustic determination of the flow resistivity of soils.
3. Acoustic determination and monitoring of soil moisture content.
4. Acoustic detection and characterisation of surface crusts, of a saturated surface layer and sub-surface layering patterns.
5. Acoustic determination of physical properties of snow.

6.1 Justification of Models used in the Characterisation of Ground Parameters

It has been shown by the many examples tabulated in Chapter 5 and in Figure 6.1, how poorly the Delany and Bazley semi-empirical relationship predicts short range propagation above sandy,silt and clay soil types. The best fit parameters for both the three parameter approximation and the Delany and Bazley semi-empirical relationship are summarised below in Table 6.1. Poor fitting is indicated by the higher values of rms error for the one parameter semi-empirical model compared to generally much lower values

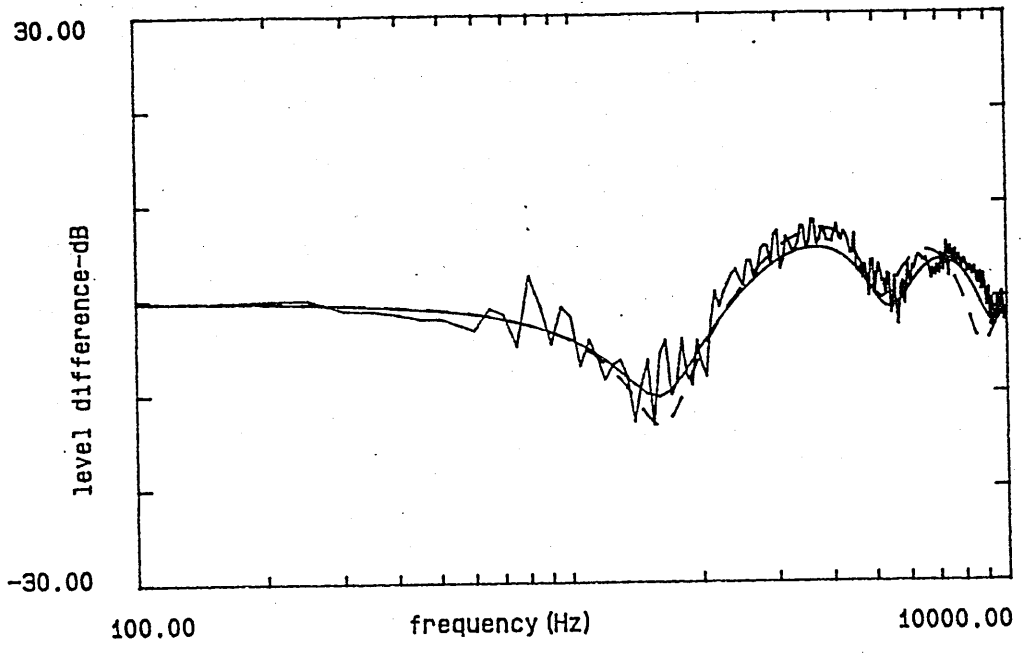

Figure 6.1 Example of Measured and Best Fit Level Difference over Sand 1, Three Parameter Fit σ_{pe} =40914, T=2.21, Ω=0.36, rms=1.88, Delany and Bazley best fit σ_e =900000, rms=7.57, geometry hs=0.24,r=1.3,hrt=0.25,hrb=0.05.

of rms error for the three parameter approximation. This is the case for every soil studied. From this it can be said that the Delany and Bazley semi-empirical relationship shown in Equation 2.23 is not approximate for characterising the homogeneous outdoor ground surfaces studied. The alternative approximation (Equation 3.33) involves three parameters and hence predicts more information on soil properties.

Table 6.1 Best Fit Ground Parameters for Various Soils

	3 para approx				Delany and Bazley	
	σ_{pe}	T	Ω	rms	σ_e	rms
Sand 1	42000	2.15	0.36	1.88	906000	7.42
Sand 2	19058	1.27	0.48	1.84	253000	4.54
Sandy Loam dry	24050	3.32	0.52	2.00	370000	10.95
Sandy loam moist	9380	1.23	0.39	1.56	218000	7.25
Clay Day 1 wheeled	14085	3.87	0.53	1.08	168000	2.29
Clay Day 1 zero	12070	1.94	0.57	1.58	106000	2.75
Clay Day 2 wheeled	3680	2.68	0.42	1.43	112700	6.34
Clay Day 2 zero	6280	3.35	0.57	1.76	91500	6.28
Silt A Day 1 cult.	8670	2.89	0.56	1.29	110000	4.40
Silt A Day 2 cult.	6040	2.24	0.49	1.23	106000	2.29
Silt A Day 2 comp.	14260	2.41	0.18	1.23	1045000	4.27

Characterisation of a ground surface using the Delany and Bazley model may be feasible if the assumption is made that the best fit effective flow resistivity σ_e is in fact a product of actual flow resistivity multiplied by porosity $\sigma\Omega$. Those soils studied which had both a homogeneous nature and independent flow resistivity and porosity measurements made upon them are shown in Table 6.2. Deduced flow resistivities and porosities for each soil using the above relationship, are shown in columns 6 and 7. Immediately it can be seen that the values of deduced porosity are greater than unity and therefore meaningless. To obtain a sensible value of porosity the predicted values of effective flow resistivity σ_e should be less than the actual measured value σ, but for each series of measurements on each soil type they are considerably higher. This phenomenon is explained in Figures 6.2 and 6.3.

Figure 6.2 shows two curves. The solid line represents a best fit predic-

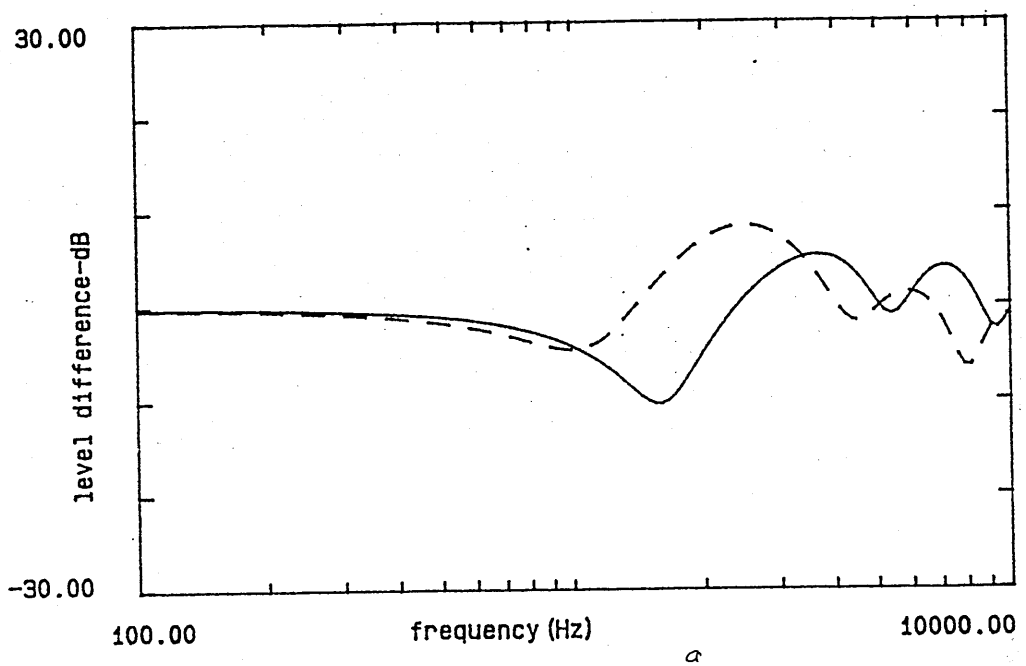

Figure 6.2 Best Fit Prediction of Level Difference over Sand 1, Three Parameter Approximation (solid line) σ_{pe} =40914, T=2.21, Ω=0.36, Delany and Bazley (broken line) σ_e =131980, geometry hs=0.24,r=1.3,hrt=0.25,hrb=0.05.

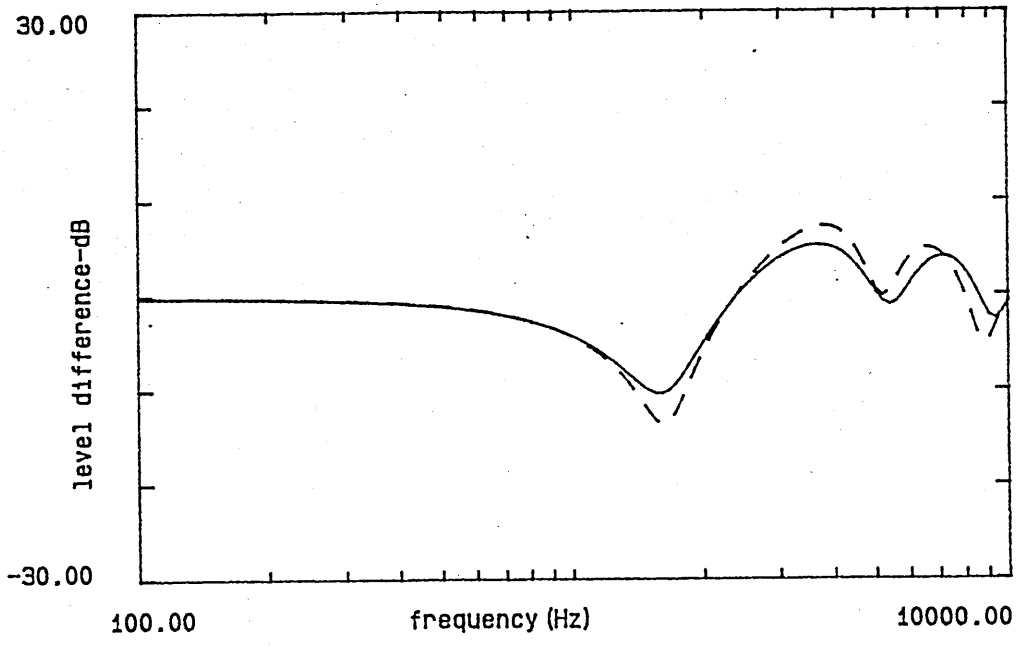

Figure 6.3 Best Fit Prediction of Level Difference over Sand 1, Three Parameter Approximation (solid line) σ_{pe} =40914, T=2.21, Ω=0.36, Delany and Bazley (broken line) σ_e =900000, geometry hs=0.24,r=1.3,hrt=0.25,hrb=0.05.

Table 6.2 Deduction of Ground Parameters from Two Different Prediction Models

Soil	meas. σ	meas. Ω	av.best fit σ_e D&B	av.rms	Pred.σ D&B	Pred.Ω D&B	Pred.Ω 3 para	av.rms
Sand 1	376000	0.35	906200	7.42	2590000	2.41	0.36	1.88
Sand 2	134700	0.47	253000	4.54	547000	1.87	0.48	1.84
Clay dry								
wheeled	81200	0.47	112700	6.34	240000	1.38	0.42	1.43
zero	41230	0.55	91500	6.28	166400	2.22	0.57	1.76
Sandy Loam								
dry	259000	0.49	370000	10.95	755100	1.42	0.52	2.00
moist	54000	0.33	218000	7.25	660600	4.03	0.39	1.56

tion from fitting level difference data over sand 1. The best fit parameters are an effective flow resistivity of 40914, porosity of 0.36 and tortuosity of 2.21. Using this information together with a deduced value of 0.55 for the pore shape factor a value for $\sigma\Omega$ of 131980 can be calculated from the relationship $\sigma_{pe} = sp^2\sigma\Omega$. The prediction according to this value of $\sigma\Omega$ and the Delany and Bazley model is plotted as the broken line in Figure 6.2. It can be seen that the two prediction curves are very dissimilar, with the ground effect dip for the single parameter empirical model occurring at a much lower frequency. In order to fit the Delany and Bazley model to the level difference data the effective flow resistivity parameter σ_e must be increased to 900000, shown in Figure 6.3, when the two ground effect dips come into line at roughly the same frequency. This results in the predicted effective flow resistivity always being larger than the measured σ and hence deduced porosities greater than unity. The deduction of porosities from values of single parameter effective flow resistivity σ_e and actual flow resistivity σ relies on good measurements of the actual flow resistivity, which are notoriously difficult to ensure. Nevertheless with an independently measured porosity of 0.36, a predicted σ_e value of 900000 results in a σ value of 2500000 which is far larger than the measured value of 376000. Meanwhile the three pa-

rameter approximation prediction of σ using the relationship $\sigma_{pe} = sp^2\sigma\Omega$ and the values of effective flow resistivity of 40914, porosity of 0.36 and tortuosity of 2.21, together with a deduced value of 0.55 for the pore shape factor, gives a value for σ of 366000 which is much more comparable with the measured value of 376000.

These examples show the problems of having to know either the soil porosity or actual flow resistivity of the soil from non-acoustic measurements in order to determine any additional information on ground characterisation using the Delany and Bazley semi-empirical relationship. It would therefore appear sensible to use a more sophisticated three parameter approximation prediction model which does not rely on a non acoustically determined flow resistivity to deduce porosity and *visa versa.*

6.2 Acoustic Determination of the Air Porosity of Soils

6.2.1 Determination of Air Porosity at the Surface

Level difference measurements can be used to determine air porosity at the soil surface. Table 6.3 is a summary of acoustically determined porosities compared to measured air porosity values for all the different soil types studied and a percentage error of prediction is also presented.

For these soils, whether sand, clay or silt based, predicted air porosities are usually higher than measured porosity values. This is probably because the acoustic reflection technique samples to a shallower depth than the core technique, particularly at higher frequencies, hence it is sampling that region of the soil profile with little overburden and possibly a lower bulk density. Those % errors which are negative indicate an acoustically deduced porosity which is less than the measured porosity.

Where the homogeneous model has been used and the predicted value of porosity is close to the measured value, that is having a small % error, it may be inferred that the soil is homogeneous at least to the depth of the core sample. Porosities of sands 1 and 2 are well determined with an error of

Table 6.3 Comparison of Acoustically Deduced and Measured Air Porosity for all Soil Types

Soil	model	treatment	layer	pred.Ω	meas.Ω	% error	av.rms	av.sample depth cm
Sand 1	h			0.36	0.35	3	1.88	0 - 3
Sand 2	h			0.48	0.47	2	1.84	0 - 3
Sand 3	ml	crusted	t	(0.13)	0.14	-7	1.73	0 - 1
			b	(0.31)	0.27	15	"	1 - 5
Sandy	h	dry		0.52	0.49	6	2.00	0 - 5
Loam	h	moist		0.39	0.33	18	1.56	0 - 5
	ml	wet	t	(0.11)	0.11	0	3.12	0 - 1
			b	(0.39)	0.28	39	"	0 - 5
Clay	h	zero		0.57	0.55†	4	1.58	0 - 3
(day1)	h	wheeled		0.53	0.62†	-14	1.08	0 - 3
Clay	h	zero		0.57	0.55	4	1.76	0 - 3
(day2)	h	wheeled		0.42	0.47	-11	1.43	0 - 3
Silt A	h	cultivated		0.56	0.54	4	1.29	0 - 3
(day1)								
Silt A	h	cultivated		0.49	0.66†	-26	1.23	0 - 6
(day2)	h	compacted		0.18	0.23	-22	1.24	0 - 3
Silt A	h	cultivated		0.47	0.53	-11	1.32	0 - 6
(day3)	ml	compacted	t	0.23	-		2.59	
			b	(0.32)	0.32	0	"	0 - 3
Silt B	ml	controlled	t	0.15	-		3.01	
		wheeling	b	(0.48)	0.48	0	"	0 - 3
Silt B	ml	poor	t	0.12	-		3.89	
		practise	b	(0.40)	0.44	-9	"	0 - 3

† possible core sampling error

( ) assumed parameter for layer model fitting

$\leq 3\%$ as are the porosities for the clay zero treatment sites for both days and silt A Day 1 (4% error), and the dry sandy loam (6% error). Sands 1 and 2, and to a certain extent the dry sandy loam, had a single-grained structure which could be described as fairly homogeneous. The silt A (day1) profile was noted as a loose, well aggregate crumb structure which was moist and uniform down to a depth of 8cm which probably accounts for the low error value here.

The worst predictions of porosity using the homogeneous model are for the silt A site, (day 2), with an error of approximately -26% for both soil treatments, for the clay wheeled treatment (day 1) -14% and for the moist, sandy loam with an error of 18%. A possible explanation for the error on the cultivated silt is inaccuracy in the measured porosity resulting from poor core sampling. For the compacted silt on the same day the %error (-22%) magnifies the actual difference between acoustically predicted and measured porosity which is only 0.05 and which is felt acceptable at this time. For the clay (day 1) the poor core sampling obviously effects the % error calculation of -14%, however the low rms error value of 1.08 suggests a good fit to the data and the acoustically determined porosity of 0.53 is considered to be more reliable than the measured value of 0.62. For the moist sandy loam soil the 18% error can possibly be explained by non-uniform moisture content throughout the moistened soil. As a consequence the profile may be inhomogeneous. This possibility is substantiated by data obtained on the same soil using a probe microphone, these data are discussed later in Section 6.2.2.

For soils fitted with a layered model, porosity comparisons can be made between the upper and lower layers. In the fitting procedure for layer situations as described in Section 4.4.1 either the upper or lower layer porosity, in some cases both, were set equal to the average, or within the range, of measured porosities, (Indicated by brackets in Table 6.3). This accounts for the zero or very low error values between acoustically determined porosity and measured air porosity values.

For the wet sandy loam the upper layer porosity was set to that mea-

sured, (0.11). The extremely high error of 39% for the lower layer is a reflection of the over simplicity of the double layer model, and the measured porosity being calculated from a sample 0-5cm deep. In hindsight it would have been more worthwhile to extract core samples from 1-6cm deep.

The sampling of crusts for porosity calculation was not possible on the silt soils because of their dry and brittle nature hence no comparison is possible for the upper layers. The high rms error values obtained when fitting data on the Silt B treatments of controlled wheeling and poor practise are not likely to be the result of poor prediction using a layered model but a consequence of spurious reflections from the sugarbeet crop. Probe results mentioned in Section 5.4.4 and discussed later in Section 6.5 confirm the presence of a crust on these treatments and the values of σ_{pe} and T predicted suggest a harder less porous crust on the poor practise site as the values in Table 6.3 suggest.

The most successful fitting of a layered situation was over Sand 3 with errors of -7% and 15% for the upper and lower layer porosities respectively. The predicted values of porosity were set close to measured air porosity values in the fitting procedure.

From studying the predictions of porosity it may be said the level difference technique can distinguish between the different wheeling treatments for the clay sites. It can also show changes in surface porosity from day to day. Note for example the changes between days 1, 2 and 3 on the cultivated silt site. The technique also provides a starting point for determining profiles of porosity with depth.

6.2.2 Determination of Air Porosity with Depth

The procedure for the determination of air porosity with depth from conjunctive use of probe and level difference results has been described in Section 4.4.3. In this section a few profiles are chosen for discussion whilst attention is drawn to Appendix B which includes a further listing of other profiles determined for the various soils. Acoustically determined porosity profiles are compared to conventionally measured air porosity profiles.

Table 6.4 Comparison of an Acoustically Deduced Porosity Profile and Measured Air Porosity - Sand 1

Depth cm	T_o	Ω_o	T_d	Ω_d	Meas. Ω	Meas. Depth
Surface	2.15	0.36			0.36	0 - 3cm
0 - 1			21.21*	0.02		
1 - 2			2.16	0.36		
2 - 3			2.12	0.36		
3 - 4			2.22*	0.34	0.34	3 - 6cm
4 - 5			2.28*	0.33		
5 - 6			2.12*	0.36		
6 - 7			2.57*	0.28		

The deduction of porosity profiles assumes that the grain shape factor n' remains constant with depth. The grain shape refers either to the shape of the individual grains, as in the case of sands, or, in soils, to the shape of the soil aggregates or quasi-stable small clods where the individual soil particles are bonded together. For a sand it is unlikely that n' will change with depth unless there occurs different banding of sands with different grain shapes. Individual quartz grains are not easily compressed and do not absorb water therefore they are unlikely to change shape. Mineral soils, however, have an inherently unstable structure which responds to changes in biological activity, cultivation practises and daily weather patterns. It is therefore unlikely that the structure of the soil at the surface will resemble the structure at lower levels in the profile. However for the relatively shallow depths of soil studied here 0 - 10cm it is assumed in the first instance that n' remains constant with depth. This assumption is most likely to be true on homogeneous soils. Tables 6.4, 6.5 and 6.6 show porosity with depth deductions for Sand 1 and Silt A Day 1 and the dry sandy loam soil all of which have low % errors (3% and 4% and 6%) respectively between acoustically predicted and conventionally measured air porosities near the surface. The values of T_o, Ω_0, T_d and Ω_d are included in the tables as examples of the relationship between T and Ω .

In Tables 6.4, 6.5 and 6.6 a point of discussion is the obvious pattern that

Table 6.5 Comparison of an Acoustically Deduced Porosity Profile and Measured Air Porosity - Silt day1

Depth cm	T_o	Ω_o	T_d	Ω_d	Meas. Ω	Meas. Depth
Surface	2.89	0.56			0.54	0 - 6cm
2 - 4			3.91	0.47		
4 - 6			6.11	0.37		
6 - 10			8.58*	0.31	0.35	6 - 9cm

Table 6.6 Comparison of an Acoustically Deduced Porosity Profile and Measured Air Porosity - Sandy loam (dry)

Depth cm	T_o	Ω_o	T_d	Ω_d	Meas. Ω	Meas. Depth
Surface	3.32	0.52			0.49	0 - 5cm
0 - 1			3.48	0.51		
1 - 3			3.89	0.48		
3 - 5			9.81	0.29		
				av 0.43		

when T remains fairly constant with depth, as in the case of the sand below 2cm (approximately 2.5), then the deduced values of porosity with depth also remain fairly constant. For Sand 1 there is close agreement between the predicted and measured profiles below 2cm. This is despite the nature of this sand which included a variety of grain shapes and sizes. An explanation may be that the mixing of different grains was such that acoustically the profile did appear uniform except very close to the surface. The probed results of high T values close to the surface are consistent for the three profiles mentioned in Appendix B but the level difference technique does not determine an equally tortuous surface. Later analysis however revealed that the high effective flow resistivity and tortuosity values for the surface interval 0-1cm were wrong due to an error in estimation of the depth interval studied, which as explained in Section 5.1.1 was in fact 0-2cm. Thus with a new value of T of 2.36 at the 0-2cm interval Table 6.4 values now change to those shown in Table 6.7.

Table 6.7 Reanalysed Comparison of an Acoustically Deduced Porosity Profile and Measured Air Porosity - Sand 1

Depth cm	T_o	Ω_o	T_d	Ω_d	Meas. Ω	Meas. Depth
Surface	2.15	0.36			0.36	0 - 3cm
0 - 2			2.36*	0.32		
2 - 3			2.16	0.36		
3 - 4			2.12	0.36		
4 - 5			2.22*	0.34	0.34	3 - 6cm
5 - 6			2.28*	0.33		
6 - 7			2.12*	0.36		
7 - 8			2.57*	0.28		

From studying the decrease of porosity with depth on the silt and sandy loam soils, Tables 6.5 and 6.6, the conclusion can be made that porosity decreases as tortuosity increases. This implies that a relatively high value of T within a profile indicates a more compacted layer with a lower porosity, if, n' remains constant. Tortuosity therefore could be seen as an important indicator of porosity behaviour with depth when studying probed profiles of σ_{pe} and T alone. When an increase in T, which from the above indicates a possible decrease in porosity, coincides in a probed profile with a marked increase in σ_{pe} then from the relationship $\sigma_{pe} = sp^2\sigma\Omega$ it can be deduced that the $sp^2\sigma$ value has been increased and may indicate an increase in flow resistivity of the soil.

Some deduced profiles show a discrepancy between measured and predicted porosity values at depth. Table 6.8 shows a profile of porosity with depth for the wheeled treatment on the clay soil, Day 2. The prediction of 0.27 for the porosity in the top two centimetres is not a very good prediction of the value of 0.47 obtained from the core sampled from 0 - 3cm. However it should be noted that the probe technique senses a crust formation as discussed later which the core sampling destroyed.

For those sites where a known crust feature was present the deduction of porosity with depth would be of most interest. However the layered model used here does not provide T_o value at the surface unless the 9 parameter

Table 6.8 Comparison of an Acoustically Deduced Porosity Profile and Measured Air Porosity - Clay Day 2

Depth cm	Ω_d	Meas. Ω	Meas. Depth
Surface		0.47	0 - 3cm
0 - 2	0.27		
2 - 4	0.57		
4 - 7	0.33	0.28	3 - 6cm

Table 6.9 Comparison of an Acoustically Deduced Porosity Profile and Measured Air Porosity - Sandy loam (moist)

Depth cm	T_o	Ω_o	T_d	Ω_d	Meas. Ω	Meas. Depth
Surface	1.23	0.39			0.33	0 - 5cm
0 - 2			5.20*	0.001		
2 - 4			1.30*	0.35		
4 - 6			4.77*	0.001		

model mentioned in Section 3.6.3 was used.

The profiles determined for the moist sandy loam soil, Table 6.9, were very poorly predicted compared to measured porosities. This may be because the profile is inhomogeneous with depth and it is not correct to assume the grain shape factor remains constant with depth. This inhomogeneity is also indicated by the large error (18%) between measured and predicted porosities at the surface.

A summary of the above discussion shows that the prediction of porosity with depth is successful on soils which are homogeneous within the top 0 - 10cms. Otherwise accuracy of prediction will be poor for three possible reasons;

1. Non homogeneity with depth.
2. Grain shape factor n' is not constant with depth (most likely to occur under non-homogeneous conditions).
3. Dissimilarity between deduced level difference and probed tortuosity

values. The more localised probe measurement is picking up features the level difference technique cannot sense.

6.3 Acoustic Determination of the Flow Resistivity of Soils.

The discussion of this objective involves three considerations.

1. The use of $sp^2\sigma$ plus conventionally measured flow resistivity to obtain measured values of sp^2.
2. The validity of using $sp^2\sigma$ as an indicator of flow resistivity .
3. The use of σ_{pe} and T for inferring effective flow resistivity.

From the level difference measurements σ_{pe} and Ω are determined directly from the homogeneous model fitting. Using the relationship $\sigma_{pe} = sp^2\sigma\Omega$ simple division enables the deduction of $sp^2\sigma$. For the layered model a value of σ_{pe} can be deduced from the determined parameters σ_e ($\sigma_e = sp^2\sigma/\Omega$) and Ω using the relationship $\sigma_{pe} = \sigma_e\ \Omega^2$. Division of σ_{pe} by Ω^2 results in the deduction of $sp^2\sigma$. The parameter $sp^2\sigma$ includes the flow resistivity σ of the soil multiplied by the square of a pore shape factor sp^2. This flow resistivity parameter cannot be used to deduce actual flow resistivity σ unless sp^2 is known. Nevertheless where independent measurements of flow resistivity are available the usefulness of $sp^2\sigma$ (acoustically determined) as a comparative measure of air permeability may be assessed. Of the soils studied flow resistivity measurements were made on Sands 1, 2 and 3 , Clay Day 2 zero and wheeled sites, Silt B controlled wheeling and poor practise treatments and sandy loam under all three moisture regimes. The average of the range of these measured values has been used in conjunction with mean level difference parameters to suggest a value of sp^2 and hence deduce a range of values of $sp^2\sigma$. Values calculated for each soil type are shown in Table 6.10.

Using the predicted mean values of σ_{pe} and Ω from level difference measurements, columns 5 and 6 and the average measured flow resistivities,

Table 6.10 Deduction of Flow Resistivity from an Inferred Value of Pore Shape Factor

Soil type	Feature	Layer		Level σ_{pe}	Diff. Ω	Av.Meas. Flow resistivity	Inferred sp^2	Inferred range of $sp^2\sigma$
			max	48311	0.35			138000
Sand 1			mean	42000	0.36	376000	0.31	117000
			min	36802	0.38			97000
			max	21450	0.44			48750
Sand 2			mean	19060	0.48	134000	0.31	39700
			min	10750	0.50			21500
Sand	crust	upper	mean	84500	0.13			650000
3	beneath	lower	mean	9610	0.31	70900	0.44	31000
			max	4622	0.44			10500
Clay day2	wheeled		mean	3680	0.42	81200	0.11	8900
			min	2985	0.40			7500
			max	6620	0.58			11400
Clay day2	zero		mean	6280	0.57	41230	0.27	11000
			min	5730	0.56			10200
			max	28810	0.47			61300
Sandy Loam	dry		mean	24050	0.52	259000	0.17	44000
			min	20270	0.52			38200
			max	10237	0.39			26200
Sandy Loam	moist		mean	9380	0.39	54000	0.44	23800
			min	8708	0.41			21200
Sandy	wet	upper	mean	34800	0.11	1500800	0.21	315000
Loam		lower	mean	9000	0.39	54000	0.43	23100
Silt B	controlled	upper	mean	13500	0.15			90000
	wheeling	lower	mean	8430	0.48	68450	0.26	17800
Silt B	poor	upper	mean	36000	0.12	1477000	0.20	300000
	practise	lower	mean	6528	0.40	144000	0.11	15840

column 7, a value of the squared pore shape factor, sp^2, can be inferred, column 8, for the different soil types using the relationship $\sigma_{pe} = sp^2\sigma\Omega$. Using these values of sp^2 a range of effective flow resistivities $sp^2\sigma$ has been calculated, column 9, for the maximum, mean and minimum values of predicted σ_{pe} and associated porosity. These values of $sp^2\sigma$, when examined can be used to infer knowledge about relative flow resistivity values at the surface for each soil type.

Relatively high values of $sp^2\sigma$ are inferred for Sands 1,2 and 3, and for the dry sandy loam. The wet sandy loam also has a high flow resistivity inferred from a $sp^2\sigma$ of 315000. The two different treatments on the clay soil and the moist soil have comparatively much lower flow resistivities. These differences may be in part explained by the soil structure. The single grain structured sands and pulverised, almost dust-like, dry sandy loam are relatively compacted and likely to have a high flow resistivity. The high value for the very wet soil is probably a combination of a change in structure after the application of water and the additional water filling or blocking the formerly air connected pores. However the clay sites were supporting a growing crop of winter wheat. It may be that the root system within the soil has helped create a looser structure and therefore lowered the flow resistivity. A reason for the low flow resistivity of the moist sandy loam soil may be that aggregation of soil particles took place when moisture was added. This is discussed in Section 6.4.

The use of a measured value of flow resistivity to obtain a value of sp^2 and hence a range of $sp^2\sigma$ creates three problems. Firstly measuring flow resistivity is not easy and the process may destroy the soil structure. Even if care is taken and reasonable results are possible these may be misleading because of two other problems.

The second problem arises from using a measured flow resistivity value that has been measured on a non-representative sample of the soil. This is shown on the two clay treatments. The acoustically deduced parameters σ_{pe} and Ω for the wheeled and zero sites when used to calculate $sp^2\sigma$ and would suggest the wheeled plot has a surface that has a lower flow resistivity

than that of the zero site. This is attributed to surface cracking and will be discussed again later. In situ measurements of flow resistivity as made by Wall [111] were made such as to avoid any noticeable cracks. Hence these measured flow resistivities are for a small sample of soil possessing macro-scale pore structure. Inferred values of sp^2 although falling within the theoretical limits are probably untrue and may explain the very low value of sp^2 on the wheeled site. The deduction of flow resistivity at the surface using the level difference technique can show a flow resistivity of a larger area which may have advantages in the case of cracked clays. On the other hand it is interesting to note that the probe measurements for this site show a looser surface on the zero plot than the wheeled plot. This discrepancy will be discussed later.

The third problem associated with the use of a measured flow resistivity is that the sample extracted maybe too deep to represent the feature of interest. This problem is demonstrated on Sand 3 the crusted sand. The measurements of flow resistivity using the Leonards Apparatus were made on samples 5cm in length. Such a large sample is likely to provide a poor indication of the flow resistivity of the crust. Also it was quite likely that the crust was altered during core extraction and location into the Leonards apparatus. If the measured flow resistivity 70900mks rayls/m is used in conjunction with the predicted σ_{pe} and Ω, an sp^2 value of 9.16 is deduced for the crust. This is well beyond the theoretical limits. A better value for sp^2 may be 0.31 as obtained for the other sands studied. This value implies a flow resistivity of 2000000mks rayls/m and an $sp^2\sigma$ value of 650000 for the crust . For the sand beneath the crust a value of 0.44 for sp^2 can be deduced. This is rather high and implies that 70900mks rayls/m is probably an unrealistic value for the flow resistivity of the lower layer as well. This again is explained by damage to the sample during flow resistivity measurements.

For acoustic soil structure monitoring and measurement of flow resistivity, *in situ*, it would be ideal not have to rely on conventionally measured flow resistivity at all. Hence it is important to consider whether studying the values of σ_{pe} and $sp^2\sigma$, can be indicative of flow resistivity where either flow

resistivity measurements are not measured or cannot be made at sufficiently small depth intervals.

An indication of the usefulness of effective flow resistivity follows from a comparison. Treatments on the same soil type on which both acoustic and conventional soil measurements have been made can be compared to those where only acoustic measurements were made. On Silt B both the controlled wheeling and poor practise treatments had a 1cm thick crust present. For the poor practise treatment flow resistivity measurements were made for 0-3cm and 3-6cm intervals. Table 6.10 shows that the measured flow resistivity 1477000mks rayls/m for the 0-3cm interval is significantly higher than the measured value for the lower layer which was 144000mks rayls/m. This implies that although the crust was only 1cm thick it was influencing the flow resistivity measurement of the 0-3cm thick core sample. Using the measured flow resistivity 1477000mks rayls/m and the acoustically determined values of $\sigma_{pe}$and Ω a value for $sp^2\sigma$ of 300000mks rayls/m can be deduced for the poor practise site. For the controlled wheeling site no successful flow resistivity measurements were made close to the surface. However using the values of σ_{pe} and Ω from the level difference measurements an $sp^2\sigma$ of 90000mks rayls/m can be deduced for the top 1cm. This value is greater than the value of $sp^2\sigma$ for the lower layer (17800) deduced from a combination of acoustically determined and conventionally measured flow resistivity. Comparison of these results suggests that the crust on the controlled wheeling site has a higher flow resistivity than the soil beneath. Comparison of the controlled wheeling plot value of $sp^2\sigma$ (90000) with the poor practise site value of (300000) suggests that the controlled wheeling site has a lower flow resistivity than the crust on the poor practise site. This interpretation is supported by field notes and probe results as discussed in Section 6.5. Also the fact that it was possible to extract core samples and monitor the flow resistivity over the upper layer suggests the crust on the poor practise site was denser and of a more compact nature.

The combined use of level difference and probe deduced parameters enables the calculation of porosity with depth Ω_d as discussed in Section 6.2.2.

Table 6.11 Monitoring Flow Resistivity with Depth on a Sand

Depth cm	σ_{pe}	T_d	Ω_d	Inferred $sp^2\sigma$
0 - 1	30600	21.21	0.02	1530000
1 - 2	6880	2.16	0.36	19000
2 - 3	7110	2.12	0.36	20000
3 - 4	9650	2.22	0.34	28400
4 - 5	8710	2.28	0.33	26400
5 - 6	7900	2.12	0.36	22000
6 - 7	7360	2.57	0.28	26300

Table 6.12 Monitoring Flow Resistivity with Depth on a Dry Sandy Loam soil

Depth cm	σ_{pe}	T_d	Ω_d	Inferred $sp^2\sigma$
0 - 1	23840	3.48	0.51	46740
1 - 3	34160	3.89	0.48	71166
3 - 5	29250	9.81	0.29	100862

Using these deduced values of Ω_d and the respective values of σ_{pe} for each depth interval from probe measurements, it is possible to deduce the variation in $sp^2\sigma$ and hence the profile of flow resistivity with depth. Rearranging Table 6.4 slightly an example of this deductive process is shown in Tables 6.11 for sand 1. Another example this time for a dry sandy loam is shown in Table 6.12.

For the sand results in Table 6.11 the probe deduced $sp^2\sigma$ values show a fairly homogeneous horizon except for the surface 0 - 1cm interval. This has been shown in reanalysis to be in error due a mistaken depth interval which, as explained in Section 5.1.1,was infact 0-2cm close to the surface. Hence with the new value for the 0-2cm included Table 6.11 should be written as Table 6.13.

Uniform values of $sp^2\sigma$ suggest a fairly constant flow resistivity with depth. For the dry sandy loam results in Table 6.12 the values of $sp^2\sigma$ suggest a decreasing flow resistivity with depth. It is also noted in Table 6.12

Table 6.13 Remonitoring Flow Resistivity with Depth on a Sand

Depth cm	σ_{pe}	T_d	Ω_d	Inferred $sp^2\sigma$
0 - 2	8149	2.36	0.32	25550
2 - 3	6880	2.16	0.36	19000
3 - 4	7110	2.12	0.36	20000
4 - 5	9650	2.22	0.34	28400
5 - 6	8710	2.28	0.33	26400
6 - 7	7900	2.12	0.36	22000
7 - 8	7360	2.57	0.28	26300

Table 6.14 Monitoring Flow Resistivity with Depth on a Crusted Sand

Depth cm	σ_{pe}	T_d	Ω_o	Inferred $sp^2\sigma$
0 - 1	106950	5.97	0.13	822692
1 - 2	47520	3.22	0.31	153290
2 - 3	21020	1.92	0.31	67806

that $sp^2\sigma$ (46740) for the 0-1cm interval is very close to the $sp^2\sigma$ deduced from level difference measurements (44000) over the same soil shown in Table 6.10.

The third consideration is whether values of σ_{pe} and T may be used to indicate flow resistivity. This is particularly important for probe measurements at depth where layering may occur at smaller intervals than conventional techniques can measure. In Table 6.14 conjunctive use of acoustically determined porosities using the layered model and σ_{pe} and T values from probe measurements allows the deduction of $sp^2\sigma$ for both the crust and the sand beneath. The large difference between values of $sp^2\sigma$ for the crust 822700 and 153300 for the sand beneath suggests that the crust has a much higher flow resistivity than the substrate.

It is tempting to study just the value of σ_{pe} to monitor effective flow resistivity. From the results in Table 6.12 if the values of σ_{pe} alone had been studied it would have been possible to deduce the existence of a harder more compacted layer at the 1 - 3 cm interval. However the value of T

is also an important indicator. The trend noted in Section 6.2.2 was that porosity values decreased as tortuosity increased. In Table 6.12 when the deduced porosity at depth is used together with the σ_{pe} value the resulting $sp^2\sigma$ suggests a lower flow resistivity between 3-5cm. From this it can be stated that where a relatively high value of σ_{pe} coincides in a profile with a relatively high value of T then porosity is likely to have decreased and flow resistivity increased.

The procedure demonstrated in Tables 6.11 and 6.12 is likely to be successful on those soils that have been described as homogeneous with depth because sensible values of porosity with depth have been deduced. However the results for the crusted sand 3 indicate a similar procedure will be successful for a layered soil.

As a summary of this discussion it is shown that the behaviour of $sp^2\sigma$ can be indicative of flow resistivity both at the surface of a soil as measured by level difference measurements and at depth within a soil profile as deduced from a combination of level difference and probe measurements. It is also suggested that the combination of a discrete increase in both σ_{pe} and T within a probed profile with depth is indicative of a decrease in porosity and an increase in flow resistivity.

6.4 Acoustic Determination and Monitoring of Soil Moisture Content.

Considering the level difference results given in Table 6.15 it appears that after initial application of water to a moist state the permeability of the sandy loam soil is actually increased compared to its permeability in a dry state. This is suggested by the decrease in the values of σ_{pe} from 24050mks rayls/m to 9380mks rayls/m and a decrease in the tortuosity (T) from 3.32 to 1.23. It is also supported by the independent measurements of flow resistivity which fall from an average of 259000mks rayls/m to 54000mks rayls/m. The same phenomena has been observed in the field on the wheeled clay site, before and after a summer thunderstorm of 20 minutes duration during

which approximately 1.5mm of rain fell. After an initial application of water the value of σ_{pe} decreases although unexpectedly T increases. This increase may be due to an increase in the grain shape factor n' rather than a decrease in porosity.

Table 6.15 Effect of Water Application to Soil on Acoustically Deduced Parameters

Soil type	Treatment	Moisture status	σ_{pe}	T	Ω
Sandy Loam		dry	24050	3.32	0.52
		moist	9380	1.23	0.39
		wet	34800	-	0.11
Clay	wheeled	before rain	9390	6.82	0.45
	wheeled	after rain	6650	10.41	0.48

For the sandy loam soil an explanation of the decrease in flow resistivity may be that the application of water causes the fine, dry, dust-like soil particles to aggregate together and form soil crumbs. This aggregation results in a possible structure change from a dense, closely packed soil composed of small soil particles to a relatively less dense soil. This explanation is supported by the decrease in the average dry bulk density from $1.25kg/m^3 \times 10^{-3}$ to $1.09kg/m^3 \times 10^{-3}$ determined from the core samples taken under dry and moist conditions respectively.

Subsequent applications of water to achieve a very wet state resulted in an increase in flow resistivity. There must be a turning point in the trend which should be indicated by acoustically determined flow resistivity and further work could show this. It is likely that this turning point will be different for different soil types The eventual increase in flow resistivity is likely to be accounted for by the increased moisture content filling the former air-filled pores. A second contribution maybe the slaking of the surface area which became more marked as water application continued. Slaking meant soil crumbs at the surface were, in-part, destroyed by water action and soil particles saturated and reorientated into a thin highly impermeable layer. This would account for the successful modelling of the soil structure by

a thin high flow resistivity layer above a more porous soil as discussed in Section 5.2.3.

From outdoor level difference measurements (Table 6.15) rainfall on the wheeled clay site (Day 4) resulted in a similar pattern of acoustically deduced σ_{pe} to that monitored on the sandy loam. The effective flow resistivity decreases from 9390mks rayls/m to 6650mks rayls/m although for the clay T increases from 6.82 to 10.41. It is suggested that the soil was moistened not saturated. Saturation would result in an increase in σ_{pe}. Moistening is likely because of the relatively small amount of rainfall and the protection offered from the crop cover which would also protect the surface and prevent destruction of soil crumbs at the surface and hence slaking.

As well as monitoring the changes to structure when water is applied (wetting phase) acoustic techniques were also found to be sensitive to monitoring a drying phase. Figures 6.4, 6.5, 6.6 and 6.7 show four level difference spectra from the two differing treatments on the clay soil.

Figures 6.4 and 6.5 were made over wet clay conditions, Figures 6.6 and 6.7 were made on the same sites when field conditions were noticeably drier. A marked difference can be seen between the wet and dry condition and between each treatment. Comparable differences between normal and zero wheeled sites are less well seen. However these are just individual examples. A total of 23 measurements were made in all to test repeatability. Table 6.16 shows average values of level difference deduced parameters σ_{pe},T and Ω for the two treatments on both days.

On Day 1 the average σ_{pe} value is higher for the wheeled plot, 14000mks rayls/m compared to 12300mks rayls/m for the zero traffic plot. The surface is less porous with a more tortuous path for the sound waves to follow indicated by the higher T value of 3.87. On Day 2 for both treatments the σ_{pe} values are reduced by roughly a factor of 2. The weather for the two weeks preceeding Day 2 had been relatively dry with only 7mm of rainfall, compared to 33mm in the two weeks preceeding Day 1 [114], consequently the plots had dried out. This drying phase as the soil drained would increase the air permeability of both treatments and this is indicated in the decrease

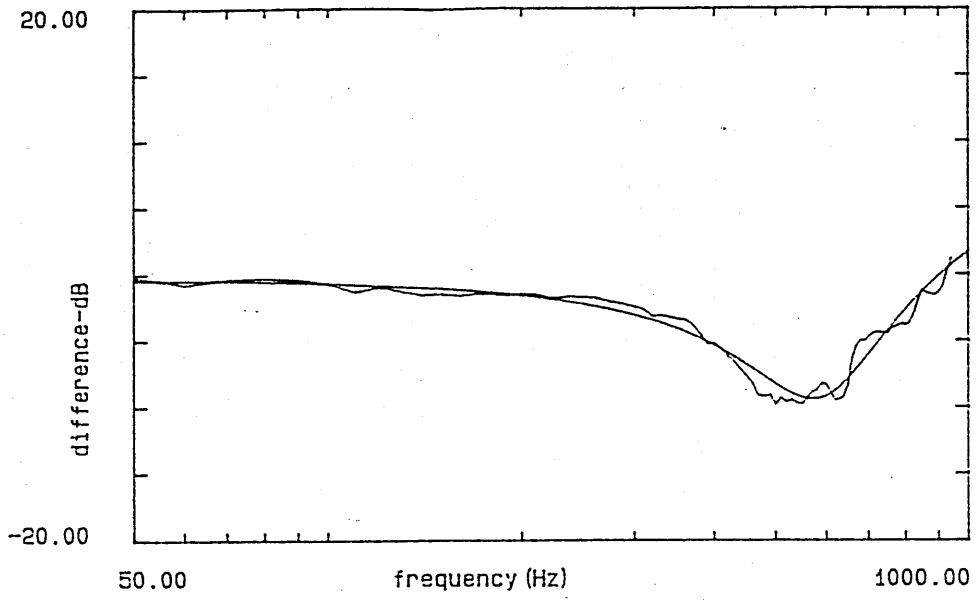

Figure 6.4 Measured and Predicted Level Difference for Clay Soil Wheeled Site under Wet Conditions hs=0.44m, r=1.75m, hrt=0.54m, hrb=0.1m, rms=1.09. Predicted parameters σ_{pe} =17300, T=4.50, Ω=0.59

Table 6.16 Comparison of Predicted Ground Parameters for two Clay Soil Treatments under Wet and Dry Field Conditions

	Soil	Treatment	Moisture	σ_{pe}	T	Ω	Meas.Ω	% water(vol)
Day 1	Clay	wheeled	wet	14000	3.87	0.53	0.62	0.19†
		zero	wet	12300	2.00	0.57	0.55	0.18†
Day 2	Clay	wheeled	dry	3680	2.68	0.42	0.47	0.19
		zero	dry	6275	3.35	0.57	0.55	0.17

† possible core sampling error

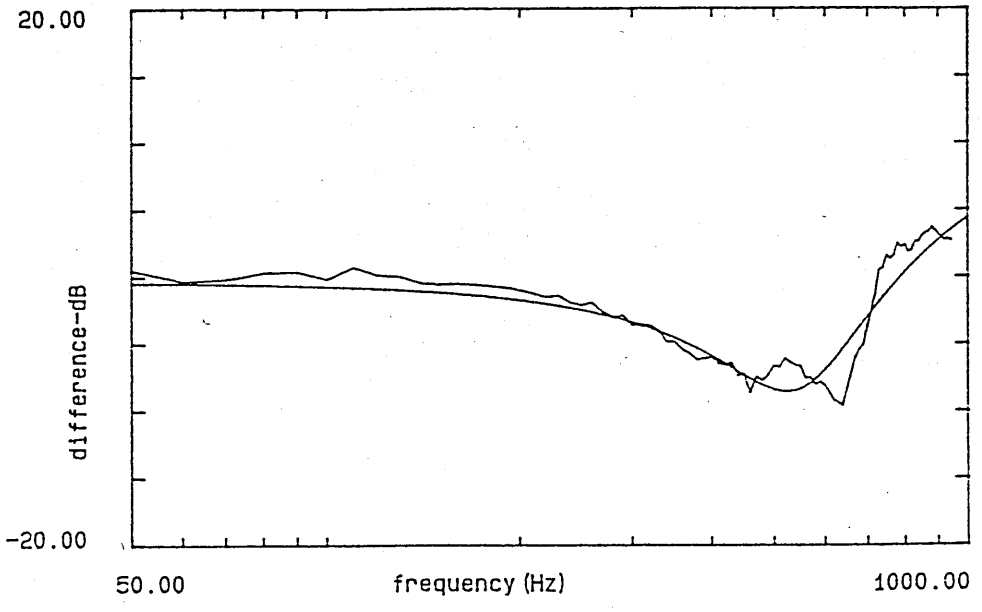

Figure 6.5 Measured and Predicted Level Difference for Clay Soil Zero Site under Wet Conditions hs=0.44m, r=1.75m, hrt=0.54m, hrb=0.1m, rms=1.71. Predicted parameters σ_{pe} =13210, T=2.67, Ω=0.61

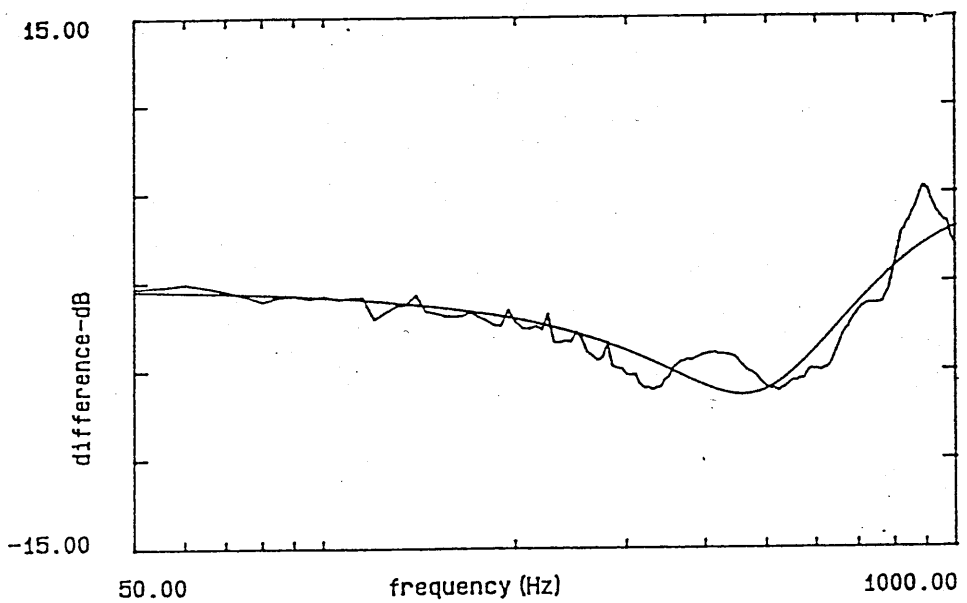

Figure 6.6 Measured and Predicted Level Difference for Clay Soil, Wheeled Site, under Dry Conditions hs=0.54m, r=1.75m, hrt=0.53m, hrb=0.1m, rms=1.42. Predicted parameters σ_{pe} =4622, T=2.16, Ω=0.43.

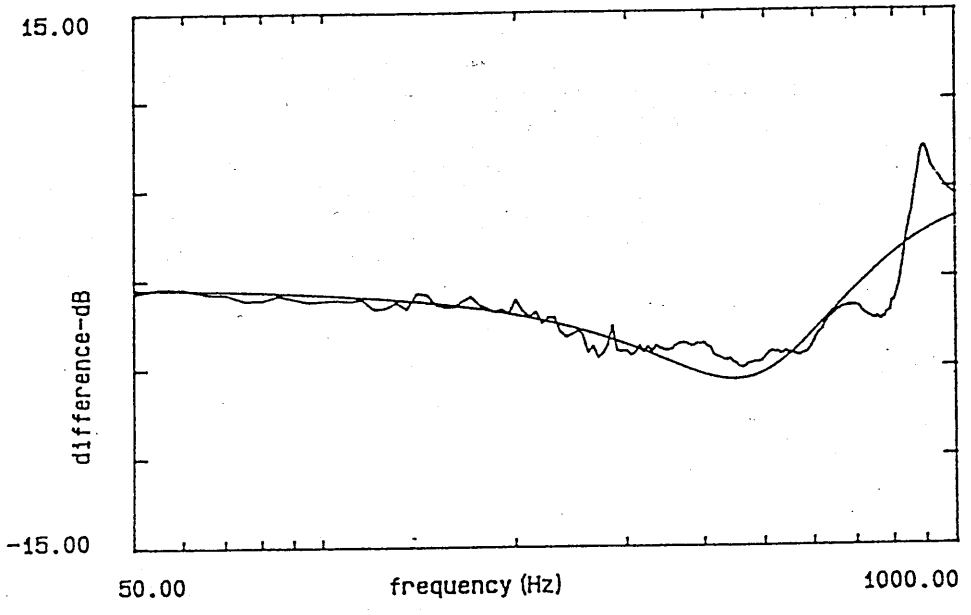

Figure 6.7 Measured and Predicted Level Difference for Clay Soil, Zero Site, under Dry Conditions hs=0.5m, r=1.77m, hrt=0.53m, hrb=0.1m, rms=1.61. Predicted parameters σ_{pe} =6620, T=2.97, Ω=0.58.

of the effective flow resistivity, σ_{pe} values for both sites. However the measured moisture contents %volume for 0 - 3cms on both dry and wet days were approximately equal to 0.19%(vol) and do not support this, although there is some doubt over the wet clay sample figures. Nevertheless, it is suggested that the acoustic reflection technique was sensing a cracked clay feature over a larger area, which the smaller core samples could not. On Day 2, both sites had become more permeable to air flow due to the presence of large cracks. Both field notes and the lower value of 3680mks rayls/m for σ_{pe} suggest that the wheeled site had suffered a more severe degree of cracking. Past monitoring of the wheeled and zero treatments indicated that the occurrence and pattern of shrinkage cracks was generally less severe on the zero treatment plots, Chamen et al [115].

6.5 Acoustic Detection and Characterisation of Surface Crusts, of a Saturated Surface Layer and Sub-surface Layering Patterns.

The presence of a surface crust was usually obvious whilst experiments were being undertaken. A further indication was the attenuation measured using the probe microphones. Greater attenuation over a given depth interval close to the surface compared to that over a similar interval at depth would imply the presence of a crust. These two pieces of information justified the use of the layered model to fit the level difference spectra.

From the fitting of this model it is possible to determine the porosity Ω and an effective flow resistivity, σ_e , of both the crust and the soil layer beneath and hence σ_{pe} from the relationship $\sigma_{pe} = sp^2\sigma\Omega$, as well as being able to estimate the crust depth. Table 6.17 represents an abbreviated form of Table 6.3, for ease of discussion and shows all predicted and measured porosities for soil surfaces where crusts were known to occur. Assumed values are shown in brackets. Included here also are the wet Sandy Loam predictions.

A direct comparison of predicted and measured crust porosities is avail-

Table 6.17 Deduced Ground Parameters for Various Layered Soils

Soil	Model	Feature	Layer	Pred.Ω	Meas.Ω	%error	rms	sample depth
Sand 3	ml	crusted	t	(0.13)	0.14	-7	1.73	0 - 1
			b	(0.31)	0.27	15	"	1 - 5
Silt A (day3)	ml	compacted	t	0.23	-		2.59	
			b	(0.32)	0.32	0	"	0 - 3
Silt B	ml	cultivated wheeling	t	0.15	-		3.01	
			b	(0.48)	0.48	0	"	0 - 3
Silt B	ml	poor practise	t	0.12	-		3.89	
			b	(0.40)	0.44	-9	"	0 - 3
Sandy loam	ml	wet	t	(0.11)	0.11	0	2.92	0 - 1
	.		b	(0.39)	0.27	39	"	0 - 5

able only on the sand (-7%) error and wet sandy loam soil (0%) error. The porosities for both upper and lower layers on both soils are, in general, well predicted because they are set close to the measured air porosities during the fitting procedure, as described in Section 4.4.1. However for the other soils the a measured value of air porosity was not available. For the silt soils it was difficult to sample the 0 - 1cm interval alone due to crust fragility. If predicted crust porosities on the silt are compared to the 0-3cm core measurements error percentages are extremely high $\approx$73% for the poor practise silt. Where measured porosities were not available the upper layer porosity had to be iterated to minimise the rms fitting error value. This works well on Silt A, but for Silt B rms discrepancy values remained high. It was thought that reflections from the sugar beet crop caused spurious reflections and subsequent difficulty in curve fitting. Consequently these data must be interpreted with caution.

It is clear the surface crusts have a lower air porosity than the soil beneath. The data also indicates that both silt treatments experienced surface crusting but the poor practise site was more severly affected having a lower porosity. Field notes show that this was indeed the case. Furthermore, Hil-

lel [38] shows that soils become increasingly prone to crusting as their initial average aggregate size is reduced. Therefore is was to be expected that a poorly managed site with a somewhat worse soil structure was likely to be prone to more severe crust formation. Although this interpretation has to be regarded with caution, due to high rms fitting error, it is supported by probe measurements, see Table 6.19. Higher σ_{pe} and T values were deduced, close to the surface, on the poor practise site compared to lower values on the controlled wheeling site suggesting a more compact, harder layer.

The sandy loam produces the worst prediction of the lower layer porosity with an error of 39%. The porosity inserted into the multi-layer model for the lower layer was set equal to that predicted from level difference measurements over the moist soil condition, 0.39, which has already been discussed as probably uncharacteristic. The measured porosity 0.28 was taken at an interval of 0 - 5cm which included the saturated surface layer. A better solution would have been to take core samples from 1 - 6cm depth below the visibly very wet surface layer. This value would probably have been around 0.33, compatible with the measured air porosity from the moist soil, and thus reduce the apparent % error in the acoustically deduced value to 18% which is slightly more tolerable.

From the relationships $\sigma_{pe} = sp^2\sigma\Omega$, and $\sigma_{pe} = \sigma_e\Omega^2$ it is possible to deduce $sp^2\sigma$ from the predicted level difference parameters as shown in Table 6.18. An inference of crust or saturated layer flow resistivity is then possible. Table 6.18 suggests that Sand 3 has the highest inferred flow resistivity and the hardest crust with an $sp^2\sigma$ value of 650000mks rayls/m . The wet sandy loam is ranked second (315000mks rayls/m), with the poor practise silt (300000mks rayls/m), followed by , the wheeled silt (90000mks rayls/m), and the loosest crust being on the compacted silt A (69000mks rayls/m). It is interesting that this order is not replicated for the lower layer except for the sand and the wheeled silt. The depth of each layer was set to the observed depth of the layers, 1cm for all sites.

The results presented above indicate the level difference technique can detect the presence of surface crusts and potentially, determine their physical

Table 6.18 Inference of Flow resistivity for Layered Soils

Soil	Model	Feature	Layer	σ_e	Ω	layer depth	$sp^2\sigma$	σ_{pe}
Sand3	ml	crusted	t	5000000	(0.13)	(1)	650000	85400
			b	100000	(0.31)		31000	9610
Silt A	ml	compacted	t	300000	0.23	(1)	69000	15870
			b	75000	(0.32)		24000	7680
Silt B	ml	controlled	t	600000	0.15	(1)	90000	13500
		wheeling	b	(36600)	(0.48)		17600	8430
"	"	poor	t	2500000	0.12	1	300000	36000
		practise	b	(40800)	(0.40)		16320	6530
sandy	ml	wet	t	2875000	(0.11)	(1)	315000	34800
loam			b	(59200)	(0.39)		23100	9000

parameters and depth without invasive sampling. A more detailed picture on variation of acoustically deduced parameters with depth is revealed by probe microphone measurements.

In the discussion of objective 2 a combination of high σ_{pe} and T deduced from propagation constant measurements was seen as an indicator of increasing flow resistivity and decreasing porosity. Hence by looking for such combinations detected by the probe microphones it is possible to deduce crust or saturated layer flow resistivity. The detection of surface crusts and the wetted layer using the probe microphone is illustrated in Table 6.19. The high σ_{pe} and T values close to the surface suggest a higher flow resistivity and a lower porosity than the layers beneath. Table 6.19 shows crust features on all the sites mentioned above and also includes the possible detection of a crust on the clay (day2) sites.

The ordering of acoustic hardness as discussed above is not quite the same for the probe measurements. The most obvious features, the sand having the hardest crust with an σ_{pe} value of 106950 and 5.97 for T, and a potentially more severe crust on the poor practise silt than on the wheeled silt are the same. The wet sandy loam and the poor practise silt are very similar in acoustic hardness. The probe technique also indicates a slight

Table 6.19 Probe Microphone Detection of Surface Crusts

Soil	Treatment	Depth cm.	σ_{pe}	T	Feature	Inferred Depth cm
Sand3		0 - 1	106950	5.97	crust	1
		1 - 2	47520	3.22		
		2 - 3	21020	1.92		
		3 - 4	21120	19.30		
Silt A	compacted	0 - 1	6865	8.65*		
		0 - 2	1295	1.86		
		0 - 0.5	61717	4.37		
		0.5 - 1	25553	1.44		
		0 - 1	83377	3.21		
Silt B	cult.	0 - 2	16470	9.35*	crust	2
	wheeling	2 - 4	7480	7.00*		
	poor	0 - 2	53260	24.00*	crust	2
	practise	2 - 4	4050	12.64*		
		4 - 6	6530	5.98		
Sandy	wet	0 - 1	53930	9.24	crust	1-2
Loam		1 - 3	13290	5.39	crust	
		3 - 5	9500	4.74		
		5 - 6	9490	6.15		
Sandy	wet	0 - 1	66560	51.80	crust	1-3
Loam		1 - 2	10850	9.11	crust	
		2 - 3	4530	11.45		
		3 - 4	4580	4.57		
		4 - 5	12730	9.87		
clay	wheeled	0 - 2	3740	4.16*	crust	2
(day 2)		2 - 4	2090	1.84		
		4 - 7	7120	3.45*		
clay	wheeled	0 - 1	6860*	7.36*	crust	1
(day 3)		1 - 3	3130	3.16		
		3 - 5	1550	3.22		
"	zero	0 - 2	4780	5.03	crust	2
		2 - 4	1330	2.18		
		4 - 6	1460	1.21		

crust formation on the clay treatments, for two different days, although these do not possess the high flow resistivities and low porosities deduced for the other soils' crusts.

Comparing all sites higher values of σ_{pe} and T may represent a more tightly bonded or cohesive structure and hence indicate the strength of the surface layer. The sand crust and wet sandy loam layer could be carefully picked away from the soil beneath for sampling hence the structure was fairly rigid. However the silt crust would 'snap' and crumble to individual grains like dust with pressure from the fingers. This may account for the highly variable and unreliable probe results obtained on this soil. In some instances the actual insertion of the probe destroyed the weak crust.

Comparing the saturated layer values of σ_{pe} and T to those for dry crusts a similarity is seen. This means the technique does not discriminate between a dry, physically hard crust like that on the silt and the very wet surface layer on the sandy loam. It is only visual observation of the physical conditions at the time of experimentation that explains the difference. This may cause difficulties when using acoustical techniques to study parameters with depth. For example when T increases has the porosity decreased because of a compacted layer or has the moisture content increased. More work needs to be done to study the effects of wetting and drying.

Discrepancies between probe and level difference prediction of physical parameters are to be expected due to the more localised nature of the probe technique. This is clearly shown in the prediction of layer depth. The level difference technique predicted the crust thickness to be 1cm at all sites . This was fixed in the fitting procedure at 1cm from observations made at the field sites. A value of 2cm was also tried in the predictions for sand 3 and the wet sandy loam cases. However this change made no difference to the predicted curve. This is to be expected as shown in Figure 3.7, where for a very high flow resistivity and low porosity the limiting depth of penetration, assuming a limiting value of 10dB attenuation, is 1cm for frequencies between 400-1000Hz.

The probe deduced parameters suggest varying depths as shown in Ta-

ble 6.20. On Silt B high σ_{pe} and T values suggest the crust has a thickness no greater than 2cm. The same depth of crust is detected for the clay although the boundary is less well defined and may even be less than 1cm. For the sand crust depth is clearly defined at 1cm thick. The major discrepancy is on the boundary between the saturated and moist soil which the probe suggests is at 2-3cm deep, although inspection by eye and reflection measurement suggest 1cm. This again suggests the lateral inhomogeneity of the wetted soil with depth from area to area and the superiority of the probe technique to monitor soil layers particularly where the boundary depth is not constant but undulating over the whole area contributing to sound reflection.

The boundary between a crust or wetted layer and the substrate below has been indicated acoustically by sharp contrasts in σ_{pe} and T values. These contrasts can also be used to pick out other layer features at depth. This is best exemplified in the snow profiles, to be discussed later, because of the greater depths to which sound can penetrate in a lower flow resistivity medium such as snow. However some limited inferences can be made about the clay soils studied. Layered features at depth were identified when the two different treatments on different days were compared. Table 6.20 shows probed profiles for the wheeled and zero treatment plots on wet, Day 1, and dry, Day 5.

From Table 6.20 a harder layer is indicated at 4-6cm on the zero treatment plots for both days. For the wetter day the values of σ_{pe} and T are higher not only for the 4-6cm layer but also at every interval down through the profile indicating that moisture content may also be playing an important role by decreasing air porosity and increasing flow resistivity. It was possible to make measurements to 10cm under dry conditions compared to only 8cm under wet conditions. This again indicates a lower flow resistivity for the zero treatment site under dry conditions.

On the wheeled sites the detection of a harder layer at 4-6cm is difficult. Measurements below 6cm could not be made successfully due to background noise. The presence of the hard layer could be deduced from the high σ_{pe} and

Table 6.20 Deduction of Hard Layers at Depth Using a Probe Microphone

Soil	Treatment	Moisture Status	Depth cm	σ_{pe}	T	Feature	% H_2O	Depth cm
Clay (day 1)	wheeled	wet	0 - 2	4090	10.20		0.19	0-3
			2 - 4	81770	55.80	Harder	0.42	3-6
	zero	wet	0 - 2	2550	4.08		0.20	0-3
			2 - 4	6294	8.33			
			4 - 6	9443	25.00	Harder	0.31	3-6
			6 - 8	5943	16.98			
Clay (day 5)	wheeled	dry	0 - 2	755	3.19		0.21	0-3
			2 - 4	915	4.39			
			4 - 6	19454	33.14	Harder	0.37	3-6
Clay (day 5)	zero	dry	0 - 2	1193	4.19		0.15	0-3
			2 - 4	1506	2.77			
			4 - 6	6378	7.30	Harder	0.29	3-6
			6 - 8	1526	2.80			
			8 - 10	1282	3.04			

T values at 4 - 6cm under dry conditions and 2 - 4cm under wet conditions.

One interesting feature of note is that under dry conditions on Day 5 (8/9/86) the measurements were made at the end of the summer and under these dry conditions the soil had experienced cracking. This is indicated by the low σ_{pe} values between 0 and 4cms below which there is possibly a more compact or wetter layer. It could be inferred that the cracks may be 4cms in length.

Conclusions of this discussion are that level difference measurements can be used to detect the presence of surface crusts and saturated surface layers and to some extent determine their physical parameters and layer depth. For finer details of variation with depth on a more localised scale and for checking the depth, continuity and undulations in crust/substrate boundaries the probe technique is more useful. Initial analysis of probe measurements made on Sand 1 showed larger effective flow resistivities and tortuosities close to the surface which possibly inferred the presence of a crust feature. This was

despite there being no visible crust and the successful fitting of the level difference measurements using the three parameter homogeneous approximation. This inconsistency was later explained (see Section 5.1.1) by an error of 1cm in the estimation of the first depth interval. This error was caused by the misleading construction of the probe microphone, used for this series of measurements. For all other measurements made over soil and discussed above an improved two microphone technique was used. These probes had the microphone diaphragms actually in line with the probe end holes and the depth graduations exactly marked on the outer probe casing. Results which suggest a surface layer using these real depths are likely to be true and indeed in most cases are corroborated in several ways. These include visual detection of a crust, detection using measurements of air permeability and porosity and better fitting of the level difference measurements using the layered prediction model.

Other conclusions reached in this section are that sub-surface layering has also been seen on the clay sites and the parameters of these layers are seen to change with the moisture status of the soil. Cracking on the wheeled site under dry conditions, is also amenable to acoustic investigation.

6.6 Acoustic Determination of Physical Properties of Snow.

The snow properties determined from acoustic measurements will include air porosity, effective flow resistivity and layering within profiles.

6.6.1 Air porosity

Porosities deduced from level difference measurements are presented in Table 6.21. Direct comparison between measured and predicted porosities can be made for sites A2b and C. The predicted porosities are in both cases higher than measured porosities . The 15% error for both sites is apparently a rather poor prediction. However the low values of rms fitting error indicate that the parameters predicted are likely to be accurate. As consid-

Table 6.21 Comparison of measured and predicted porosities for snow

Site		Location	pred.Ω	meas.Ω	% error	rms	depth meas.Ω
A2b		KRC	0.88	0.76	16	0.68	0 - 5
			0.88	0.73	20		0-15
B	category 1	Road	0.90			0.41	
B	category 2	Road	0.63			0.53	
C		pine trees	0.60	0.52	15	0.90	0 - 5
			0.60	0.60	0	"	0-15
D		poplars	0.45			0.69	

ered in Section 3.7 the sound penetration with depth in snow is likely to be around 10-15cm, at 1KHz. If the measured porosities are averaged for the top 15cm then the % error increases to 20% for Site A but reduces to 0% for Site C. For the other sites where no measured porosities were made close to the surface the small rms fitting errors (rather lower than those obtained typically for soils) give confidence in the acoustically deduced values of air porosity.

6.6.2 Porosity with depth

Porosity profiles with depth cannot easily be deduced for snow. This is because the assumption that n' the grain shape factor remaining constant with depth is known not to be true [98]. As snow ages sintering occurs where individual snow crystals change from a generally flat to a more rounded shape. Hence, at the surface new fallen snow is more likely to be composed of flat shaped crystals whilst snow that has aged and been exposed to weather will be composed of more rounded grains. At depth older snow also continues to undergo this metamorphosis with time. The probe microphone is able to sense to greater depths in snow compared to those in soil and in doing so passes through snow layers of different ages depending the snowfall history. Deduced porosity profiles will therefore be misleading if the assumption of the grain shape factor remaining constant with depth is made. It is proposed

to discuss later how acoustic measurements could be used to monitor this sintering process.

6.6.3 Effective Flow Resistivity

From studying $sp^2\sigma$, in Table 6.22, a suggestion is made that the KRC, Site A has the snow cover with the highest flow resistivity. This is unexpected because of the very high air porosity 0.88. A related observation here is that from examination of columns 4 and 5 the highest porosity values are associated with the highest tortuosity values. This implies from the relationship $T = \Omega^{-n'}$, that n' is at the upper end of the previously known limit (9 for mica chips), which suggests physically the snow is composed of flat shaped crystals. The snow at least for the KRC site was known to be newly fallen within 24hrs before measurements hence it was likely to be very porous and composed of flat crystals, thus the highly tortuous nature of the air path around flat snow crystals within the snow frame could account for the high flow resistivity. On the other hand whilst it is true that high tortuosity might be associated with high flow resistivity so might a small hydraulic radius of the pores.

At both tree areas and for some measurements over the road, lower tortuosity values are associated with lower porosity values. This implies n' has decreased and suggests a different structure. Field notes report for the tree sites that a hard surface crust existed. Crusts on snow are likely to occur where melting and refreezing has caused a structural change which includes an increase in the density. This would explain the prediction of low porosities and the inferred low values of n' indicate a more spherical shaped crystal composition. Hence acoustic measurements could be used to monitor the sintering process. The higher average σ_{pe} and T values of 1570 and 1.58 beneath the poplar trees suggest a higher flow resistivity for this site compared to an σ_{pe} value of 1420 and T of 1.11 for the pine trees. This difference is also indicated in Table 6.25 showing the probe deduced parameters for these sites.

It is interesting to note from probe measurements in Table 6.23 that

Table 6.22 Deduction of Effective Flow Resistivity at Four Different Snow Sites from Acoustic Measurements

Site		σ_{pe}	T	Ω	$sp^2\sigma$	n'
Site A2b	max	3810	2.83	0.92	4140	
KRC	mean	3470	2.70	0.88	3940	7.76
	min	3120	2.57	0.85	3670	
Site B	max	2280	3.25	0.91	2500	
Road Category 1	mean	2010	2.55	0.90	2240	8.88
	min	1750	1.85	0.90	1920	
Site B	max	1560	1.35	0.62	2520	
Road Category 2	mean	1270	1.10	0.63	2020	0.21
	min	1120	1.00	0.56	2000	
Site C	max	1690	1.32	0.57	2960	
Pine trees	mean	1420	1.11	0.60	2370	0.20
	min	1130	1.00	0.59	1920	
Site D	max	1580	1.58	0.45	3510	
Poplar trees	mean	1570	1.58	0.45	3480	0.57
	min	1550	1.58	0.45	3450	

at depth, in snow as with soils high tortuosities are associated with more compacted layers ie those with a higher density and lower porosity.

6.6.4 Subsurface Layering and Surface Crusts on Snow

Acoustic measurements using the probe microphone technique can monitor layers of alternating soft and hard snow, defined by measured densities, within profiles up to 30cm deep. Table 6.23 shows two examples from Site A1 and Site A2b.

The presence of a harder layer at depth is clearly seen at both sites. This is indicated by the high σ_{pe} and T values at 9.5-11cm for the first profile and 16-18cm for the second, which correspond to measured porosities of 0.56 and 0.58 respectively. The presence of the layer at different levels indicates an undulating boundary. It is postulated that this harder layer was the former snow surface and was a hard crust which was then subsequently buried to different depths as snow drifted across the exposed area. At the time of

Table 6.23 Acoustic Deduction of Hard Layers within Two Snow Profiles

Depth cm	σ_{pe}	T	σ_{pe}	T	density kg/m^3 $\times 10^{-3}$	meas.Ω	depth of sample
0 - 4	2990	2.40	6530	1.15	0.38	0.58	0
4 - 6	2150	1.98	2890	1.25	0.32	0.65	5
6 - 9.5	1690	1.43	1600	0.95			
9.5- 11	12820	5.83*	13680*	4.23*	0.40	0.56	10
11 - 13	5030*	4.50*	5280	2.92			
13 - 15	1350*	1.37*	1040*	1.09	0.23	0.75	15
0 - 2	3520	3.00*	5100*	2.14	0.22	0.76	0
2 - 8	2960	3.07	3490	2.55	0.22	0.76	5
8 - 16	2050	3.96	2170	1.89	0.29	0.68	10
16 - 18	23920	13.94	30330	15.75	0.38	0.58	15
18 - 24	4030	1.62	2590	1.44	0.29	0.69	20
24 - 30	2570	2.36	2130	1.95	0.30	0.67	30

these measurements the snow above the layer is fairly homogeneous and relatively less compact. The measurements made at site A2b were made in the level difference area of reflection and it is interesting to note the close correspondence of the predicted parameters for the low frequency model, σ_{pe} = 3470 and T = 2.7 for the level difference technique with those deduced from probe measurements σ_{pe} = 3520 and T = 3.0. The good fit of the level difference model also indicates homogeneity.

The layers acoustically detected above are relatively thin, 2cm, compared to the depth of the entire profile, c.50cm. The detection of layers is therefore dependent on the sampling interval chosen between measurements. At Site A2a another probed profile had fewer successful measurements made at larger depth intervals. These can be seen in Table 6.24.

The stratigraphy notes for this site presented indicate the presence of a hard layer at 12cm. This is consistent with the measurements made at site A1 However the layer is only very thin probably less than 1cm and it is not detected by the density samples or the larger probe intervals, the layer probably falling within the 10 - 20cm interval. It is thought that if

Table 6.24 Deduction of Snow Parameters from a Probed Snow Profile

Depth cm	σ_{pe}	T	σ_{pe}	T	density $kg/m^3 \times 10^{-3}$	meas.Ω	depth of sample
0 - 7	1060	2.26	2520	1.23	0.30	0.67	0 - 5
7 - 10	2990	2.45	4810	1.01	0.24	0.73	5 - 10
					0.22	0.76	10 - 15†
10- 20	2600	1.33	1130	1.39	0.26	0.71	15 - 20

† hard layer at 12cm mentioned in stratigraphy description

sufficiently small depth intervals are studied with the acoustic technique then this could reveal information on snow layering undetectable by the conventional density sampling procedure. However, in snow the lower flow resistivity means that greater depth intervals are required to give measurable attenuation than in soils.

The probe technique has determined the presence and enabled deduction of the properties of hard snow layers, probably former surface crusts, that have subsequently become buried. The technique was also successful in the detection of crusts at the current snow surface. Table 6.25 shows profiles obtained from measurements beneath the pine trees and in the poplar woods and road vicinities.

The 0 - 2cm measurements for the first three sites were found to be unreliable probably due to leaking holes. Below two centimetres however the predicted parameters imply a compacted layer close to the surface overlying a relatively less dense profile beneath. The 5 - 18 cm interval probe measurement for the poplar area was probably leaking and is therefore not included here. The parameters deduced when compared to the profiles in Site A1 and A2b in Table 6.23 suggest a more dense structure throughout the entire depth of each profile. Field notes remark that the entire profile beneath the pine trees was difficult to penetrate when digging a snow pit. When the side walls had been exposed certain hard layers at, the surface, 6.5, 15.5 and 30cm remained intact while the looser powdery snow caved away from the faces. This alteration of powdery snow and harder layers

Table 6.25 Deduction of Surface crusts from probed Snow Profiles

Location	Depth cm	σ_{pe}	T	σ_{pe}	T	density $kg/m^3 \times 10^{-3}$	meas. Ω	depth
Pine Trees	0 - 2	1660	0.03	2860	1.85	0.44	0.52	0 - 5
	2 - 5	9000	37.3	5520	29.25	"	"	
	5 - 10	4370	12.6	3740	7.57	0.32	0.65	9
	10 - 15	460	0.87	260	0.93			
	15 - 22	5450	13.1	6050	12.00	0.28	0.69	16
	22 - 25	3610	1.08	3530	2.00	0.35	0.61	22.5
Poplars	0 - 5	17750	7.79	19400	9.02			
Road	0 - 5	10530	35.1	5320	33.3			
	5 - 20	1580	1.61	560	1.23			
Site A 3	0 - 2	8600	28.58	12700	34.69*	0.22	0.76	0 undisturbed snow 1 week old
	2 - 5	320	1.29	1320*	1.51*	0.21	0.77	5 hard 10cm
	5 -10	7490	10.88	7230	6.82			
	10 -15	7000	2.46	5770	4.08	0.33	0.64	10
	15 -30	2050	2.01	1890	1.86			

could explain the extremely loose layer indicated at 10 - 15cm where little attenuation was measured between the two depths.

Chapter 7

Summary and Implications for Future Work

The purpose of this thesis was to investigate the feasibility of using acoustic methods to determine the porosity of air-filled connected pores, the flow resistivity, pore tortuosity and effects of moisture content over the upper 0.1m of various soil types, and for deeper depths of snow. A summary of the discussion shows that the level difference and probe microphone methods have been used successfully to determine various ground parameters. Air porosities were acoustically deduced, for some soils, to within 10% of the measured value. Profiles of acoustically deduced porosity with depth compared well with measured values particularly for sand. An effective flow resistivity parameter $sp^2\sigma$ was deduced acoustically for several different soil types including sand, silt and clay.

The acoustical techniques developed had reasonable success at determining the physical properties and monitoring surface crusts and subsurface layering with depth in soils and snow. The use of a multi-layered model enabled the deduction of soil parameters for a two layer situation, usually a harder crust over a looser substrate. It is questionable just how successful the level difference measurements for layered soils were due to the rather crude fitting procedure used and the question of sound penetration with depth. Nevertheless the probe microphone technique proved successful in suggesting a structural change between the upper and lower layers and en-

abled the monitoring of changes in flow resistivity, porosity and tortuosity at depth at smaller intervals than conventional techniques could measure. This suggests the possible *in situ* acoustical determination of profiles associated with soil surface capping which conventional techniques destroy. For snow the insertion of the probe microphone into surface crusts in some cases damaged them nevertheless the technique was successful at locating and monitoring layers of alternating soft and hard snow, defined by measured densities, within profiles up to 0.3m deep. It was sensitive to thin layers only a few centimeters thick which were not noted in the density measurements and to undulations in the boundaries between layers. Undulations between boundaries were particularly noticed in the snow where former surface crusts were buried beneath varying depths of wind blown snow. In the analysis of level difference measurements made over snow, predictions were made assuming an externally reacting homogeneous medium. Probe measurements for the same snow suggest a layered structure in some locations. This fact plus the knowledge that sound penetration is possible to deeper depths in snow indicates that future deduction may need to use an externally reacting multi-layered impedance model to improve parameter prediction.

Changes in acoustically deduced air porosity, effective flow resistivity and tortuosity were noticed for varying soil moisture contents and an artificially saturated sandy loam soil seemed to be characteristic of a thin low permeability layer above a higher permeability substrate. Probe microphone measurements corroborated this structure and from changes in the deduced effective flow resistivity and tortuosity could locate the depth, undulations and lateral variation in the position of a wetting front within the soil profile. This suggests the possibility of using acoustical techniques to monitor soil moisture content and distribution. To study this the idea of permanently placed buried probe microphones is attractive, possibly in close proximity to soil resistance blocks which are sensitive to soil moisture content. If suitably protected from moisture the microphones could remain buried and monitor the formation and deformation of surface crusts during wetting and drying phases of the soil. The changes in acoustically deduced soil properties

brought about by water application to soils needs clarifying and effort put into understanding the relationships involved.

To study this behaviour it is proposed to set up experiments on artificially managed soils, during both wetting and drying phases. The feasibility of monitoring crust formation, aggregate shape and change on moisture application, swelling, shrinking and hysteresis effects can then be explored. Field measurements are proposed at irrigation trial sites which are currently monitored by gravimetric and neutron probe techniques for moisture content. Field measurements are also proposed at trial sites which are currently monitored for natural surface capping formation. This monitoring consists of tests for seed germination and penetrometer measurements. Acoustical measurements of air porosity and air permeability will complement these. When both sets are used together a comprehensive assessment of crust structure and thickness is feasible.

Further investigation is necessary to understand the effect of a root zone on level difference and probe measurements. It is proposed to establish small pits and tubs of previously prepared soils. Within these some will remain plant free as controls and others will be planted to create a root zone. Acoustic measurements can then be made to compare parameter predictions with and without roots. The effect of water application on both planted and control tubs can also be potentially monitored acoustically.

Results showed that the acoustic techniques used could distinguish physical differences in soil properties between different wheeling treatments. Research into the area of soil influencing both probe and level difference measurements as a function of source-receiver geometry, frequency and surface impedance, may offer a method for monitoring changes of air permeability in the localised environment of wheel tracks. Such experiments are proposed in the environment of a large soil bin where special equipment is available for creating agricultural machinery wheelings under controlled soil conditions. The effect of wheeling on soil air porosity, air permeability and structure will be monitored acoustically and compared and contrasted with densities measured using a gamma probe. It is realised that the confines of a soil bin

with side walls and the close proximity of wheeling equipment may require the development of an acoustic pulse technique to eliminate any unwanted reflections.

To obtain more information on soil characteristics from acoustic measurements it may be possible to use a four parameter model to fit both level difference and propagation measurements. This would offer the opportunity of deducing air-filled porosity Ω, actual flow resistivity σ, a pore shape factor sp^2 and a grain shape factor n' simultaneously. Monitoring of thin sections of soil or snow by image analysis could offer independent measurements of pore and grain shape. Then, in view of the Bruggeman relationship $T = \Omega^{-n'}$ if the grain shape factor is known values of porosity and the effective flow resistivity $sp^2\sigma$ can be calculated with depth throughout a profile. After sufficient investigations deduced values of the pore shape and grain shape factors may begin fall into predictable patterns for particular soil types at particular soil moisture contents. Thus look up tables or nomographs could be prepared of these parameters. Using the relationships $\sigma_{pe} = sp^2\sigma\Omega$ and $T = \Omega^{-n'}$ these tables would allow deductions of the air permeability at the surface and at depth entirely from acoustic measurements. The deduction of n' throughout a snow profile will also provide an acoustic method of monitoring the sintering process in snow.

At present a fitting routine iterating the four parameters involved is not available. However, an example of a prediction curve using the four parameter model is shown in Figure 7.1 together with a measured propagation constant for 0-1.5cm on Sand 2. Using the σ_{pe} =24240 and T=1.55 values deduced earlier (see Section 5.1.2) for this data, a measured porosity Ω of 0.48 and an inferred value of $sp^2 = 0.31$, typical of the sands studied, a value of σ =162900mks rayls/m can be deduced from the relationship $\sigma_{pe} = sp^2\sigma\Omega$. Using these values of σ, T, Ω, and sp^2 the predicted propagation constant for the four parameter model fits the measured data better, particularly the real part at high frequencies, than the propagation constant predicted using just the $\sigma_{pe}$and T parameters and the low frequency approximation, as shown in Figure 7.2.

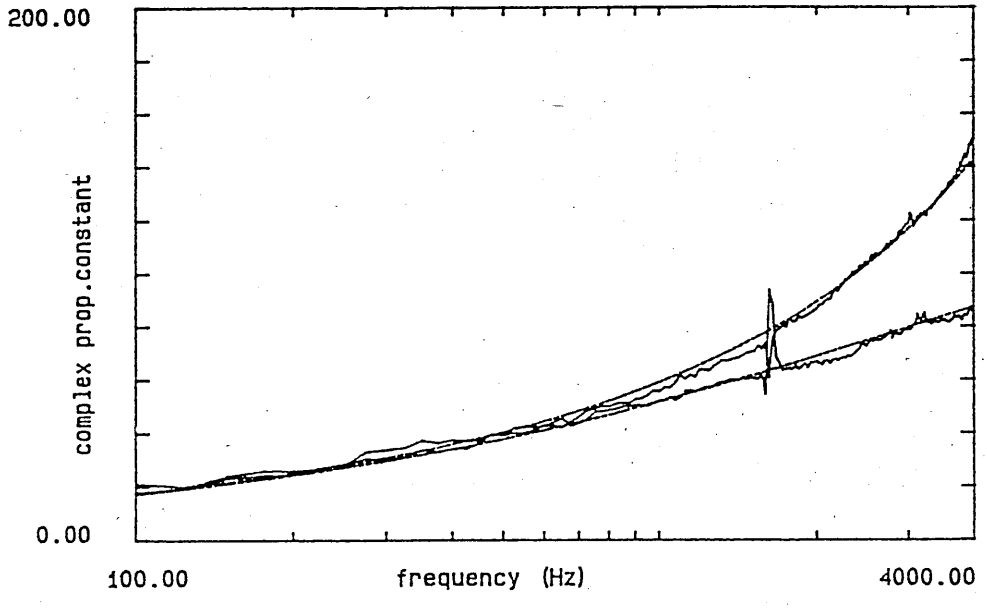

Figure 7.1 Measured and Predicted Propagation Constant using a Four Parameter Homogeneous Model, Deduced parameters σ =162900, $\Omega = 0.48$, $sp^2 = 0.31$ and T = 1.55 depth 0-1.5cm

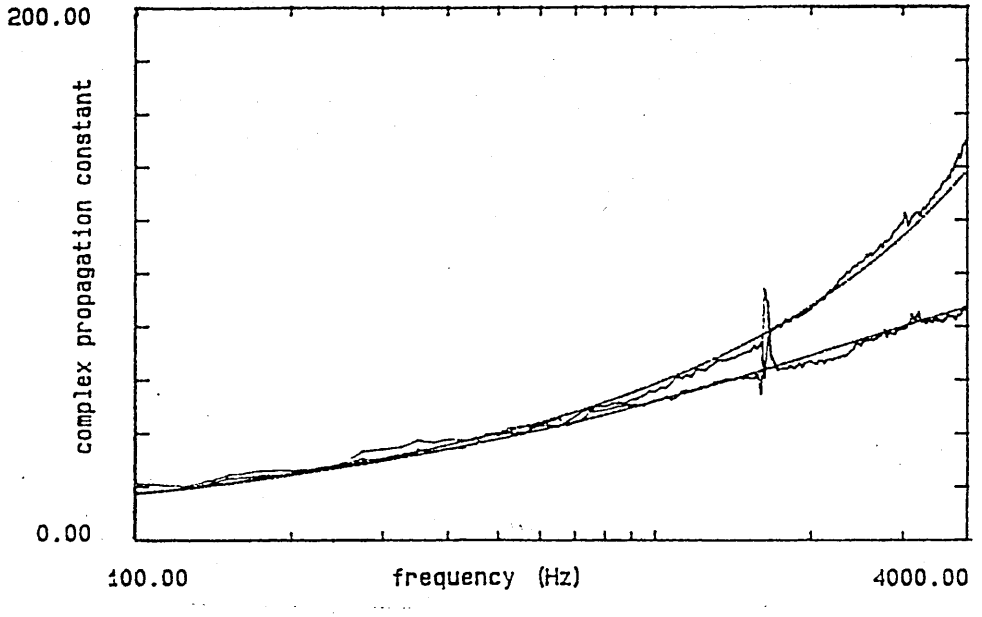

Figure 7.2 Measured and Predicted Propagation Constant using a Three Parameter Homogeneous Model σ_{pe} =24240 T=1.55 depth 0-1.5cm

A fitting routine based on four parameters was not undertaken for this study because it was felt wise to begin with a simple approximation involving less parameters and slowly build up the number of parameters involved. The work here shows that simple two and three parameter approximations can monitor changes effectively in different soil types under different conditions. If, in the first instance, a more complicated model had been used from the outset the issues and patterns indicated in this work may well have been swamped in a sea of numbers. Another reason for concentrating on the three parameter approximation chosen was the problem of level difference fitting, three parameters produced a certain amount of ambiguity, four would have been even worse.

In an effort to scale down the size of operations a single frequency approximation approach has been used successfully to deduce soil parameters from propagation constant measurements. The broad band averaging technique had problems when data were poorly behaved with frequency and was also heavily dependent on computer time and access to modelling subroutines required to manipulate the complex calculations involved at every frequency. The alternative single-frequency technique involved inspection of the measured values of the real and imaginary parts of the propagation constant and the choice of two individual data points for the deduction of an effective flow resistivity and tortuosity. For the low frequency/high flow resistivity approximation the choice of data points is likely to be a low frequency point for the effective flow resistivity and a high frequency point for the tortuosity. For the high frequency/low flow resistivity approximation data points at as high a frequency as possible should be chosen for both parameters. The success of this technique, illustrated by many examples throughout the thesis, indicates that it may be feasible to scale down the entire field measurement and analysis operation. Measurements may be made in a select frequency band, and an approximation based procedure used to develop a practical, minimum instrumentation, acoustic surveying technique. In future research it is proposed to compare further the results of using selected low and high frequency bands with those obtained using broad band sound for the probe

microphone measurements in several different soil types. It is also proposed that if distinct frequency bands are chosen then agricultural equipment's self noise may be used to determine soil properties from received signals at pre-buried microphones and microphones on a boom mounted on the machinery. This will involve the recording of machinery spectra in the field for frequency composition and engineering design of suitable protection and cabling for the buried and boom microphones.

Bibliography

[1] Attenborough K. Acoustical characteristics of rigid fibrous absorbent and granular materials. *J. Acoust. Soc. Am.*, 73:785–799, 1983.

[2] Hillel D. *Introduction to Soil Physics.* Academic Press, London, 1982.

[3] Avery B.W. and Bascombe C.L., editors. *Soil Survey Laboratory Methods.* Soil Survey, 1982. Harpenden, U.K.

[4] Low A.J. Study of soil structure in the field and laboratory. *J.Soil Science*, 5(1):57–74, 1954.

[5] Leamer R.W. and Shaw B. A simple apparatus for measuring non-capillary porosity on an extensive scale. *J.Am.Soc.Agron.*, 1003–1008, 1941.

[6] Jamison V.C. and Reed I.F. Durable asbestos tension tables. *Soil Science*, 67:311–318, 1949.

[7] Haarst G.G. Van der and Stakman W.P. Soil moisture retention curves. ii. directions for use of the sand box apparatus, range pf 0 to 2.7. Inst. Land and Water Management Research. Wageningen, Netherlands.

[8] Hunter R. *Instructions for Routine Determination of the Pore Size Distribution and Air Permeability of Soil Cores at SIAE.* Technical Report, Scottish Institute of Agricultural Engineering, SIAE, Bush Estate, Penicuik, Midlothian, 1983.

[9] Vomocil J.A. *Agronomy Monograph No.9.* Academic Press. New York, 1965.

[10] Page J.B. Advantages of the pycnometer for measuring the pore space in soils. *Soil Science Soc.Am.*, proc.1947. Vol.12:81–84, 1948.

[11] R.P. Janse. Sound absorption at the soil surface. *Centre for Agricultural Publishing and Documentation*, 89–123, 1969.

[12] Kummer F.A. and Cooper A.W. Soil porosity determinations with the air pressure pycnometer as compared with the tension method. *Agricultural Engineering*, 26:21–23, 1945.

[13] Russell M.D. A simplified air-picnometer for field use. *Proc.Soil Sci.Soc.Am.*, 14:736–776, 1950.

[14] Pidgeon J.D. *A portable air pycnometer for rapid field measurement of air-filled porosity.* Departmental Note DNSSN/169, NIAE Scottish Station, Bush Estate, Penicuik., 1974.

[15] Grable A.R. *Compaction of Agricultural Soils.* Am. Soc. Agr. Eng. Monograph, 1971. pp 154 - 164 Effects of compaction on content and transmission of air in soils.

[16] Beuhrer T.F. *Movement of Gases through Soil as a Criterion of Soil Structure.* Technical Bull. 39, University of Arizona, University of Arizona Tucson Arizona USA, 1932.

[17] Childs E.C. *An Introduction to the Physical Basis of Soil Water Phenomena.* J.Wiley and Sons Ltd. London, 1969. pp 179-201.

[18] Kirkham D. Field methods of determination of air permeability of soils in its undisturbed state. *Soil Sci. Soc. Amer. Proc.*, 11:93 – 99, 1947.

[19] Grover R.L. Simplified air permeameters for soil in place. *Soil. Sci. Soc. Amer. Proc.*, 19:414 – 418, 1955.

[20] Brooks R.M. and Reeve R.C. Measurement of air and water permeability in soils. *Trans. Am. Soc. Agr. Eng.*, 2:125 – 128, 1959.

[21] Green R.D. and Fordham S.J. *A Field Method for Determining Air Permeability in Soil.* Technical Bulletin 29, Ministry for Agriculture, Fisheries and Food, HMSO London, 1975. pp 273 - 288.

[22] Wilde S.A. and Steinbrenner E.C. Determination of air permeability of soil by means of a sphygamomanometer. *Jl. of Forestry*, 48(12):840 – 841, 1950.

[23] Imre J. Experiments on the air permeability of forest soils by radium emanation method. *Canadian Jl. of Earth Sciences*, 3:419 – 429, 1966.

[24] Evans D.D. and Kirkham D. Measurement of the air permeability of soil in situ. *Soil Sci. Soc. Amer. Proc.*, 14:65 – 73, 1949.

[25] Alpan B. An experimental method for determining the air permeability of partly saturated soils. *Soil Science*, 94(4):263 – 269, 1962.

[26] Tanner C.B. West european methods for soil structure determination. page 43, West European Working Group on Soil Structure of the ISSS, 1967.

[27] Kirkham D. Proposed method for field measurement of permeability of soil beneath the water table. *Soil Sc. Soc. Amer. Proc.*, 10:58–69, 1945.

[28] Janse A.R.P. and Bolt G.H. The determination of the air permeability of soils. *Netherlands Jl. of Agricultural Science*, 8:124 – 131, 1960.

[29] Taylor S.A. and Ashcroft G.L. *Physical Edaphology.* W.H.Freeman and Co., 1972.

[30] Bell J.P. *Neutron Probe Practise.* Technical Report 19, Institute of Hydrology, Institute of Hydrology Wallingford England, 1976.

[31] Grant D.R. Measurement of soil moisture near the surface using a neutron moisture meter. *J. Soil Science*, 26:124–129, 1975.

[32] Gurr C.G. Use of gamma rays in measuring water content and permeability in unsaturated columns of soil. *Soil Science*, 94:224–229, 1962.

[33] Fergurson H. and Gardner W.H. Water content measurement in soil columns by gamma ray absorption. *Soil Sci. Soc. Am. Proc.*, 26:11–14, 1962.

[34] Soane B.D. Dual energy gamma ray transmission for coincident measurement of water content and dry bulk density of the soil. *Nature*, 214:1273–4, 1967.

[35] Gurr C.G. and Jakobsen B. Gamma probe for measurement of field bulk density and water content. In Emerson W.W., Bond R.D., and Dexter A.R, editors, *Modification of Soil Structures*, pages 127–33, J.Wiley, Chichester, 1978.

[36] Marshall T.J. and Holmes J.W. *Soil Physics.* Cambridge University Press, 1979.

[37] Rijtema P.E. *The Calculation of Non-Parallelism of Gamma Access tubes, Using Soil Sampling Data.* Technical Bulletin 67, Institute for Land And Water Management, Institute for Land and Water Management, Wageningen, The Netherlands, 1969.

[38] Hillel D. Crust formation on loessial soil. In *Proc. of Transaction of 7th International Congress of Soil Science*, pages 330–339, Madison. Wisc. USA, 1960.

[39] de Bie J.E.G.M. and J.M.M. Groenewoud. *Several Manners to find the Normalized Specific Impedance of an Arbitrary Soil Type Pt.1 The Inclined Track Method.* PhD thesis, Catholic University, Nijmegen, Toernooiveld, Netherlands.

[40] Delany M.E. and Bazley E.N. Acoustical properties of fibrous absorbent materials. *Applied Acoustics*, 3:309–322, 1970.

[41] Attenborough K. Acoustical impedance models for outdoor ground surfaces. *J. Sound & Vib.*, 99(4):521–544, 1985.

[42] Embleton T.F.W. and Piercy J.E.and Daigle G.A. Effective flow resistivity of ground surfaces determined by acoustical measurements. *J. Acoust. Soc. Am.*, 74(4):1239–1244, 1983.

[43] Prout J.N. Some measurements of the absorption coefficients of soil using the impedance tube technique. *Noise Con.*, 7(6):20–23, Nov-Dec 1961.

[44] Talaske R.H. *The Acoustic Impedance of a Layered Forest Floor.* report, Noise Control Laboratory, NCL, Pennsylvania State University, University Park PA. USA, 1980.

[45] Chung J.Y. and Blaser D.A. Transfer function method of measuring in-duct acoustic properties. *J. Acoust. Soc. Am*, 68(3):825 – 913, 1980.

[46] Heisler G.M., McDaniel O., and Dahl M. Measurements of normal-incidence impedance of six forest floors by the tube method. In *Proceedings of the Second Symposium on Long Range Sound Propagation and Acoustic/Seismic Coupling Vol2.*, pages 408–427, University of Mississippi, Physical Acoustics Research Group, Department of Physics and Astronomy., February 1985.

[47] Glaretas C. *A New Method for Measuring the Acoustic Impedance of the Ground.* PhD thesis, Pennsylvania State University, Pennsylvania State University, PA, USA, 1981.

[48] Oura H. Reflection of sound at snow surface and mechanism of sound propagation in snow. *Low Temperature Science*, 9:179–186, 1952.

[49] Ishida T. Acoustic properties of snow. *Contributions from the Intensity of Low Temperature Science Series A.*, 20:23–63, 1965.

[50] Tillotson J.G. Attenuationof sound over snow covered fields. *J. Acoust. Soc. Am.*, 171–173, 1965. Letter to the Editor.

[51] Buser O. A rigid frame model of porous media for the acoustic impedance of snow. *J. Sound & Vib.*, 111(1):71–92, 1986.

[52] S.M. Lee and J.C. Rogers. Characterization of snow by acoustic sounding: a feasibility study. *J. Sound & Vib.*, 99(2):247–266, 1985.

[53] Dickinson P.J. and Doak P.E. Measurement of the normal acoustic impedance of ground surfaces. *J. Sound & Vib.*, 13(3):309–322, 1970.

[54] Legouis T. and Nicholas J. Phase gradient method of measuring acoustic impedance of materials. *J. Acoust. Soc. Am.*, 81(1):44–50, 1987.

[55] Daigle G.A. and Stinson M.R. Measurement of normal incidence impedence of outdoor ground surfaces in the frequency range 20-500hz. *J. Acoust. Soc. Am.*, Suppl.1 (78):586, 1985.

[56] van der Heijden L.A.M., de Bie J.G.E.M., and Groenewoud J. A pulse method to measure the impedance of semi natural soils. *Acustica*, 51(3):193–197, 1982.

[57] J.S. Bolton and E. Gold. The determination of acoustic reflection coefficients by using cepstral techniques: i: experimental procedures and measurements of polyurethane foam ii: extensions of the technique and considerations of accuracy. *J. Sound & Vib.*, 110(2):179–202, 1986.

[58] Van der Heijden L.A.M. *The Influence of Vegetation on Acoustic Properties of Soils.* Kripps, 1984.

[59] Embleton T.F.W., Piercy J.E., and Olson N. Outdoor sound propagation over ground of finite impedance. *J. Acoust. Soc. Am.*, 59(2):267–277, Feb 1976.

[60] Mansbach P.A. and Holmer C.I. *Techniques for the Measurement of Acoustic Impedance of Ashphalt.* Report No. NBSIR 78 - 1541, US Environment Protection Agency, Office of Noise Abatement and control, October 1978.

[61] Habault D. and Corsain C. Identification of acoustical properties of a ground surface. *J. Sound & Vib.*, 100(2):169–180, 1985.

[62] Chessel C.I. Propagation of noise along a finite impedance boundary. *J. Acoust. Soc. Am.*, 62:825–834, 1977.

[63] Rasmussen K.B. Sound propagation over grass-covered ground. *J. Sound & Vib.*, 78(2):247–255, 1981.

[64] Soom A. and Gu R-R. Average excess attenuation during sound propagation from an isotropic source above grassland. *J. Acoust. Soc. Am.*, 70(4):1129–1139, Oct. 1981.

[65] Parkin P.H. and Scholes W.E. The horizontal propagation of sound from a jet engine close to the ground at radlett. *Jl. Sd. Vib*, 1(1):1 – 18, 1968.

[66] Foss R.E. Effects of wind and ground plane attenuation on sound propagation near the ground. *J. Acoust. Soc. Am.*, 66(4):1088–1092, Oct 1979.

[67] Nicolas J., Embleton T., and Piercy J. Authors reply to "comments on "precise model measurements versus theoretical prediction of barrier insertion loss in the presence of ground. *J. Acoust. Soc. Am.*, 74(4), Oct 1983.

[68] Wempen J. Ground effect on long range sound propagation. In *Proc. I.O.A. One Day Meeting on Outdoor Sound Propagation*, Institue of Acoustics, September 1987. unpublished.

[69] Cramond A.J. and Don C.G. Reflection of impulses as a method of determining acoustic impedance. *J. Acoust. Soc. Am.*, 75(2):382–389, 1984.

[70] Don C.J. and Cramond A. Soil impedance measurements by an acoustic pulse tecnique. *J. Acoust. Soc. Am.*, 77(4):1601, 1985.

[71] Martens M.J.M., Van der Heijden L.A.M., Wathus H.H., and Van Rems W.J.J.M. Classification of soils based on acoustic impedance, air flow resistivity and other physical soil parameters. *J. Acoust. Soc. Am.*, 78(3):970–980, Sept. 1985.

[72] Bolen L.N. and Bass H.E. Effects of ground cover on the propagation of sound through the atmosphere. *J. Acoust. Soc. Am.*, 69(4):950–954, April 1981.

[73] Zuckerwar A.J. Acoustic ground impedance meter. *J. Acoust. Soc. Am.*, 73(6):2180–2186, June 1983.

[74] Attenborough K. Near grazing sound propagation over open flat continuous terrain. *Bulletin Acoustics Australia*, 13(1):23–29, 1985.

[75] Wilde S.A. *Forest Soils.* Ronald, New York, 1958.

[76] Aylor D.E. Noise reduction by vegetation and ground. *J. Acoust. Soc. Am.*, 51(1):411–414, 1972.

[77] Attenborough K. Acoustical properties of homogenous and inhomogenous ground surfaces. In *Sound Propagation in Forrested Areas and Shelterbelts*, pages 43–55, 1986.

[78] Huck M.G., Klepper B., and Taylor H.M. Diurnal variations in root diameter. *Plant Physiology*, 45:529–530, 1970.

[79] Cramond A.J. and Don C.G. Effects of moisture content on soil impedance. *J. Acoust. Soc.Am.*, 82(1):293–301, July 1987.

[80] Nyborg N., Rudnick I., and Schilling S. Experiments on acoustic absorption in sand and soil. *J. Acoust. Soc. Am.*, 22(4):422–425, 1950.

[81] Proc. of the Physical Society of London. *The Absorption of Sound in a Homogeneous Porous Medium*, 1946.

[82] Attenborough K., Bass H.E., and Bolen L.N. Sound transmission into plane porous ground surfaces. *Acoustic Letters*, 6(6):87–90, 1982.

[83] Attenborough K., Sabatier J.M., Bass H.E., and Bolen L.N. The acoustic transfer function at the surface of a layered poroelastic soil. *J. Acoust. Soc. Am.*, 79(5):1353–1358, 1986.

[84] Richards T.L., Attenborough K., Heap N.W., and Watson A.P. Penetration of sound from a point source into a rigid porous medium. *J. Acoust. Soc. Am.*, 78(3):956–963, Sept 1985.

[85] Van Hoof H.A.J.M. *Acoustic and Seismic Measurements in Seismic Boxes.* Technical Report FEL 1986-47, TNO Physics and Electronics Laboratory, August 1986.

[86] Attenborough K. Personal Communication.

[87] Ohagki M., Takemura H., and Fujino K. Sound velocity, attenuation constant and absorption coefficient in dry snow pack. unpublished.

[88] Ferrero M.A. and Sacerdote G.G. Parameters of sound propagation in granular absorbent materials. *Acustica*, 1:137–142, 1951.

[89] Attenborough K. and Hess H.M. Acoustical surveying of porous soils. In *14th International Symposium on Acoustical Imaging-The Hague.*, 1985.

[90] Price M.A. *Sound Propagation in Woodland.* PhD thesis, Open University, Milton Keynes, UK., 1986.

[91] Nicolas J., Berry J.L., and Daigle G.A. Propagation of sound above a finite layer of snow. *J. Acoust. Soc. Am*, 77(1):67 – 73, 1985.

[92] Donato R.J. Impedance models for grass covered ground. *J. Acoust. Soc. Am.*, 61(6):1449–1452, June 1977.

[93] Soom A.A. and Bollinger J.G. Snowmobile noise emission and propagation. In *Proceedings Third Symposium on University Research in*

Transportation Noise, pages 39 – 48, University of Utah USA, November 1975.

[94] Bohlender D.A., Babolt F., Irwin P.J., and Mathews T. A pulse harmonic technique for the study of sound propagation in the atmosphere. *J. Sd & Vib.*, 105(2):283–290, 1986.

[95] Zwikker C. and Kosten C.W. *Sound Absorbing Materials.* Elsevier, Amsterdam, 1949.

[96] Attenborough K. and Buser O. On the application of rigid porous models to imepedance data for snow. *J. Sd & Vib.*, 124(1), 1988.

[97] Zarek J.H.B. Sound absorption in flexible porous materials. Academic Press Inc. Ltd., 1978.

[98] Buser O. Personal Communication.

[99] Attenborough K. and Heap N.W. Sound attenuation over ground cover. *Shock and Vibration Digest*, 7(10):73–85, 1975.

[100] Attenborough K., Hayek S.I., and Lawther J.M. Propagation of sound above a porous half space. *J. Acoust. Soc. Am.*, 68:1493–1501, 1980.

[101] Quartarao L.R. *A Theoretical Investigation of Sound Propagation above a Half-Space of Extended Reaction.* Master's thesis, Pennsylvania State University, 1983.

[102] Chien C.F. and Soroka W.W. A note on the calculation of sound propagation along an impedance surface. *J. Sound & Vib.*, 69(2):340–343, 1980.

[103] Huisman W.H.T., Martens M.J.M., and van Asseldonk W. Measured and modelled temperature effects on outdoor sound transmission. *Proc. Inst. of Acous.*, 9, 1987.

[104] Brekhovskikh L.M. *Waves in Layered Media.* Academic Press, 1960.

[105] Biot M.A. Theoryof propagation of elastic waves in a fluid saturated porous solid.(2) higher frequency range. *J. Acoust. Soc. Am.*, 28(2):168–178, 1956.

[106] Sabatier J.M., Bass H.E., Bolen L.M., Attenborough K., and V.V.S.S. Sastry. The interaction of airborne sound with the porous ground: the theoretical formulation. *J. Acoust. Soc. Am.*, 79(5):1345–1352, May 1986.

[107] Johnson J.B. On the application of biot's theory to acoustic wave propagation in snow. *Cold regions Science and Technology*, 6:49–60, 1982.

[108] Bogordskii V.V., Gavirilo V.P., and Nikitin V.A. Characteristics of sound propagation in snow. *Soviet Physics*, 20:121–122, 1974.

[109] *NAG FORTRAN Library Manual.* Numerical Algorithms Group Ltd., mk12 vol.3 edition, March 1987.

[110] Leonard R.W. Simplified flow resistance measurements. *J. Acoust. Soc. Am.*, 17(3), 1946.

[111] Wall E.H. *Measurement of Air Permeability in Soils.* Master's thesis, Silsoe College, Cranfield Institute of Technology, Silsoe, Bedforshire, 1986.

[112] Stanton M.A. *Determination of Pore Continuity by a Measurement of Air Permeability.* Master's thesis, Silsoe College, Cranfield Institute of Technology, Silsoe, Bedforshire, 1985.

[113] Ball B.C., the late Harris W., and Burford J.R. A laboratory method to measure gas diffusion and flow in soil and other porous materials. *J.Soil Science*, 32:323–333, 1981.

[114] Meterological Results from Met. Office Data for Wrest Park, Silsoe, Bedfordshire.

[115] Chamen W.C.T., Cope R.E., Geikie A., and Stafford J.V. *A Long Term Experiment to Compare the Effect of Different Tyre/Soil Contact Pressures on Soil and Crop Responses when Growing Winter Wheat.* Departmental Note DN1263, National Institute of Agricultural Engineering, National Institute of Agricultural Engineering, Silsoe, Bedford, Feb 1985.

Symbols

a	phase constant
b	attenuation constant
d	layer thickness
f	frequency
i	$\sqrt{(-1)}$
J_n	Bessel function of nth order
K	permeability
K_a	intrinsic permeability
k_b	bulk propagation constant in the medium
k_o	bulk propagation constant in air
n'	grain shape factor
Npr	Prandtl number
T	tortuosity $= q^2 = \Omega^{-n'}$
sp	pore shape factor ratio
Z_c	normalised characteristic impedance
σ_{pe}	effective flow resistivity $= \sigma_e \Omega^2 = sp^2 \sigma \Omega$
σ_e	effective flow resistivity $= sp^2 \sigma / \Omega$
σ	flow resistivity mks rayls/m
Ω	volume porosity of connected air-filled pores
γ	ratio of specific heats
ρ_o	density of air
ρ_b	effective density of air in rigid porous medium
ρ_s	dry bulk density of soil
ρ_g	soil particle density
ρ_i	density of ice
ϕ^o	phase in degrees

Glossary

Absorption Coefficient the ratio of sound energy absorbed by a surface to the total sound energy which strikes it.

Acoustics the science of sound.

Acoustical relating to acoustics.

Amplitude the maximum value, the peak.

Anechoic almost totally sound-absorbent at a very wide range of frequencies. An anechoic chamber gives almost Free Field conditions.

Attenuation The difference between the sound level in (dB) measured (or predicted) at two points. In this case usually between microphones buried at different depths in soil or snow.

Audio Frequency a frequency within the audible range of about 20Hz to 20000Hz.

Band a segment of the frequency spectrum, eg. an octave or third octave.

Characteristic Impedance a measure of the qualities possessed by a substance carrying sound waves which indicates the ratio of the root mean square sound pressure level at a point to the rms particle velocity. It is equal to the product of the density ρ and the speed of sound in the substance c.

Decibel (dB) (One tenth of a Bel): A means of denoting the ratio of two quantities when the range of values is very great. A Bel can be described as the number of tenfold increases the lower quantity must be given to equal the higher ie $\log_{10}(i_1/i_2)$. Sound pressure is the commonest quantity expressed in decibels, in which case the lower quantity is usually $2 \times 10^{-5} Nm^{-2}$, known as the reference pressure.

Diffraction the diversion of the direction of travel of a wave other than by reflection or refraction.

Dry Bulk Density ρ_b The mass of dry soil per unit bulk volume of soil kgm^{-3}.

Echo reflected sound which arrives a long enough time after its direct equivalent to be heard as a separate sensation.

Excess Attenuation The difference between the sound level (in dB) measured (or predicted) at a certain location above a surface, minus that which would be expected at that location in the absence of any ground surface (known as the Free Field case).

Field region of acoustic interest.

Field Capacity The water content in a soil after ample irrigation of rainfall, when the rate of downward movement of water has substantially decreased, usually 1-3days after irrigation or rain. Water content at field capacity is expressed as a mass or volume fraction of soil water. It can also be defined in relation to moisture release curves as 0-0.2 bar.

Free Field a region in which no significant reflections of sound occur

Flow Resistance The ratio of the pressure gradient to the induced flow velocity across a given porous sample.

Flow Resistivity The flow resistance per unit length.

Frequency The number of times a vibrating system or particle completes a repetitive cycle or movement in a period of one second, expressed in Hertz or 'cycles per second'.

Gradient A variation of the local speed of sound with height above ground causing a refraction of sound. It is most commonly caused by rising or falling temperature with altitude or by differences in wind speed.

Hysteresis The relationship between matric potential and soil water content V_w for a given soil is not unique and varies depending on whether the soil is drying or weeting. This is due to hysteresis. The soil water content at a given suction is higher when the soil is drying than when it is wetting.

Impedance a measure of the complex ratio of force (or pressure) to velocity see also Characteristic Impedance.

Level Difference The difference between the sound level in (dB) measured (or predicted) at two vertically separated microphones above a ground surface.

Noise unwanted sound

Octave the interval between two sounds one of which has a frequency twice that of another.

Oscillation variation in the magnitude of a quantity above and below a certain level over a certain time (or distance).

Peak Sound Pressure Level the value in decibels of the maximum sound pressure level

Permanent Wilting Point The water content a soil reaches at a time when water extraction by plants has ceased. Based on the assumption that above 15bars suction, plants will wilt and not recover even when placed in a saturated atmosphere. It is an idealised concept which depends in reality on not only the soil but the plant and the weather. Neverthelass it is seen as a good approximation for most soils. The water content at permanent wilting point is expressed as a mass or volume fraction of the soil water.

Phase A measure of whether a sound or other periodic function is 'in step' or 'out of step'. It is measured as an angle in degrees or in radians. If, for example, one sine wave lags behind another so that it is always at its minimum while the other is at its maximum, it is π radians or 180^o out of phase.

Plane wave A wave in which the Wave Fronts are parallel with one another and at right angles to the direction of propagation.

Pure Tone A sound whose wave form is Sinusoidal.

Random Noise Strictly speaking, a fluctuating quantity (sound or electronic) whose amplitude distribution with time is Gaussian. Generally, noise due to random pressure or other fluctuations resulting in a continuous spectrum.

Refraction The bending of sound by passage from one medium to another or in a gradient.

Resonance When a system is vibrating as a result of a forced excitation at a certain frequency, if the amplitude of vibration deminishes as a result of raising or lowering the frequency of the exciting force then the system is in resonance.

Resonant Frequency A frequency at which resonance occurs.

Root Mean Square (rms) Value The values of a fluctuating quantity are squared, averaged and then the square root is extracted.

Sine Wave A wave which varies with time or distance as the trigonometric function, the sine.

Sinusoidal Varying as the sine of an angle

Soil Structure The aggregation of primary soil particles into units which are separated from each other by surfaces of weakness. An individual natural soil aggregate is called a ped in contrast to a clod caused by disturbance.

Sound Wave motion in an elastic medium, or the sensation of hearing this may produce.

Sound Pressure Level The rms (usually) values of the pressure fluctuations above and below atmospheric pressure caused by the passage of a sound wave, expressed in decibels re 2 x $10^{-5} Nm^{-2}$.

Sound Shadow The acoustical equivalent to a light shadow, usually partially penetrated as a result of diffraction.

Spherical Wave A wave in which the Wave Fronts form concentric spheres.

Wave A disturbance propagated in a medium

Wave Front A theoretical surface which is made up of points at which the phase of a wave is the same. In the case of a sine wave the wave front joins points of equal amplitude and phase.

Wavelength The perpendicular distance between two Wave Fronts in which the phases differ by one complete period. It is equal to the speed of sound divided by the frequency and is usually represented by λ.

White Noise Noise of a statistically random nature having equal energy at every frequency over a particular band.

Appendix A

FORTRAN program listings

A.1 DIF2VS

```
c       program dif2vs
c    Program to calculate field at two vertically separated microphones
c       in dB and the difference between them.

        character*20 ifile1,ifile2,ofile1,ofile2,infinp
        dimension df(400,4),dn(400,4),an(250),af(250),dbn(250),dbf(250)
        dimension diff(250),fr(250)
        common/head/idat(3),itim(3),sh,rh,sd,rmh,rmd,iav
        common/hed2/fsa,ga,amks,fsb,gb,bmks

        type*,'interactive or from data file? interactive =1'
        accept*,int
        if(int.eq.1)goto 10
        nin=10
        nout=9
        type*,'input filename containing input data'
        read(5,2)infinp
        open(unit=10,name=infinp,type='old')
        goto 15
10      nin=5
        nout=6
c
c       Read in data and put data required for analysis into arrays;
c        i.e.195 points-every other point from 50hz to 2kHz (10Hz apart)
c       or 190 points- every other point from 50Hz to 1KHz (5Hz apart)

15      write(nout,*)'first (top) microphone data filename?'
        read(nin,2)ifile1
        write(nout,*)'nicolet channel?  A=1  B=2'
        read(nin,*)ichn
c       write(nout,*)'sound level meter used? 1=old,2=new 0=none'
```

```
c       read(nin,*)islmn
        islmn=0
        call slmset(islmn,vrefn,attn,itrn,nin,nout)
        write(nout,*)'    '

25      write(nout,*)'second (bottom) microphone data filename?'
        read(nin,2)ifile2
        write(nout,*)'channel? A=1, B=2'
        read(nin,*)ichf
c       write(nout,*)'sound level meter used? 1=old,2=new  0=none'
c       read(nin,*)islmf
        islmf=0
        call slmset(islmf,vreff,attf,itrf,nin,nout)

        write(nout,*)'output file for dB difference?'
        read(nin,2)ofile1
        write(nout,*)'output file dB at microphones'
        read(nin,2)ofile2

2       format(a)

        write(nout,*)'frequency range of nicolet 1000Hz=1  2000Hz=2'
        read (nin,*)ifr

        if(ifr.eq.1)ii=190
        if(ifr.eq.2)ii=195
        open(unit=2,name=ifile1,type='old')
        open(unit=3,name=ofile1,type='new')
        open(unit=4,name=ofile2,type='new')

c       delete header blocks of easch data file by calling rddat then
c       reads in data for both the upper & lower mics.

        call rddat
        gainn=ga
        if(ichn.eq.2) gainn=gb
        read(2,40)((dn(j,k),k=1,4),j=1,400)
40      format(1x,4e10.3)
        close(unit=2)

        open (unit=2,name=ifile2,type='old')
        call rddat
        gainf=ga
        if(ichf.eq.2) gainf=gb
        read(2,50)((df(j,k),k=1,4),j=1,400)
50      format(1x,4e10.3)
        close(unit=2)
```

```
      if (ifr.eq.1)goto 80
c     set up arrays for top microphone data and frequencies 2000Hz.
      jk2=9
      freq=40.0
      do 45 k2=1,ii
      freq=freq+10
      jk2=jk2+2
      fr(k2)=freq
      an(k2)=dn(jk2,ichn)
45    continue
c     set up array for bottom microphone data up to 2000Hz
      jk3=9
      do 55 k3=1,ii
      jk3=jk3+2
      af(k3)=df(jk3,ichf)
55    continue
      goto 60
c     set up arrays for top microphone data up to 1000Hz
80    jk2=19
      freq=45.00
      do 70 k2=1,ii
      freq=freq+5.0
      jk2=jk2+2
      fr(k2)=freq
      an(k2)=dn(jk2,ichn)
70    continue
c     set up array for lower microphone up to 1KHz range
      jk3=19
      do 75 k3=1,ii
      jk3=jk3+2
      af(k3)=df(jk3,ichf)
75    continue

cc    Use data to calculate field at microphones first adjusting
c        data for gain of tape recorder and S.L.M.

60    do 200 j=1,ii

      fre=fr(j)

c     Adjust for gain on nagra tape recorder.
       an(j)=an(j)*gainn/141.421
       af(j)=af(j)*gainf/141.421

c     convert from volts to dB
      dbn(j)=attn+20*alog10(an(j)/vrefn)
```

```
        dbf(j)=attf+20*alog10(af(j)/vreff)
        diff(j)=dbn(j)-dbf(j)

90      write(3,100)alog10(fre),diff(j)
100     format(1x,2f12.6)
        write(4,150)alog10(fre),dbn(j),dbf(j)
150     format(1x,3f12.6)
200     continue
        stop
        end


        subroutine slmset(islm,vref,att,itr,nin,nout)
        itr=1
        write(nout,*)'tape recorder output voltage of calibration tone?'
        read(nin,*)vo
        if(itr.eq.0) goto 10
        write(nout,*)'at tape attenuator setting?'
        read(nin,*)tatt
        gain=10**(tatt/20.)
        vi=vo*gain/141.421
10      if(itr.eq.0)vi=vo
        vref=vi/(10**0.2)
        if(islm.eq.2) goto 310
        if(islm.eq.0)goto 320
        write(nout,*)' slm attenuator setting for measurement?'
        read(nin,*)att
        return
310     write(nout,*)'slm scale used for measurement?'
        write(nout,*)'   lower  - 25 to 105 = 1'
        write(nout,*)'   middle - 45 to 125 = 2'
        write(nout,*)'   upper  - 65 to 145 = 3'
        read(nin,*)att
        if(att.eq.1) vref=vref*100.
        if(att.eq.2) vref=vref*10.
        att=120
        return
320     continue
        att=120
        return
        end
```

A.2 CAL

```
c Program CAL to transfer data from the Zenith format to noraml.
      dimension freq(401),difmag(401),phase(401)
      character*80 dummy,input,output
```

```
      parameter (factor=57.296)
1     print*, ' What is the name of input file'
      read(*,'(a)')input
      print*, ' What is the name of output file?'
      read(*,'(a)')output
      print*,' What is the calibration constant?'
      read(*,*)const
      open(2,status='new',file=output)
      open(3,status='old',file=input)
      read(3,'(a)')dummy
      read(3,'(a)')dummy
      print*,' Total points, no. of points to be discarded at beginning'
      print*,' and spacing points required?'
      read(*,*)npoint,ndisca,nspace
      np1 = ndisca + 1
      do 10 i = 1, npoint
10    read(3,*)freq(i),difmag(i),phase(i)
      do 20 j = np1, npoint, nspace
20    write(2,'(1p3e15.4)')alog10(freq(j)),difmag(j)+const,
     *                     phase(j)*factor
      close(2)
      close(3)
      print*, ' Do you want another set (0/1)?'
      read(*,*)ians
      if (ians .eq. 1)goto 1
      stop
      end
```

A.3 OSABCALC

```
c     program OSABCALC
c     hmhess 13/11/87

      dimension freq(200),zdf(200),zdn(200),rdf(200),rdn(200)
      dimension atten(200),phasex(200),phase(200),phase2(200),sigmape(200)
      dimension t(200)
      complex*8 kb,kb2
      real*16 t1,cc,dd,ee,xx,ff
      character*20 ifile1,ifile2,ofile1,ofile2
      pi=3.141592653
      co=344.0
      rho=1.2
      gamma=1.4

      type*,'interactive or from data file?  interactive = 1'
      accept*,int
      if(int.eq.1)goto 10
```

```
      nin=10
      nout=9
      type*,'input filename containing input data'
      read(5,2)infinp
      open(unit=10,name=infinp,type='old')
      goto 15
10    nin=5
      nout=6
2     format(a)
15    write(nout,*)'deepest probe normalised TF data filename?'
      read(nin,2)ifile1
      write(nout,*)'shallow probe normalised TF data filename?'
      read(nin,2)ifile2
      write(nout,*)'no. of column(s) and data points?'
      read(nin,*)icoldat,ipoint
      write(nout,*)'output format required?'
      write(nout,*)'ioput=1,freq mag,phase of ntf'
      write(nout,*)'ioutp=2,freq,a,b,sigmape,t plus average values sig
& t'
      read(nin,*)ioutp
77    write(nout,*)'output file name?'
      read(nin,2)ofile1
      if(ioutp.eq.1)goto 17
      write(nout,*)'output file for sigmape and t averages'
      read(nin,2)ofile2
17    write(nout,*)'diff.in depth in metres between the two probes'
      read(nin,*)d
      write(nout,*)'low freq. or high freq. model? high=1'
      read(nin,*)hilo
34    open(unit=2,name=ifile1,type='old')
      open(unit=3,name=ifile2,type='old')
      open(unit=4,name=ofile1,type='new')
      if(ioutp.eq.1)goto 35
      open(unit=9,name=ofile2,type='new')
35    tott=0.0
      totsig=0.0
      icount=0.0
      icount2=0.0
      do 300 j=1,ipoint
      read(2,40)freq(j),zdf(j),rdf(j)
      read(3,40)freq(j),zdn(j),rdn(j)
40    format(1p3e15.4)
      atten(j)=zdf(j)-zdn(j)
      phase(j)=rdf(j)-rdn(j)
c     to account for every flip of phase.
      diff=phase(j)-phase(j-1)
      if(diff.le.-120.0)k=k+1
```

```
      if(diff.ge.120.0)k=k-1
      phasex(j)=phase(j)+(360.0*k)
      phase2(j)=sqrt(phasex(j)*phasex(j))
c     calc of real a and imag b of prop constant
      b=(atten(j)*alog(10.0))/(20.0*d)
      b=sqrt(b*b)
      a=(pi*phase2(j))/(180.0*d)
      a=sqrt(a*a)
      fr=10**freq(j)
      kb=cmplx(a,b)
      kb2=kb*kb
      if(hilo.eq.1)goto 99
c     low freq/high flow res. model for soils
      t(j)=real(kb2)/(6.241e-05*8.14*fr*fr)
      sigmape(j)=Aimag(kb2)/(6.241e-05*4.0*fr)
      goto 98
99    t1=(2*pi*fr)/co
c     high freq. model
      cc=(gamma-1)/sqrt(0.76)
      type*,'cc=',cc
      dd=real(kb2)/aimag(kb2)
      ee=(dd-1)+cc*(dd+1)
      xx=(-ee+sqrt(ee*ee+8*cc))/(4*cc)
      ff=1-(2*cc*xx)+2*(cc**2)*(xx**2)
      t(j)=(ff*aimag(kb2))/((1+cc)*xx*(t1**2))
      sigmape(j)=2*pi*fr*xx**2*t(j)*rho
98    if(t(j).gt.0)goto 275
      tott=tott+0.0
      totsig=totsig+0.0
      icount=icount
      goto 276
275   tott=tott+t(j)
      totsig=totsig+sigmape(j)
      icount=icount+1
c     write data to files
276   if(ioutp.eq.2)goto 120
100   write(4,40)freq(j),atten(j),phase2(j)
      goto 300
120   write(4,121)freq(j),a,b,sigmape(j),t(j)
121   format (1x,3f10.4,1x,1pe11.4,x,1pe11.4)
300   continue
      if(ioutp.eq.1)goto 600
      totsig=totsig/icount
      tott=tott/icount
      write(9,*)'******  ******* ******** *******'
      write(9,*)'average sigmape     =',totsig
      write(9,*)'average t           =',tott
```

```
600     stop
        end
```

A.4 PROPAB1

```
c    program PROPAB1
c    program to calculate transfer functions from two data files,(edited
c    nicolet data) and calculate an equalised transfer function
c    and to calculated the real and imaginary part of the propogation
c    constant ie.a and b and sigmape and T
c     hmhess5/2/88

        common/head/idat(3),itim(3),sh,rh,sd,rmh,rmd,iav
        common/hed2/fsa,ga,amks,fsb,gb,bmks
        character*20 ifile1
        character*20 ifile2
        character*20 ofile
        character*20 ofile2
        dimension eqphs2(200),eqphs(200),sigmape(200),T(200),eqphsx(200)
        complex tfeq,tf1,tf2,kb,kb2
        pi=3.141592653

c  choose and open input and output files.
        type*,'interactive or from data file? int=1'
        accept*,int
        if(int.eq.1)goto 10
        nin=10
        nout=9
        open(unit=10,name='propin.dat',type='old')
        goto 15
10      nin=5
        nout=6
15      write(nout,*)'inputfile 1 ?'
        read(nin,2) ifile1
        write(nout,*)'inputfile 2 ?'
        read(nin,2) ifile2
        write(nout,*)'output file?'
        read(nin,2) ofile
c       type*,'do you require average values of sigmape and t y=1 '
c       read(nin,2)iav
c       if(iav.eq.0)goto 17
        write(nout,*)'output file for averages?'
        read(nin,2)ofile2
17      write(nout,*)'whats the diff. in depth between the two probes
     *  in metres'
        read(nin,*)dd
        write(nout,*)'difference in db gain between the surface & buried
```

```
mics as
     *  indicated on the measuring amps ie +70dB-+60dB=+10dB'
        read(nin,*)corr
        write(nout,*)'frequency range of nicolet'
        write(nout,*)'                500Hz=1'
        write(nout,*)'               1000Hz=2'
        write(nout,*)'               2000Hz=3'
        write(nout,*)'               5000Hz=4'
        write(nout,*)'              10000Hz=5'
        read(nin,*)ifr
c  set output required.
c  ioutp=1    writes the frequency and the magnitude and phase of the
c              two transfer functions. NB in volts not dBs.
c  ioutp=2    writes frequency and the magnitude and phase of the
c             equalised transfer function. in dBs
c  ioutp=3    writes the frequency and real and imaginary parts of the
c             propagation constant ie. a and b and sigmape and T.
        write(nout,*)'output format required'
        write(nout,*)'ioutp=1  Freq.,mag.& phase of the two TFs'
        write(nout,*)'ioutp=2  Freq.,mag.& phase of EQ TF.'
        write(nout,*)'ioutp=3  Freq.,real(a) & imag(b),sigmape,T'
        read(nin,*)ioutp
2       format(a)
        open(unit=1,name=ifile1,type='old')
        open(unit=2,name=ifile2,type='old')
        open(unit=3,name=ofile,type='new')
        open(unit=4,name=ofile2,type='new')
c       delete header blocks by calling rddat
        call rddat2(1)
        call rddat2(2)

        freq=100.0
        if(ifr.eq.1)ii=39  !all these
        if(ifr.eq.2)ii=39  !changed to start at 100Hz
        if(ifr.eq.3)ii=9   !others start at
        if(ifr.eq.4)ii=7  !changed to start at 100hz
        if(ifr.eq.5)ii=1   !50Hz
        do 50 j=1,ii
        read(1,3)a,b,c,d
        read(2,3)e,f,g,h
50      continue

        if(ifr.eq.1)ij=181
        if(ifr.eq.2)ij=157
        if(ifr.eq.3)ij=195
        if(ifr.eq.4)ij=157   !changed 5/2/88 to start at 100Hz
        if(ifr.eq.5)ij=199
```

```
        tott=0.0
        totsig=0.0
        icount=0

        do 150 i=1,ij

c read data and calculate two transfer functions.

        read(1,3)a,b,c,d
        read(1,3) amag1,bmag1,coh1,quad1
c       type*, amag1,bmag1,coh1,quad1
        read(2,3)e,f,g,h
        read(2,3) amag2,bmag2,coh2,quad2
c       type*, amag2,bmag2,coh2,quad2
3       format(1x,4e10.3)
        pmag1=amag1*amag1
        pmag2=amag2*amag2
        rtf1=coh1/pmag1
        rtf2=coh2/pmag2
        atf1=quad1/pmag1
        atf2=quad2/pmag2
        tf1=cmplx(rtf1,atf1)
        tf2=cmplx(rtf2,atf2)
        tfeq=tf2/tf1
        rtfeq=real(tfeq)
        atfeq=aimag(tfeq)
        tmag1=sqrt(coh1*coh1+quad1*quad1)/pmag1
        tmag2=sqrt(coh2*coh2+quad2*quad2)/pmag2
        phase1=atan2(quad1,coh1)
        phase2=atan2(quad2,coh2)
c
c  equalise the two transfer functions.
c
        eqmag=tmag2/tmag1
c       puts eqmag into dB
        eqmag=20*alog10(eqmag)
        eqmag=eqmag+corr
        eqphs(i)=phase2-phase1
c       puts phase from radians into degrees
        eqphs(i)=eqphs(i)*57.29578

c       to account for every flip of phase
        diff=eqphs(i)-eqphs(i-1)
        if(diff.le.-340.0)k=k+1
        if(diff.ge.340.0)k=k-1
        eqphsx(i)=eqphs(i)+(360*k)
```

```
      eqphs2(i)=sqrt(eqphsx(i)*eqphsx(i))

c     calculate the imag value of the propogation constant in dB/m.
      b=(eqmag*alog(10.0))/(20.0*dd)
      b=sqrt(b*b)
c     calculates the real part of the propagation constant
c     this converts degrees back to radians per metre.
      a=(pi*eqphs2(i))/(180.0*dd)
      a=sqrt(a*a)
      kb=cmplx(a,b)
      kb2=kb*kb
      T(i)=Real(kb2)/(6.241E-05*8.14*freq*freq)
      sigmape(i)=Aimag(kb2)/(6.241E-05*4.0*freq)
      if(t(i).gt.0)goto 275
      tott=tott+0.0
      totsig=totsig+0.0
      icount=icount
      goto 276
275   totsig=totsig+sigmape(i)
      tott=tott+t(i)
      icount=icount+1
276   fr=alog10(freq)
      if(ioutp.eq.1) goto110
      if(ioutp.eq.2) goto 120
      if(ioutp.eq.3) goto 130
110   write(3,111) fr,tmag1,phase1,tmag2,phase2
111   format(1x,5f12.5)
      goto 140
120   write(3,121) fr,eqmag,eqphs2(i)
121   format(1x,5f12.5)
      goto 140
130   write(3,131) fr,a,b,sigmape(i),T(i)
131   format(1x,3f10.4,1x,1pe11.4,x,1pe11.4)
140   if(ifr.eq.1)crem=2.5
      if(ifr.eq.2)crem=5.0
      if(ifr.eq.3)crem=10.0
      if(ifr.eq.4)crem=25.0
      if(ifr.eq.5)crem=50.0
      freq=freq+crem
150   continue
c     if(iav.eq.0)goto 200
      totsig=totsig/icount
      tott=tott/icount
      write(4,*) ' --*--*---*-----*----*---*--*--'
      write(4,*) 'average sigmape = ',totsig
      write(4,*) 'average T  = ',tott
200   stop
```

```
      end
c  read header block from data files

      subroutine rddat2(ichi)
      common/head/idat(3),itim(3),sh,rh,sd,rmh,rmd,iav
      common/hed2/fsa,ga,amks,fsb,gb,bmks
c  read scaling data

      read(ichi,100)(idat(j),j=1,3)
      read(ichi,100)(itim(j),j=1,3)
  100 format(1x,3i6)
      read(ichi,101)sh,rh,sd,rmh,rmd
  101 format(1x,5f12.6)
      read(ichi,102)iav
  102 format(4x,i3)
      read(ichi,103)fsa,ga,amks
      read(ichi,103)fsb,gb,bmks
  103 format(1x,3f12.6)
      return
      end
```

A.5 NTFCALC

```
c     program NTFCALC
c     hmhess 21/10/87

      character*20 ifile1,IFILE2,ofile1,infinp
      complex dn,df,tf
      pi=3.141592653

      type*,'interactive or from data file?  interactive = 1'
      accept*,int
      if(int.eq.1)goto 10
      nin=10
      nout=9
      type*,'input filename containing input data'
      read(5,2)infinp
      open(unit=10,name=infinp,type='old')
      goto 15
10    nin=5
      nout=6
2     format(a)
15    write(nout,*)'deepest probe normalised TF data filename?'
      read(nin,2)ifile1
      write(nout,*)'shallow probe normalised TF data filename?'
      read(nin,2)ifile2
      write(nout,*)'no. of column(s) and data points?'
```

```
      read(nin,*)icoldat,ipoint

77    write(nout,*)'output file name?'
      read(nin,2)ofile1
34    open(unit=2,name=ifile1,type='old')
      open(unit=3,name=ifile2,type='old')
      open(unit=4,name=ofile1,type='new')

      do 300 j=1,ipoint
      read(2,40)freq(j),dn
      read(3,40)freq(j),df
40    format(1p3e15.4)
      tf=(dn/df)
c     write data to files

100   write(4,110)freq(j)tf
110   format(1x,e13.6,1x,e13.6,1x,e13.6)

300   continue
      stop
      end
```

A.6 COPY5

```
c     program MTU_prb_manip5.for
c     program to manipulate the  michigan snow data
c     extended reaction and high freq/low flow res. approx.
c     hmhess 12/8/87

      character*20 ifile1,ofile1,infinp,ofile2
      dimension atten(400),phase(400)
      dimension sigmape(400),T(400),phase2(400),PHASEX(400)
      real*16 r,p,q,t1,cc,dd,ee,xx,ff
      complex*8 kb,kb2
      pi=3.141592653
      co=328.3
      rho=1.317
      gamma=1.4

      type*,'interactive or from data file?  interactive = 1'
      accept*,int
      if(int.eq.1)goto 10
      nin=10
      nout=9
      type*,'input filename containing input data'
      read(5,2)infinp
```

```
      open(unit=10,name=infinp,type='old')
      goto 15
10    nin=5
      nout=6
15    write(nout,*)'probe normalised TF data filename?'
      read(nin,2)ifile1
      write(nout,*)'no. of column(s) and data points?'
      read(nin,*)icoldat,ipoint

      write(nout,*)'output format required'
      write(nout,*)'ioutput=1 freq,mag and phase of NTF'
      write(nout,*)'ioutput=2 freq,a,b,sigmape and T'
      read(nin,*)ioutp

77    write(nout,*)'output file name?'
      read(nin,2)ofile1
      if(ioutp.eq.1)goto 17

      write(nout,*)'output file for sigmape and T averages'
      read(nin,2)ofile2

17    write(nout,*)'whats the diff in depth btwn two probes in metres'
      read(nin,*)depth

      write(nout,*)'whats the height of the source in metres?'
      read(nin,*)hst

      write(nout,*)'distance from probes to speaker'
      read(nin,*)rs

c     high freq approx only looks at data above 1khz

2     format(a)
54    write(nout,*)'frequency range of analyzer'
      write(nout,*)'                          2000Hz=3'
      write(nout,*)'                          5000Hz=4'
      write(nout,*)'analysed up to 5kHz but studied up to 4KHz=5'
      write(nout,*)'   "      "  "  "    "     "    "  "  2kHz=6'
      read(nin,*)ifr

34    open(unit=2,name=ifile1,type='old')
      open(unit=3,name=ofile1,type='new')
      if(ioutp.eq.1)goto 35
      open (unit=4,name=ofile2,type='new')
35    freq=1000.0
      if(ifr.ge.4)ii=160
```

```
      do 36 i=1,ii
      read(2,40)c,d
36    continue

c     if(ifr.eq.3)ij=380
      if(ifr.eq.4)ij=316
      if(ifr.eq.5)ij=246
      if(ifr.eq.6)ij=83
      tott=0.0
      totsig=0.0
      icount=0
      do 300 j=1,ij

c     dummy line to read in every other line

      read(2,40)e,v
      read(2,40)dn,df
40    format(e13.6,e13.6)
c     calc phase and magnitude of the propagation constant

      phase(j)=ATAN2(df,dn)
c     puts phase from radians into degrees
      phase(j)=phase(j)*57.29578

      atten(j)=sqrt(df*df+dn*dn)
      atten(j)=20*alog10(atten(j))
      atten(j)=sqrt(atten(j)*atten(j))

c     to account for every shift in phase
      if(phase(j-1).eq.0.00)k=0.0
      if(phase(j-1).eq.0.0)goto777
      diff=phase(j)-phase(j-1)
      if(diff.le.-120.0)k=k-1
      if(diff.ge.120.0)k=k+1
777   PHASEX(J)=PHASE(J)-(360.0*K)
      phase2(j)=sqrt(phaseX(j)*phaseX(j))

c
c     calc to account for extended reaction
c     based on ' Richards,Attenborough,Heap and Watson
c     eqns 26 & 27
c     0.97 = sin(theta)**2
c     where atan(theta)=hst/distance of probe to speaker rs
c     sin**2(theta) will vary with changes in geometry
c     adjustment for electrovoice speaker height with 3k cross over

      if(freq.lt.1500)goto 400
```

```
        hs=hst-0.2
c       hs=hst+0.2
        goto 401
400     hs=hst
401     theta=rs/hs
        theta=atan(theta)
        sthe=(sin(theta))**2

c       calculation of real a and imag b parts of prop constant
c       taking into account extended reaction

        G=(atten(j)*alog(10.0))/(20.0*depth)
        F=(pi*phase2(j))/(180*depth)
        t1=(2*pi*freq)/co
        p=f**2-g**2+(t1**2*sthe)
        q=g**2*f**2
        r=0.5*(p+sqrt(p**2+(4*q)))
        a=sqrt(r)
        b=(g*f)/a

555     kb=cmplx(a,b)
31      format(x,e10.4,x,e10.4)
        kb2=kb*kb

c       calculation of t and sigma pe using high freq/low flow res
        cc=(gamma-1)/sqrt(0.76)
        dd=real(kb2)/aimag(kb2)
        ee=(dd-1)+cc*(dd+1)
        xx=(-ee+sqrt(ee*ee+8*cc))/(4*cc)
        ff=1-(2*cc*xx)+2*(cc**2)*(xx**2)
        t(j)=(ff*aimag(kb2))/((1+cc)*xx*(t1**2))
        sigmape(j)=2*pi*freq*xx**2*t(j)*rho

701     totsig=totsig+sigmape(j)
        tott=tott+T(j)
        icount=icount+1
        fr=alog10(freq)

        if(ioutp.eq.2)goto 120



100     write(3,110)fr,atten(j),phase2(j)
110     format(1x,3f12.6)
119     goto 122

120     write(3,121)fr,a,b,sigmape(j),T(j)
```

```
121     format(1x,3f10.4,1x,1PE11.4,x,1PE11.4)

122     if(ifr.eq.2)crem=2.5
        if(ifr.eq.3)crem=5.0
        if(ifr.ge.4)crem=12.25

        freq=freq+crem
300     continue
        if(ioutp.eq.1)goto 600
        totsig=totsig/icount
        tott=tott/icount

        write(4,*)' *****     ******     ******     *******    ******'
        write(4,*)'average sigmape       =',totsig
        write(4,*)'average T             =',tott

600     stop
        end
```

A.7 COPY6

```
c       program copy6.for
c       program to manipulate the  michigan  data
c       includes local and extended reaction and calc.a and b from
c       the low freq/high flow res. eqn 6 in memo.
c       and to account for soils ie 344 instead of 328 for snow.
c       NB the value in the equation for T also changes for soil and snow
due
c       to a diiferent value of rho0 (1.2 for soils) (1.317 for snow)
c       this makes the change form 8.14 to 9.10 in the T equation.
c       hmhess 8/2/88

        character*20 ifile1,ofile1,infinp,ofile2
        dimension atten(400),phase(400)
        dimension sigmape(400),T(400),phase2(400),phasex(400)
        real*16 r,p,q,t1,cc,dd,ee,ff,xx
        complex kb,kb2
        pi=3.141592653
c       co=344.0
        co=328.4
        type*,'interactive or from data file?  interactive = 1'
        accept*,int
        if(int.eq.1)goto 10
        nin=10
        nout=9
        type*,'input filename containing input data'
```

```
        read(5,2)infinp
        open(unit=10,name=infinp,type='old')
        goto 15
10      nin=5
        nout=6

15      write(nout,*)'probe normalised TF data filename?'
        read(nin,2)ifile1
        write(nout,*)'no. of column(s) and data points?'
        read(nin,*)icoldat,ipoint

        write(nout,*)'output format required'
        write(nout,*)'ioutput=1 freq,mag and phase of NTF'
        write(nout,*)'ioutput=2 freq,a,b,sigmape and T'
        read(nin,*)ioutp

        write(nout,*)'local=1 or extended=2 reaction model?'
        read(nin,*)loex

77      write(nout,*)'output file name?'
        read(nin,2)ofile1
        if(ioutp.eq.1)goto 17

        write(nout,*)'output file for sigmape and T averages'
        read(nin,2)ofile2

17      write(nout,*)'whats the diff in depth btwn two probes in metres'
        read(nin,*)dd

        write(nout,*)'whats the height of the source in metres'
        read(nin,*)hst

        write(nout,*)'distance from probes to speaker'
        read(nin,*)rs

2       format(a)
54      write(nout,*)'frequency range of analyzer'
        write(nout,*)'                          1000Hz=2'
        write(nout,*)'                         2000Hz=3'
        write(nout,*)'                         5000Hz=4'
        write(nout,*)'analysed up to 5kHz but studied up to 4KHz=5'
        write(nout,*)'   "      " " "    "     "   " " 2kHz=6'
        write(nout,*)'analysed up to 5kHz but studied up to 1kHz=7'
        read(nin,*)ifr

34      open(unit=2,name=ifile1,type='old')
        open(unit=3,name=ofile1,type='new')
```

```
      if(ioutp.eq.1)goto 35
      open (unit=4,name=ofile2,type='new')

35    freq=100.0

      if(ifr.eq.2)ii=79
      if(ifr.eq.3)ii=39
      if(ifr.ge.4)ii=15
c     if(ifr.ge.4)ii=30
      do 36 i=1,ii
      read(2,40)c,d
36    continue

      if(ifr.eq.2)ij=360
      if(ifr.eq.3)ij=380
      if(ifr.eq.4)ij=392
      if(ifr.eq.5)ij=319
      if(ifr.eq.6)ij=159
c     if(ifr.eq.7)ij=60
      if(ifr.eq.7)ij=75
      tott=0.0
      totsig=0.0
      icount=0

      do 300 j=1,ij

c     dummy line to read in every other line
      read(2,40)e,v
      read(2,40)dn,df
40    format(e13.6,e13.6)

c     calc phase and magnitude of the propagation constant

      phase(j)=ATAN2(df,dn)
c     puts phase from radians into degrees
      phase(j)=phase(j)*57.29578

      atten(j)=sqrt(df*df+dn*dn)
      atten(j)=20*alog10(atten(j))
      atten(j)=sqrt(atten(j)*atten(j))

c     to account for every shift in phase
      if(phase(j-1).eq.0.0)k=0.0
      if(phase(j-1).eq.0.0)goto777
      diff=phase(j)-phase(j-1)
      if(diff.le.-120.0)k=k-1
      if(diff.ge.120.0)k=k+1
```

```
777     phasex(j)=phase(j)-(360.0*k)
        phase2(j)=sqrt(phasex(j)*phasex(j))
        if(loex.eq.1)goto 222
c
c       calc to account for extended reaction
c       based on  Richards,Attenborough,Heap and Watson
c       eqns 26 & 27
c       where tan(theta)=hs/distance of probe to speaker
c       sin**2(theta) will vary with changes in geometry
c       adjustment for electrovoice speaker height with 3k
c       crossover

        if(freq.lt.1500)goto 400
        hs=hst-0.2
c       hs=hst+0.2
        goto 401
400     hs=hst
401     theta=rs/hs
        theta=atan(theta)
        sthe=(sin(theta))**2


        G=(atten(j)*alog(10.0))/(20.0*dd)
        F=(pi*phase2(j))/(180*dd)
        t1=(2*pi*freq)/co
        p=f**2-g**2+(t1**2*sthe)
        q=g**2*f**2
        r=0.5*(p+sqrt(p**2+(4*q)))
        a=sqrt(r)
        b=(g*f)/a

        goto 555

c       calculate the imaginary value of prop.constant in dB/m
222     b=(atten(j)*alog(10.0))/(20.0*dd)
        b=sqrt(b*b)
c       calculate the phase of prop constant
c       this converts degrees back to radians per metre
        a=(pi*phase2(j))/(180*dd)
        a=sqrt(a*a)

555     kb=cmplx(a,b)
31      format(x,e10.4,x,e10.4)
        kb2=kb*kb

c       low frequency approximation for snow
        T(j)=Real(kb2)/(6.241E-05*9.10*freq*freq)
```

```
c       low frequency approximation for soils
c       T(j)=Real(kb2)/(6.241E-05*8.14*freq*freq)
        sigmape(j)=Aimag(kb2)/(6.241E-05*4.0*freq)

        totsig=totsig+sigmape(j)
        tott=tott+T(j)
        icount=icount+1

        fr=alog10(freq)

c       write data to files

        if(ioutp.eq.2)goto 120

100     write(3,110)fr,atten(j),phase2(j)
110     format(1x,3f12.6)
119     goto 122

120     write(3,121)fr,a,b,sigmape(j),T(j)
121     format(1x,3f10.4,1x,1PE11.4,x,1PE11.4)

122     if(ifr.eq.2)crem=2.5
        if(ifr.eq.3)crem=5.0
        if(ifr.ge.4)crem=12.25

        freq=freq+crem
300     continue
        if(ioutp.eq.1)goto 600
        totsig=totsig/icount
        tott=tott/icount

        write(4,*)' *****     ******     ******     *******    ******'
        write(4,*)'average sigmape       =',totsig
        write(4,*)'average T             =',tott

600     stop
        end
```

A.8 LDFIT

```
c
c driver propram to calculate apparent flow resistivity, porosity and
c tortuosity by means of least  squares fit. nag routine e04ajf is used.
c to run this fitting routine after compiling this program, type
c link ldfit,range,error,sys$naglib/lib
c
      implicit real*8(a-h,o-z)
```

```
      real*8 k0
      character*35 ifile2,ifile3
      real hs,hrb,hrt,r,v0,freq1,freq2,freqt,ddata1,ddata2,ddata3,
     *     tort1,tort2,poro1,poro2
      dimension freq(405),rtfreq(405),k0(405),c4pik0(405),diff(405)
      dimension xc(3),fvecc(405),pred(405),w(39),iw(5),bl(3),bu(3)
      common /given/hs,hrb,hrt,r,v0
      common /const/pi,pi2,rtpi,factor,rho0,rho0v0,term
      common /data/freq,rtfreq,k0,c4pik0,diff,pred,fact1,fact2
      common /ndata/m,iext
      ibound=0
      lw=39
      liw=5
      n=3
      factor=1.0
      gamma=1.4d0
      pi=3.1415926d0
      pi2=2.0d0*pi
      rtpi=dsqrt(pi)
      pi4=4.0d0*pi
      print*,'*********************************************************'
      print*,'*         interactive fitting routine for               *'
      print*,'*              the determinaton of                      *'
      print*,'*       apparent flow resistivity, porosity            *'
      print*,'*              and   Tortuosity                         *'
      print*,'*           Optional choices of using                   *'
      print*,'* (i)  locally reacting or extended reaction surfaces *'
      print*,'* (ii) snow or soil                                     *'
      print*,'*********************************************************'
      print*
1     print *,' name of the input file?'
      read(*,999)ifile2
      print*, ' do you want to save the predicted data (0/1)'
      read(*,*)ians
      if(ians .eq. 1) then
       write(*,*)' name of the output file?'
       read(*,999)ifile3
       open(unit = 3, file =ifile3,status='new')
      endif
      open(unit = 2, file =ifile2,status='old')
      print *, 'input hs, and r !'
      read(*,*)hs,r
3     print *, 'input height of bottom and top mics !'
      read(*,*)hrb,hrt
      if(hrt .le. hrb)goto 3
10    print *, 'input the minimun and maximun values of sigma'
      read(*,*)sigma1,sigma2
```

```
      if(sigma1 .lt. 0.0 .or. sigma1 .ge. sigma2)then
       type *, ' incorrect specification of sigma'
       goto 10
      endif
12    print *, 'input the minimun and maximun Tortuosity'
      read(*,*)tort1,tort2
      if(tort1 .lt. 0.0 .or. tort1 .ge. tort2)then
       type *, ' incorrect specification of Tortuosity'
       goto 12
      endif
13    print *, 'input the minimun and maximun porosity'
      read(*,*)poro1,poro2
      if(poro1 .lt. 0.01 .or. poro1 .ge. poro2 .or.
     *   poro2 .gt. 1.0)then
       type *, ' incorrect specification of porosity'
       goto 13
      endif
14    print *, 'What is the starting value for porosity?'
      read(*,*)poros
      if((poro2-poros)*(poros-poro1) .lt. 0.0)goto 14
15    print *, 'input the minimun and maximun frequencies'
      read(*,*)freq1,freq2
      if(freq1 .lt. 0.0 .or. freq1 .ge. freq2)then
       type *, ' incorrect specification of Frequency'
       goto 15
      endif
17    print *, ' What type of surfaces are you using?'
      print *, ' 1 : locally reacting'
      print *, ' 2 : extended reaction'
      read(*,*)iext
      if(iext .lt. 1 .or. iext .gt. 2)goto 17
18    print *, ' What type of grounds are you using?'
      print *, ' 1 : snow'
      print *, ' 2 : soil'
      read(*,*)igrd
      if(igrd .eq. 1)then
       rho0=1.317d0
       v0=328.0
      else if(igrd .eq. 2)then
       rho0=1.2d0
       v0=343.0
      else
       goto 18
      endif
      rho0v0=rho0*v0
      pi2v0=pi2/v0
19    print *, ' What constant values are you using?'
```

```
      print *, ' 1 : term = 9.10d0 (snow)'
      print *, ' 2 : term = 8.29d0 (soil)'
      read(*,*)iconst
      if(iconst .eq. 1)then
       term = 9.10d0
      elseif(iconst .eq. 2)then
       term = 8.29d0
      else
       goto 19
      endif
      xc(1)=0.5*(sigma1+sigma2)/sigma2
      bl(1)=sigma1/sigma2
      bu(1)=1.0
      fact1 = 4.0d0*sigma2
      xc(2)=0.5*(tort1+tort2)/tort2
      bl(2)=tort1/tort2
      bu(2)=1.0
      fact2 = tort2
      xc(3)=poros
      bl(3)=poro1
      bu(3)=poro2
      i = 0
20    continue
      read(2,*,end=25)ddata1,ddata2,ddata3
      freqt=10.0**ddata1
      if((freqt-freq1)*(freqt-freq2) .gt. 0)goto 20
      i = i + 1
      diff(i) = dble(ddata2)
      freq(i) = dble(freqt)
      rtfreq(i) = dsqrt(freq(i))
      k0(i)=pi2v0*freq(i)
      c4pik0(i)=pi4*k0(i)
      goto 20
25    m = i
      close(unit=2)
      call funct1(n,xc,fc)
      sum = fc
      factor=dsqrt(sum)
30    ifail=1
      call e04jaf(n,ibound,bl,bu,xc,fsumsq,iw,liw,w,lw,ifail)
      if(ifail .eq. 2)then
       print *,' ifail =',ifail
       goto 30
      endif
      sigma=sigma2*xc(1)
      tort=tort2*xc(2)
      print *,' ifail      =',ifail
```

```
      print *,' sigma      =',sigma
      print *,' tortuosity =',tort
      print *,' porosity   =',xc(3)
      print *,' RMS error  =',dsqrt(fsumsq*sum/m)
      call funct1(n,xc,fc)
      if(ians.eq.1)write(3,'(1p2e15.4)')(dlog10(freq(i)),pred(i),i=1,m)
      print *,' do you want another one (0/1)?'
      read(*,*)icon
      if(icon .eq. 0)stop
      if(ians .eq. 1)close(unit=3)
      goto 1
999   format(a)
      end
c (rev. 1 9/9/87  by   k m li)
c subroutine funct1(n,xc,fc)
c this subroutine is used to determine the ground parameters, alpha and
c sigma, by the method of least squares fit. this subroutine is requested
c by the nag routine e04fdf.
c m  : no. of experimental points.
c n  : no of parameters (it is 2 in this case).
c xc : unknown parameters, where xc(1) = sigma, xc(2) = Tortuosity and
c                                xc(3) = porosity.
c fc : sum of differences between the predicted and experimental values.
c
c the source-observer geometry is passed through the common steatement
-
c 'given'. some other constant parameters are passed via 'const', 'data'
c and 'ndata' respectively.
c freq   : frequency of the received signals,
c k0     : wave numbers of the received signals,
c diff   : level difference of two microphones at heights hr1 and hr2
c          respectively,
c pred   : predicted level difference and
c factor : scaling factor for efficient use of the nag routine. it is
the
c          sum of squares of the initial value of alpha and sigma. this
c          value should be evaluated first before actually calling the
c          nag routine. 'factor' is set to 1 initially.
c
      subroutine funct1(n,xc,fc)
      implicit real*8(a-h,o-z)
      real*8 k0
      real hs,hrb,hrt,r,v0
      complex*16 p1,p2,p3,beta,rp,pe,pe2,wiz,f,zc,k6,
     *           nre,mre,sthnre,b,n1,m1,beta0,beta1
      dimension xc(n),pred(405),phr1(3),phr2(3),cth1(3),cth2(3),
     *          rr1(3),rr2(3),
```

```
     *          freq(405),rtfreq(405),k0(405),c4pik0(405),diff(405)
      parameter (rate=0.0)
      common /given/hs,hrb,hrt,r,v0
      common /const/pi,pi2,rtpi,factor,rho0,rho0v0,term
      common /data/freq,rtfreq,k0,c4pik0,diff,pred,fact1,fact2
      common /ndata/m,iext
      si=fact1*xc(1)
       si2=si/pi2
      tu=fact2*xc(2)
      fc = 0.0
c
c determination of the path lengths (both direct and indirect).
c
      call range(hs,hrb,r,v0,rate,rd1,phd1,id1,cth1,rr1,phr1,ir1)
      call range(hs,hrt,r,v0,rate,rd2,phd2,id2,cth2,rr2,phr2,ir2)
      do 10 i = 1, m
       zre=term*freq(i)*tu
       k6=7.9d-3*rtfreq(i)*cdsqrt(dcmplx(zre,si))
       zre1=rho0*tu/0.75d0
       zim=si2/freq(i)
       zc=dcmplx(zre1,zim)/xc(3)
       beta=k6*rho0v0/(zc*pi2*freq(i))
       p1=cdexp(dcmplx(0.0d0,k0(i)*phd1))/(c4pik0(i)*rd1)
       p2=(0.0d0,0.0d0)
       p3=(0.0d0,0.0d0)
       if(ir1 .gt. 0)then
        do 15 i1 = 1, ir1
         if(iext .eq. 1)then
          rp=(cth1(i1)-beta)/(cth1(i1)+beta)
          b=(1.0,0.0)
         else if(iext .eq. 2)then
          sthsq=1-cth1(i1)*cth1(i1)
          sth=dsqrt(sthsq)
          nre=(k6/k0(i))**2
          mre=beta*beta/nre
          sthnre=cdsqrt(1.0d0-sthsq/nre)
          beta0=beta*sthnre
          rp=(cth1(i1)-beta0)/(cth1(i1)+beta0)
          n1=cdsqrt(1.0d0-1.0d0/nre)
          m1=cdsqrt(1.0d0-mre)
          beta1=cdsqrt(1.0d0-beta*beta)
          b=(cth1(i1)+beta0)*n1/((cth1(i1)+beta*n1/m1)*sthnre)
     *     *cdsqrt((m1+beta*n1*cth1(i1)+sth*beta1)/(2.0d0*sth*beta1))
     *     /m1**3
         else
          print *,' Error in choosing the type of surface !'
          stop
```

```
          endif
          p2=p2+rp*cdexp(dcmplx(0.0d0,k0(i)*phr1(i1)))
     *          /(c4pik0(i)*rr1(i1))
          pe=cdsqrt(dcmplx(0.0d0,k0(i)*phr1(i1)*0.5d0))*(cth1(i1)+beta)
          pe2=dcmplx(0.0d0,-1.0d0)*pe
          call w(pe2,wiz)
          f=1.0d0+dcmplx(0.0d0,rtpi)*pe*wiz
          p3=p3+(1.0d0-rp)*b*f*cdexp(dcmplx(0.0d0,k0(i)*phr1(i1)))
     *          /(c4pik0(i)*rr1(i1))
15       continue
        endif
        aptot1=cdabs(p1+p2+p3)
        p1=cdexp(dcmplx(0.0d0,k0(i)*phd2))/(c4pik0(i)*rd2)
        p2=(0.0d0,0.0d0)
        p3=(0.0d0,0.0d0)
        if(ir2 .gt. 0)then
         do 17 i2 = 1, ir2
          if(iext .eq. 1)then
           rp=(cth2(i2)-beta)/(cth2(i2)+beta)
           b=(1.0,0.0)
          else if(iext .eq. 2)then
           sthsq=1-cth2(i2)*cth2(i2)
           sth=dsqrt(sthsq)
           nre=(k6/k0(i))**2
           mre=beta*beta/nre
           sthnre=cdsqrt(1.0d0-sthsq/nre)
           beta0=beta*sthnre
           rp=(cth2(i2)-beta0)/(cth2(i2)+beta0)
           n1=cdsqrt(1.0d0-1.0d0/nre)
           m1=cdsqrt(1.0d0-mre)
           beta1=cdsqrt(1.0d0-beta*beta)
           b=(cth2(i2)+beta0)*n1/((cth2(i2)+beta*n1/m1)*sthnre)
     *     *cdsqrt((m1+beta*n1*cth2(i2)+sth*beta1)/(2.0d0*sth*beta1))
     *     /m1**3
          else
           print *,' Error in choosing the type of surface !'
           stop
          endif
          p2=p2+rp*cdexp(dcmplx(0.0d0,k0(i)*phr2(i2)))
     *          /(c4pik0(i)*rr2(i2))
          pe=cdsqrt(dcmplx(0.0d0,k0(i)*phr2(i2)*0.5d0))*(cth2(i2)+beta)
          pe2=dcmplx(0.0d0,-1.0d0)*pe
          call w(pe2,wiz)
          f=1.0d0+dcmplx(0.0d0,rtpi)*pe*wiz
          p3=p3+(1.0d0-rp)*b*f*cdexp(dcmplx(0.0d0,k0(i)*phr2(i2)))
     *          /(c4pik0(i)*rr2(i2))
17       continue
```

```
        endif
       aptot2=cdabs(p1+p2+p3)
       pred(i)=20.0d0*dlog10(aptot2/aptot1)
10     fc=fc+((pred(i)-diff(i))/factor)**2
       return
       end
```

A.9 POROS3

```
c     porosity
c    this program calculates the porosity of soil samples
c    all you have to know is the volume of the soil sampler and the wet
and
c    dry weights of the soil samples and the weight of the sample tin.
        real mw,ms
        gd=2.65
c       vt=105.78
c     input variables
4000    type*,'depth cm ='
        accept*,depth
        type*,'volume of sample='
        accept*,vt
        type*,'sample no='
        accept*,sample
        type*,'wt. of tin = '
        accept*,tin
c       type*,'wt of wet mass + tin = '
        type*,'wt of wet mass = '
        accept*,wmt
        type*,'wt of dry mass + tin ='
        accept*,amst
c   calc of weight of wet(if necessary) and dry mass without tin
c       wm=wmt - tin
        wm=wmt
        ms=amst - tin
c       type*,'wm=',wm,'ms=',ms
c   calc of wet mass (g)
        mw=wm-ms
c       type*,'mw=',mw
c   calculation of dry bulk density dbd
        dbd= ms/vt
        type*,'dbd=',dbd
c   open output file
       open (unit=20,name = 'porosity.dat',type='new')
c   calculation of total porosity,and percentages of water
c   (wat),solids (sol) and air porosity (ap)
       totp = 100-(dbd/gd)*100
```

```
      wat=(mw/vt)*100
      sol=((ms/gd)/vt)*100
      ap= 100-sol-wat
      write (20,7000)sample
7000  format(10x,'sample = ',f12.3)
      write(20,7500)depth
7500  format(3x,'depth cm  =',f6.2)
      write (20,8000)totp,wat,sol,ap
8000  format(' totp= ',f6.2,3x,'wat= ',f6.2,3x
     1 'sol = ',f6.2,3x,'ap= ',f6.2)
c   do you want another go? y = 1
      type*,'do you want another go  yes=1'
      accept*,ans
      if (ans .eq. 1) go to 4000
      stop
      end
```

Appendix B

Other Porosity Profiles with Depth

Table B.1 Deduction of Porosity with Depth for Sand 1

Depth cm	T_o	Ω_o	T_d	Ω_d	Meas.Ω	Depth meas.
surface	2.15	0.36		0.36		0 - 3cm
1-2			12.90	0.03		
2-3			2.49	0.29		
3-4			2.34	0.32		
4-5			2.60	0.27		
5-6			2.18	0.35	0.34	3-6cm
6-7			2.17	0.35		

Table B.2 Deduction of Porosity with Depth for Sand 1

Depth cm	T_o	Ω_o	T_d	Ω_d	Meas.Ω	Depth meas.
surface	2.15	0.36			0.36	0-3cm
0 - 1			13.14*	0.03		
1 - 2			2.26*	0.33		
2 - 3			2.08	0.38		
3 - 4			2.32	0.33	0.34	3 - 6cm

Table B.3 Deduction of Porosity with Depth for Sand 2

Depth cm	T_o	Ω_o	T_d	Ω_d	Meas.Ω	Depth meas.
surface	1.27	0.48			0.47	0 - 3cm
0-1			3.38	0.02		
1-2			2.15	0.10		
2-3			1.85	0.15		
3-4			1.35	0.40		
4-5			1.85	0.15		
5-6			1.65	0.21		
6-7			1.59	0.24		

Table B.4 Deduction of Porosity with Depth for Sand 2

Depth cm	T_o	Ω_o	T_d	Ω_d	Meas.Ω	Depth meas.
surface	1.27	0.48			0.47	0 - 3cm
0-1.5			1.55	0.26		
2-3.5			1.11	0.48		
3.5-4			3.27	0.02		
4-5			2.25	0.08		
5-6			1.85	0.15		
6-7			2.10	0.10		

Table B.5 Deduction of Porosity with Depth for Silt A, Cultivated site, Day 2

Depth cm	T_o	Ω_o	T_d	Ω_d	Meas.Ω	Depth meas.
surface	2.24	0.49			0.65†	0 - 6cm
2 - 4			3.72	0.31		
4 - 6			8.95	0.14		
4 - 6			11.90	0.11	0.17	6 - 9cm

† possible core sampling error

Appendix C

Results for Sand 1

Table C.1 Best fit ground parameters from Level Difference Measurements for Sand 1

	3 para approx				Delany and Bazley	
	σ_{pe}	T	Ω	rms	σ_e	rms
Sand 1	36802	2.11	0.38	1.56	790000	6.48
	37482	2.08	0.37	1.84	820000	7.48
	41292	2.20	0.36	1.91	900000	7.59
	40914	2.21	0.36	1.88	887000	7.57
	48175	2.13	0.35	2.06	1020000	7.72
	48311	2.16	0.35	2.04	1020000	7.71
average	42000	2.15	0.36	1.88	906000	7.42

Table C.2 Ground Parameters Deduced from Other Measurements using Probe Microphone in Sand 1

depth(cm)	σ_{pe}	T
1-2	17302*	12.90*
2-3	10231*	2.49*
3-4	12332	2.34*
4-5	7395*	2.60*
5-6	8126	2.18*
6-7	10431	2.17*
0-1	14470*	13.14*
1-2	7278	2.26*
2-3	7252	2.08*
3-4	9082	2.53*
4-5	20845	5.57*
5-6	4376	0.94*
6-7	6203	2.32*

* Deduced using Approximation Technique

Table C.3 Measured Flow Resistivities for Sand 1, using Air Flow-Rig

Soil	sample	σ mks rayls/m
Sand 1	1	387000
	2	326800
	3	351600
	4	438000
	average	376000

Table C.4 Measured Soil Parameters for Sand 1.

Soil	Depth cm	water	soilds	air	av. air
Sand1	0 - 3	0.10	0.56	0.35	
	0 - 3	0.08	0.58	0.35	0.35
	3 - 6	0.07	0.56	0.36	0.36
	6 - 9	0.07	0.56	0.37	
	6 - 9	0.11	0.60	0.29	0.33

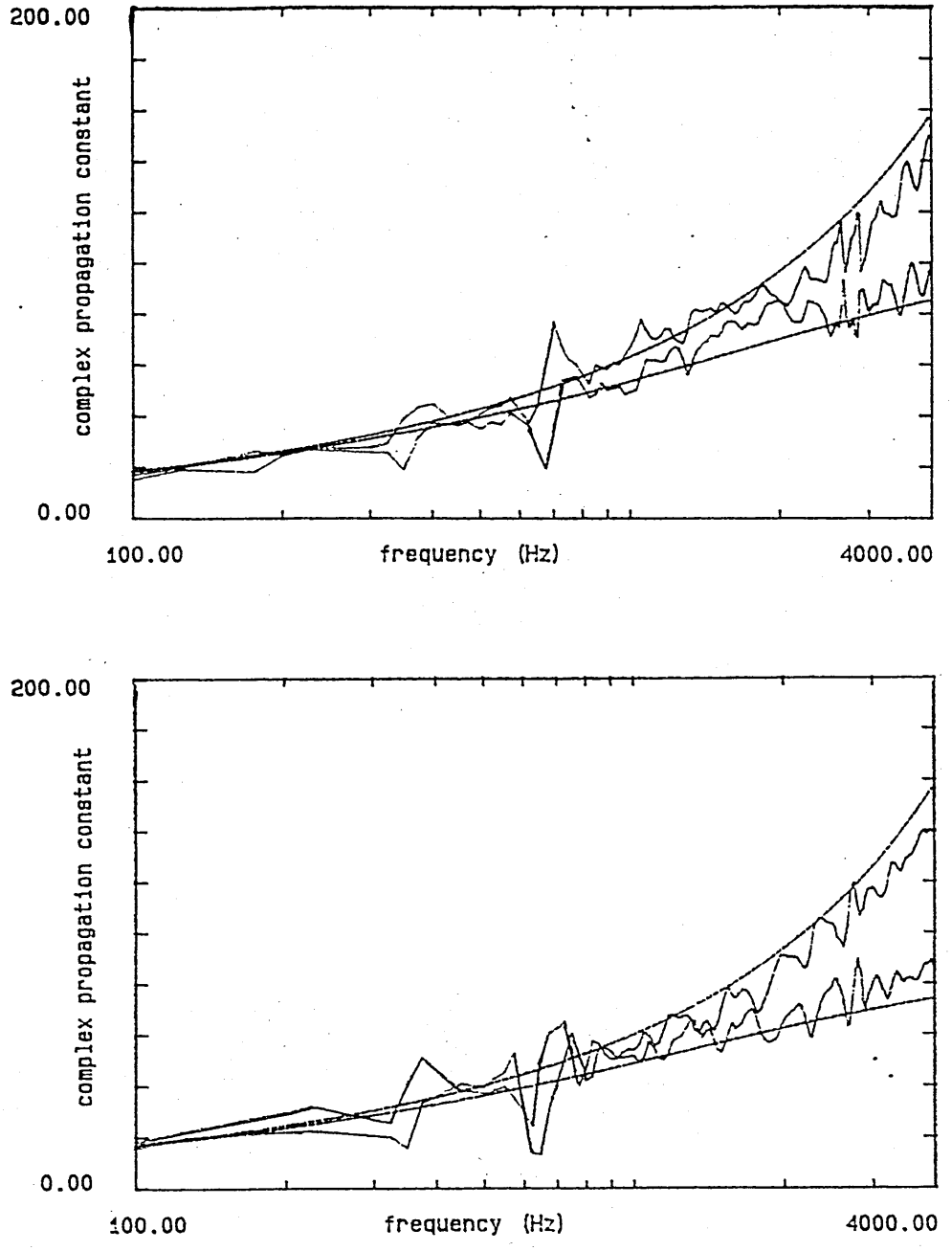

Figure C.1 Examples of Measured and Predicted Propagation Constant in Sand with depth a)0-1cmσ_{pe} =27060 T=2.37, b)1-3cmσ_{pe} =23490 T=2.60

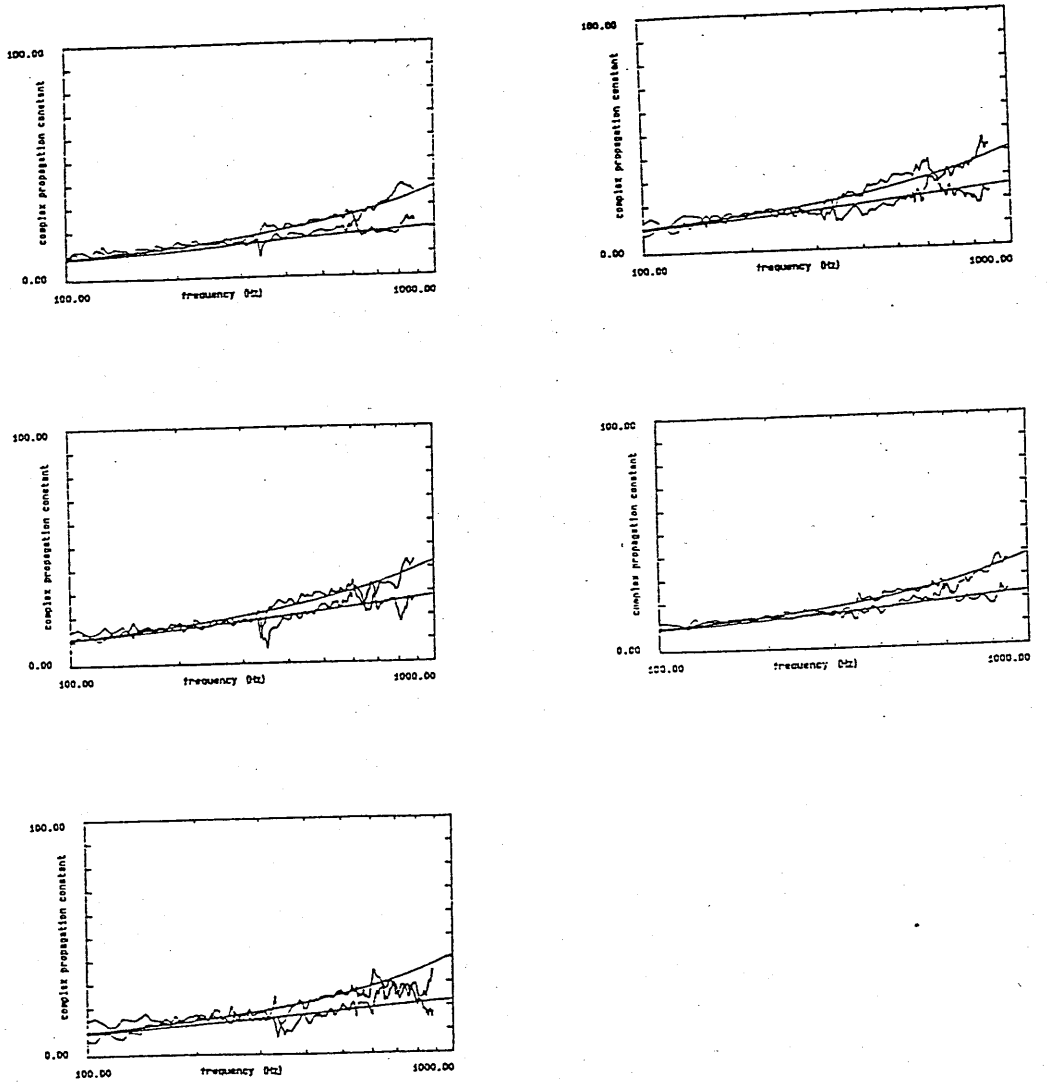

Figure C.2 Examples of Measured and Predicted Propagation Constant in Sand with depth a)1-2cmσ_{pe} =6880 T=2.16, b)2-3cmσ_{pe} =7110 T=2.12, c)3-4cm σ_{pe}=9652 T=2.22 d)4-5cmσ_{pe} =8707 T=2.28, e)6-7cmσ_{pe} =7350 T=2.57.

Appendix D

Results for Sand 2

Table D.1 Measured Flow Resistivities for Sand 2, using Air Flow-Rig

Soil	sample	σ mks rayls/m
Sand2	1	109200
	2	141200
	3	153700
	average	134700

Table D.2 Measured Soil Parameters for Sand 2.

Soil	Depth cm	water	soilds	air	av. air
Sand2	0 - 3	0.02	0.50	0.49	
	0 - 3	0.02	0.51	0.47	
	0 - 6	0.02	0.52	0.46	0.47

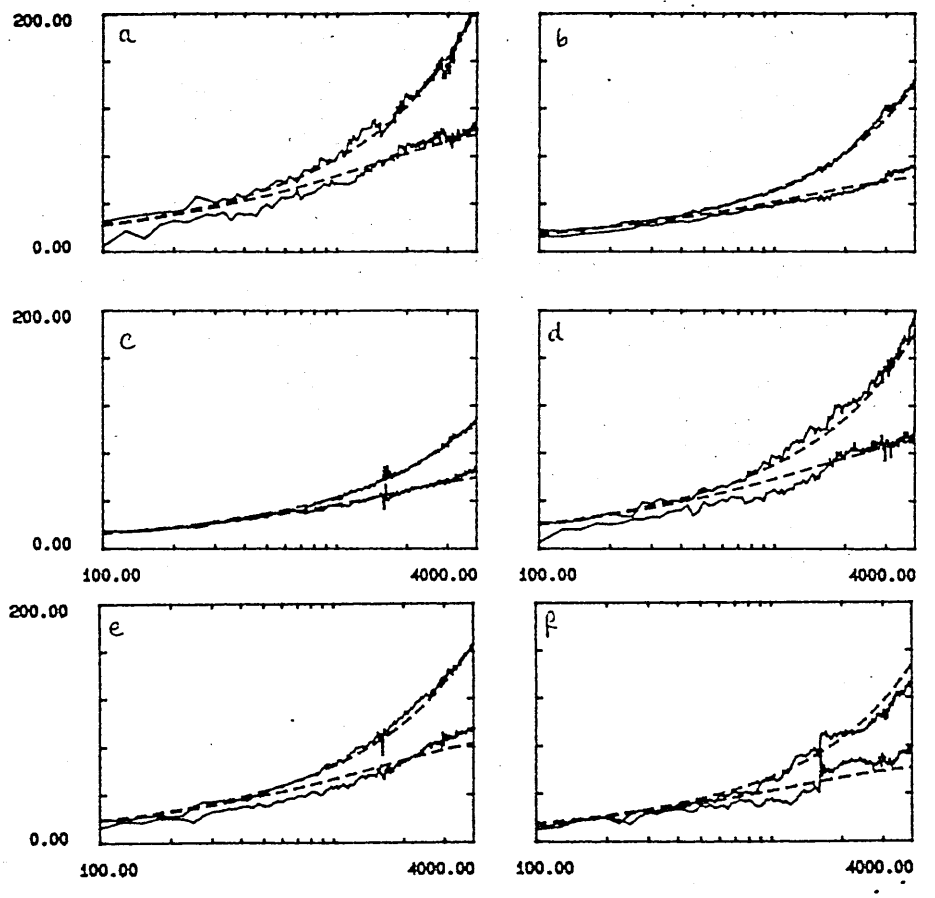

Figure D.1 Examples of Measured and Predicted Propagation Constant in Sand with depth a)0-1cmσ_{pe} =40343 T=4.3, b)1-2cmσ_{pe} =17774 T=2.12, c)2-3.5cm σ_{pe}=13159 T=1.11 d)3.5-4cmσ_{pe} =33250 T=3.27, e)4-5cmσ_{pe} =27708 T=2.77, f)5-6cm σ_{pe}=18477 T=2.43

Table D.3 Ground parameters deduced from Other Measurements using Probe Microphone in Sand 2

Location	Depth(cm)	σ_{pe}	T
Tray	0-1	11156	3.12
	0-1	40343	4.3
	1-2	17774	2.12*
	2-3	16812	2.77*
	4-5	27708	2.77*

* Deduced using Approximation Technique

Appendix E

Results for Sand 3

Table E.1 Measured Soil Parameters for Sand 3.

Soil	Depth cm	water	soilds	air	av. air
Sand3	0 - 1	0.42	0.44	0.13	
	0 - 1	0.26	0.60	0.13	
	0 - 1	0.34	0.48	0.16	0.14
	1 - 6	0.13	0.55	0.32	
	1 - 6	0.14	0.57	0.29	
	1 - 6	0.14	0.55	0.31	
	1 - 6	0.17	0.59	0.24	
	1 - 6	0.11	0.51	0.39	0.31

Table E.2 Measured Flow Resistivities for Sand 3, using Leonards Apparatus

Soil	sample	Run #	σ mks rayls/m
Sand3	1	1	69460
		2	78240
	2	1	71800
		2	71230
		3	69730
	3	1	71230
		2	68300
		3	67500
	average		71000

Table E.3 Ground parameters deduced from all Measurements using Probe Microphone in Sand 3

Location	Depth(cm)	σ_{pe}	T
Sand 3	0-1	95430	9.05
	1-2	47550	3.22
	2-3	64740	10.64
	3-4	59430	21.21
	4-5	47550	12.16
	0-1	223220	761.0
	1-5	21130	10.08

Appendix F

Results for Sandy Loam (dry)

Table F.1 Parameters Deduced from all Level Difference Measurements on a Sandy Loam (dry)

	3 para approx				Delany and Bazley	
	σ_{pe}	T	Ω	rms	σ_e	rms
Sandy Loam	22290	1.06	0.59	1.93	210000	3.84
	25660	2.73	0.50	1.35	350000	5.35
	26410	2.80	0.51	1.35	350000	5.30
	20270	4.46	0.52	2.91	390000	19.94
	28810	4.29	0.47	1.57	530000	11.38
	20870	4.59	0.53	2.91	390000	19.90
average	24050	3.32	0.52	2.00	370000	10.95

Table F.2 Measured Flow Resistivities for Sandy Loam dry, using Air Flow-Rig

Soil	sample	σ mks rayls/m
Sandy Loam dry	1	284000
	2	306000
	3	212000
	4	236000
	average	259000

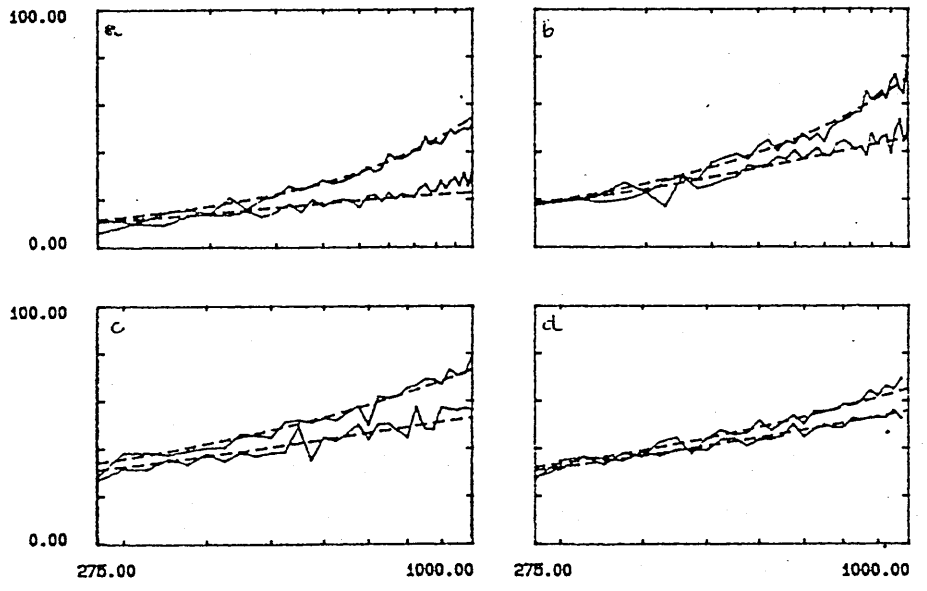

Figure F.1 Examples of Measured and Predicted Propagation Constant in Sandy Loam (dry) with Depth, a)0-2cm σ_{pe}=10113 T=5.26 b)3-5cmσ_{pe} =26227 T=6.31, c)0-1cmσ_{pe} =31255 T=5.44, d)0-2cmσ_{pe} =29152 T=2.40,

Table F.3 Measured Soil Parameters for Sandy Loam dry.

Soil	Depth cm	water	soilds	air	av. air
Sandy Loam Dry	0 - 5	0.04	0.48	0.48	
	0 - 5	0.03	0.48	0.49	
	0 - 5	0.04	0.46	0.49	
	0 - 5	0.04	0.46	0.49	
	0 - 5	0.03	0.46	0.51	
	0 - 5	0.03	0.48	0.48	
	0 - 5	0.03	0.45	0.51	0.49

Appendix G

Results for Sandy Loam (moist)

Table G.1 Parameters Deduced from all Level Difference Measurements on a Sandy Loam (moist)

	3 para approx				Delany and Bazley	
	σ_{pe}	T	Ω	rms	σ_e	rms
	9324	1.33	0.39	1.16	230000	5.61
	8708	1.02	0.41	1.09	170000	7.00
	9766	1.23	0.38	1.82	230000	9.02
	8873	1.27	0.38	1.16	230000	5.61
	10237	1.29	0.39	1.82	230000	9.02
average	9381	1.23	0.39	1.56	218000	7.25

Table G.2 Measured Flow Resistivities for Sandy Loam moist, using Air Flow-Rig

Soil	sample	σ mks rayls/m
Sandy Loam moist	1	90890
	2	38967
	3	36235
	4	47600
	average	54000

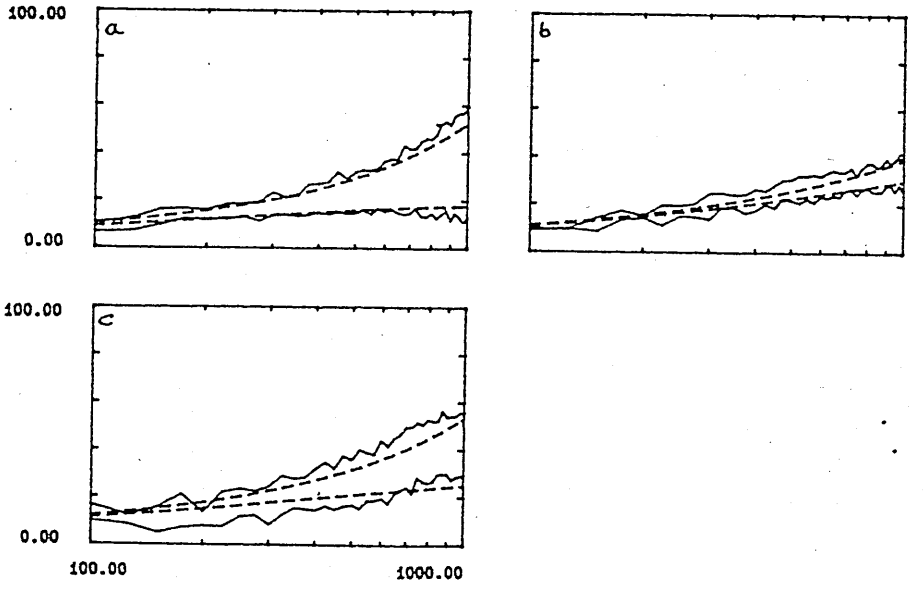

Figure G.1 Examples of Measured and Predicted Propagation Constant in Sandy loam (moist) with Depth a)0-2cm σ_{pe}=7470 T=5.20* b)2-4cmσ_{pe} =9510 T=1.3*, c)4-6cmσ_{pe} =10643 T=4.77*.

Table G.3 Measured Soil Parameters for Sandy Loam Moist.

Soil	Depth cm	water	soilds	air	av. air
Sandy Loam Moist	0 - 5	0.20	0.42	0.38	
	0 - 5	0.24	0.46	0.29	
	0 - 5	0.23	0.45	0.31	
	0 - 5	0.23	0.44	0.33	
	0 - 5	0.26	0.48	0.26	
	0 - 5	0.20	0.43	0.37	
	0 - 5	0.19	0.41	0.40	0.33

Appendix H

Results for Sandy Loam (wet)

Table H.1 Deduced Parameters from all Level Difference Measurements for Sandy Loam (wet).

Measurement	Layer	σ_e	Ω	Depth(cm)	rms
1	Top	2000000	(0.11)	(1)	3.28
	Bottom	(59200)	(0.39)		
2	Top	2000000	(0.11)	(1)	3.35
	Bottom	(59200)	(0.39)		
3	Top	5000000	(0.11)	(1)	2.92
	Bottom	(59200)	(0.39)		
4	Top	2500000	(0.11)	(1)	2.93
	Bottom	(59200)	(0.39)		

Table H.2 Measured Flow Resistivities for Sandy Loam Wet, using Air Flow-Rig

Soil	sample	σ mks rayls/m
Sandy Loam wet	1	2172200
	2	1498600
	3	831600
	average	1500000

Table H.3 Measured Soil Parameters for Sandy Loam Wet.

Soil	Depth cm	water	soilds	air	av. air
Sandy Loam Wet	0 - 1	0.32	0.64	0.04	
	0 - 2	0.27	0.53	0.19	0.11
	0 - 5	0.28	0.50	0.23	
	0 - 5	0.22	0.46	0.32	
	0 - 5	0.29	0.47	0.30	0.28

Table H.4 Ground Parameters Deduced from Other Measurements using Probe Microphone in Sandy Loam (wet)

depth(cm)	σ_{pe}	T
0-1	66560	37.150
0-2	28650	10.76
0-2	28620	21.78
0-2	30020	10.58
1-2	6694	5.34
1-2	10846	2.34
1-3	7385	10.77
2-4	16198	7.58
2-4	4118	8.49
3-4	4582	4.57
3-5	8300	6.83
4-6	8435	8.66
5-6	14448	7.68

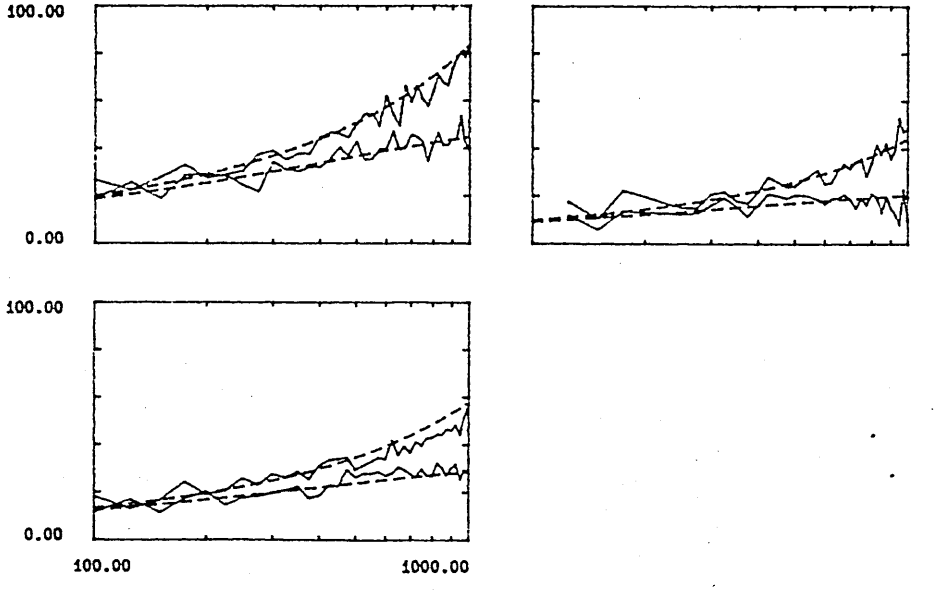

Figure H.1 Examples of Measured and Predicted Propagation Constant in Sandy loam (wet) with Depth, a)0-2cm σ_{pe}=30020 T=10.58 b)1-3cmσ_{pe} =7237 T=3.3, c)1-3cmσ_{pe} =13290 T=5.39.

Appendix I

Results for Clay Soils

I.1 Day1

Table I.1 Parameters Deduced from All Level Difference Measurements for Clay Soil both Wheeled and Zero Treatments Day 1

	3 para approx				Delany and Bazley	
	σ_{pe}	T	Ω	rms	σ_e	rms
wheeled	17300	4.50	0.59	1.09	163000	2.53
	13760	3.91	0.53	1.06	160000	2.33
	12556	3.51	0.50	1.09	190000	1.90
	12712	3.55	0.51	1.09	160000	2.40
zero	10510	2.14	0.55	2.74	90000	1.70
	10140	1.38	0.51	3.56	110000	1.70
	10180	1.34	0.55	3.62	110000	1.30
	11460	1.13	0.56	3.58	100000	1.57
	15015	2.17	0.61	1.66	118000	2.30
	12970	2.02	0.56	1.72	118000	4.40
	13210	2.67	0.61	1.71	109000	5.65
	11370	2.10	0.58	1.31	106000	3.06
	13785	2.50	0.64	1.30	100000	3.07

Table I.2 Ground parameters deduced from all Probe Measurements for Clay Wheeled and Zero Sites Day 1

Site	Depth cm	σ_{pe}	T
Wheeled	0 - 2	730	1.67
	0 - 2	7180	16.86
	0 - 2	4350	12.04
	2 - 4	81767	55.8
	0 - 4	22925	22.9
Zero	0 - 2	3620	4.94
	0 - 2	4520	4.07*
	0 - 2	625	4.04
	0 - 2	670	2.44
	0 - 2	300	2.71
	0 - 2	5590	6.28*
average		2553	4.08
	2 - 4	4220	4.66*
	2 - 4	5130	8.28*
	2 - 4	6790	6.55
	2 - 4	1100	7.23
	2 - 4	10200	15.6
	2 - 4	10180	3.25
average		6270	7.95
	4 - 6	7210	25.04
	4 - 6	8270	27.04
	4 - 6	12851	22.73
average		9943	25.0
	6 - 8	4786	19.86
	6 - 8	4313	14.1
average		4100	16.98

Table I.3 Measured Soil Parameters for Clay Day 1.

Site	Depth cm	water	soilds	air	av. air
Wheeled	0 - 3	0.21	0.19	0.59	
	0 - 3	0.17	0.17	0.65	0.62
	3 - 6	0.45	0.38	0.16	
	3 - 6	0.39	0.36	0.23	0.20
	6 - 9	0.45	0.40	0.15	0.15
Zero	0 - 3	0.19	0.21	0.60	
	0 - 3	0.22	0.26	0.52	0.55
	3 - 6	0.30	0.34	0.36	
	3 - 6	0.31	0.27	0.42	
	3 - 6	0.28	0.29	0.43	
	3 - 6	0.34	0.28	0.28	0.40
	6 - 9	0.51	0.41	0.08	
	6 - 9	0.46	0.38	0.16	
	6 - 9	0.54	0.38	0.08	0.10

I.2 Day 2

Table I.4 Parameters Deduced from all Level Difference Measurements on Clay Wheeled and Zero Sites, Day 2

	3 para approx				Delany and Bazley	
	σ_{pe}	T	Ω	rms	σ_e	rms
wheeled	4622	2.16	0.43	1.42	104000	4.77
	3785	2.0	0.40	1.25	106000	4.49
	2985	3.16	0.40	1.31	127000	6.98
	3327	3.41	0.44	1.74	114000	9.04
zero	6230	3.66	0.56	1.94	98000	7.40
	5730	3.81	0.56	1.87	93000	6.52
	6350	2.99	0.58	1.63	87000	5.66
	6620	2.97	0.58	1.61	88000	5.56

Table I.5 Parameters Deduced from all Probe Measurements for Clay Wheeled and Zero Sites, Day 2

Site	Depth cm	σ_{pe}	T
Wheeled	0 - 2	3740	4.16*
	0 - 2	3770	4.07*
	0 - 2	3700	4.26*
average		3740	4.16*
	2 - 4	2090	1.84
	4 - 7	7120	3.45*
Zero	0 - 2	1467	3.36
	0 - 2	393	3.36
	2 - 5	414	0.92

Table I.6 Measured Soil Parameters for Clay, Day 2

Site	Depth cm	water	soilds	air	av. air
Wheeled	0 - 3	0.25	0.35	0.40	
	0 - 3	0.15	0.25	0.60	
	0 - 3	0.24	0.33	0.43	0.47
	3 - 6	0.28	0.40	0.32	
	3 - 6	0.34	0.43	0.23	
	3 - 6	0.29	0.40	0.31	0.26
	6 - 9	0.38	0.49	0.13	
	6 - 9	0.34	0.43	0.23	
	6 - 9	0.29	0.35	0.36	0.24
Zero	0 - 3	0.19	0.25	0.56	
	0 - 3	0.17	0.28	0.55	0.55
	3 - 6	0.21	0.29	0.50	
	3 - 6	0.19	0.28	0.53	0.51
	6 - 9	0.26	0.34	0.40	
	6 - 9	0.24	0.31	0.45	0.42

I.3 Day 3

Table I.7 Parameters Deduced from all Probe Measurements on Clay, Wheeled and Zero Sites, Day 3

Site	Depth cm	σ_{pe}	T
Wheeled	0 - 1	6860*	7.36*
	1 - 2	5671	3.45*
	1 - 3	2845*	2.03*
	1 - 3	1658	3.17
	1 - 3	4884	4.30
average		3130	3.16
	2 - 3	761	0.7
	2 - 5	1247	2.31
	3 - 5	1551	3.22
Zero	0 - 2	1115	3.61
	0 - 2	2393	4.65*
	0 - 2	5373	7.63
	0 - 2	4810*	3.38*
	0 - 2	10120	5.58
average		4780	5.03
	2 - 4	1449	1.46
	2 - 4	1220	2.91
average		1334	2.18
	4 - 6	1456	1.21

I.4 Day 4

Table I.8 Ground Parameters Deduced from all Level Difference Measurements on Clay, Wheeled Before and After Rain.

	Soil	Site	σ_{pe}	T	Ω
before	wheeled	9340	7.00	0.45	1.46
rain		9200	7.25	0.45	1.47
		9640	6.21	0.44	1.33
		av. 9390	6.82	0.45	
After	wheeled	6340	11.3	0.49	1.09
Rain		7710	11.22	0.50	1.07
		7040	10.2	0.49	1.25
		6710	11.15	0.50	1.39
		6710	10.48	0.48	1.38
		5390	8.11	0.42	1.35
average		6650	10.41	0.48	

I.5 Day5

Table I.9 Parameters Deduced from all Probe Measurements on Clay, Wheeled and Zero Sites, Day 5

Site	Depth cm	σ_{pe}	T
Wheeled	0 - 2	283	1.27
	0 - 2	1228	5.11
	average	755	3.19
	2 - 4	954	5.42
	2 - 4	876	3.37
	average	915	4.39
	4 - 6	24509	39.0
	4 - 6	14399	26.4
	average	19454	33.14
Zero	0 - 2	1304	6.21
	0 - 2	769	3.90
	0 - 2	1506	2.47
	average	1193	4.19
	2 - 4	1354	2.21
	2 - 4	336	3.80
	2 - 4	2828	2.31
	average	1506	2.77
	4 - 6	8371	8.46
	4 - 6	4386	6.14
	average	6378	7.30
	6 - 8	1424	3.53
	6 - 8	1628	2.08
	average	1526	2.8
	8 - 10	1282	3.04

Appendix J

Results for Silt A

J.1 Day 1

Table J.1 Ground Parameters Deduced from all Level Difference Measurements for Silt A, Cultivated Site, Day1.

	3 para approx				Delany and Bazley	
	σ_{pe}	T	Ω	rms	σ_e	rms
cultivated	8591	2.81	0.54	1.21	130000	6.50
	8753	2.97	0.58	1.38	90000	2.29
	av 8672	2.89	0.56	1.29	110000	4.40

Table J.2 Parameters Deduced from all Probe Measurements on Silt A Cultivated Sites, Day 1

Site	Depth cm	σ_{pe}	T
Culti-	0 - 2	3020	4.21
vated	2 - 4	2020	3.91
	2 - 4	1030	1.08*
	4 - 6	14190*	6.11*
	6 - 8	2525	4.51
	6 - 10	10550	8.58*

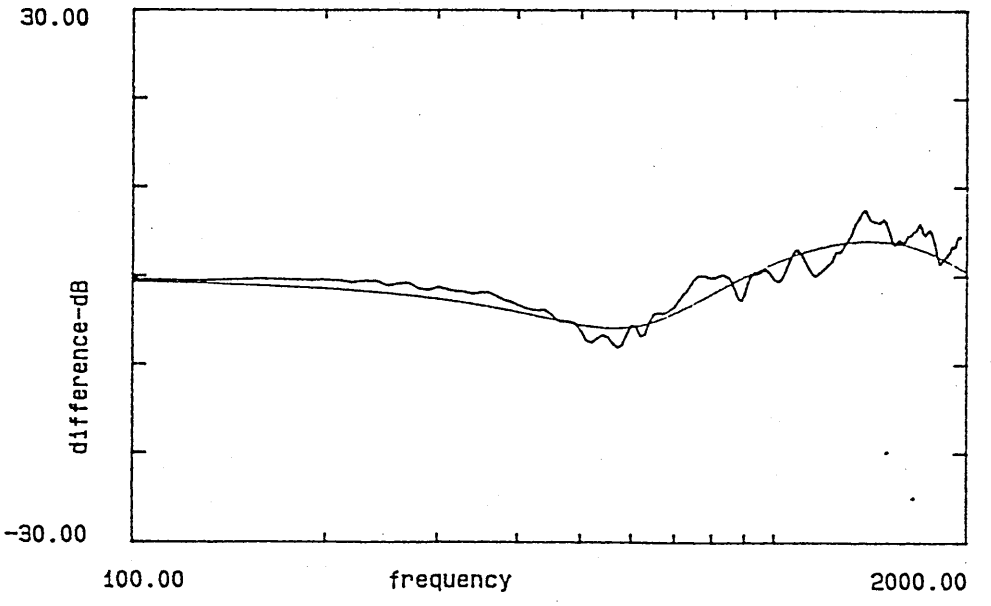

Figure J.1 Examples of Best Fit Predictions from Level Difference Measurements over Silt A, Cultivated Site, Day 1. Geometry hs=0.45m, r=1.75m, hst=0.45m, hrb=0.1m, Deduced σ_{pe} =8590, T=2.81, Ω=0.54 rms=1.21

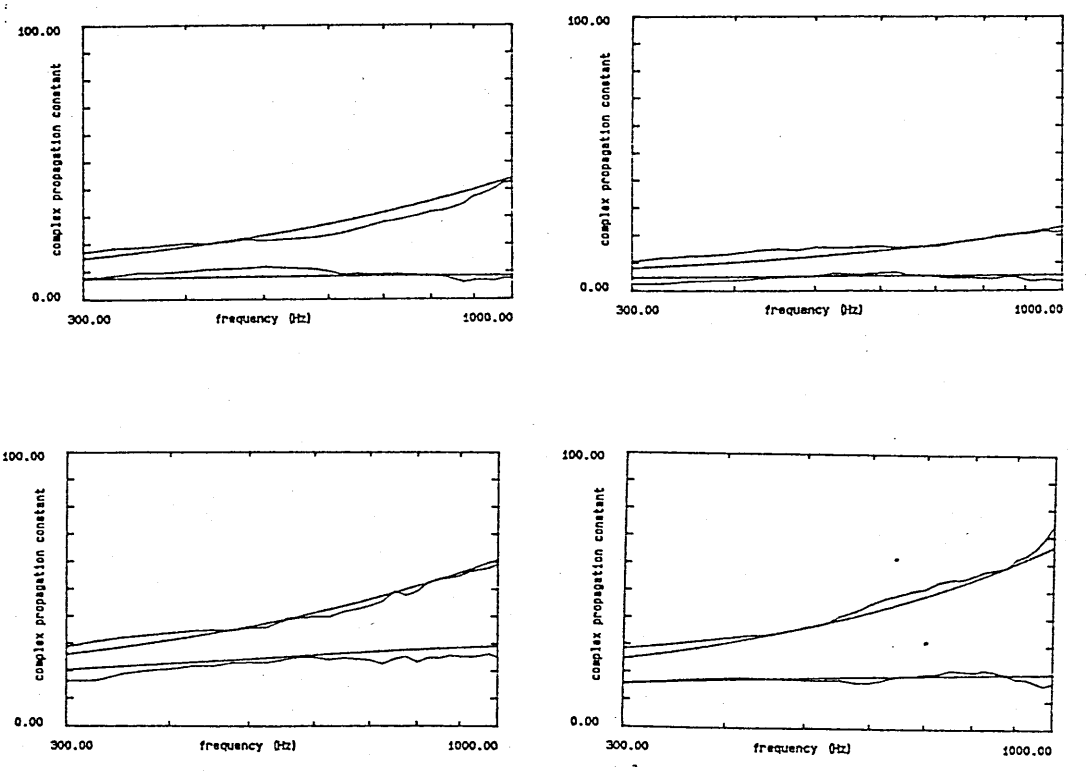

Figure J.2 Examples of Measured and Predicted Propagation Constant in Silt A, Cultivated Site, Day 1, a) 0-2cm σ_{pe}=3020 T=4.21 b) 2-4cmσ_{pe} =1032 T=1.08* c) 4-6cm σ_{pe}=14190* T=6.11* d)6-10cmσ_{pe} =10550 T=8.58*

Table J.3 Measured Soil Parameters for Silt A, Day 1

Site	Depth cm	water	soilds	air	av. air
Cultivated	0 - 6	0.20	0.26	0.54	
	0 - 6	0.18	0.22	0.60	
	0 - 6	0.22	0.28	0.50	
	0 - 6	0.20	0.25	0.55	0.54
	6 - 9	0.35	0.37	0.28	
	6 - 9	0.25	0.31	0.44	0.35

J.2 Day 2

Table J.4 Ground Parameters Deduced from all Level Difference Measurements for Silt A, Cultivated and Compacted Sites, Day2.

	3 para approx				Delany and Bazley	
	σ_{pe}	T	Ω	rms	σ_e	rms
Cultivated	5887	2.45	0.49	1.27	110000	7.32
	5831	2.49	0.52	1.20	90000	2.64
	6400	1.78	0.46	1.23	120000	2.85
	av 6039	2.24	0.49	1.23	106000	4.27
Compact	17075	2.94	0.18	1.38	1600000	1.15
	11444	1.88	0.19	1.11	490000	3.43
	av.14260	2.41	0.18	1.24	104500	2.29

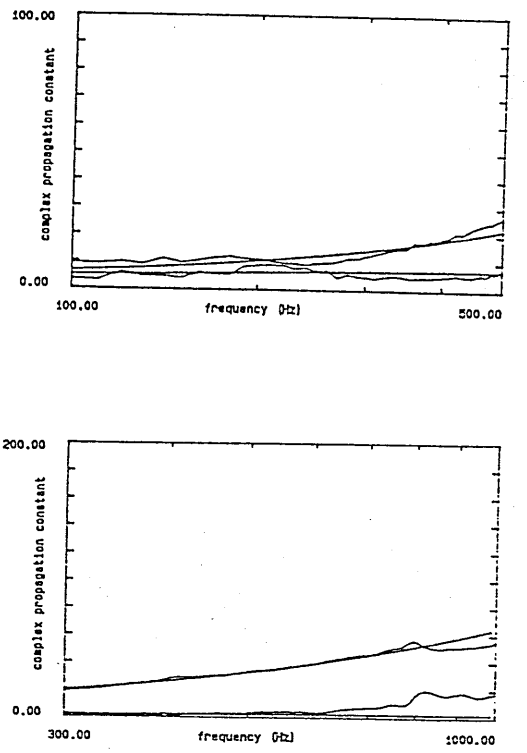

Figure J.3 Examples of Measured and Predicted Propagation Constant with depth in Silt A , Cultivated Site, Day 2, a)2-4cm σ_{pe}=2527 T=3.72 b)4-6cmσ_{pe} =3246 T=8.95

Table J.5 Measured Soil Parameters for Silt A, Day 2

Site	Depth cm	water	soilds	air	av. air
Cultivated	0 - 6	0.17	0.21	0.62	
	0 - 6	0.15	0.20	0.65	
	0 - 6	0.12	0.21	0.67	
	0 - 6	0.13	0.19	0.68	
	0 - 6	0.11	0.21	0.68	0.66
	6 - 9	0.45	0.46	0.09	
	6 - 9	0.35	0.42	0.23	
	6 - 9	0.41	0.47	0.12	
	6 - 9	0.31	0.41	0.28	0.18
compacted	0 - 3	0.28	0.49	0.23	
	0 - 3	0.31	0.45	0.24	0.23

J.3 Day 3

Table J.6 Ground Parameters Deduced from all Level Difference Measurements for Silt A, Cultivated Site, Day 3.

Site	σ_{pe}	T	Ω	rms
cultivated	4384	2.54	0.47	1.41
	4298	2.20	0.48	1.14
	4483	2.60	0.48	1.40
	av 4370	2.44	0.474	1.32

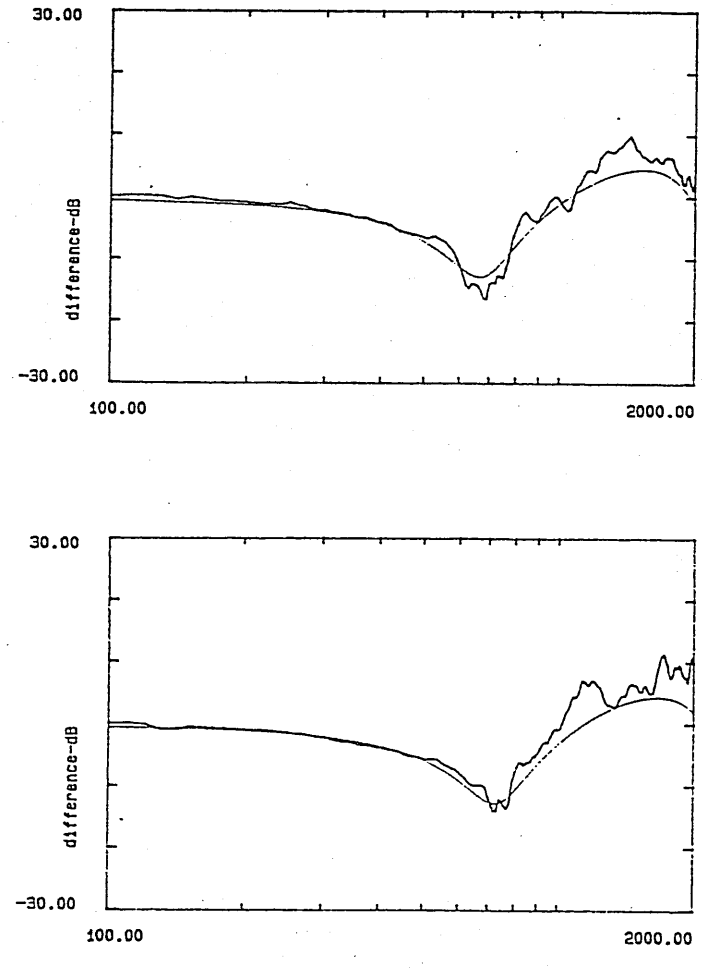

Figure J.4 Examples of Best Fit Predictions from Level Difference Measurements over Crusted Silt A, compacted site, Day 3. a) Geometry hs=0.45m, r=1.75m, hst=0.50m, hrb=0.1m, Deduced parameters for Upper Layer σ_e =300000, Ω=0.21, for Lower Layer σ_e =100000, Ω=0.32 rms=2.23 b) Geometry hs=0.45m, r=1.75m, hst=0.45m, hrb=0.1m, Deduced parameters for Upper Layer σ_e =300000, Ω=0.25, for Lower Layer σ_e =50000, Ω=0.32 rms=2.96

Table J.7 Ground Parameters Deduced from all Level Difference Measurements for Silt A, Compacted Site, Day3.

Site	Layer	σ_e	Ω	Depth cm	rms
compacted	t	300000	0.25	(0.01)	2.96
	b	50000	(0.32)		
	t	300000	0.21	(0.01)	2.23
	b	100000	(0.32)		

Table J.8 Measured Soil Parameters for Silt A, Day 3

Site	Depth cm	water	soilds	air	av. air
Cultivated	0 - 6	0.15	0.35	0.50	
	0 - 6	0.12	0.30	0.58	
	0 - 6	0.15	0.33	0.52	0.53
	6 - 9	0.27	0.36	0.37	
	6 - 9	0.31	0.40	0.29	0.33
Compact	0 - 3	0.18	0.44	0.38	
	0 - 3	0.24	0.50	0.26	0.32
	3 - 6	0.37	0.55	0.07	0.07
	6 - 9	0.36	0.51	0.13	0.13

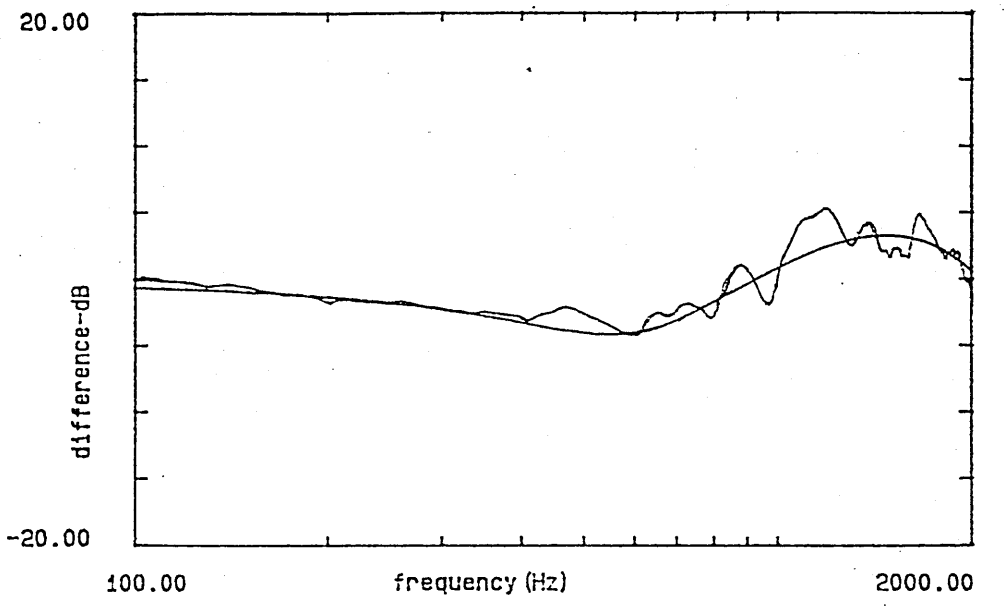

Figure J.5 Example of Best Fit Prediction from Level Difference Measurements over Silt A, Cultivated Site, Day 3. Geometry hs=0.45m, r=1.75m, hst=0.45m, hrb=0.1m, Deduced σ_{pe} =4300, T=2.20, Ω=0.48, rms=1.14.

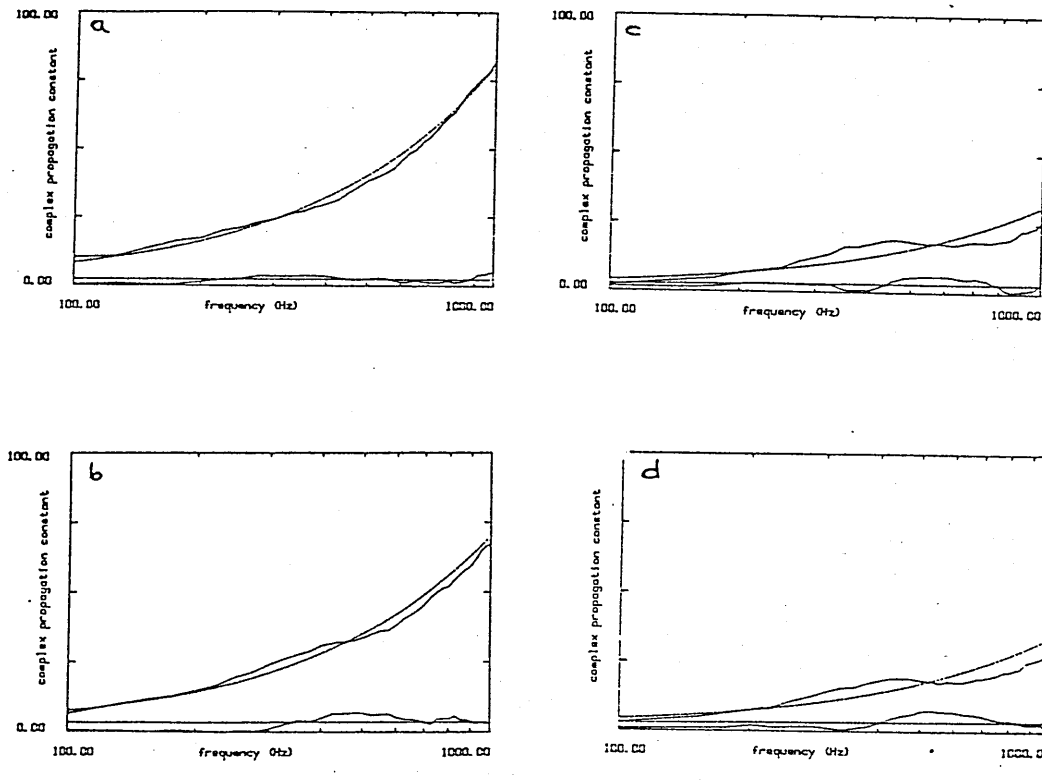

Figure J.6 Examples of Measured and Predicted Propagation Constant in Silt A, Cultivated Site, Day 3, a) 0-2cm σ_{pe}=1520 T=13.9 b) 1-2cm σ_{pe} =2020 T=10.43 c) 2-4cm σ_{pe}=780 T=2.08 d)2-4cmσ_{pe} =940 T=2.48.

Appendix K

Results for Silt B

Table K.1 Ground Parameters Deduced from all Level Difference Measurements for Silt B, Cultivated Wheelings and Poor practise Sites.

Site	Layer	σ_e	Ω	Depth cm	rms
Cultivated Wheelings	t	700000	0.15	(0.01)	2.39
	b	(36600)	(0.48)		
	t	500000	0.15	(0.01)	3.27
	b	(36600)	(0.48)		
	t	700000	0.15	(0.01)	2.37
	b	(36600)	(0.48)		
	t	500000	0.15	(0.01)	3.80
	b	(36600)	(0.48)		
Poor practise	t	2500000	0.12	(0.01)	3.84
	b	(40800)	(0.42)		
	t	2500000	0.12	(0.01)	3.94
	b	(40800)	(0.42)		

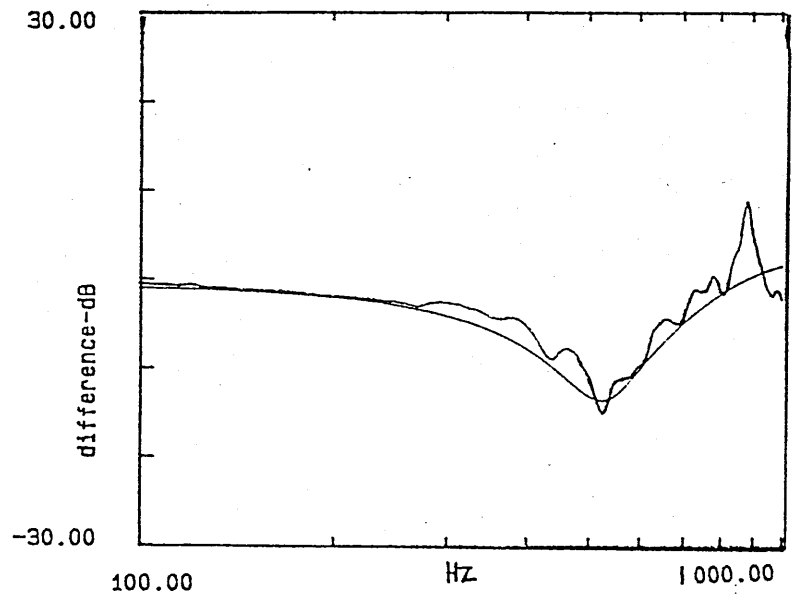

Figure K.1 Example of Best Fit Prediction from Level Difference Measurements over Crusted Silt B, controlled wheeling site. a) Geometry hs=0.65m, r=1.76m, hst=0.65m, hrb=0.1m, Deduced parameters for Upper Layer σ_e =700000, Ω=0.15, for Lower Layer σ_e =36600, Ω=0.48 rms=2.37.

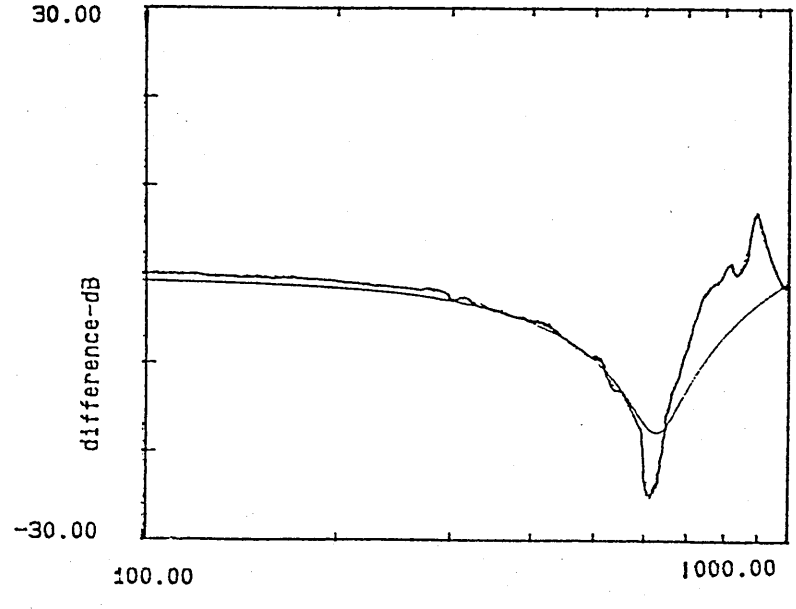

Figure K.2 Example of Best Fit Prediction from Level Difference Measurements over Crusted Silt B, poor practise site. a) Geometry hs=0.46m, r=1.76m, hst=0.55m, hrb=0.1m, Deduced parameters for Upper Layer σ_e =2500000, Ω=0.12, for Lower Layer σ_e =40800, Ω=0.40 rms=3.94.

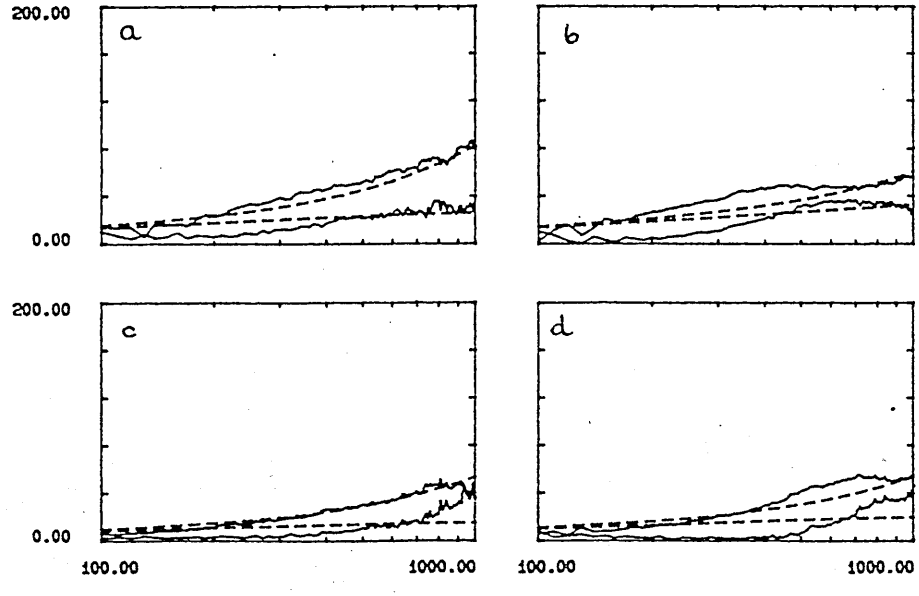

Figure K.3 Examples of Measured and Predicted Propagation Constant in Silt B, Controlled Wheeling Site, a) 0-2cm σ_{pe}=17175 T=13.06 b) 0-2cmσ_{pe} =15757 T=5.65 c) 2-4cm σ_{pe}=6520 T=5.64 d)2-4cmσ_{pe} =8430 T=8.36.

Table K.2 Parameters Deduced from all Probe Measurements on Silt B Controlled Wheeling and Poor practise Sites.

Site	Depth cm	σ_{pe}	T
Cultivated	0 - 2	15757	4.65*
Wheeling	0 - 2	17175	13.06*
average		16422	8.85
	2 - 4	8438	8.36
	2 - 4	6520	5.64
Poor practise	0 - 2	44397	49.9*
	0 - 2	38697	27.1*
	0 - 2	90747*	20.7*
	2 - 4	1582	5.03
	2 - 4	6512	20.26
	4 - 6	6525	5.98

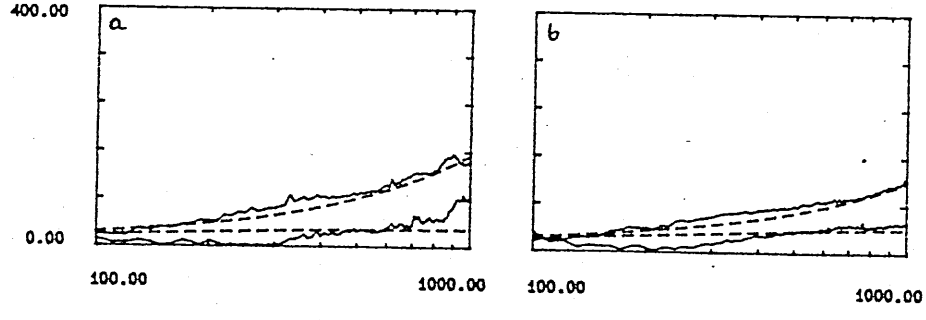

Figure K.4 Examples of Measured and Predicted Propagation Constant in Silt B, Poor Practise Site, a) 0-2cm σ_{pe}=44397 T=49.9 b) 0-2cmσ_{pe} =38697 T=27.10

Table K.3 Measured Soil Parameters for Silt B

Site	Depth cm	water	soilds	air	a.v. air
Cultivated	0 - 3	0.16	0.44	0.43	
Wheeling	0 - 3	0.16	0.38	0.46	
	0 - 3	0.15	0.40	0.44	
	0 - 3	0.07	0.38	0.59	0.48
	6 - 9	0.31	0.23	0.50	0.27
Poor	0 - 3	0.10	0.38	0.51	
Practise	0 - 3	0.11	0.37	0.52	
	0 - 3	0.12	0.49	0.39	
	0 - 3	0.12	0.46	0.42	
	0 - 3	0.15	0.42	0.43	0.44
	3 - 6	0.17	0.46	0.37	
	3 - 6	0.25	0.61	0.14	
	3 - 6	0.25	0.64	0.11	
	3 - 6	0.15	0.46	0.39	
	3 - 6	0.18	0.52	0.30	
	3 - 6	0.23	0.58	0.19	0.25
	6 - 9	0.23	0.51	0.26	
	6 - 9	0.19	0.45	0.37	
	6 - 9	0.22	0.52	0.26	
	6 - 9	0.22	0.56	0.22	
	6 - 9	0.20	0.46	0.34	0.29

Table K.4 Measured Flow Resistivities for Silt B

Treatment	Depth cm	σ mks rayls/m
Cultivated wheeling	0 - 3	62300
	3 - 6	74600
Poor practise	0 - 3	2200000
	0 - 3	1536900
	0 - 3	691360
	0 - 3	144000

Appendix L

Results for Snow

L.1 Site A2a

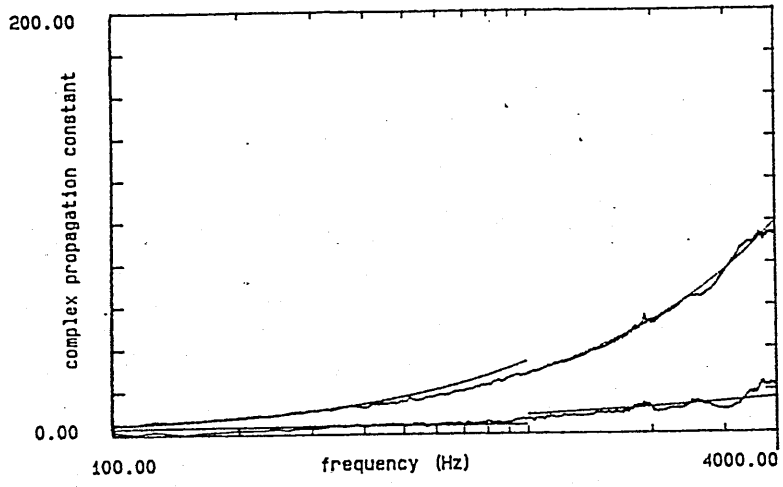

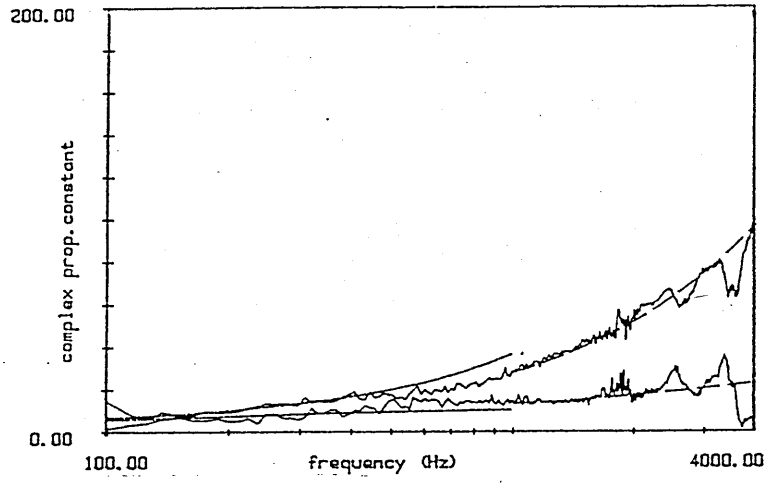

Figure L.1 Examples of Measured and Predicted Propagation Constant in Snow Site A2a, Parameters Deduced a) 0-7cm Low frequency Model σ_{pe}=1060 T=2.26 High Frequency Model σ_{pe} 2520 T=1.23, b) 7-10cm Low frequency Model σ_{pe}=2992 T=2.45 High Frequency Model σ_{pe} 4815 T=1.23

L.2 Snow Site A2b

Table L.1 Ground Parameters Deduced from Level Difference Measurements for Snow Site A2b.

Site	σ_{pe}	T	Ω	rms
KRC	3810	2.83	0.92	0.72
	3120	2.57	0.85	0.64
average	3470	2.7	0.88	0.68

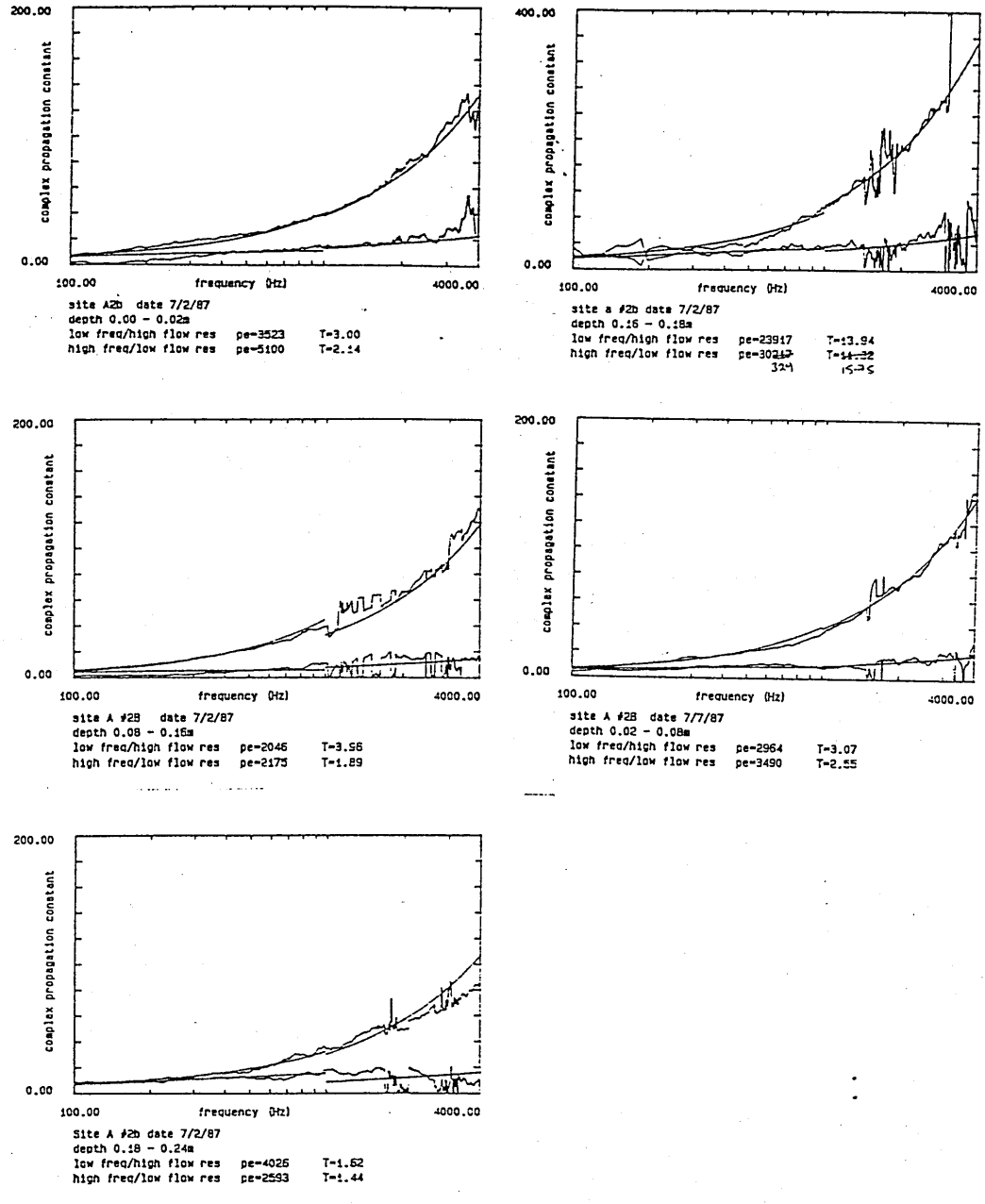

Figure L.2 Examples of Measured and Predicted Propagation Constant in Snow Site A2b, Parameters as labelled beneath plots.

L.3 Snow Site B

Table L.2 Ground Parameters Deduced from all Level Difference Measurements for Snow Site B.

Site	σ_{pe}	T	Ω	rms
Road	2276	3.25	0.91	0.52
Category 1	1751	1.85	0.90	0.31
average	2010	2.55	0.90	0.41
Road	1118	1.35	0.56	0.64
Category 2	1170	1.04	0.66	0.31
	1560	1.0	0.62	0.58
	1237	1.0	0.67	0.59
average	1270	1.10	0.63	0.89

L.4 Snow Sites C&D

Table L.3 Ground Parameters Deduced from all Level Difference Measurements for Snow Site C & D.

Site	σ_{pe}	T	Ω	rms
Site C	1430	1.0	0.65	
	1690	1.32	0.57	
	1135	1.0	0.59	
average	1420	1.11	0.60	
Site D	1581	1.58	0.45	0.66
	1553	1.58	0.45	0.72
average	1567	1.58	0.45	0.69

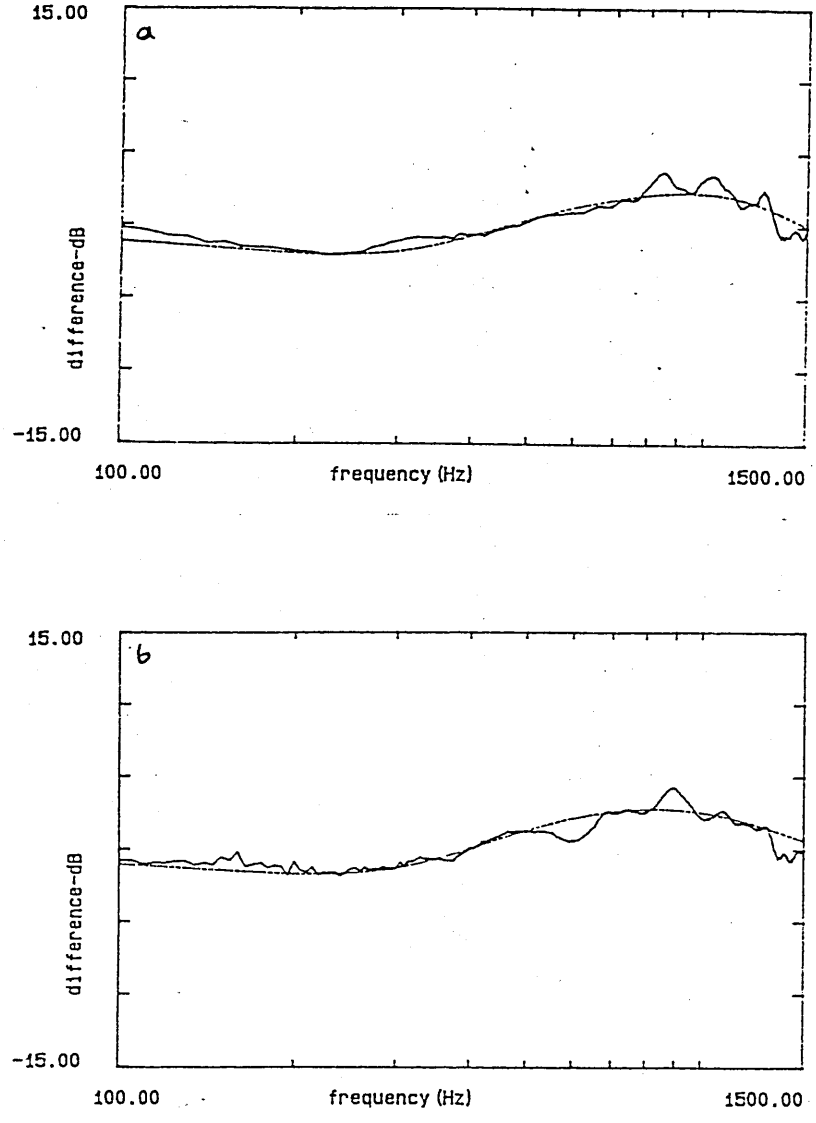

Figure L.3 Examples of Best Fit Predictions from Level Difference Measurements over Snow A2b, a) Geometry hs=0.5m, r=1.63m, hst=0.5m, hrb=0.1m, Deduced σ_{pe} =3120, T=2.57, Ω=0.85, rms=0.64 b) Geometry hs=0.5m, r=1.93m, hst=0.5m, hrb=0.1m, Deduced σ_{pe} =3810, T=2.83, Ω=0.92, rms=0.72

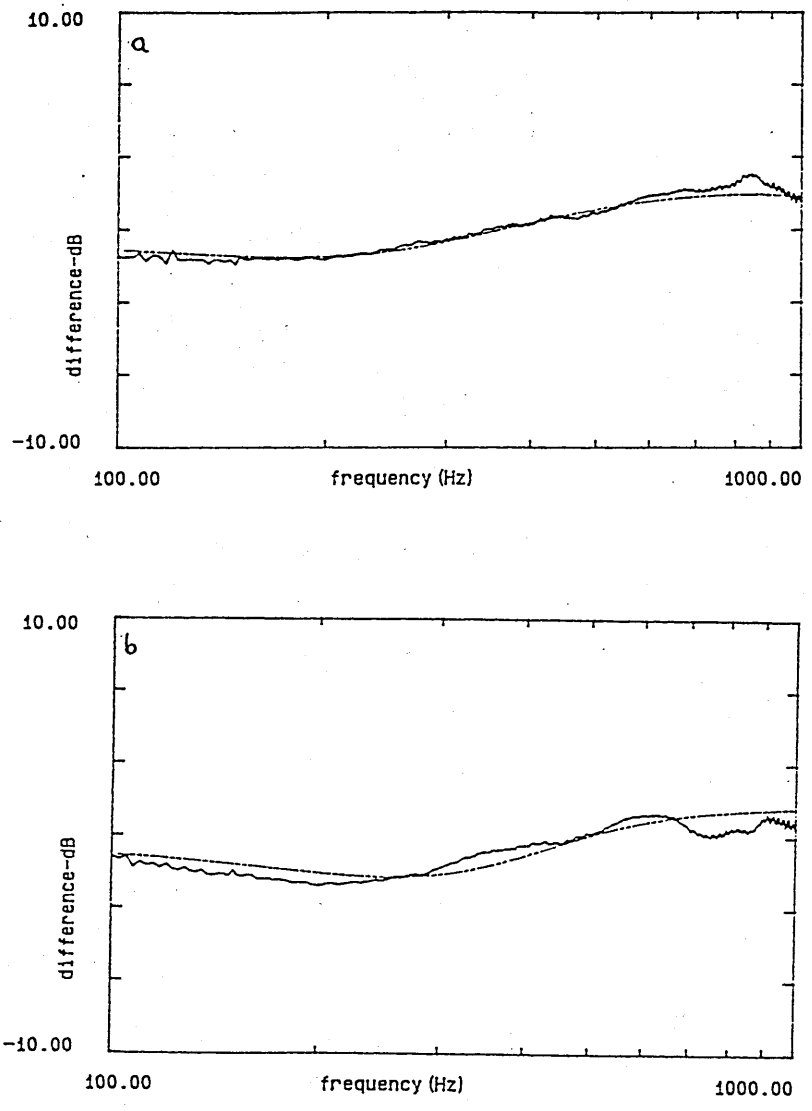

Figure L.4 Examples of Best Fit Predictions from Level Difference Measurements over Snow B, a) Geometry hs=0.5m, r=1.25m, hst=0.37m, hrb=0.1m, Deduced σ_{pe} =1750, T=1.85, Ω=0.9, rms=0.31 b) Geometry hs=0.5m, r=1.5m, hst=0.6m, hrb=0.2m, Deduced σ_{pe} =1170, T=1.00, Ω=0.66, rms=0.31

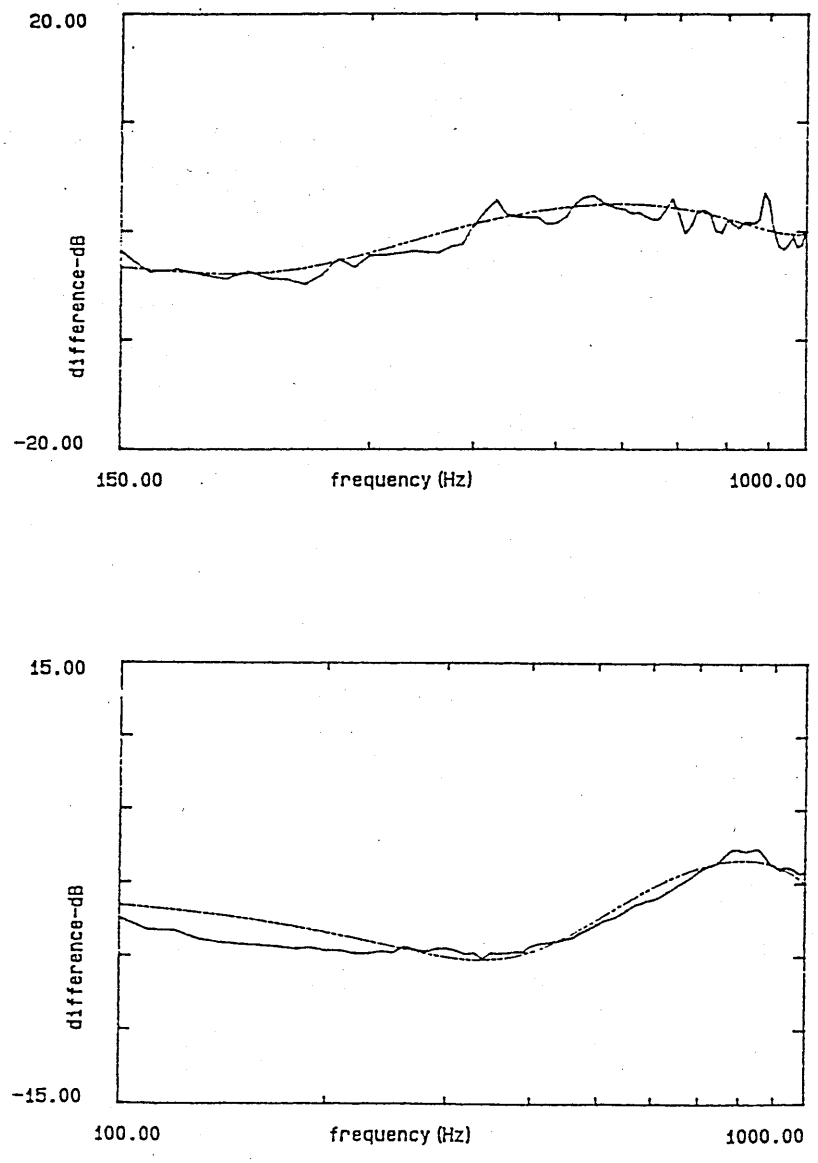

Figure L.5 Examples of Best Fit Predictions from Level Difference Measurements over Snow, a) Site C; Geometry hs=0.5m, r=0.95m, hst=0.52m, hrb=0.1m, Deduced σ_{pe} =1135, T=1.00, Ω=0.59, rms=0.81
b)Site D; Geometry hs=0.55m, r=1.07m, hst=0.53m, hrb=0.05m, Deduced σ_{pe} =1580, T=1.58, Ω=0.45, rms=0.66